Dynamic Protein-based Nanoparticles for Drug Delivery Applications

Dissertation

zur Erlangung des akademischen Grades

"Doktor der Naturwissenschaften"

im Promotionsfach Chemie

am Fachbereich Chemie, Pharmazie, Geographie und Geowissenschaften

der Johannes Gutenberg-Universität in Mainz

vorgelegt von

Elena Steiert

geboren am 16. Dez. 1991 in Villingen-Schwenningen

Mainz, Januar 2020

Dekan: ██████████████

Erstgutachter: ███████████████

Zweitgutachter: ██████████████

Datum der Einreichung: ████████

Datum der mündlichen Prüfung: ████████

EIDESSTATTLICHE ERKLÄRUNG

Die vorgelegte Dissertation wurde am Institut für Pharmazie und Biochemie der Johannes Gutenberg-Universität in Mainz zur Erlangung des Grades „Doktor der Naturwissenschaften" angefertigt.

Erstgutachter: ███████████████

██████████████████

███████████████████

Zweitgutachter: ███████████████

██████████████████

███████████████████

Hiermit erkläre ich an Eides statt, dass ich die vorliegende Dissertation selbstständig und nur mit den angegebenen Hilfsmitteln angefertigt habe. Diese Dissertation wurde noch nicht als Prüfungsarbeit für eine andere Prüfung eingereicht. Zudem wurden bisher weder die gleiche, noch Teile der Abhandlung als Dissertation bei einer anderen Fakultät oder einem anderen Fachbereich eingereicht.

Ort, Datum   Elena Steiert

DANKSAGUNG

ABSTRACT

Proteins are natural polymers, which depict promising materials for the preparation of nanoparticles due to their biocompatibility, biodegradability and low toxicity. Moreover, proteins are attractive substances as a result of the simplicity and versatility in their surface modification using bioorganic chemistry.

This PhD thesis presents the development of several different protein-based nanoparticle systems, composed of high surface PEGylated enzymes. The modification changes the enzyme solubility behavior and allows a particle formation by an emulsion-based preparation technique. This process preserves the enzyme structure and activity and the prepared particles need no cross-linking in order to be stable.

The preparation technique was advanced to approve the encapsulation of large, hydrophilic enzymes which can act as biotherapeutics in bacterial infection treatment. The encapsulation of the antibacterial payload leads to no activity impairment and the payload can sustained release at the local area of bacterial infections. These results open up the possibility to transfer this particle preparation technique universally to various enzymes as particle material and the encapsulation of diverse hydrophilic payloads.

Additionally, the emulsion technique was applied in this work to develop stimuli-responsive protein-based nanoparticle systems, which allows a triggered payload release. An acid-sensitivity was obtained through cleavable vinyl ether groups distributed within the PEG backbone. The prepared particles disassembled in acidic conditions, as it occurs for example in the endo-lysosomal pathway, while they were stable in a physiological neutral environment. After the encapsulation of a hydrophilic payload into these nanoparticles, an acid triggered payload release could be shown.

Furthermore, a nanoparticle system was developed with a redox-responsivity, which was obtained using a disulfide linker between the enzyme and PEG. The linker has the additional property of degrading itself after the disulfide cleavage. The prepared nanoparticles have the ability to decompose in reductive conditions, while the nearly unmodified enzyme can be regained due to the linker property. In the future, this enzyme recovery from the particle material could be exploited, that the protein-based nanoparticles itself can be used as a biotherapeutic agent.

ZUSAMMENFASSUNG

Proteine sind natürliche Polymere, die aufgrund ihrer Biokompatibilität, ihrer biologischen Abbaubarkeit und ihrer geringen Toxizität vielversprechende Materialien für die Herstellung von Nanopartikeln darstellen. Darüber hinaus sind Proteine attraktive Substanzen, da sie durch die Anwendung der bioorganischen Chemie einfach und vielseitig oberflächenmodifiziert werden können.

In dieser Arbeit wird die Weiterentwicklung eines proteinbasierten Nanopartikelsystems präsentiert, das aus Enzymen besteht, die mit mehreren Polyethylenglykol (PEG)-Ketten modifiziert wurden. Die Modifikation verändert das Löslichkeitsverhalten des Enzyms und ermöglicht dadurch eine Partikelbildung durch eine Emulsions-basierte Herstellungstechnik. Dieses Verfahren bewahrt die Enzymstruktur und -aktivität und die hergestellten Nanopartikel müssen nicht vernetzt werden, um stabil zu sein.

Die Herstellungstechnik wurde weiterentwickelt, um die Einkapselung großer, hydrophiler Enzyme zu gewährleisten, die als Biotherapeutika bei der Behandlung von bakteriellen Infektionen wirken können. Die Einkapselung der antibakteriellen Wirkstoffe führt zu keiner Beeinträchtigung ihrer Aktivität und die Substanzen können in lokaler Nähe von bakteriellen Infektionen über einen längeren Zeitraum freigesetzt werden. Diese Ergebnisse eröffnen die Möglichkeit, diese Partikelpräparationstechnik universell auf verschiedene Enzyme als Partikelmaterial zu übertragen und verschiedene hydrophile Nutzlasten einzuschließen.

Zusätzlich wurde in dieser Arbeit die Emulsionstechnik genutzt, um Protein-basierte Nanopartikelsysteme zu entwickeln, die sich durch bestimmte externe Reize auflösen können, wodurch eine kontrollierte Wirkstofffreisetzung ermöglicht wird. Eine Säureempfindlichkeit wurde durch säurespaltbare Vinylethergruppen erhalten, die im PEG-Rückgrat verteilt waren. Die hergestellten Partikel konnten unter sauren Bedingungen, wie sie beispielsweise in dem endo-lysosomalen Weg auftreten, zerlegt werden, während sie in physiologisch neutraler Umgebung stabil waren. Nach dem Einschluss einer hydrophilen Modellverbindung konnte die durch Säure ausgelöste Wirkstofffreisetzung nachgewiesen werden.

Darüber hinaus wurde ebenso ein Nanopartikelsystem mit Redox-Empfindlichkeit entwickelt, das unter Verwendung eines Disulfid-Linkers zwischen dem Enzym und PEG erhalten wurde. Der Linker besitzt die zusätzliche Eigenschaft sich nach der Disulfid Spaltung selbst aufzulösen. Die hergestellten Nanopartikel konnten unter reduzierenden Bedingungen abgebaut werden, während durch die Linkereigenschaft das nahezu unmodifizierte Enzym zurückgewonnen wurde. In Zukunft könnte diese Zurückgewinnung des Enzyms aus dem Partikelmaterial genutzt werden, um die proteinbasierten Nanopartikel selbst als Biotherapeutikum einzusetzen.

TABLE OF CONTENT

1 INTRODUCTION

1.1 NANOCARRIERS IN MEDICINE

Nanotechnology, which deals with materials in the nanoscale size, has evolved exceedingly the last decades.[1] This revolutionary technology is applied in the most different areas, for example in solar energy[2], cosmetics[3], agriculture[4] or in food safety[5]. Especially in medicine, nanotechnology achieved great success. The so-called nanomedicine deals with nanomaterials, which are applicable for diagnosis, prevention and treatment of diseases.[6] Particularly, nanomaterials for the targeted site-specific drug delivery is a promising application. The goal is to deliver the right amount of the drug to desired sites in the body, such as tumors or diseased tissues, while minimizing the undesirable side effects of the drugs on non-affected areas. For delivery, the drugs can be attached or encapsulated into nanocarriers, which exhibit several advantages. On the one hand, insoluble drugs are administrable this way and moreover, the encapsulation protects the drug against enzymatic degradation, for example by proteases.[7] Additionally, due to encapsulation, the drug elimination by kidney or the immune system is reduced, whereby the administered drug doses can be decreased. Consequently, it follows a side effect reduction.[8] Furthermore, attached targeting ligands on nanocarrier surfaces results in specific receptor binding between drug carriers and targeted cells. This so-called active-targeting provides an even more addressed drug delivery.[9]

In summary, nanomedicine offers several benefits over common drugs, which includes the improved drug efficiency as well as pharmacokinetics, pharmacodynamics and further the drug encapsulation results in reduced systemic toxicity.[10] The success in drug delivery using nanocarriers is obvious, considering that more than 50 nanomedicines are FDA approved and in clinical use.[11] Figure 1 summarizes important events in nanomedicine over the last 55 years and in the following introduction, some of them will be discussed more in detail.

After the general introduction in nanomedicine in this section, the succeeding one will present different types of nanocarriers, their biodistribution, cellular uptake, and drug release.
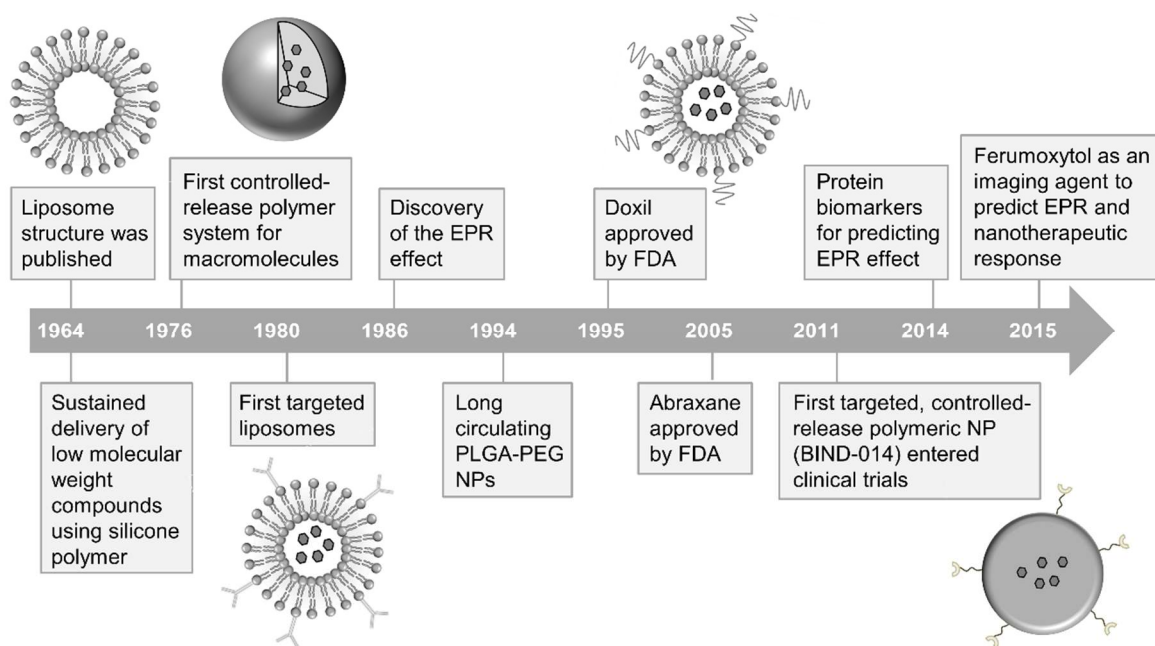
Figure 1: Timeline of milestones in nanomedicine over the last decades. Redrawn from Shi *et al.*[12]

1.1.1 DIFFERENT TYPES OF NANOCARRIERS

Nanocarriers are defined as colloidal particulate systems, based on macromolecular materials and their size ranging between 1–1000 nm.[13] In general, nanoparticles not only vary in their size, but also in their material. A selection of the most commonly used nanomaterials for drug delivery is summarized in Figure 2. On the whole, a main distinction can be made between inorganic and organic nanoparticles.[14] Inorganic nanomaterials are for example composed of gold[15] or silica[16], but a major drawback of these nanomaterials is often their toxicity.[17]
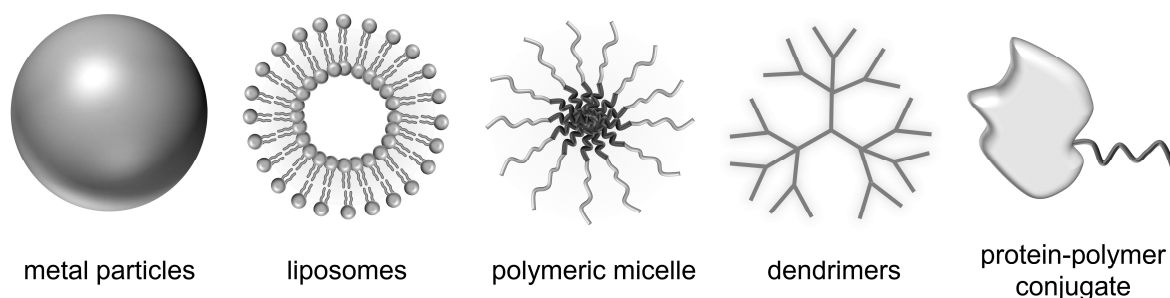
Figure 2: Summary of nanoparticles, which can be used for drug delivery applications. Redrawn from Sun *et al.*[18] and Ekladious *et al.*[19].

In general, as organic nanocarriers, particularly polymer- or lipid-based materials are described. Considering lipid-based carriers, the most common investigated particles are liposomes. This particle system consists of a lipid bilayer, which is mainly composed of the

amphiphilic phospholipids, enclosing an inner water core. Within these liposomes, the hydrophilic head of the phospholipids is oriented to the water core or the aqueous exterior. Accordingly, the hydrophobic tails of the bilayer are directed towards each other.[20] With regard to hydrophobic and hydrophilic areas within the particle system, the encapsulation of hydrophobic drugs in the lipid bilayer, as well as hydrophilic payloads in the inner core, is possible, which highlights the advantage of this type of nanocarrier.[21] Here, Doxil® needs to be emphasized, which is the first approved nanocarrier in clinical application. Doxil® is a delivery system for the anticancer drug doxorubicin (DOX), which is based on poly(ethylene glycol) modified (PEGylated) liposomes.[20] The additional PEG attachment on the liposome surface leads to a prolonged circulation time of the nanocarrier system.[22] This so-called "stealth-effect" will be discussed more in detail in Section 1.1.2. Nevertheless, Doxil® was just the beginning of FDA approved liposomal-based formulations of drug delivery systems, hence in the succeeding years many more followed.[23]

After discussing lipid-based nanocarriers, now a closer look at polymer particles will follow. Polymer nanocarriers can be constructed of synthetic or natural polymers. Both backbones provide beneficial properties for nanoparticle preparation due to their stability and their customization ability by surface modification.[7] To start off, the synthetic polymer particles will be considered, which have the ability to form for example micelles. They are composed of amphiphilic block copolymers, which can self-assemble above their critical micelle concentration (CMC).[24] In addition, amphiphilic block copolymers can build up polymersomes by forming a bilayer membrane.[25] Moreover, also dendrimers, which are hyperbranched globular polymers, belong to this subgroup of synthetic polymer particles.[26] Additionally, the conjugation of therapeutics and synthetic polymers results in nanocarriers of this group due to their size around 10 nm. Amongst other things, this type of nanosystem includes polymer-drug and polymer-protein conjugates, which can be used as biotherapeutics.[27] These polymer conjugations beneficially affect the properties of therapeutics, like improved solubility, circulation time, immunogenicity and safety.[19] Already 1977 Abuchowski *et al.* proved these advantages after PEG attachment to proteins.[28] Taking into account that until now ten PEGylated proteins are approved by the FDA, the outstanding properties of these nanocarrier systems are highlighted.[29] Likewise, the PEGylation is also considered as the gold standard for the preparation of polymer-drug conjugates. As a result, additionally to the already mentioned approved polymer-protein conjugates, six conjugations of polymers and drugs are on the market and five of them are based on the PEG attachment.[19] The FDA approved conjugates described in this section are summarized in Table 1.

Table 1: FDA approved PEG-therapeutic conjugates. Modified from Ekladious *et al.*[19]

Name	Polymer	Therapeutic	Indication	Year
Adagen	PEG	Adenosine deaminase (ADA)	ADA severe combined immunodeficiency	1990
Oncaspar	PEG	L-asparaginase	Acute lymphoblastic leukaemia	1994
PegIntron	PEG	Interferon α2b	Hepatitis C	2001
Pegasys	PEG	Interferon α2a	Hepatitis B, hepatitis C	2002
Neulasta	PEG	Granulocyte colony-stimulating factor	Chemotherapy-induced neutropenia	2002
Somavert	PEG	human growth hormone receptor antagonist	Acromegaly	2003
Macugen	PEG	Anti-vascular endothelial growth factor aptamer	Neovascular age-related macular degeneration	2004
Mircera	PEG	Epoetin beta	Anaemia associated with chronic kidney disease	2007
Cimzia	PEG	Anti-tumor necrosis factor Fab´	i.a. Crohn's disease and rheumatoid arthritis	2008
Krystexxa	PEG	Uricase	Chronic gout	2010
Plegridy	PEG	Interferon β1a	Relapsing multiple sclerosis	2014
Movantik	PEG	Naloxone	Opioid-induced constipation	2014
Adynovate	PEG	Factor VIII	Haemophilia A	2015
Palynziq	PEG	Phenylalanine ammonia lyase	Phenylketonuria	2018
Jivi	PEG	Factor VIII	Haemophilia A	2018

Despite the advantages, PEG also exhibits a limitation due to the lack of biodegradability. As a result, higher molecular weight PEGs can cause accumulation in human tissues. Additionally, anti-PEG antibodies were discovered in patients, which lead to a fast clearance of PEG containing conjugates by the immune system.[30] For this reason, efforts are made to find PEG alternatives or degradable PEG variants. For example, poly(2-oxazoline) represents a capable PEG alternative. However, this polymer needs further investigations in-depth concerning pharmacokinetics, pharmacodynamics and biodistribution.[31] The most promising PEG alternative is the poly(*N*-(2-hydroxypropyl) methacrylamide)[32], which is as drug-polymer conjugate in clinical trial tests. In summary, the efforts in finding a PEG alternative are great, but until now none of them are FDA

approved. Nevertheless, it has to be emphasized that the benefits of PEG outweighing over the limitations, as a result, PEG is still considered as the gold standard.[30] Anyway, with regard to overcoming the absence of biodegradability, degradable PEG backbones were developed. For example, Hawker *et al.* synthesized a promising acid-sensitive PEG by introducing vinyl ether moieties, whose synthesis could be improved by the group of Holger Frey.[33] *Via* anionic ring opening copolymerization (AROP) of ethylene oxide (EO) and 3,4-epoxy-1-butene (EPB), PEG with several allylic moieties was synthesized. These allyl residues were isomerized with a Wilkinson's catalysts resulting in pH-sensitive vinyl ether moieties. The advantages of this synthetic route above the previously described one are the improved narrow molecular weight distribution and good control over the distribution of cleavage sites. Furthermore, the stability in physiological neutral conditions could be proven while a fast vinyl ether cleavage at a reduced pH value of 4.9 with a half-life time of around one day could be shown. Additionally, concerning the non-modified hydroxyl end group of this polymer, conjugation reactions are possible.[33b] Recently, an acid-sensitive hydrogel based on PEG bearing vinyl ether units has been developed.[34] However, until now, this degradable PEG variant was not tested in protein or drug conjugation.

Although, synthetic polymer nanosystems are frequently used, in comparison nanoparticles based on natural polymers exhibit some advantages, due to non-toxicity, biodegradability and biocompatibility.[35] An example of natural polymer nanoparticles is based on acetylated dextran, which was prepared by an emulsion-based method. On the one hand, using this particle system the successful siRNA delivery was proven[36] and in further studies, the active-targeting by attachment of targeting structures on the dextran particles was developed[37]. Another example of natural polymer-based nanocarriers are micelles prepared by the self-assembly of polysaccharide amphiphilic building blocks.[38]

Until now, two types of natural polymer nanoparticles are FDA approved: Abraxane and Ontak.[11] Both examples of natural drug delivery systems are based on proteins. Abraxane was approved in 2005. This nanoparticle system consists of albumin, which encapsulates paclitaxel, an antitumor drug against metastatic breast cancer, *via* hydrophobic interactions. Considering the poor water solubility, free paclitaxel had to be administered in the toxic solvent Cremophor EL, which could be circumvented by the encapsulation in the protein particles. Thus, these 130 nm albumin particles also prevent the additional administration of strong antihistamines or dexamethasone, which otherwise had to be given to protect against an immune reaction triggered by the Cremophor EL solvents. In addition to the original goal of reducing the toxicity of paclitaxel, Abraxane demonstrates improved pharmacokinetics and increased tumor inhibition due to enhanced endothelial binding and tumor uptake of the nanoparticles.[39] Three years later, in 2008, Ontak was approved for the treatment of malignant disorders. In contrast to Abraxane, Ontak is a

particle system based on an engineered fusion protein of interleukin-2 (IL-2) and diphterietoxin, which is a toxin since it inhibits the protein biosynthesis in eukaryotes. As a result of IL-2, the particles gained an active targeting function against various hematological malignancies, where appropriate receptors are overexpressed.[40]

Since this thesis focuses on protein nanoformulations, section 1.2 will be more specific about this type of nanocarrier.

1.1.2 BIODISTRIBUTION OF NANOCARRIERS

Succeeding the introduction of different nanocarrier types, this section will present their biodistribution and the related difficulties but also benefits after the nanoparticle administration.

In general, the most popular way of drug administration is the oral uptake, in consideration that it is not painful. However, the oral application of nanoparticles is rather unfavorable, due to several compartments in the human body have to be overcome until reaching the targeted area. At first, nanoformulations have to survive extremely acidic conditions and the presence of proteases in the stomach. Subsequently, nanoparticles reach the small intestine, where it is exposed to extreme enzymatic digestion. Finally, to gain a systemic effect, the nanocarrier has to enter the bloodstream by absorption of enterocytes in the small intestine.[41] However, for systemic administration and to circumvent the extreme conditions in the stomach and small intestine, nanoparticles can be applied directly into the bloodstream. Hence, after intravenous administration, the nanocarriers have the first contact with blood and their components like plasma proteins. The plasma proteins have the ability to rapidly bind on the particle surfaces to a high extent, which results in a so-called protein corona. The extent of the corona formation depends on the particle size, charge, shape and hydrophobicity. Mostly, albumin, immunoglobulin G, fibrinogen or apolipoproteins interact with the particle surfaces. The binding of plasma proteins has various advantages, like an improved circulation time and reduced toxicity of the nanoparticle system.[42] For example, positively charged nanocarriers can disturb the negatively charged plasma membrane, causing cell death. Protein corona attachment on the nanoparticle surface leads to charge shielding, resulting in an increased nanoformulation safety.[43] However, the protein corona has a drawback in targeted drug delivery, due to targeting function on particle surfaces could be covered. Additionally, complement proteins also contain to plasma proteins. The complement system is a part of the innate immune system and interactions with particles, called opsonization, can lead to an immune response by phagocytic cells. To reduce immunogenicity, the gold standard so far is the PEGylation of nanocarrier surfaces, which is described as a "stealth effect".

Presumably, it is caused by steric repulsion, due to the adsorption of water molecules on PEG.[42] In addition, PEGylation has the advantage of charge shielding. The immune system confounds negatively charged nanoparticles with pathogens like bacteria since they also exhibit a negative charge. As a result, these nanoparticles would lead to an increased uptake by phagocytic cells. Thus, the shielding of the negative charge by PEG ensures reduced immunogenicity.[44] Moreover, with regard to the side effects of positively charged particles, which was already discussed at the protein corona attachment, this cytotoxicity is also decreased by PEG attachment.[45] Nevertheless, the stealth effect results not only in reduced immunogenicity and cytotoxicity but further in overall decreased protein corona adsorption. Additionally, Landfester *et al.* proved that the stealth effect not only depends on the reduced protein adsorption due to PEG-attachment but also in the preferred binding of certain plasma proteins, like clusterin. The binding of this plasma protein leads to reduced unspecific cellular uptake and enables the nanocarrier to reach specifically targeted cells.[46]

An additional challenge after the intravenous application of nanosystems is the quick elimination out of the blood by renal or hepatic clearance. If nanoparticles are smaller than the renal extraction cut off of around 10 nm, it results in the particle elimination.[47] Mostly, nanoparticles are bigger, which avoids the renal clearance. The elimination of nanocarriers by the liver is initiated by the interaction between immune cells and nanoparticles, ensuing the transport to the hepatic cells. However, as a result of PEGylation, the immune response is reduced, which further prevents the elimination by the liver.[48] Nevertheless, particles with sizes above 200 nm can accumulate in the liver and spleen due to fenestrated endothelial pore sizes of 200–500 nm.[49] But the unwanted clearance of nanocarriers by the kidney, liver or spleen can be circumvented in the main due to nanoparticle size adjustment.

Within the bloodstream, nanocarriers have the possibility to reach desired tissues or cells for example through active targeting, which was already mentioned. However, certain areas, like tumors, can also be reached preferably without the need of targeting structures on the nanoparticle surface, which is called passive targeting. This effect was first described by Maeda *et al.* in 1986, which observed an increased drug accumulation in tumors.[50] This passive targeting is substantiated by an enhanced permeability and retention (EPR) of the blood vessels, the so-called EPR-effect, which is caused by several factors. The rapid proliferation during tumor growth results in a low density of endothelial cells and thus to the loss of tight junctions. Consequently, larger gaps between cells emerge.[51] Furthermore, the EPR-effect is caused by tumor angiogenesis, the formation of new blood vessels. Tumors need fast angiogenesis to ensure a sufficient supply of nutrients and oxygen to cells.[52] In consideration of rapid blood vessel formation, the basement membrane is defective or completely missing.[53] The resulting openings of the blood

vessels in the tumor are typically in the size range of 100–400 nm.[54] For this reason, nanosystems smaller than this size limit of 400 nm, can penetrate from the blood vessels into the tumor tissue and accumulate there. Nevertheless, nanoformulations with a size of 100 nm revealed the best results concerning the EPR-effect.[55] In comparison, normal, endothelial cells of non-diseased blood vessels have a distance of 5 nm.[56] Consequently, free drugs with a smaller size than 5 nm have the ability to penetrate into healthy tissues. In contrast, most nanocarriers are too big, which highlights the advantages of nanoparticles as drug delivery systems especially in cancer treatment.[57]

1.1.3 CELLULAR UPTAKE OF NANOCARRIERS

After explaining the possible entry of nanocarriers from the bloodstream into tissues, this section will focus on the particle uptake in cells, after reaching their extracellular membrane. In literature several mechanisms are described, how nanoparticles overcome the cell membrane to get into the cell. Mostly, the particles are taken up by endocytosis. During this mechanism, inside of cells a vesicle, a so-called endosome, is formed, consisting of the cell membrane, which enclosed the nanocarrier. The endocytosis can be divided into two main mechanism types, the phagocytosis and pinocytosis. Nanoparticles larger than 500 nm are preferably taken up in cells *via* the phagocytosis mechanism, and smaller ones *via* pinocytosis. The pinocytosis can be further subdivided into four procedures: the clathrin-mediated endocytosis, caveolin-mediated endocytosis, clathrin- and caveolin-independent endocytosis and macropinocytosis. All nanoparticle uptake mechanisms strongly depend on their size, shape and surface properties.[58] An overview of the cellular nanoparticle uptake mechanisms is summarized in Figure 3.

Phagocytosis, clathrin- as well as caveolin-dependent endocytosis describe receptor-mediated uptakes of nanoparticles. For this reason, in these endocytosis mechanisms, the nanocarriers need ligands on their surface, which have the ability for cell receptor interactions. For example, phagocytosis is induced after opsonin attachment. Receptors on cell surfaces recognize the attached complement proteins on nanoparticles, due to ligand-receptor interactions, which results in the cellular uptake. This mechanism is mainly performed by phagocytes, but also other cell types have a phagocytic activity, however to a lower extent. Additionally, the clathrin-dependent endocytosis is responsible for the receptor-mediated uptake of specific molecules. Thus, clathrin-coated endosomes with sizes of 100–150 nm are formed, but mostly resulting in degradative lysosomes. This uptake mechanism depends strongly on the charge of nanocarriers, especially positively charged particles are particularly preferred taken up by this route.[59] In contrast, the receptor-mediated endocytosis by caveolin builds vesicles with a size around 50–80 nm, which normally do not end in a degradative lysosome. For this reason, this is the most

appealing nanoparticle uptake mechanism, since the cargos undergo no degradation during this pathway. Cells without clathrin or caveolin can use the clathrin- and caveolin-independent pathway. For instance, growth hormones, extracellular fluids or interleukin-2 using this pathway to penetrate into cells. Macropinocytosis, which occurs in almost all cell types, is a non-specific endocytic mechanism by taking up high volumes of extracellular fluids. Using this pathway, large nanoparticles can penetrate into cells, by forming vesicles around 0.5–10 μm. All in all, based on their properties, nanoparticles can be taken up in cells by each described mechanism.[60]
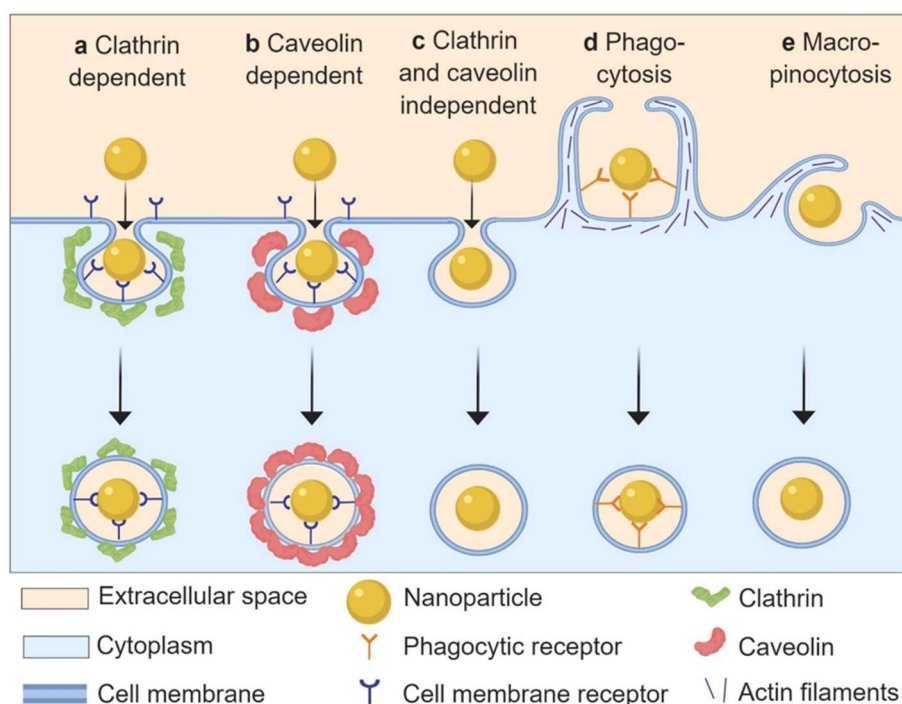
Figure 3: Cellular uptake mechanism of nanoparticles by endocytosis, which can be differentiated between clathrin and caveolin dependent, or clathrin and caveolin independent pathway as well as phagocytosis and macropinocytosis. Reprinted from Donahue *et al.*[61], Copyright (2019), with permission from Elsevier.

After nanoparticle initialization by endocytosis, nanoparticles are located in vesicles inside the cells, following by different intracellular trafficking ways, which are summarized in Figure 4.

For example, the endosome can evolve to a late endosome and subsequently merging with a lysosome. This mechanism is accompanied by a pH decrease to a value of 5.[18] Afterwards, an escape of the nanoparticles out of the vesicle is possible, resulting in the released nanoparticles in the cytosol. On the other hand, if the nanocarriers do not escape, the particles could also be degraded in the lysosome or transported out of the cell by exocytosis. However, if the endosomes do not evolve in a late endosome, a nanoparticle escape can occur directly after cellular uptake.
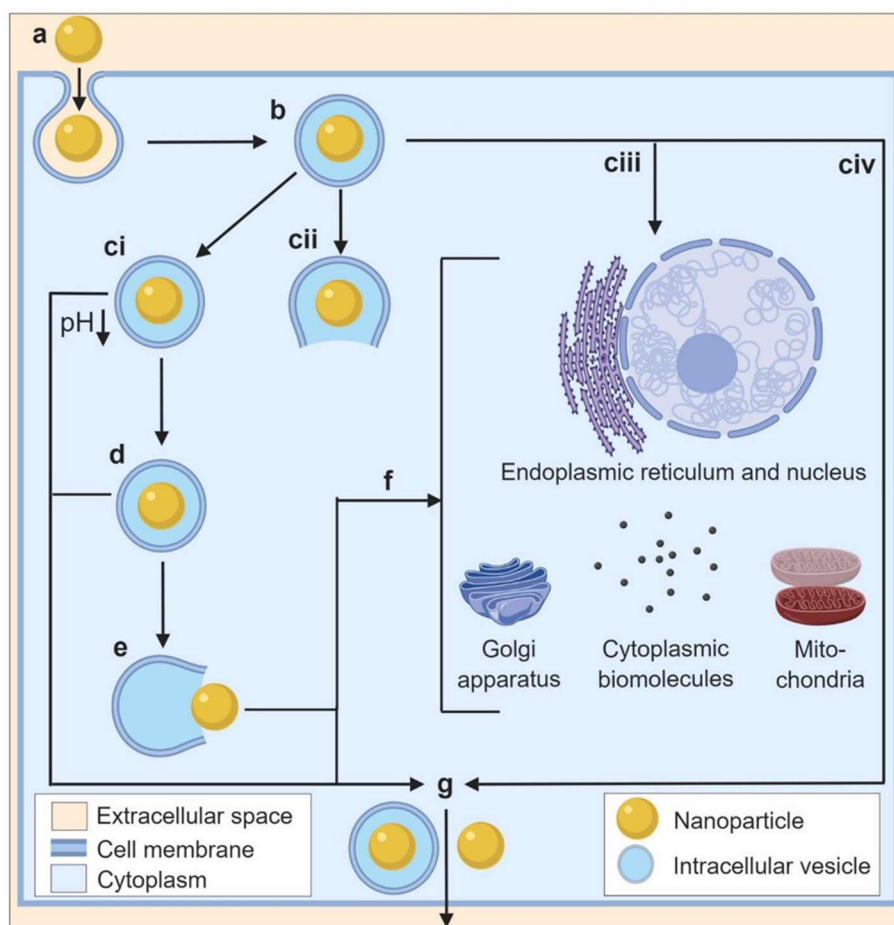
Figure 4: Summary of intracellular pathways of nanocarriers after endocytosis (a). After cellular uptake, the particles are in the endosome (b) that can evolve to a late endosome which is characterized by a decreased pH value (ci). Additionally, this vesicle can fuse with lysosomes (d). However, nanoparticles can also undergo endosomal escape (cii, e) resulting in particle release in the cytosol where reaching of the organelles or compartments is possible (f). Furthermore, endosomes can transport the nanoparticles directly to other organelles (ciii), but also all vesicles or released particles can undergo exocytosis (civ, g). Reprinted from Donahue *et al.*[61], Copyright (2019), with permission from Elsevier.

In conclusion, after cellular uptake, the vesicles with the enclosed nanosystems have several options for further processing. Nevertheless, for drug delivery systems the endosomal and lysosomal escape are mostly of interest.[61]

1.1.4 DRUG RELEASE OUT OF NANOCARRIERS

This section will focus on the final drug release out of the nanocarrier system, which should preferably occur in diseased tissues or cells. This drug release can be classified into two major mechanisms, the sustained and the stimuli-responsive release. The sustained release describes drug leakage over a longer period of time. With this method, a constant drug level in cells or tissues is obtained by diffusion- or solvent controlled release out of

the particle system.[62] The release rate depends on the particle constitution and how the drug can overcome the particle material.[18] But mostly, for the treatment of diseases a triggered drug release is preferred, whereby a more controlled drug delivery is ensured. Such a stimuli-responsive particle material needs endogenous or exogenous stimuli for drug release. Examples for endogenous stimuli include pH-, redox- or enzyme-responsiveness. In contrast, changes in ultrasonic intensity, light or electric pulses belong to the group of exogenous stimuli. Appropriate stimuli lead to a nanocarrier material change, resulting in for example linker cleavage of conjugates or particle disassembly, whereby the encapsulated drug can be released in a controlled manner.[63] The different drug release possibilities are summarized in Figure 5. Considering that parts of this thesis focus on acid- and redox-responsive nanocarriers the following paragraphs will give a closer look at these two endogenous stimuli.
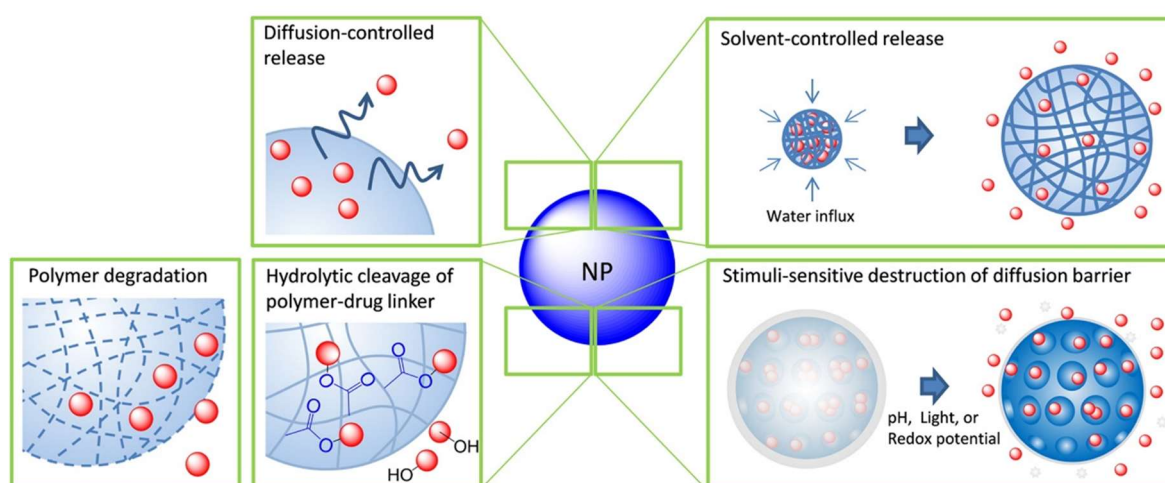
Figure 5: Drugs in nanoparticles can release through different mechanisms. The sustained release by diffusion or induced by solvent describes a slow drug leakage out of the nanoparticle system. In contrast, the stimuli-responsive drug release is an induced mechanism for example by polymer degradation or the cleavage of a polymer-drug conjugate. Reprinted from Lee *et al.*[62], Copyright (2015), with permission from Elsevier.

pH-responsiveness is a reliable stimulus in different diseases. For example, in inflammation or tumors, the tissue environment has a decreased pH value. In tumors, the fast angiogenesis results in nutrition and oxygen deficiency. For this reason, the metabolism has to switch to glycolysis, which forms acidic metabolites. As a result, the pH of the environment decreases to a value of 6.5. In comparison, healthy tissues exhibit a pH value of 7.4. Thus, acid-sensitive nanocarriers lead to a spatial-controlled drug release in tumors.[64] Not only tissues but also intracellular compartments, like lysosomes with a pH value of 5 can trigger the payload release of acid-sensitive nanoparticles.[65]

Moreover, differentiate reductive environments in the body makes redox-sensitive nanocarriers an interesting tool for the controlled drug release. The tripeptide glutathione

(GSH) plays an important role as an antioxidant inside of cells. The most crucial function is the involvement in reductive processes, due to GSH containing a sulfhydryl group. Hence, GSH has the ability to cleave disulfide bonds.[66] The intracellular GSH concentration is frequently higher (10 mM) compared to the blood plasma (2 μM). Additionally, in cancer cells, the GSH concentration is even tenfold higher than in healthy cells. For this reason, redox-sensitive nanocarriers are an interesting target for stimuli-responsive drug delivery.[67]

Figure 6 summarizes some of the most frequently used acid or redox cleavable groups, like acetals, hydrazones and disulfides. In acetals, two oxygen atoms are attached to the same carbon atom. Acidic conditions lead to oxygen protonation, whereby the linked carbon atom is activated. Subsequently, a water molecule can attack the carbon, resulting in the acetal cleavage to aceton and two alcohol molecules.[68] In hydrazones, a nitrogen-carbon double bond occurs, with a second bound nitrogen to the first one. The cleavage mechanism is similar to the described one of acetals. Protonation of the amine which is linked to the carbon atom leads to carbon activation, which can be attacked by water molecules. As a result, the hydrazone bond can be cleaved to a hydrazine and a ketone molecule.[69] Like mentioned before, disulfide bonds can be cleaved in reductive conditions for example by GSH, which results in two sulfhydryl groups while GSH is oxidized to glutathione-disulfide (GSSG).[67]
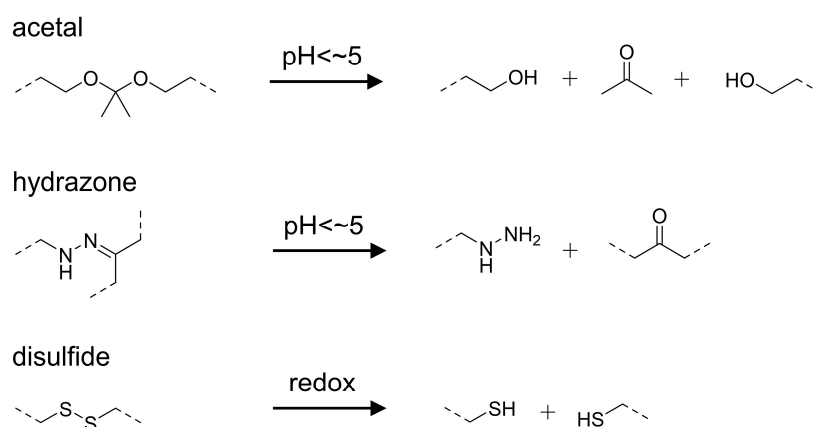
Figure 6: Examples of linkers in stimuli-responsive nanosystems. Acetals and hydrazones are acid-sensitive linker, which decompose at pH values below 5. Disulfides are cleaved by reductive conditions, resulting in sulfhydryl groups. Redrawn from Fleige *et al.* and Binauld *et al.*[67-68]

1.1.5 STIMULI-RESPONSIVE NANOCARRIERS

After describing the general concept of stimuli-responsive nanosystems for triggered drug release, this section will present examples of such particle types. Since this thesis partly deals with polymers and protein-polymer conjugates bearing stimuli-responsive groups, such examples will be discussed more in detail.

With regard to acid-responsive polymer particles, often the polymer bears several cleavage sites in the backbone.[70] Recently Li *et al.* described a pH-responsive polymer microsphere, where multiple acetal groups were introduced in the polymer backbone. The decrease in pH value results in acetal cleavage and particle disassembly. This particle system was proved to encapsulate the anticancer drug DOX and release it in acidic conditions.[71] In section 1.1.1, a similar approach but based on a natural nanoparticle backbone has already been mentioned. The basic building block of this nanosystem is dextran, whose hydroxyl groups were acetylated. This modification results in a changed solubility, which enables a nanoparticle preparation *via* an emulsion technique. These nanoparticles were successfully used for siRNA encapsulation. Acidic conditions lead to acetal cleavage within the dextran chains, resulting in a changed solubility and consequently in nanoparticle disassembly and siRNA release.[36]

In contrast, in redox stimuli-responsive polymer nanoparticles, the reductive cleavage site is predominantly introduced by two described methods: disulfide bond as linker (Figure 7a) or as cross-linkage of the shell particle material (Figure 7b).[72]
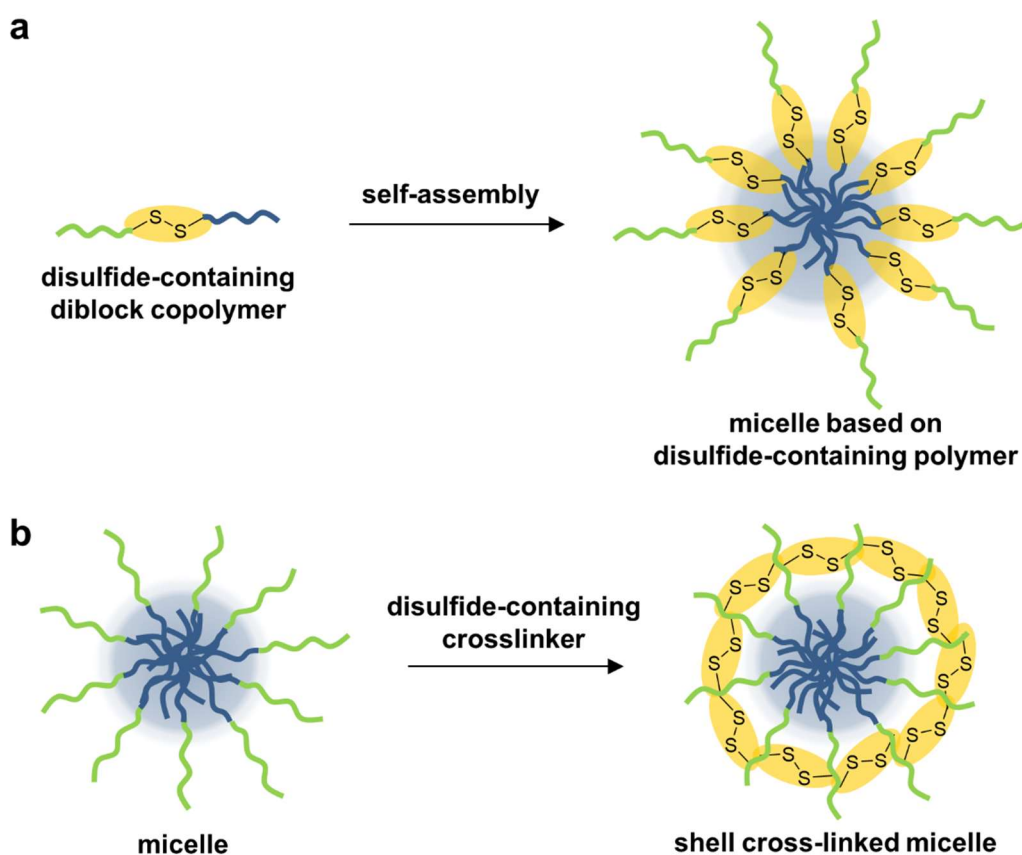
Figure 7: Depiction of different strategies to obtain reductive-labile polymer nanoparticles. a) The reductive-sensitivity can be obtained *via* a disulfide bond within the polymer chain or b) *via* disulfide-containing cross-linkage between different polymer chains after particle formation. Redrawn from Huo *et al.*[72a]

For example, biodegradability could be obtained through diblock copolymers which were linked *via* a disulfide bond. These polymers formed micellar shapes, in which for example DOX was encapsulated. Reductive conditions lead to disulfide cleavage of the diblock copolymer, which did not result in particle disassembly but in DOX release.[73] An example of a particle shell cross-linking was described by Han *et al.*, where a block copolymer was synthesized with thiol groups in the side chains. After particle formation by self-assembly, the thiol-groups were cross-linked, resulting in redox-responsive disulfide bonds. DOX, as a model anticancer drug, was effectively encapsulated into this nanocarrier system and could increasingly release after exposure in a reductive environment.[74]

In contrast, in protein-polymer as well as polymer-drug conjugates, the acid or redox-responsive group is mostly between the polymer and the active molecule linkage.[75] For example, the group of Tanja Weil described the cytochrome *c* modification using boronic acid groups and the subsequent interaction with salicylhydroxamate functionalized PEG. This interaction is reversible, which can detach in acidic conditions.[76] In protein-polymer conjugates, only a few approaches deal with a degradable polymer backbone. Yurkovetskiy *et al.* described the conjugation of trypsin with a polymer, which contains several acid-labile acetal groups in the polymer backbone.[77] Another example was described by the Wurm group, in which bovine serum albumin (BSA) was conjugated with poly(phosphate) that is cleavable in basic conditions.[78] A drawback of this system includes the cleavage in alkaline conditions, which normally exists only in the intestinal tract in the ileum.[79] A similar approach was proven by the Maynard group. Therefore, a thiol-modified lysozyme was conjugated *via* a disulfide bridge with a polymer, bearing several ester bonds within the backbone. Basic conditions lead to ester cleavage. However, in addition, the whole polymer chain can cleaved off in reductive conditions due to the disulfide bond.[80] Nevertheless, in regard to these examples, it becomes more clear, that in protein-polymer conjugates the stimuli-responsiveness, which can be addressed *in vitro* or *in vivo*, is mostly gained through the linker group. Additionally, drawbacks of the described protein-polymer examples are their absence of the recovery of unmodified proteins. In all cases, traces of polymer or linker molecules remaining on the protein surface. If the proteins are used as biotherapeutics, this may be undesirable, which is also confirmed with drug-polymer conjugates. For this reason, the next section will focus on stimuli-responsive linker groups, which lead to therapeutic recovery.

With regard to disulfide as a linker group, the aim of regaining a traceless therapeutic is limited due to drugs have to bear a sulfhydryl group. To circumvent this disadvantage, a new chemical linker was developed in the last years. By using a so-called self-immolative linker, redox-responsive disulfide bridges can be introduced between a thiol-free drug and a polymer. These linkers have the ability to be completely replaced, which results in the

regained, unmodified drug.[81] Figure 8 summarizes examples of disulfide self-immolative linkers and the reactions after disulfide reduction.

For instance, Zelikin *et al.* described a polymer-drug conjugate consisting of ribavirin, an antiviral agent, conjugated to poly(methacrylic acid). The conjugation was performed between the ribavirin hydroxyl-group and the polymer carboxylic acid using a disulfide self-immolative linker. The linker introduction results in a redox-responsiveness of this prodrug with a carbamate group between the linker and ribaverin. Increased GSH concentrations lead to disulfide reduction. Subsequently, the free sulfhydryl group reacts with the carbamate, resulting in a cyclic thiocarbamate and regained free, unmodified ribavirin.[82] In addition, the self-immolative degradability was not only used for drug conjugation, but also for the preparation of stimuli-responsive polymer particles. In this example, free drugs are encapsulated in the particle system and are not bound to the degradable polymer backbone. A trigger results in polymer self-immolative degradation, whereby the drug is released.[83] This concept of self-immolative degradability was also described for traceless reversible protein-polymer conjugation.[84]
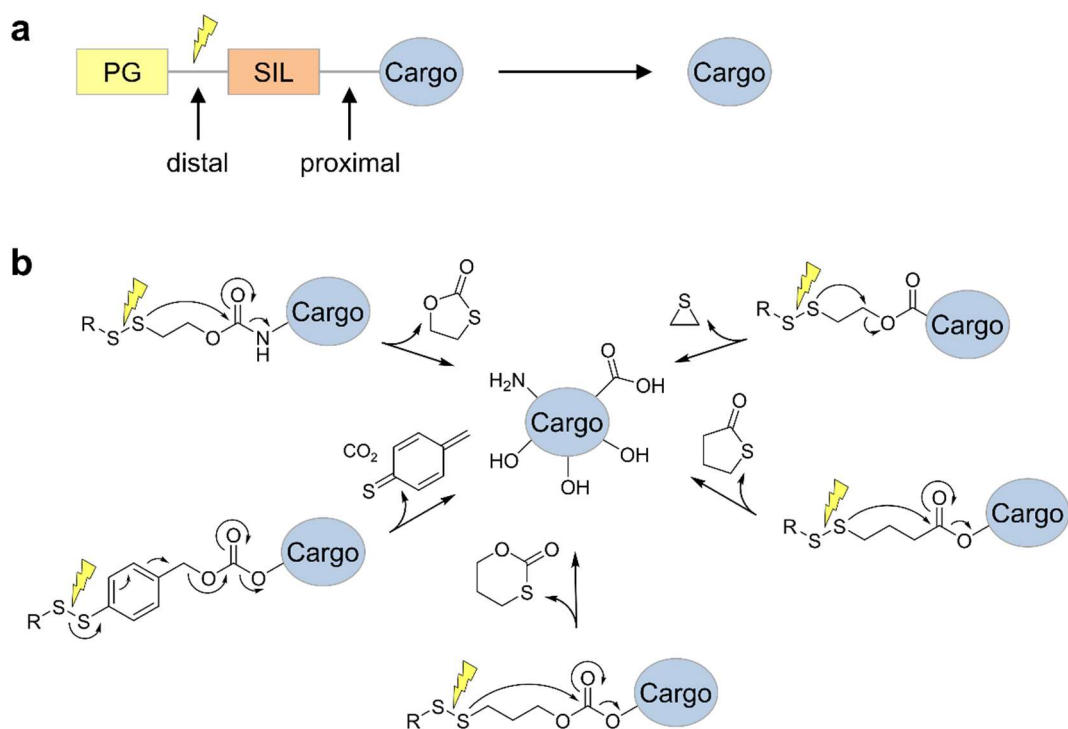
Figure 8: a) Representation of the general principle of the self-immolative linker. A stimulus results in the distal removal of a protecting group (PG), following by a fast removal of the self-immolative linker (SIL), whereby the unmodified cargo at the proximal end is released; b) Examples of disulfide self-immolative linkers and their reaction mechanism triggered by disulfide cleavage, which results in cargo release. The various functional groups like amines, carboxylic acids and hydroxyl groups of the cargos can be regained during this mechanism. Redrawn from Riber *et al.*[81]

Another example was recently reported by Guo *et al.*, which developed a polymer nanogel for traceless protein delivery using a self-immolative linker (Figure 9). The polymer backbone was synthesized with dithioethyl carbonate side chains, which were coupled with amine groups of the protein lipase, resulting in dithioethyl carbamate bonds. The protein-polymer coupling induced the nanogel formation. GSH treatment reduced the disulfides and the free thiol group reacted with the carbamate linkage, which recovered the unmodified protein. Moreover, a regained enzymatic lipase activity of 87% was observed.[85] Nevertheless, the disulfide cleavage was investigated in a GSH concentration of 0.6 M, which does not represent physiological conditions in cells.
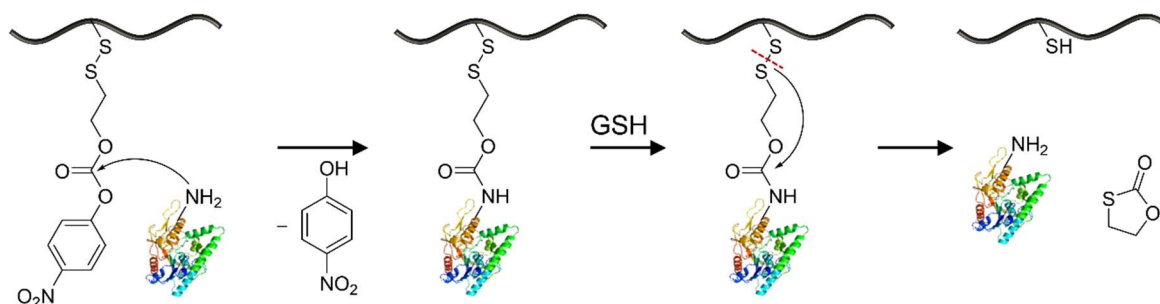
Figure 9: Polymer sidechains bearing dithioethyl carbonate chains, which react with amine functionalities of the lipase. The formed dithioethyl carbamate linkage represents the self-immolative linker. Increased GSH concentrations lead to disulfide reduction. The produced thiol-group reacts with the carbamate, which results in the regained, unmodified lipase. Redrawn from Guo *et al.*[85]

1.2 PROTEIN-BASED NANOCARRIERS

After introducing nanomedicine in general and its concept of biodistribution, cellular uptake and cargo release, this chapter will now focus on protein-based nanoparticle in depth.

Nanocarriers based on proteins gained a special interest in the last years. This type of nanoparticles is currently one of the most investigated drug delivery systems in clinical trials, but until now only a few are FDA approved.[23] In living organisms, proteins are responsible to fulfill various roles. For example, proteins are capable for molecular transport, are part of the immune system and catalyze reactions. As mentioned before in section 1.1.1, as a drug delivery system, natural polymers such as proteins are more beneficial above synthetic ones due to nontoxicity, biodegradability and biocompatibility.[35] Another advantage of proteins for nanocarriers over synthetic polymers is their unique structure with several addressable functional groups in the backbone. Proteins possess carboxylic acids, amines and thiols, which can be useful for protein modification by utilizing the toolbox of bioorganic chemistry. Thus, proteins can be covalently modified, which is a beneficial appliance in nanomedicine for example for

attachment of target structures. In contrast, most synthetic polymers are homogeneous and only bear individual functional groups. Again, it emphasizes the advantages of using proteins as drug delivery systems.[86] Furthermore, due to the amphiphilic nature of proteins, the encapsulation of both, hydrophilic as well as hydrophobic drugs, is possible.[35a]

Protein nanoparticles can be distinguished between natural and artificial protein assemblies. For example, protein-cages like ferritins[87] and heat shock proteins[88] but also virus-like-particles[89] belonging to protein nanostructures occurring in nature. In common, these natural protein nanocarriers self-assemble to form their unique shapes.[90]

In contrast, artificial protein-particles have to be forced to form particles, since they lack the ability to self-assemble. Mainly, there are two synthetic strategies to obtain protein structures. Both of them are based on changed solubility behavior. On the one hand, these altered properties can be achieved through protein denaturation or through protein modification using polymers.[91] In the following section, these two strategies to prepare artificial protein nanoparticles will be explained more in-depth.

1.2.1 NANOPARTICLE PREPARATION BY DENATURATION OF PROTEINS

Various proteins can be used as a backbone for the preparation of the forced assembly in nanoparticles, induced by denaturation. For example, globular proteins like albumin are a frequently used material as nanoparticle backbone.[92] In globular proteins most non-polar amino acids are directed into the interior of the spherical structure and polar groups to the outside. Protein denaturation causes a structural change, resulting in more non-polar amino acids on the outside of the protein structure.[93] As a result of hydrophobic interactions between denaturized proteins, nanoparticles can be formed.[92] There are several nanoparticle preparation techniques, which make use of protein denaturation like thermal desolvation[94], gelation[95] and emulsification[96].

The globular protein albumin is an often-used material for the preparation of protein-nanoparticles, especially in the application of the desolvation technique, which is represented in detail in Figure 10. Marty *et al.* first described the desolvation technique[97] and Langer *et al.* optimized it by using human serum albumin (HSA) as particle backbone resulting in HSA-particles with sizes between 50–280 nm.[94, 98] Herein, the protein is dissolved in an aqueous solution and a desolvating agent like acetone or ethanol is added dropwise. As a result, the tertiary structure of the protein changes, which leads to aggregation of denaturized proteins. Considering the general particle instability of these prepared protein-nanocarriers, they had to be stabilized by cross-linking using for example glutaraldehyde. This developed particle system can be used for drug encapsulation by

combining the drug and the protein in the aqueous solution.[99] Moreover, this method was proven to be suitable for the encapsulation of poorly soluble drugs.[100]
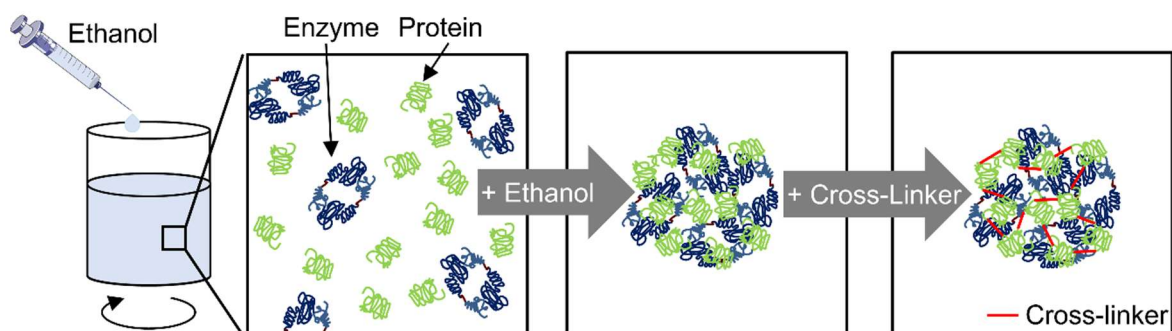
Figure 10: Schematic illustration of protein particle preparation using the desolvation technique. The protein is dissolved in water and the slow addition of a desolvating agent like ethanol results in protein aggregation. For particle stabilization the proteins are subsequently cross-linked. Redrawn from Estrada *et al.*[101]

In contrast, thermal gelation describes the aggregation of proteins, initiated by heat, which results in protein denaturation. As described in the previous section, intermolecular hydrophobic interactions of the denaturized proteins form particular structures.[102] For example, using the globular protein lactoferrin, nanoparticles with a size of around 110 nm were prepared after a heat treatment at 75 °C.[103] In the emulsification method, two possibilities for albumin particle stabilization are commonly used, the thermal or the chemical stabilization. In both approaches, albumin is dissolved in aqueous solution and homogenized with an oil phase, e.g. cotton seed oil, which results in a water-in-oil emulsion. The protein in the water droplets can either be stabilized by cross-linking using e.g. formaldehyde, or by thermal denaturation. In the latter case, the emulsion is added to a preheated oil-phase with a temperature around 140–180 °C, thus resulting in stabilized albumin particles by heat denaturation. Using the emulsification method, larger particles with sizes between 300–1000 nm are formed.[99c, 104]

Most of the above-described preparation methods include cross-linking for nanoparticle stabilization, for which intent the functional groups of the respective proteins can be used. For example, 2,4-toluene diisocyanate (TDI) is a cross-linking agent, which reacts unselectively with hydroxyl and amine groups on protein surfaces.[105] Moreover, amines can be cross-linked using glutaraldehyde or formaldehyde, which are the most frequently used cross-linking groups.[91, 106] However, cross-linking includes some disadvantages like the toxicity of the cross-linking agents and possible chemical reactions with nanoparticle payloads.[106] Additionally, cross-linking leads to surface amine loss. For this reason, the possibility of further targeting reactions or PEGylation of nanoparticles is limited. One possibility to avoid surface amine loss is to protect them during cross-linking using dimethylmaleic anhydride (DMMA). As a result, the amines can be recovered after the

reaction.[107] Furthermore, to circumvent the described disadvantages, particle stabilization can be carried out using disulfide chemistry. Therefore, intramolecular disulfide bonds of albumin could be reduced, and after protein aggregation, intermolecular disulfide bonds can be formed for particle stabilization.[108]

1.2.2 ASSEMBLY OF PROTEIN-POLYMER CONJUGATES

After describing the artificial particle preparation by protein denaturation, this section will focus on particles based on protein-polymer conjugates. Although protein-polymer conjugates have already been discussed in section 1.1.1 and 1.1.5, however, in this chapter, these conjugates will be used to describe their use for the formation of particles. First, general methods of protein-polymer conjugation will be explained and following a description of the particle preparation.

Mainly, three different approaches for protein-polymer conjugate preparation are described, which are summarized in Figure 11: the *grafting to, grafting from* and *grafting through* method.

The *grafting to* method is the most commonly used approach. Here, the protein and functionalized polymer are covalently linked after polymer synthesis. Naturally occurring reactive groups on the protein surface like amines, carboxylic acids and thiols are used for the polymer attachment. A further advantage of this method is, that the polymer synthesis can be performed in a non-aqueous solution, meanwhile, the protein is not exposed to these conditions, which are relatively harsh overall.[109] Disadvantages of this method include the rather low graft density, especially during the attachment of longer polymer chains, but also the difficult purification by separation of non-attached polymers.[110] Both other methods describe controlled polymerization using mostly atom transfer radical polymerization (ATRP) or reversible-addition fragmentation transfer (RAFT) in the presence of a functionalized protein. In the *grafting from* method the protein is functionalized with a polymerization initiator, which enables the direct polymer growth from the protein core. An advantage over the *grafting to* method is the more efficient reaction due to reduced steric hindrance and in addition the easier purification.[111] The *grafting to* and *grafting from* method summarizes approaches, where only one protein molecule is involved. In contrast, using the *grafting through* method, several proteins can be attached to the polymer backbone. Here, polymerization is carried out with a monomer bearing protein reactive functional groups. Accordingly, after polymerization, several proteins can be attached to the polymer backbone.[112]
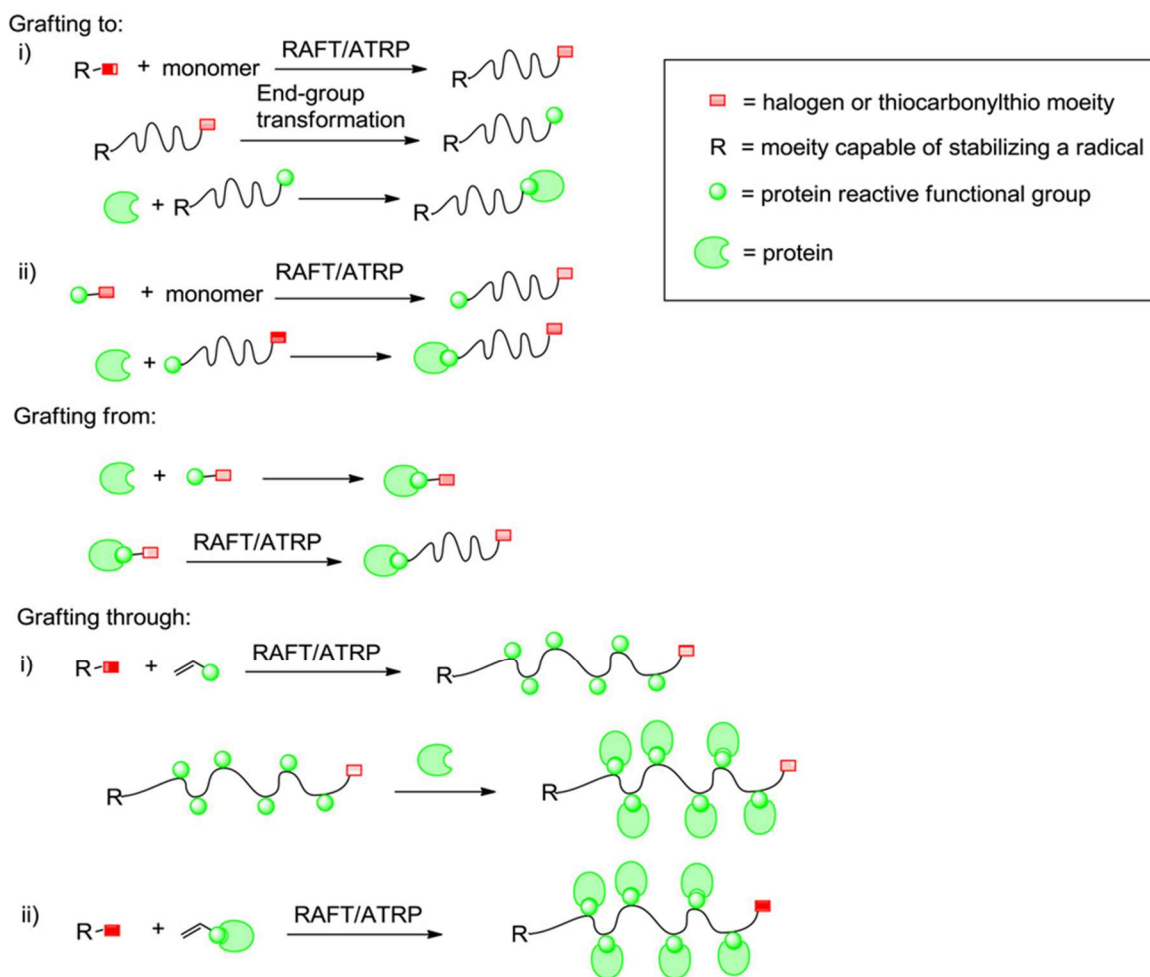
Figure 11: Representation of different methods for the preparation of protein-polymer conjugates. In general, the conjugate formation can be divided into three major procedures: *grafting to, grafting from* and *grafting through*. Reprinted from Grover *et al.*[112a], Copyright (2010), with permission from Elsevier.

The attachment of hydrophobic polymers to hydrophilic proteins or vice versa, hydrophilic polymers to hydrophobic proteins, is advantageous, due to a gained amphiphilicity of the conjugate. With this changed behavior, these conjugates have the ability to self-assemble, which can be exploited to form nanoparticular shapes.[113] Different possibilities for this type of particle preparation will be discussed in the following.

For example, a denaturized protein backbone can be used for the polymer conjugation. Denaturation leads to the accessibility of all functional protein groups, which are normally directed inwards of the globular proteins. Subsequent attachment of several hydrophilic polymer chains results in an amphiphilic material, which has the ability to self-assemble. Different working groups described the denaturation of the BSA polypeptide backbone and the subsequent PEGylated. After self-assembly, the obtained particles were successfully used as a drug delivery system for example for the encapsulation of anticancer drugs.[114]

In contrast, also the intact structure of proteins can be used for the preparation of protein-polymer conjugates. In the following examples, the polymer attachment on proteins will be differentiated between the site-selective and the high ratio surface modification. The site-selective protein-polymer conjugation describes the targeted attachment of one or only a small amount of polymer chains onto the protein surface. Since polymer attachment can result in a decreased protein activity, a low number of polymers on the protein surface is advantageous.[115] The difficulty of site-selective polymer attachment on proteins includes, that functional groups like the amines of lysine residues are multiply abundant and therefore hard to address site-selectively. In contrast, cysteine is a rarely available amino acid and therefore the sulfhydryl-group is a suitable target for site-selective modification.[116]

Olsen *et al.* described a site-selective polymer attachment on the green-fluorescent protein (GFP). The used GFP bears a sulfoethyl thioester group, which was conjugated with the cysteine activated diblock copolymer poly(dimethylacrylamide)-*b*-poly(*N*-isopropyl-acrylamide) (PDMA-*b*-PNAPAM). Polymers have an aggregation ability above their so-called lower critical solution temperature (LCST), due to resulting predominate hydrophobic interactions between polymer chains. As a result of transferring these polymer properties onto the newly formed conjugate, the protein-polymer construct can self-assemble into micelles above the polymers LCST.[113, 117] The formed thermo-responsive particles show a size of 15.3 nm at 50 °C, compared to the monomer form of 5.5 nm at room temperature.[118] Additionally, the Olsen group examined the protein dependence of the self-assembling ability in the protein-polymer conjugates. It was shown, relying on the proteins' properties like charge and size, that different shapes are formed during the self-assembly.[119]

Another example of self-assembled protein-polymer conjugates was described by the Stenzel group. A most frequently used site-selective polymer attachment on BSA includes the cysteine-34 modification. This cysteine group can be used as attachment point without the impairment of the protein activity.[120] In the Stenzel group, this type of site-selective BSA modification was used for the attachment of maleimide functionalized poly(methyl methacrylate) (PMMA). Therefore, PMMA was dissolved in DMSO and the slowly addition of an albumin containing aqueous phase followed. The conjugation to the amphiphilic protein-polymer compound and nanoparticle formation by self-assembly take place simultaneously. After DMSO removal particles between 50–220 nm were obtained. During particle formation the encapsulation of the anti-cancer agent curcumin was possible.[121] In Figure 12 the general concept of particle formation based on site-selectively modified proteins is illustrated.
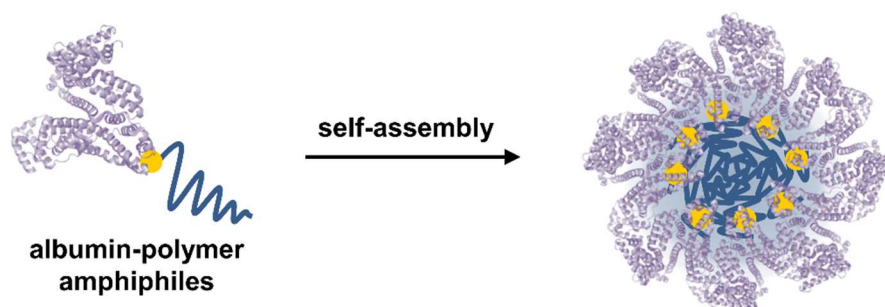
Figure 12: The conjugation of a polymer and protein results in an amphiphilic compound, which has a self-assembly behavior. Redrawn from Jiang *et al.*[120b]

After describing nanoparticles based on the site-specific linked protein-polymer conjugates, the following section will focus on high surface modified proteins. An example was described by Segura *et al.* (Figure 13).[122] After introducing 15 bromo-terminated groups on the BSA surface using 2-bromoisobutyryl bromide, this protein was suitable as a macroinitiator. Subsequently, using the *grafting from* method, the polymer synthesis by ATRP was carried out directly at the protein core, resulting in BSA-poly(dimethylamino) ethyl methacrylate (PDMA) nanoparticles (nBSA). After mixing this protein-polymer conjugate with pDNA, polyplexes were formed with a size of around 50 nm.
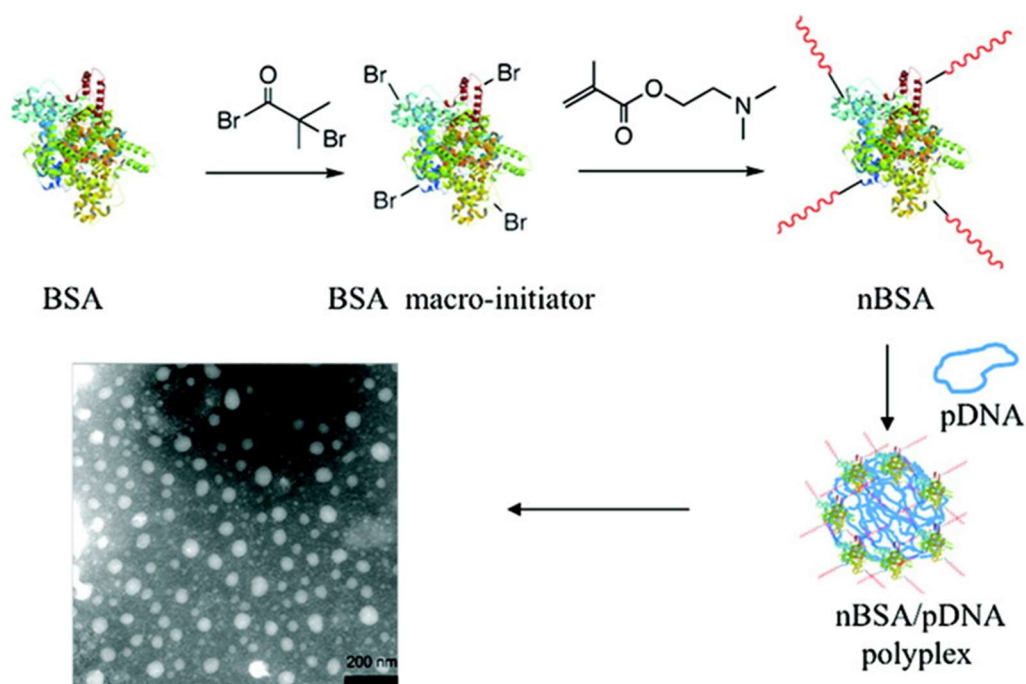
Figure 13: BSA-PDMA conjugate synthesis *via grafting-from* ATRP polymer synthesis resulting in nanoparticular BSA (nBSA). Mixing of this conjugate with pDNA leads to the formation of polyplexes with sizes around 50 nm. Reprinted from Zhang *et al.*[122], Copyright (2011), with permission from American Chemical Society.

In addition to protein-polymer conjugates which build particles by self-assembly, further particle preparation methods can be applied. For example, protein-polymer conjugates

show a surface activity at polar-apolar interfaces, for this reason, these conjugates have the ability to stabilize emulsions.[123] Based on that, the Mann group described a proteinosome preparation by an emulsion technique (Figure 14). Therefore, BSA was modified using mercapto-thiazoline-activated PNIPAAm, resulting in three attached polymer chains. After proteinosome preparation, the particles were cross-linked by PEG-bis(N-succinimidyl succinate), resulting in sizes between 20–50 μm. Enzymes were successfully encapsulated into this drug delivery system, without losing their enzymatic activity.[124]
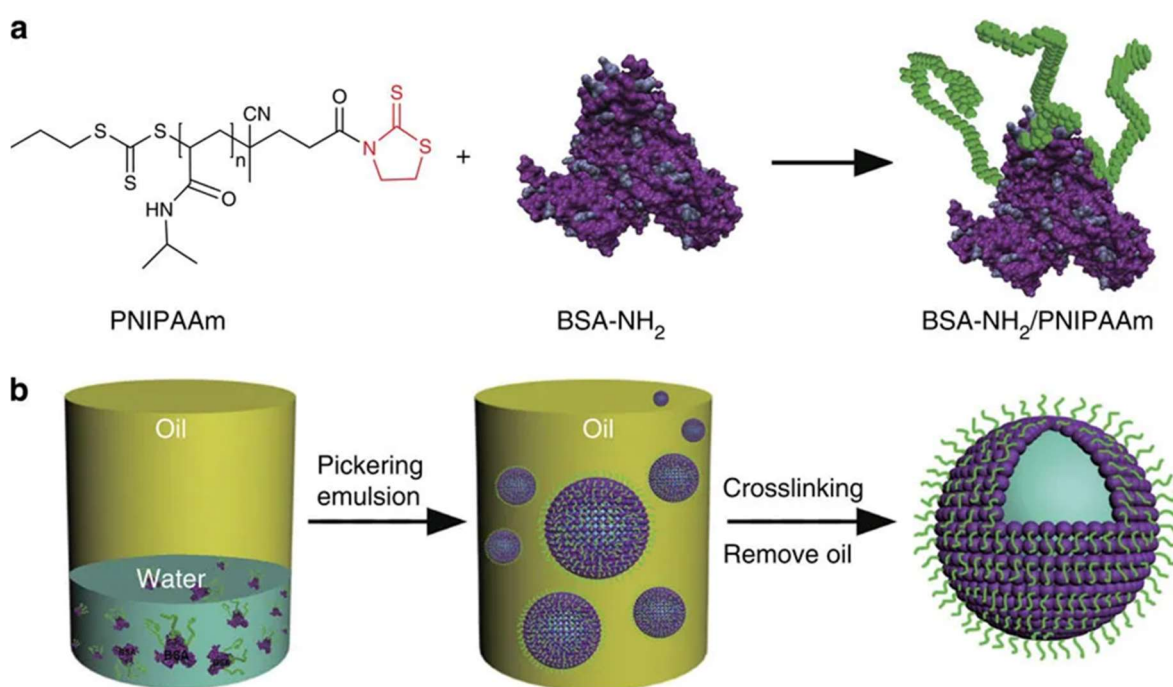
Figure 14: a) Conjugation of BSA with mercapto-thiazoline-activated PNIPAAm; b) This protein-polymer conjugate was used for particle formation with an emulsion technique. Subsequently, these particles are stabilized by cross-linking with a bifunctional PEG. Reprinted from Huang *et al.*[124], Copyright (2013), with permission from Springer Nature.

Furthermore, Xue *et al.* described a system based on urease-mPEG conjugates, which was used as a stabilizer of a water-in-water emulsion, forming droplet sizes of 200–500 nm (Figure 15). Using this approach, the main challenge of water-in-water emulsion, the instability, was improved. Additionally, within this method, the bioactivity preservation of the protein-particle material was described.[125]
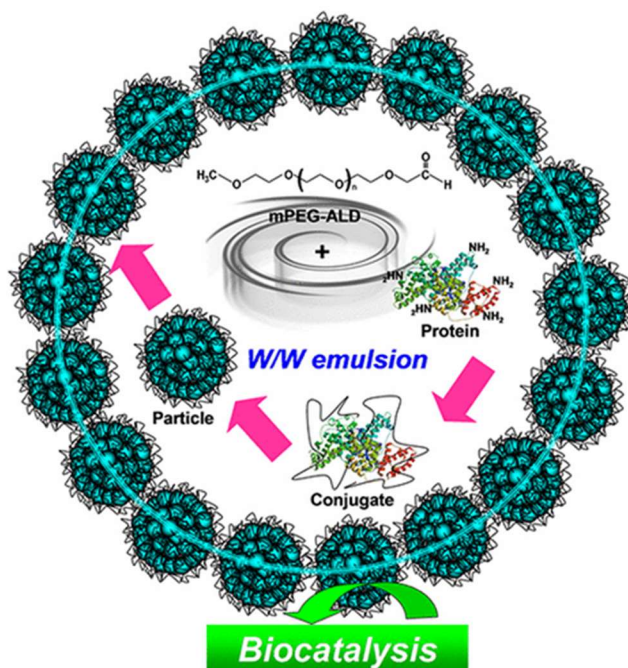
Figure 15: Protein-polymer conjugation for the stabilization of a water-in-water emulsion. During this process, the protein maintains its catalytic activity. Reprinted with permission from Xue *et al.*[125], Copyright (2017) American Chemical Society.

Our group developed a similar approach for the preparation of protein-based nanoparticles but based on an oil-in-water emulsion technique.[126] The key step in this method includes the high surface PEGylation of proteins to obtain stable protein particles. The PEG attachment changes the solubility behavior of the protein, in an amphiphilic character that allows dissolving the protein in an organic solvent such as dichloromethane (DCM) without significant loss in structure by denaturation. This DCM solution, also called oil phase, can be covered with an aqueous phase and sonication results in an oil-in-water emulsion. The oil droplets containing the PEGylated proteins and subsequent removal of the volatile organic phase leads to stable protein-particles with sizes around 100 nm. During the particle formation, the protein structure and activity are not impaired and the stabilization by cross-linking of the prepared particles is not required. Figure 16 summarizes the general concept of this so-called single emulsion method for the preparation of protein-based nanoparticles. This technique was proven by the PEGylation of lysozyme as a model protein. The approach was successfully transferred to other proteins like *β*-lactoglobulin, ovalbumin, HSA, cytochrome *c*, horseradish peroxidase, glucose oxidase and catalase.[126a, 127] Accordingly the single emulsion offers a universal method for the preparation of protein-based nanoparticles. Into this type of protein-nanoparticle, the anticancer drug doxorubicin was encapsulated and *in vitro* studies proved the intracellular drug release. Nevertheless, the nanoparticle preparation based on this method is only suitable for the encapsulation of hydrophobic drugs.[126a] To overcome this

limitation, the application of a double-emulsion technique would be purposeful, which is a frequently used method for the encapsulation of several hydrophilic drugs or biotherapeutics in polymer particles.[128] In our working group, first investigations of the preparation of protein-based nanoparticles using the double emulsion method were carried out in a master and PhD thesis.[129]
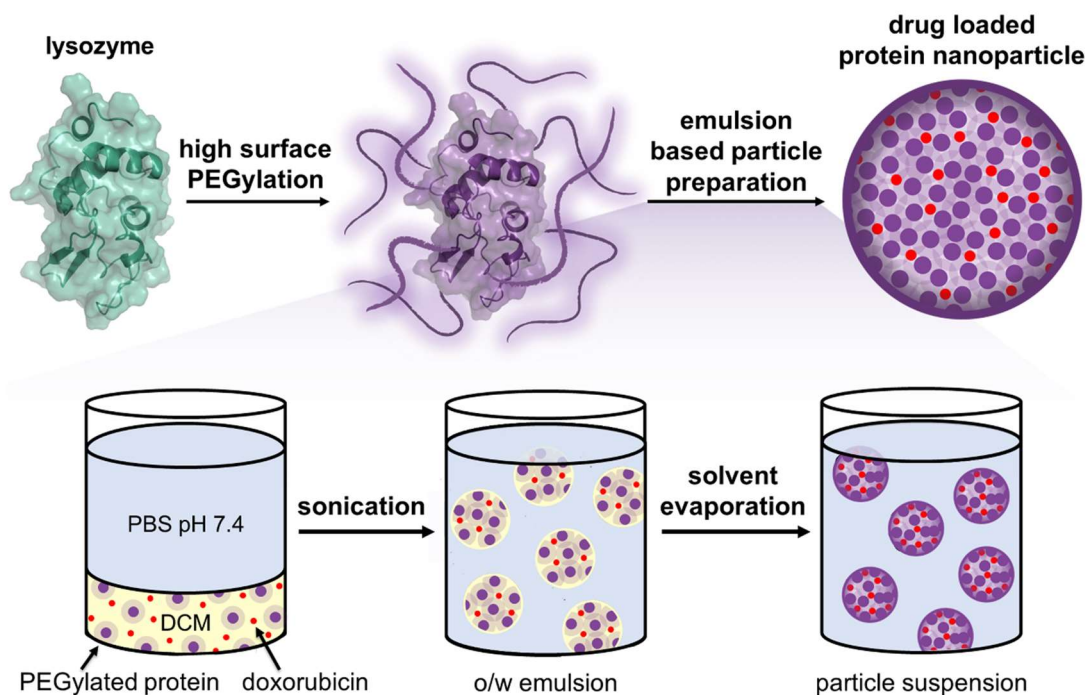
Figure 16: High surface PEGylation of lysozyme leads to an altered solubility, which enables a particle preparation by an emulsion-based method. The protein-polymer conjugate was dissolved in DCM, covered with PBS (pH 7.4) and after sonication, an oil-in-water-emulsion with the PEGylated protein in the DCM droplets is obtained. DCM removal results in a stable particle suspension. Reprinted with permission from Fach *et al.*[126a], Copyright (2016) American Chemical Society.

In summary, in this section, the preparation of nanoparticles based on proteins, which normally do not have the self-assemble ability, was discussed in-depth. This ability is gained through polymer attachment on protein surfaces. In addition, nanoparticle systems were described where the preparation technique has no impact on protein structure and activity, which opens up new possibilities of nanocarriers, which may serve as active biotherapeutics. However, this developed nanoparticle systems lack in a stimuli-responsiveness, whereby no triggered drug release is possible. For this reason, the next section will deal with protein-based nanoparticle systems, which have the ability of a triggered drug release after exposer with different stimuli.

1.2.3 STIMULI-RESPONSIVE PROTEIN-BASED NANOPARTICLES

As described in section 1.1.4, nanocarriers with a stimuli-responsiveness can release their payload in a triggered and more controlled manner. This section will focus on protein-based nanoparticles, which react in different ways to certain endogenous stimuli. For example, De Geest *et al.* described a high surface modification of BSA, starting with a macroinitiator attachment on the protein surface (Figure 17). A *grafting from* RAFT polymer synthesis using [(2,2-dimethyl-1,3-dioxolane)methyl]acrylamide (DMDOMA) directly from the protein core results in a protein-polymer conjugate which self-assembled into nanoparticles with sizes around 50–190 nm.
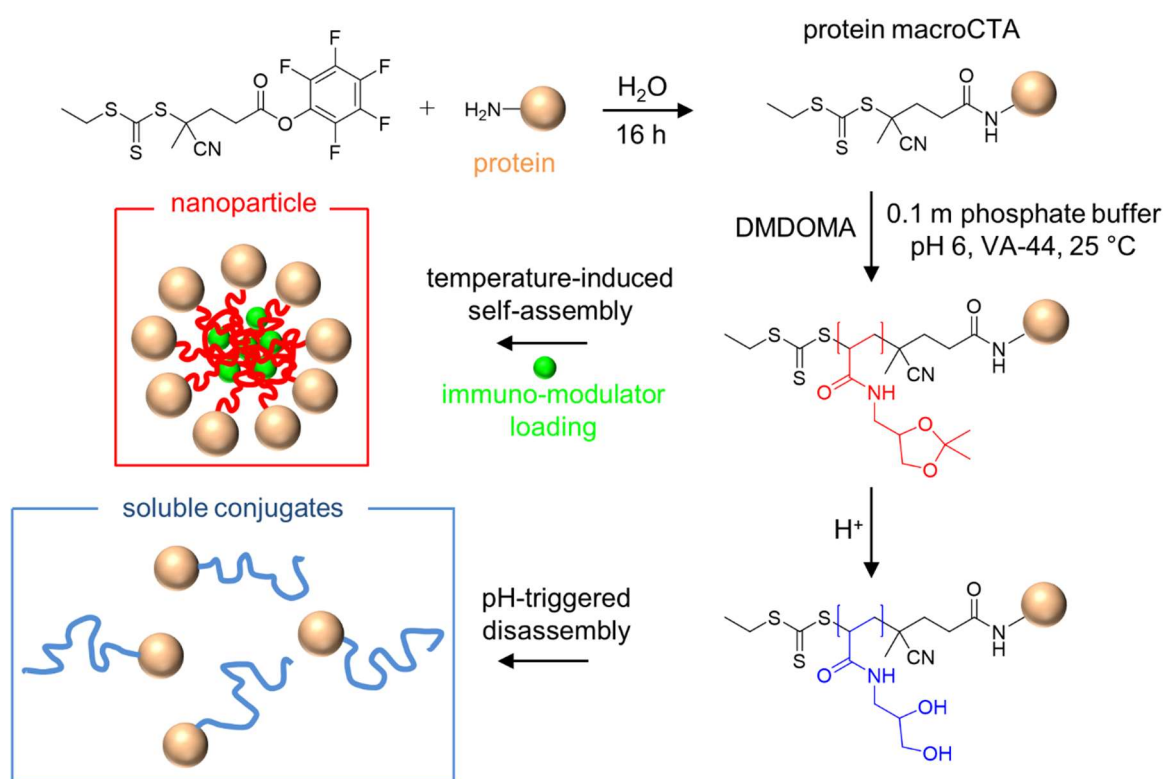
Figure 17: Acid-responsive protein-polymer conjugate synthesis *via grafting-from* RAFT polymer synthesis. This conjugate forms nanoparticles through its a self-assemble ability. Hydrophobic dioxolane units within the polymer chain result in acid-sensitivity. Reduced pH values lead to dioxolane cleavage, resulting in hydrophilic diols, which induces particle disassembly. Redrawn from Vanparijs *et al.*[130]

A stimuli-responsiveness is obtained through the hydrophobic dioxolane moieties in the polymer backbone. Acidic conditions lead to ketal cleavage, resulting in hydrophilic diol groups. The undergoing solubility switch results in the loss of the ability to self-assemble, causing the particles to dissolute.[130] However, a drawback of this system is that the polymer backbone is irreversibly attached to the protein. Furthermore, extremely acidic

conditions (pH 1) are required for particle disassembly, which does not occur in tumor tissues or in the endo-lysosomal pathway.

The Stenzel group described a different way of protein-nanoparticle degradation. Therefore, BSA was site-specifically modified with maleimide functionalized poly-(ε-caprolactone) (PCL). Subsequently, protein-based particles with sizes around 150 nm were formed by self-assembly, where the hydrophobic PCL built the core and hydrophilic BSA the shell. Incubation of the particles in trypsin and pancreatin solutions led to BSA hydrolysis and ester bond cleavage of the polymer backbone, finally resulting in an overall particle degradation. Nevertheless, the examined conditions do not reflect the *in vitro* or *in vivo* environment. The aim of the study was only to qualitatively analyze, whether an enzymatic degradation of the prepared particle system would be possible.[120a]

Another example of stimuli-responsive protein-based nanoparticles was described by Wang *et al.* (Figure 18). On the surface of BSA, several hydrazine groups were introduced, which were linked with the aldehyde functionalized copolymer poly(di(ethyleneglycol)ethyl ether acrylate-*co*-poly(ethylene glycol) methyl ether acrylate) (P(DEGA-*co*-PEGA)) to obtain a high surface modified protein. The obtained hydrazone bond between the protein and copolymer is acid-sensitive. The conjugate self-assembled temperature induced, due to the introduced temperature-responsiveness of the copolymer. For particle stabilization, carboxylic acids of the BSA molecules were cross-linked using cystamine by a carbodiimide-mediated coupling reaction. The resulting disulfide bond in the particle corona led to a redox-responsiveness of the 70 nm particle system. However, acidic conditions alone did not result in a degradation of the double stimuli-responsive particles. A full nanoparticle disassembly required both, an acidic and a reductive environment.[131] In addition, a drawback of this nanoparticle system is the remaining linker fragments on the protein surface after stimuli treatment.
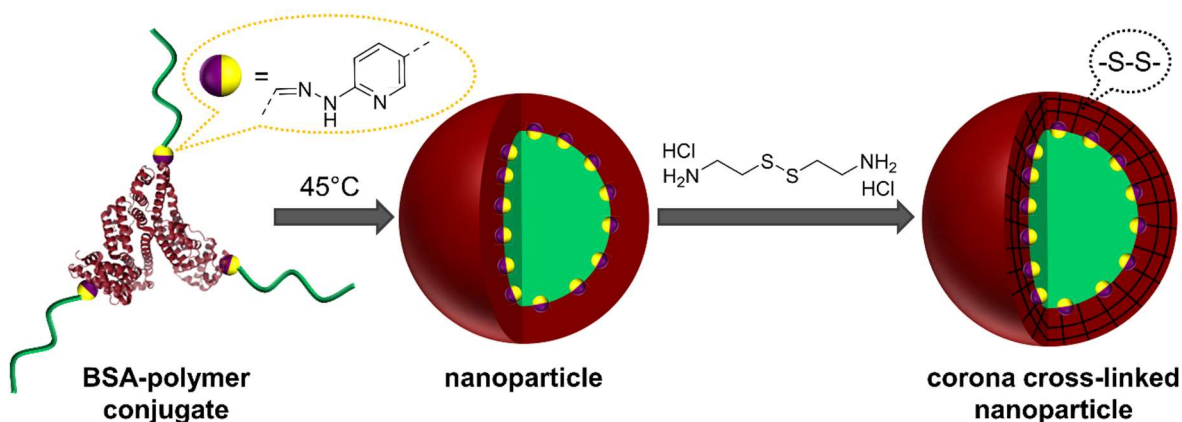
Figure 18: Preparation of multi-stimuli-responsive protein-based nanoparticles. After polymer attachment on the BSA surface resulting in an acid-sensitive hydrazone linkage, particles were formed by heat-induced self-assembly. In addition, the nanoparticles were stabilized by BSA cross-linking, which introduced redox sensitive disulfide bonds. Redrawn from Wang *et al.*[131]

To avoid this disadvantage, the DeSimone group developed a cross-linked protein nanoparticle system using a self-immolative linker, whose type of stimuli-responsiveness was earlier discussed in Section 1.1.5. The particles were produced using a particle replication in non-wetting templates (PRINT) technique, where BSA was mixed with lactose and glycerol as plasticizers. In a so-called melt-solidification strategy, the mixture was heated to 60 °C and subsequently formed in particular shapes. Considering the degradability of the produced particles in water, they were stabilized by cross-linking using dithio-bis(ethyl 1*H*-imidazole-1-carboxylate) (DIC) for amine linkage of different BSA molecules (Figure 19), where particle sizes around 3 μm were obtained. Disulfide reduction within the cross-linkages result in particle degradation and traceless linker removal to regain unmodified BSA. Consequently, this type of protein-based nanoparticles is a suitable method for triggered drug delivery.[132] Nevertheless, a disadvantage of this method includes the potential protein denaturation as a result of heating during the PRINT preparation technique.
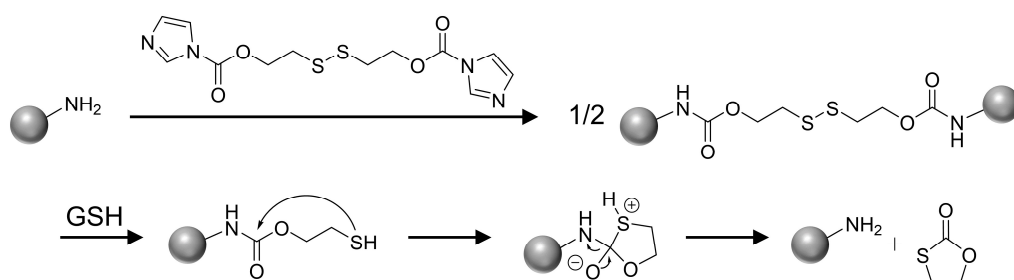
Figure 19: BSA cross-linking between amine functionalities using dithio-bis(ethyl 1*H*-imidazole-1-carboxylate) (DIC). Reductive conditions lead to disulfide cleavage and traceless linker removal on the BSA surface. Redrawn from Xu *et al.*[132]

In summary, the described examples of stimuli-responsive protein-based nanoparticles show several unresolved disadvantages. Partially harsh conditions are required for particle degradation, which will not occur in *in vitro* or *in vivo* studies. Additionally, in the case that the particle material itself should be used as biotherapeutic and consequently should have a pharmacological effect in tissues or cells, the recovery of unmodified and not denaturized protein is desirable. However, in the described examples, on the one hand, the proteins still bear linker molecules or the whole polymer backbone after treatment with certain stimuli and on the other hand, harsh preparation conditions lead to protein denaturation. For this reason, in this research area, there are still problems to overcome for the development of a protein-based nanoparticle system with triggered drug release.

1.2.4 ENZYMES AS MATERIAL FOR NANOCARRIERS

As described at the beginning of section 1.2, proteins offer several advantages as a nanocarrier backbone. Previously, this work outlined different proteins, which were used for the preparation of protein-based nanosystems. This section will now focus on the proteins used in this thesis, which all represent enzymes. In general, enzymes catalyze reactions from a substrate to a product and can be mainly divided into six different classes, oxidoreductases, transferases, hydrolases, lyases, isomerases and ligases.[133] In this work, two different enzyme classes were used, which will be explained in the following.

First of all, cytochrome *c* (Cyt) will be discussed in-depth, which belongs to the enzyme class of oxidoreductases, by catalyzing the electron transfer between two molecules. With a molecular weight of 12.4 kDa, this enzyme has a single polypeptide chain consisting of 104 amino acids.[134] The catalytic center of this enzyme is a prosthetic group, which is generally defined as a non-polypeptide unit, covalently attached to a protein and being involved in the enzymatic reactivity.[133] Here, the prosthetic functionality is a heme group, which bears an iron ion between a porphyrin ring, which is covalently attached to Cyt by two cysteine residues. Cyt has versatile roles in eukaryotes. For example, within the mitochondria intermembrane it is part of the respiratory chain and responsible for the electron transport process between complex III and complex IV. It displays the importance of this enzyme, as it is involved in the formation process of adenosine triphosphate (ATP), the major energy carrier in living organisms.[134] Another important role of this enzyme is in the intrinsic apoptotic pathway. After an apoptotic stimulus, Cyt is released from mitochondria into the cytosol. There, it binds the apoptotic protease-activating factor-1 (APAF1) which is part of the apoptosome, resulting in triggered programmed cell death.[135] Additionally, Cyt can be classified in the subgroup of peroxidases, due to the ability for the oxidation of various substrates in the presence of H_2O_2.[136] Mainly, the reaction results in H_2O_2 elimination, whereby this enzyme can regulate oxidative stress and inhibits the formation of reactive oxygen species (ROS).[137] This reaction is also catalyzed by the heme group as a prosthetic group.[134, 138] Although, in literature, Cyt is not described as nanoparticle backbone, this enzyme is used as an encapsulated drug in nanosystems, which will be described more in detail in section 1.3.

The second enzyme used in this work is lysozyme (LYZ), which belongs to the class of hydrolases. This enzyme is built up of a single polypeptide chain consisting of 129 amino acids with a molecular weight of 14.3 kDa. It occurs in almost all human secretion body fluids and tissues. LYZ is a part of the human innate immune system due to its antibacterial activity. By its glycoside hydrolase activity, this enzyme has the ability to cleave *β*-1,4-glycosidic bonds between *N*-acetylmuramic acid and *N*-acetylglucosamine residues. Considering that this polymer is a major part of the peptidoglycan layer in bacteria cell

walls, hydrolysis catalyzed by LYZ results in cell wall degradation and consequently in lysis of the bacteria.[139] LYZ is a frequently used model enzyme in various studies[126, 140] and in addition, due to its natural antibacterial activity, it is commonly applied for food preservation[141].

Figure 20 illustrates the two described enzymes Cyt and LYZ, thus a comparison of the three-dimensional structure and size is possible.
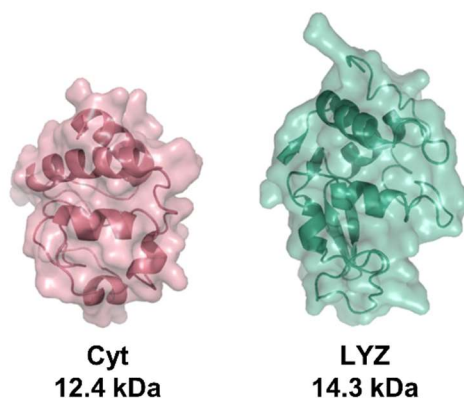
Figure 20: Detailed illustration of the three-dimensional structure of cytochrome *c* from equine heart (Cyt, red, PDB: 1hrc) and lysozyme from hen egg (LYZ, green, PDB: 2lyz).

1.3 ENZYME DELIVERY WITH NANOCARRIERS

Since proteins play important roles in the human body, they can be exploited as natural drugs. A variety of diseases like cancer, infections or genetic disorders are addressable by therapeutic proteins. Based on the role or the activity of the involved proteins, they can be divided into different groups. For example, proteins with an enzymatic activity can be used as biotherapeutic to expand an existing function in cells. Moreover, applying proteins with targeting functions like monoclonal antibodies provides the ability to address specific molecules inside the living organism.[142] In 2018 alone, 11 new antibody preparations have been approved by the FDA.[143] Also, several enzymes have been granted admission.[144] For example, asparaginase *Erwinia chrysanthemi* (Erwinaze®) was proven as a chemotherapeutic agent, for the treatment of acute lymphoblastic leukemia.[145] Nevertheless, the direct application of enzymes includes difficulties like poor stability as a result of enzymatic degradation. The enzyme encapsulation in nanoparticle systems can overcome these problems.[146] For example, due to the natural apoptotic activity of Cyt, different types of nanoparticles were used to encapsulate and thus protect this enzyme from preliminary degradation. The targeted delivery to cancer cells and Cyt release can induce programmed cell death. This type of nanocarriers has the potential to be a new generation of antitumor drugs.[147]

So far, nanocarriers have been mainly described as drug delivery systems for the treatment of cancer. However, due to the issue concerning antibiotic resistance, the development of nanoparticles for antibiotics delivery is expanding, which should lead to increased drug effectiveness.[148] Considering that LYZ is a natural antibacterial enzyme, it is an interesting biotherapeutic, which can be encapsulated in nanoparticles for the treatment of antibacterial infections. For example, the group of Jan van Hest covalently linked LYZ to viral capsid proteins, which can form particles by self-assembly (Figure 21). The resulting virus-like particles encapsulate LYZ in the core. LYZ retains its enzymatic activity during this process against small artificial substrates, which can diffuse inside of the particle. However, a release of the hydrolytic active enzyme is not possible, consequently, no antibacterial activity can be observed.[149]
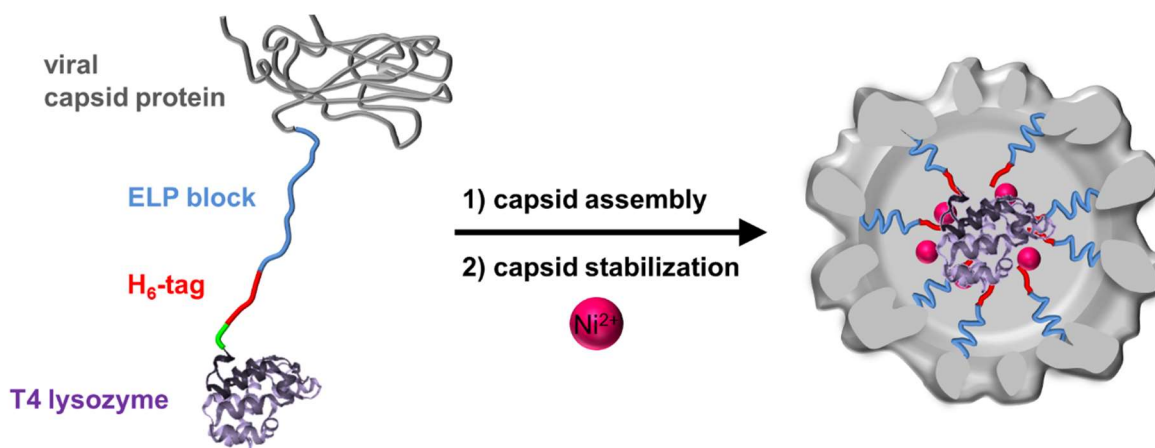
Figure 21: Schematic representation of covalently linked LYZ to viral capsid proteins. These conjugates have a self-assembly ability resulting in particles with LYZ in the core. The enzymatic activity of encapsulated LYZ was examined with small *M. Luteus* cell wall fragments, which can diffuse inside the particle core. Redrawn from Schoonen *et al.*[149]

In a similar manner, Abouhmad *et al.* developed cellulose nanocrystals. In contrast to the previously mentioned study, LYZ was covalently attached to the nanocrystal surface. Therefore, amines on the enzyme surface were linked with glutaraldehyde functionalities on the nanocrystal surface. The particles have an overall positive charge, which enhances the interaction of the particles with negatively charged bacteria. However, a drawback of this system is that LYZ is not shielded while being attached to the particle surface.[150] Another example of LYZ delivery using nanocarriers was described by the Yu group. They developed silica nanoparticles with encapsulated LYZ. The particles have the ability to attach on the bacteria surface and LYZ was sustainably released by diffusion. Nevertheless, silica nanoparticles are toxic, which is not taken into account in this work.[151]

In conclusion, the development of nanomedicine for the delivery of protein therapeutics is an interesting approach in the treatment of different diseases and is gaining more and more attention.[152]

2 MOTIVATION AND OBJECTIVES

The nanotechnology represents a remarkable research area, which is particularly in medicine a promising tool. The so-called nanomedicine provides as drug delivery vehicles outstanding advantages. As a result of drug encapsulation in nanocarriers, the drugs are protected from degradation *in vivo* and are transported in a more targeted manner to addressed tissues and cells, which results in reduced side-effects and toxicity. Especially, nanoparticles based on proteins represent promising properties due to their general biocompatibility, high biodegradability, low toxicity and their ease of modification, by using the toolkit of bioorganic chemistry.

Fach *et al.* recently reported in our working group the preparation of protein-based nanoparticles. High surface PEGylation of lysozyme (LYZ) renders the solubility in organic solvents, which opens up the possibility of the protein-based nanoparticle preparation by a single emulsion technique. The prepared nanoparticles are stable without cross-linking and the proteins exhibit a preserved structure and activity. Nevertheless, only the encapsulation of hydrophobic drugs is possible by using the single emulsion technique. For hydrophilic payloads, this method was adopted to a double emulsion technique and in first investigations in our group, PEGylated albumin was used for the encapsulation of a fluorescent model compound.

In this work, the idea was to evolve the double emulsion procedure by using PEGylated LYZ as particle material (Figure 22). Considering the issue of antibiotic resistance, as a hydrophilic drug an antibiotic agent could be encapsulated into this nanoparticle system. In view of the natural antibacterial activity of LYZ, this would be of interest, since potentially a combined effect of the particle material itself and the encapsulated hydrophilic drug could be gained. Additionally, the release behavior could provide a profound understanding of the particle characteristics. In further *in vitro* investigations, the antibacterial potency of this particle system and a possible combined effect of particle material and payload could be analyzed.
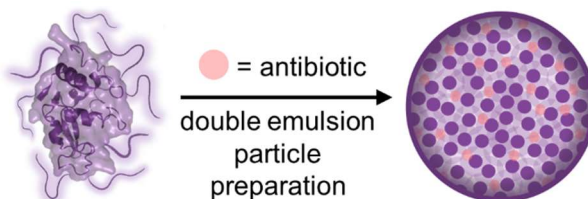
Figure 22: Encapsulation of hydrophilic antibiotics in particles composed of PEGylated LYZ using a double emulsion technique.

As described in section 1.1.4, nanocarriers with a stimuli-responsiveness can release their cargo in a controlled manner after the exposer of intrinsic stimuli. Examples of intrinsic stimuli may be the decreased pH values in tumor tissues or within the endo-lysosomal pathway after cellular uptake, but also the increased reductive conditions in the cytosol can be exploited for a controlled drug release. Nevertheless, in consideration of stimuli-responsive protein-based nanoparticles, the described examples in section 1.2.3 show several unresolved disadvantages, like for example the requirement of harsh conditions for particle preparation or particle disassembly. Based on that, the aim was to establish novel types of stimuli-responsive protein nanoparticles. Therefore, conjugates with introduced sensitivities should be applied to the already developed protein particle preparation technique in our group.

The second project of this work will focus on the development of an acid-sensitive protein-based nanoparticle system (Figure 23a). Hence, PEG with several vinyl ether moieties in the polymer backbone (section 1.1.1) should be conjugated to the model enzyme cytochrome *c* (Cyt) in order to develop a new kind of stimuli-responsive protein-PEG conjugate. This polymer attachment should introduce an acid-sensitivity into the conjugate and additionally change the solubility in organic solvents, which allow the particle preparation using the emulsion technique. Since the vinyl ether moieties are stable in physiological conditions, this property could be transferred to the prepared particles while they should degrade in a slightly acidic environment due to polymer backbone cleavage. Accordingly, model compounds could be encapsulated into the nanoparticle system in order to analyze the acid degradability of the particles more in-depth by monitoring an acid triggered payload release.
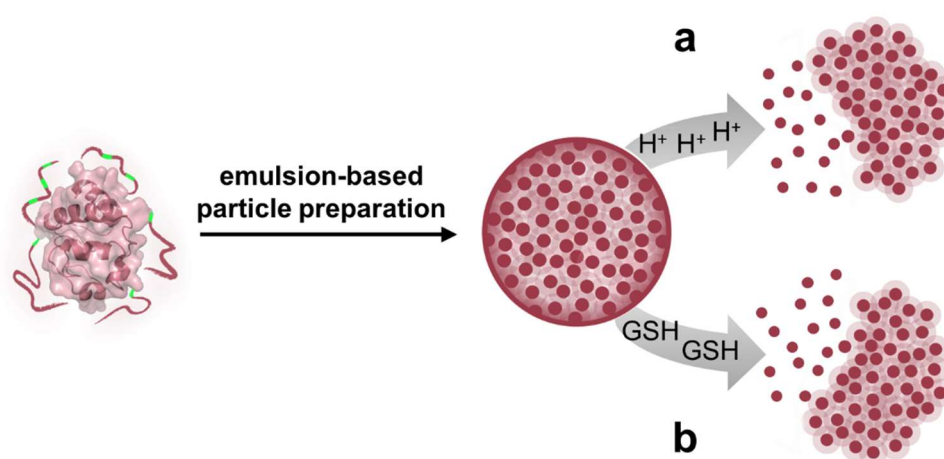
Figure 23: Development of acid- (a) and redox-responsive (b) nanoparticles based on PEGylated Cyt. Both particle types should be prepared by using the emulsions technique.

In recent years, enzymes as biotherapeutics gained more attention. For this reason, in protein nanoparticles, self-immolative linkers could be introduced to regain the native

protein after exposure with a stimulus. Furthermore, in this context reductive-labile linkages are often used (section 1.2.3), which is after the acid-responsivity the second most popular intrinsic trigger for stimuli-responsive nanocarriers. However, in the described example of such a protein-based nanoparticle system in section 1.2.3, harsh preparation conditions lead to protein denaturation.

Based on that, the third project in this thesis deals with reductive-labile protein-based nanoparticles with self-immolative properties within the particle material (Figure 23b). It was the aim to introduce a disulfide self-immolative linker (section 1.1.5) between Cyt, as a model enzyme, and PEG. Herein, the reductive-responsivity should be gained through the linker, and not due to the whole polymer backbone degradability like in the second project of this thesis. Again, a solubility change of this conjugate could allow the emulsion-based protein particle preparation. In consideration of the linker properties, these nanoparticles should be stable in non-reductive conditions and the exposer of a redox-active agent could provide the possibility of particle disassembly as a result of the linker cleavage. The idea was to recover the native, unmodified Cyt out of the nanoparticle system during this mechanism since this particle system itself could be used as biotherapeutic.

3 RESULTS AND DISCUSSION

3.1 LYSOZYME NANOPARTICLES FOR THE DELIVERY OF HYDROPHILIC ANTIBACTERIAL PAYLOADS

The first part of this chapter describes the electrophilic activation of methoxypoly(ethylene glycol) (mPEG). Subsequently, the activated mPEG will be used for enzyme PEGylation due to its obtained reactivity towards nucleophilic groups on the enzyme surface. The aim of the enzyme PEGylation is to obtain an amphiphilic protein material in order to prepare protein nanoparticles by an emulsion-based method. Following, the encapsulation of antibacterial drugs and purification of this nanoparticle system will be developed. At the end of this chapter, the antibacterial activity of this particle system will be investigated.

The majority of the data in this section was published in Macromolecular Rapid Communication, WILEY-VCH Verlag GmbH & Co. KGaA (Steiert *et al.*[153]), and is discussed in this work more in detail.

3.1.1 LYSOZYME SURFACE MODIFICATION AND ANALYSIS

First, the electrophilic mPEG activation will be described in the following section. Furthermore, the chapter will deal with the subsequent protein PEGylation and the associated analytics.

Synthesis of TFP-activated methoxypolyethylene glycol (TFP-mPEG)

Considering the low reactivity of the terminal hydroxy group of mPEG, the chemical activation is required to exploit the polymer for protein modification. Several activation methods are existing, which can be used to address different amino acids on protein surfaces. For example, reactive amino acids are lysine, cysteine, histidine, arginine, serine, threonine and tyrosine. Taking into account that lysine is the most abundant amino acid, it is exceedingly addressed for protein PEGylation. Commonly, electrophilic groups like active esters are used for the mPEG activation, as it reacts with the nucleophilic amines of the lysine.[154] *N*-hydroxysuccinimide active ester (NHS) is the electrophilic activation of choice of polymers[155] which is directly purchasable as NHS-mPEG. A disadvantage of NHS-mPEG is the fast hydrolysis rate. For this reason, Radi *et al.* analyzed different kinds of electrophilic mPEG activation. The goal was to find a high reactivity after mPEG activation and at the same time a mild protein PEGylation condition in order to preserve

the protein structure and enzymatic activity. In this publication, the activation of mPEG with an epoxy-group is described as a method of choice.[126b] After testing the reproducibility of these results, an activation with tetrafluorophenol (TFP) showed equally good outcomes.[156] Based on this, TFP was chosen for mPEG activation. An advantage over the purchasable NHS-mPEG is the higher stability of this active ester in slightly basic, aqueous conditions.[157]

Here, α-methoxy-ω-carboxy-PEG with a molecular weight of 2 kDa was modified with 2,3,5,6-tetrafluorophenol (TFP), as described previously in our group.[126b] First, the carboxylic acid of the polymer was activated with N,N'-dicyclohexylcarbodiimide (DCC), by forming an O-acylisourea intermediate. Subsequently, the hydroxy group of TFP reacts with the intermediate resulting in a TFP activated mPEG (TFP-mPEG) as beige solid in a yield of 70% (Figure 24).
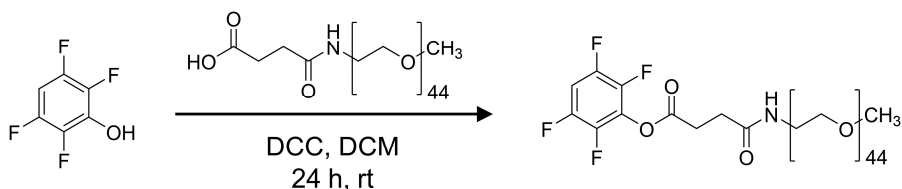
Figure 24: Electrophilic activation of α-methoxy-ω-carboxy-PEG using TFP, resulting in TFP-mPEG. Reproduced from Steiert et al.[153], Copyright (2018) WILEY-VCH Verlag GmbH & Co. KGaA.

The obtained active ester is highly reactive towards nucleophilic groups of proteins. Consequently, the protein PEGylation using TFP-mPEG will be outlined in the next section.

PEGylation of Lysozyme with TFP-mPEG

In this work, the intention of protein PEGylation is to prepare protein-based nanoparticles. If nanoparticles would solely be consisting of proteins, it would result in unstable particles in an aqueous solution due to the good water solubility of the proteins. Only the denaturation of proteins or cross-linking of the particles would result in stabilization.[35a] In our group, a new method for protein-based nanoparticle preparation was described, which was already explained in section 1.2.2. After changing the solubility behavior of proteins by PEGylation, the formation of stable protein-based nanoparticles with a mild preparation method is possible and additional cross-linking is not needed. Furthermore, this method does not lead to protein denaturation.[126]

Lysozyme (LYZ) from hen egg white, an antibacterial enzyme with a molecular weight of 14.3 kDa, was used for protein PEGylation (Figure 25).[139] High surface modification of

LYZ should lead to the described solubility switch. Seven amines of LYZ are accessible for the modification with the electrophilic activated TFP-mPEG. Six of the amines are assigning to lysine and one to the N-terminal amino group. The protein PEGylation takes place in an aqueous buffer with a slightly basic pH value of 8. Basic conditions are required for deprotonating of the ε-amines of lysine with a pK_a of 10.5. For the protein PEGylation, a threefold excess of TFP-mPEG per amine on the LYZ surface was used as already presented in our group.[126b] The PEGylation reaction was performed at room temperature for 48 hours and after the reaction time, the PEGylated protein was purified by size exclusion chromatography (SEC). This purification method is based on the separation by size, in which bigger molecules elutes faster than smaller ones.[158] Thus, the PEGylated lysozyme can be separated from the native enzyme and excess of not reacted TFP-mPEG. The advantage of this purification method compared to dialysis is the shorter time in which the purified PEGylated product is obtained. Subsequent freeze-drying results in the PEGylated lysozyme (LYZmPEG) as colorless solid.
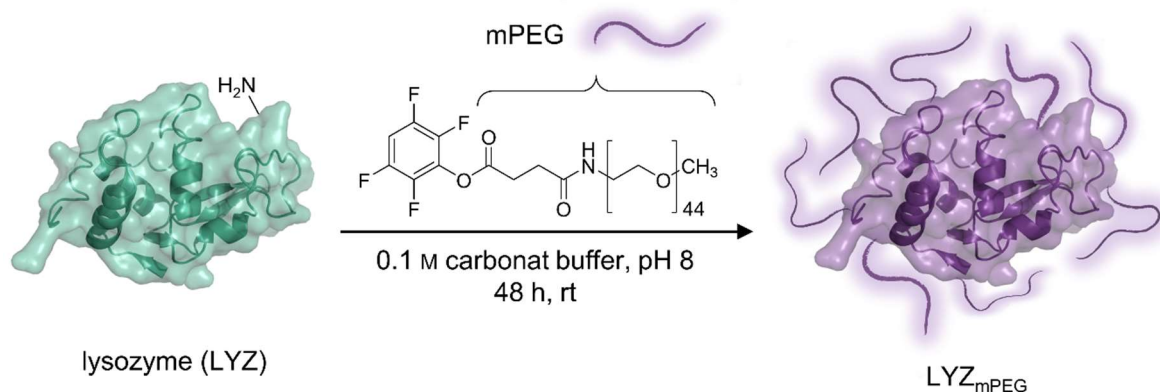
Figure 25: Surface PEGylation of lysozyme (LYZ) with TFP-mPEG, resulting in LYZmPEG. The LYZ modification takes place in an aqueous buffer under slightly basic conditions (pH 8). Seven amines are accessible on the enzyme surface for PEGylation. Reproduced from Steiert *et al.*[153], Copyright (2018) WILEY-VCH Verlag GmbH & Co. KGaA.

After PEGylation of LYZ, in the next section, the analysis of LYZmPEG regarding the molecular weight, structural integrity and enzymatic activity will follow.

Analysis of PEGylated Lysozyme

For molecular weight analysis of the resulting PEGylated LYZ, different methods were carried out. First, LYZmPEG was analyzed by sodium dodecyl sulfate-polyacrylamide gel electrophoresis (SDS-PAGE). In this analytical method, denaturized and negatively charged proteins are applied on a polyacrylamide gel and separated by their molecular weight in an electric field. The negative charge is obtained by mixing the samples with sodium dodecyl sulfate (SDS), resulting in a protein movement towards the anode in the

electric field. In the meshed polyacrylamide gel, small proteins move faster towards the anode than bigger ones, resulting in the separation of proteins based on their molecular weight.[159]

SDS-PAGE analysis of the native lysozyme shows a defined band at 14 kDa (Figure 26, lane 1 and 3). Lysozyme PEGylation leads to a protein band between 22–25 kDa (lane 2), indicating a molecular weight increase of 8 kDa. This leads to the assumption, that 4 mPEG chains are attached on the lysozyme surface due to the usage of a 2 kDa mPEG derivate.
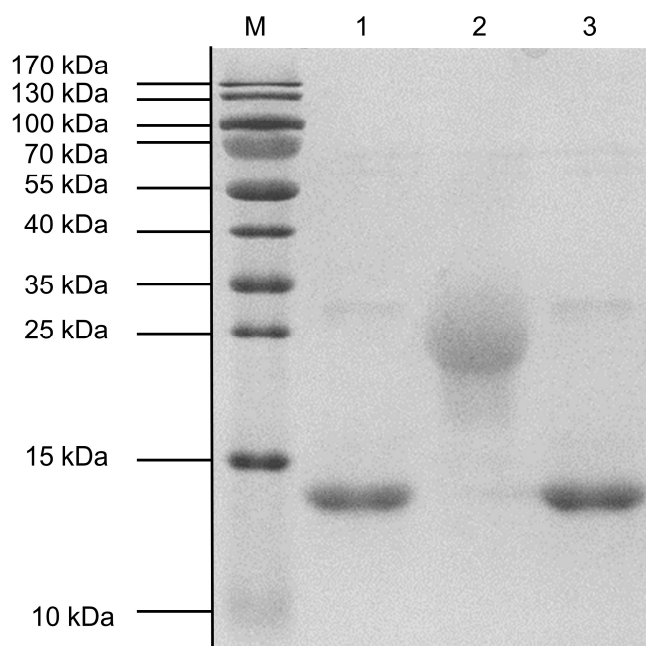
Figure 26: SDS-PAGE (15%) of native lysozyme (lane 1 and 3) and PEGylated lysozyme (lane 2). As the protein marker (M) prestained protein ladder (10–170 kDa) was used. 30 μg of the PEGylated enzyme and 15 μg of the native enzyme were analyzed (first 90 V, 60 min; then 200 V, 60 min). The SDS-PAGE shows the increase in molecular weight due to lysozyme PEGylation. Lane 2 shows no traces of native enzyme, indicating a complete conversion to LYZ$_{mPEG}$. Adapted from Steiert et al.[153], Copyright (2018) WILEY-VCH Verlag GmbH & Co. KGaA.

Considering that the SDS-PAGE suggests only an approximation of the molecular weight of the PEGylated lysozyme, LYZ$_{mPEG}$ was further analyzed by matrix-assisted laser desorption/ionization time-of-flight mass spectrometry (MALDI-ToF MS). In this analytical method, samples are dried on a matrix. Subsequent desorption by a laser results in ionization of the samples. Afterwards samples are sped up in an electric field. By measuring the time-of-flight with a detector, the mass to charge ratio can be concluded. Smaller ions reach the detector faster than bigger ones. The advantage of this frequently used method for protein molecular weight analysis is its sensitivity.[160]

The MALDI-ToF spectrum of the PEGylated lysozyme shows a broad peak between 20–24 kDa, with a maximum at 22.89 kDa (Figure 27). The second peak around 46 kDa and the third one around 69 kDa corresponds to the dimer and trimer of LYZ$_{mPEG}$. Compared to

the molecular weight of native lysozyme with 14.3 kDa, this analytical method proves that four out of seven amines of lysozyme were modified with mPEG. Thus, the results obtained by SDS-PAGE and MALDI-ToF coincide.
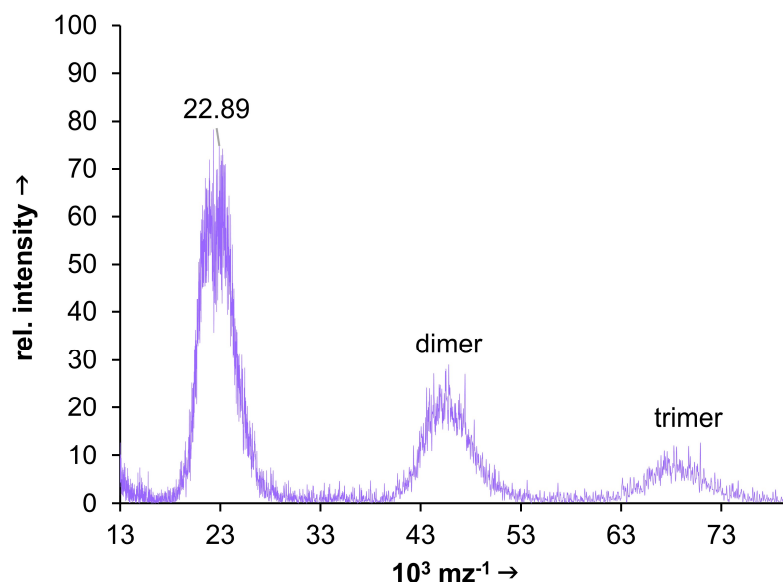
Figure 27: MALDI-ToF MS diagram of LYZ$_{mPEG}$. The diagram confirms the increase in molecular weight after PEGylation of the protein. Conversion into PEGylated enzyme was complete due to no traces of native enzyme are detectable. Reproduced from Steiert *et al.*[153], Copyright (2018) WILEY-VCH Verlag GmbH & Co. KGaA.

Both analytical methods, SDS-PAGE and MALDI-ToF MS, show no native enzyme, indicating that purification of the PEGylated product was successful or else the conversion to LYZ$_{mPEG}$ was proceeded completely. However, the second substantiation is more likely, considering the usage of a high TFP-mPEG excess. Nevertheless, presumably, some of the TFP-activated mPEG hydrolyzed during the incubation time, resulting in only 4 attached mPEG chains on the LYZ surface, even though a much larger excess was used.

The goal during PEGylation of lysozyme was to preserve the secondary structure of the enzyme, which was analyzed by circular dichroism (CD) spectroscopy. The absorbance of right- and left-handed circularly polarized light by optic active substances have different extents. Measuring the differences of these two light species, result in a respective content of the secondary structural elements of α-helices, β-pleated sheets, turns and disordered structures. In the near ultraviolet (UV) region, between 240–190 nm, are characteristic areas for secondary structural elements.[161] The CD measurements of native and PEGylated lysozyme were performed at 20 °C. The obtained spectrum of LYZ$_{mPEG}$ looks slightly different compared to that of native lysozyme (Figure 28). This result suggests that PEGylation with TFP-mPEG leads to only minor changes in the secondary structure.
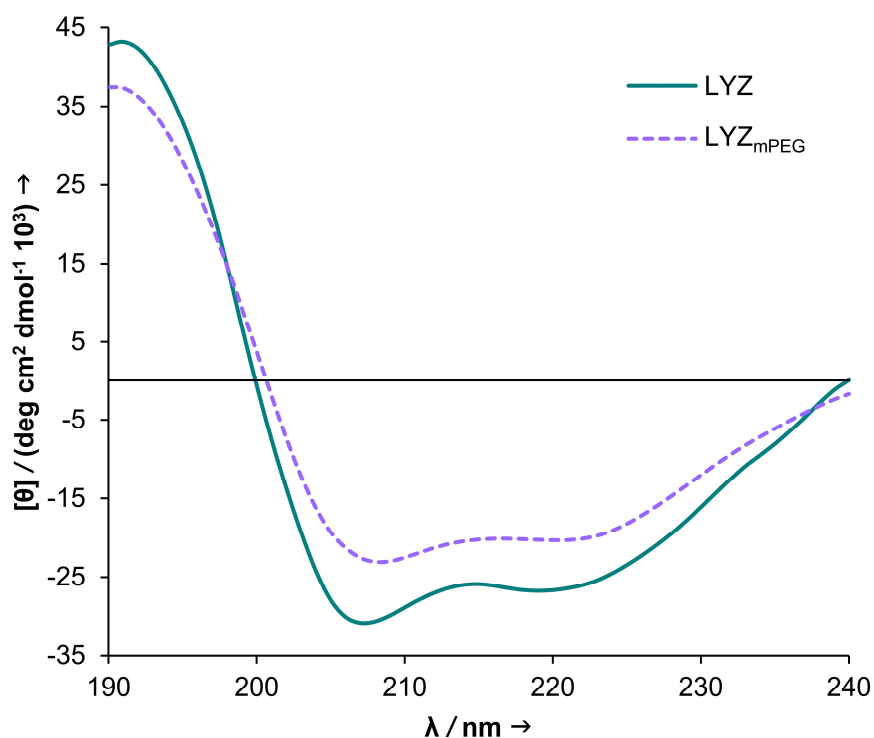
Figure 28: Circular dichroism spectra of native lysozyme (green) and PEGylated lysozyme (dotted, purple). Comparison of both CD spectra shows only minor differences, suggesting that lysozyme PEGylation with TFP-mPEG results in nearly no impairment of the secondary structure. Detailed analysis of secondary structure elements is summarized in Table 2. Reproduced from Steiert *et al.*[153], Copyright (2018) WILEY-VCH Verlag GmbH & Co. KGaA.

More precise is the evaluation of the CD spectra by DichroWeb, resulting in a detailed analysis of the percentage change of the secondary structural elements (Table 2). During PEGylation, the number of α-helices is decreased by around 13%. In contrast, β-pleated sheets are almost not existing in both, native and the PEGylated enzyme. Furthermore, there is nearly no change in the content of turns after PEGylation. In comparison, the amount of disordered structure elements increased around the changed value of α-helices. Nevertheless, the attachment of TFP-mPEG on the lysozyme surface seems to be a mild PEGylation method, resulting in a minor impairment of the secondary structure.

Table 2: Detailed calculated secondary structure elements of native and PEGylated lysozyme (in %) by DichroWeb using CONTIN. Adapted from Steiert *et al.*[153], Copyright (2018) WILEY-VCH Verlag GmbH & Co. KGaA.

	LYZ	LYZ$_{mPEG}$
α-**helices**	81.0	68.4
β-**sheet**	0.2	0.7
turns	10.3	11.3
disordered	8.6	19.8

A further goal during PEGylation of lysozyme was to preserve the initial enzymatic activity. Lysozyme is part of the human innate immune system due to its antibacterial activity. As already explained in section 1.2.4, LYZ exhibit a glycosidase activity by cleaving the *β*-1,4-glycosidic bonds between *N*-acetylmuramic acid and *N*-acetylglucosamine residues, which is a major part of the peptidoglycan layer in bacteria cell walls. As a result, LYZ can cause bacteria lysis due to cell wall degradation. The active site of lysozyme for cell wall degradation is a broad gap, consisting of six subsites and located between two domains (Figure 29). During the cleavage process, the six subsites interact with six sugar residues of the peptidoglycan layer. The strength of the *β*-1,4-glycosidic bond of the sugar is reduced between subsite four and five, resulting in targeted hydrolysis by the catalytic groups glutamic acid at position 35 and aspartic acid at position 52 of LYZ in attendance of water.[139] Consequently, the lysine residues of LYZ, which were targeted for PEGylation are not involved in the cleavage mechanism. In Figure 29 the lysine residues of lysozyme are highlighted red, where position 33 and 97 are most accessible for PEGylation, which was described by Pfister *et al.*[155] However, due to the near location of these lysines to the active site, PEGylation of lysozyme can lead to an impairment of the enzymatic activity.
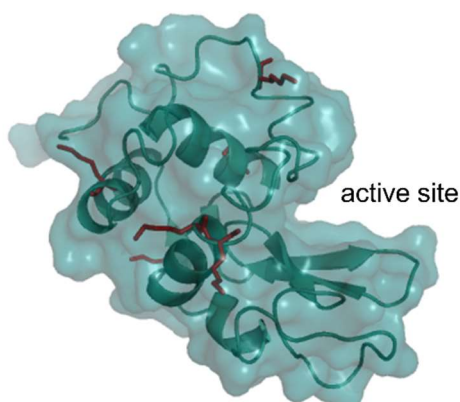
Figure 29: Lysozyme structure with red highlighted lysine residues and better exemplification of the active site, where the peptidoglycan layer cleavage takes place.

The glycosidase activity of native and PEGylated lysozyme was investigated with the artificial enzyme substrate 4-methylumbelliferyl-*β*-D-*N,N',N''*-triacetylchitotriosid. This substrate consists of three chitosan derivate units linked to a 4-methylumbelliferone by a *β*-1,4-glycosidic bond. The bound 4-methylumbelliferone shows no fluorescence. However, after cleavage of the *β*-1,4-glycosidic bond, the release of 4-methylumbelliferone results in a fluorescent signal. The fluorescence change relating to the artificial substrate cleavage by the native and the PEGylated lysozyme was observed over a period of 2.5 hours. Through comparison of the obtained fluorescence slopes, the change of the enzymatic activity after PEGylation can be determined. Results of the activity assay show that the

PEGylation of lysozyme leads only to a minor decrease in the enzymatic activity of 19%, compared to the native enzyme (Figure 30). As described, the impairment of the enzymatic activity is due to lysine PEGylation near to the active site. PEG attachment can be associated with a shielding effect, resulting in decreased active side accessibility for the substrate. However, the examined artificial enzyme substrate is smaller than the peptidoglycan layer of the natural substrate. Despite active site shielding by PEG, probably smaller substrates can easier reach it compared to bigger ones. This must be considered during the discussion of the enzyme activity results. Consequently, enzymatic activity investigations with the bigger, natural substrate can show a greater impairment. Nevertheless, the determined enzymatic activity fits the CD spectrum. Considering that the protein secondary structure is barely impaired, it also should result in only slight change in the initial enzymatic activity.
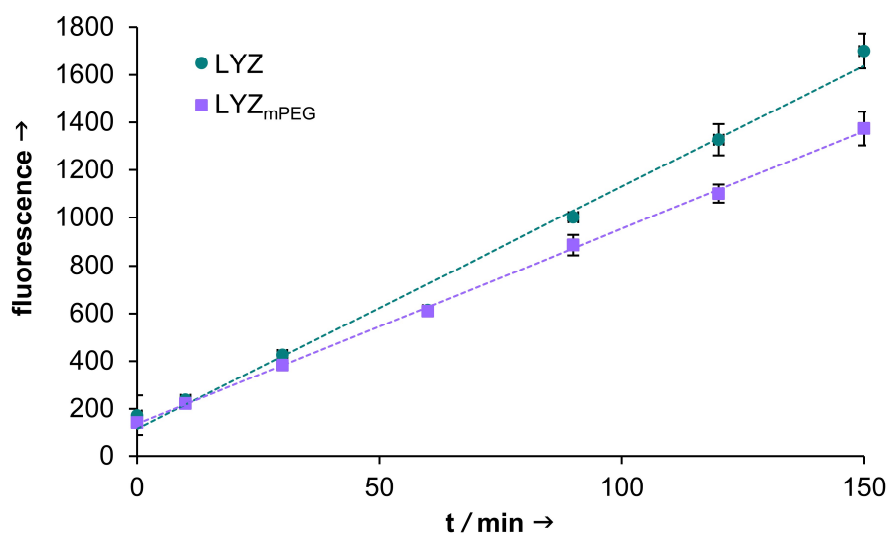
Figure 30: Results of the enzymatic activity assay of native lysozyme compared to the PEGylated lysozyme, analyzed over a period of 2.5 hours. The measured fluorescence depends on the artificial substrate cleavage. The green straight shows the enzymatic activity of native lysozyme (larger slope) and the purple straight of LYZ_{mPEG} (81% of initial enzymatic activity). Adapted from Steiert *et al.*[153], Copyright (2018) WILEY-VCH Verlag GmbH & Co. KGaA.

In summary, in this chapter, the successful LYZ PEGylation was proven due to molecular weight increase. The enzyme modification results in only minor structural changes and the enzymatic activity show a slight impairment.

3.1.2 NANOPARTICLE PREPARATION BY DOUBLE EMULSION AND ANALYSIS

After LYZ PEGylation, in the following section, the nanoparticle preparation based on LYZ_{mPEG} will be discussed. Additionally, the examination of antibacterial material encapsulation will follow. The chapter will end with nanoparticle analysis and with a payload release study.

LYZ$_{mPEG}$-Nanoparticle Preparation by Double Emulsion

The PEGylation of LYZ leads to a solubility in DCM, which allows the preparation of protein nanoparticles by a mild emulsion-based method. In section 1.2.2, it was already described that the single emulsion-based method is only suitable for the encapsulation of hydrophobic drugs. For hydrophilic ones, this method had to be adapted to a double emulsion-based technique. As the name says, two emulsions have to be prepared. Subsequently, the hydrophilic payload is present in an inner water droplet, enclosed by an oil phase, containing the particle material. Considering the water solubility, the hydrophilic payload has to be protected from the surrounding aqueous environment, which is achieved with the oil-phase. Finally, this results in nanoparticles with a hydrophilic drug in the core.

This double emulsion method is already frequently used for the preparation of polymer particles.[128c] Utilizing this technique, different hydrophilic drugs were successfully encapsulated into polymer particles, like antibiotics, nucleic acids, biopharmaceutics or anticancer drugs. The encapsulation of hydrophilic drugs is necessary to protect the drug from environmental degradation and to obtain a controlled release of the payload.[128a] This existing double emulsion method was adopted to form nanoparticles, consisting of protein-PEG as particle material.

In Figure 31 the protein-based nanoparticle preparation by a double emulsion method and encapsulation of a hydrophilic payload is represented in detail. First, the particle material, LYZ$_{mPEG}$, was dissolved in DCM and a 16-fold decreased volume of an aqueous phase compared to DCM was added. If hydrophilic compounds should be encapsulated, this aqueous phase contains the drug. Sonication results in a water-in-oil (w/o) emulsion. Water droplets, which contain the hydrophilic drug, are within the DCM solution. The particle material is presented in the surrounding oil phase. Subsequent addition of a five-fold excess of PBS (pH 7.4) compared to the DCM volume and a second ultrasonic treatment leads to a water-in-oil-in-water (w/o/w) emulsion. The inner water droplet with the hydrophilic drug is surrounded by a DCM layer containing the particle material. As a result of the DCM volatility, the oil phase is removed by stirring at room temperature. During this process, the DCM layer is getting smaller, resulting in the self-assembly of the particle material encapsulating the hydrophilic drug. For the preparation of empty protein particles by double emulsion, the first emulsion is carried out with *dd*-H$_2$O. Prepared nanoparticles based on LYZ$_{mPEG}$ as particle material is abbreviated in the following text as LYZ$_{mPEG}$-NP.
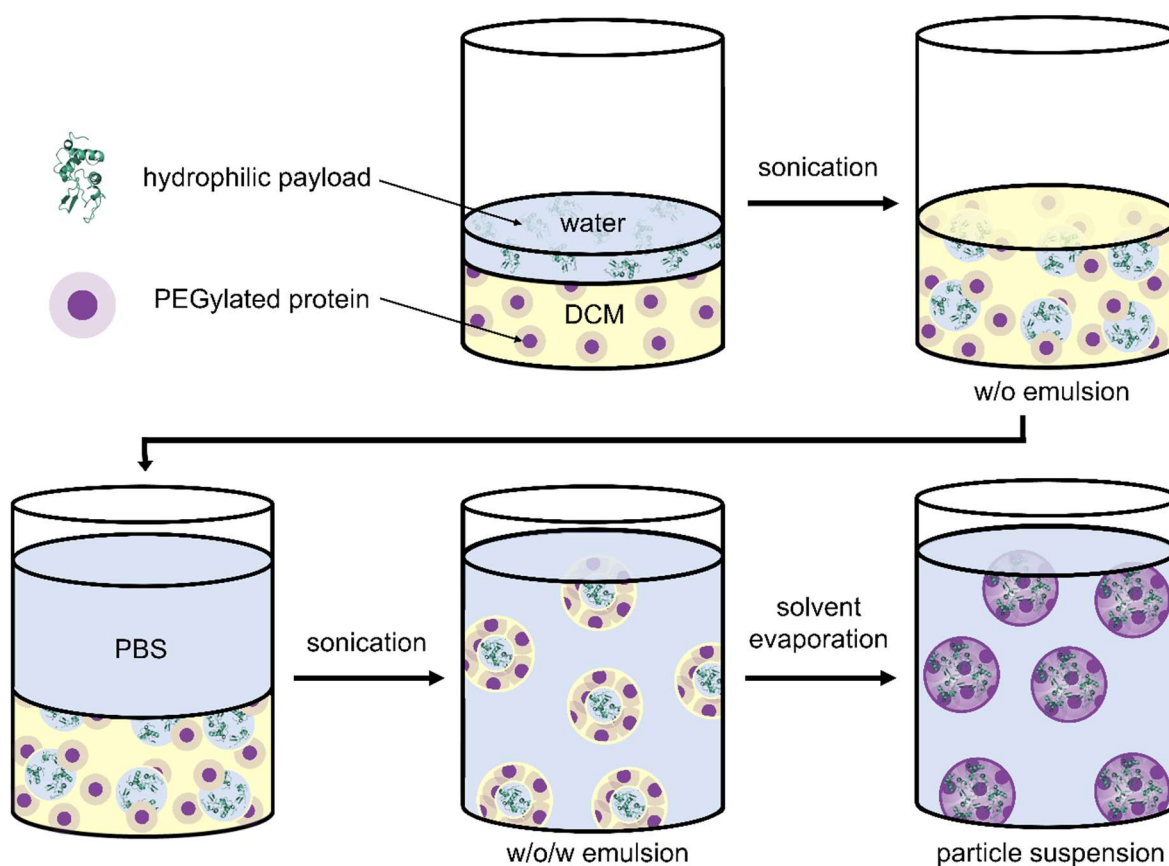
Figure 31: Protein-based nanoparticle preparation by a double emulsion method. The PEGylated lysozyme is dissolved in DCM, covered with a small amount of water containing the hydrophilic payload. A first sonication treatment results in a water-in-oil (w/o) emulsion. Addition of PBS (pH 7.4) and a second ultrasonic treatment, forms a water-in-oil-in-water (w/o/w) emulsion. After removal of the volatile DCM, stable protein-based nanoparticles with an encapsulated hydrophilic payload are obtained. Adapted from Steiert *et al.*[153], Copyright (2018) WILEY-VCH Verlag GmbH & Co. KGaA.

Encapsulation of Small Antibiotics in LYZ$_{mPEG}$-Nanoparticles

For the first studies in this project, the encapsulation of small hydrophilic antibiotics was tested, in order to potentially gain a combined effect of the particle material and the encapsulated antibacterial drug. First, gentamicin sulfate (GS) (Figure 32), an antibiotic drug against gram-positive and gram-negative bacteria was encapsulated into LYZ$_{mPEG}$-nanoparticles (LYZ$_{mPEG}$-NP(GS)). This antibiotic is assigned to the group of aminoglycosides, which inhibit the protein biosynthesis in bacteria resulting in bacteria death. A side effect of gentamicin sulfate is nephrotoxicity. Therefore, encapsulation in a nanoparticle system is advantageous to reach a more targeted release for minimizing the side effect.[128a]
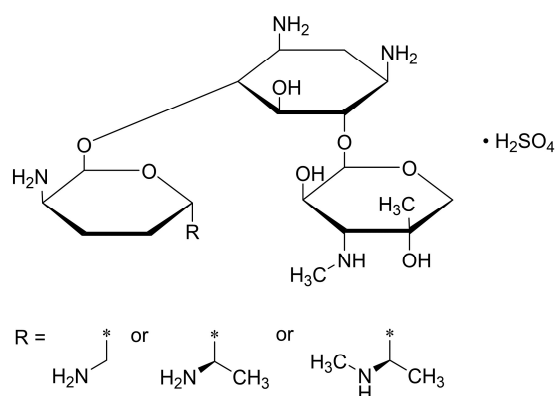
Figure 32: Structure of gentamicin sulfate, which is an antibiotic, containing to the group of aminoglycoside. In bacteria it interacts with ribosome subunits, resulting in disrupted protein biosynthesis.[162]

In a first antibacterial test, the gentamicin sulfate loaded particles were not purified for removal of not encapsulated drugs. To analyze several concentrations of the freshly prepared LYZ_{mPEG}-NP(GS) suspension, the particles were diluted in PBS (pH 7.4). Subsequently, the samples were mixed with the bacteria strain MC4100, which is an *Escherichia coli* (*E. coli*) strain, containing to gram-negative bacteria.[163] Free drug and empty particles, matching the encapsulated GS concentration and the particle material concentration of LYZ_{mPEG}-NP(GS), were also mixed with MC4100. The general antibacterial activity of empty particles, GS loaded particles and free drugs were analyzed by determination of the minimal inhibitory concentration (MIC). MIC indicates the lowest concentration of antibacterial substances which results in no visible growth of bacteria. Bacteria growth would lead to turbidity. For MIC determination, the mixtures of the three substances and the MC4100 were incubated at 37 °C for 24 hours.

Table 3: MIC determination of free GS, not purified GS-loaded and empty nanoparticles against MC4100 after 24 hours. The concentration in the table refers to the free and the encapsulated GS concentration. (+) no visible bacteria growth is observable; (-) turbidity caused by bacteria growth. *the concentration of LYZ_{mPEG}-NP refers to the particle material LYZ_{mPEG} and ranges from 0.85–27.30 μM. It matches the amount of particle material of LYZ_{mPEG}-NP(GS).

sample	Concentration of encapsulated GS [μM]					
	43.42	21.71	10.86	5.43	2.71	1.36
GS	+	+	+	+	-	-
LYZ_{mPEG}-NP(GS)	+	+	+	+	-	-
LYZ_{mPEG}-NP*	-	-	-	-	-	-

In Table 3 the results of the first antibacterial test of empty particles, GS loaded particles and free drug are summarized. Empty particles don't show antibacterial activity against the bacteria strain MC4100, indicating that there will no combined antibacterial effect of

the antibiotic and the particle material. In literature, it was shown that native lysozyme has antibacterial activity against *E. coli*, even though it is a gram-negative bacterium strain.[164] Therefore, the used bacterial strain is not considered as a reason that the empty nanoparticles show no activity. Perhaps, due to the shielding of the PEG chains on the lysozyme surface of the particle material, the active site is not accessible for big substrates like bacteria. In section 3.1.1, the enzymatic activity determination was analyzed with a small artificial substrate. Therefore, this result cannot be compared with the activity against bacteria. Furthermore, it has to be considered that lysozyme has better antibacterial activity against gram-positive bacteria strains. The substrate, the peptidoglycan layer, as the outer membrane is better reachable in gram-positive compared to gram-negative bacteria.[165] Using a gram-positive substrate would perhaps result in antibacterial activity of the particle material.

Unpurified GS loaded nanoparticles and free drugs show the same antibacterial effect at the same concentrations, which displays, that the particle preparation has no influence on the antibiotic activity. Through non-purification of the particles, it is not assured if the antibiotic was successfully encapsulated or if the drug is only in the external aqueous phase. For the analysis of this subject, this antibacterial test was repeated but gentamicin loaded particles were purified by dialysis (molecular weight cut-off (MWCO) 100 kDa) for eight hours. With a molecular weight of 576 g mol^{-1} of gentamicin, the biggest part of the not encapsulated drugs should be removed during dialysis. Repetition of the antibacterial test results in no inhibition of bacterial growth during incubation of bacteria with purified nanoparticles (Table 4).

Table 4: MIC determination of free GS and purified GS-loaded nanoparticles against MC4100 after 24 hours. The concentration in the table refers to the free GS concentration, the GS content after nanoparticle purification was not determined. (+) no visible bacteria growth is observable; (-) turbidity caused by bacteria growth.

sample	Concentration of encapsulated GS [μM]					
	43.42	21.71	10.86	5.43	2.71	1.36
GS	+	+	+	+	-	-
LYZ$_{mPEG}$-NP(GS)	-	-	-	-	-	-

This result indicates that not enough gentamicin was encapsulated into LYZ$_{mPEG}$-nanoparticles. However, much more likely is, that the drug is too small, resulting in completely diffusion out of the particle system during purification. Considering the hydrophilicity of the encapsulated gentamicin sulfate, it has the effort to move to the hydrophilic exterior milieu, resulting in a release out of the particle during purification. Presumably, the prepared LYZ$_{mPEG}$-nanoparticles are relatively wide-meshed and as a

result, the diffusion out of the particle system would occur quickly. In contrast, in literature, the successful GS encapsulation in poly(lactic-*co*-glycolic acid) (PLGA) particles by the double emulsion method was described, where the emulsion was stabilized using polyvinyl alcohol (PVA). However, after 10 days only 50% of the payload was released.[166] For this reason, it can be assumed that this type of PLGA nanoparticles is too dense. Consequently, the double emulsion method is not the reason that the GS encapsulation in the LYZ$_{mPEG}$-nanoparticles did not achieve the desired results. More likely, the nature of the particle material is crucial and how it behaves during particle preparation.

Encapsulation of a Large Antibacterial Payload in LYZ$_{mPEG}$-Nanoparticles

Based on the results of the encapsulation of a small antibiotic into the presumably wide-meshed LYZ$_{mPEG}$-nanoparticles, a large hydrophilic payload was selected for further studies. The encapsulation of active enzymes as biotherapeutics is gaining more attention due to their important role in the human body.[167] For example, enzymes control gene regulation or provide the equilibrium between cell survival and cell death.[168] The double emulsion technique is a suitable method for encapsulation of active enzymes.[169] In view of the potential combining effect of the antibacterial particle material and an antibacterial payload, native lysozyme was selected as biotherapeutic. For native lysozyme encapsulation, LYZ$_{mPEG}$-nanoparticles were prepared as described at the beginning of this section 3.1.2, resulting in LYZ$_{mPEG}$-NP(LYZ).

Fluorescence Labeling of LYZ (Cy5-LYZ)

For better distinction of the LYZ$_{mPEG}$ particle material and the encapsulated native lysozyme, the native enzyme was fluorescent-labeled with the water-soluble sulfo-cyanine 5 NHS ester (Cy5, ex. 605 nm, em. 675 nm). For protein labeling, NHS ester is the most popular functional group. The amine-reactive NHS ester of the dye reacts with ε-amino groups of lysine on the lysozyme surface. The sulfonate-group (SO_3^-) of the dye leads to no change in the reactivity, it only results in increased water-solubility due to the charged group. This is beneficial for protein modification, as a result of no requirement of DMSO for solving the dye.[170] Concerning, that too high DMSO concentrations can lead to protein denaturation.[171] Neutral or slightly basic conditions are required for protein modification. Therefore, LYZ was combined with 0.6 equivalents (eq) of sulfo-cyanine 5 NHS ester per enzyme in neutral conditions (0.1 M borate buffer pH 7) and allowed to stir for one hour while protecting from light. Primary amines of lysozyme react with the activated carboxylic acid of the dye, resulting in a stable amide bond between the protein and Cy5 (Cy5-LYZ) (Figure 33). The mixture was purified by SEC and after freeze-

drying, Cy5-LYZ was obtained as blue solid. The quantification, how many amines of the lysozyme were modified with the Cy5 dye, was performed with a Cy5 standard. Cy5 was dissolved in 0.1 M borate buffer pH 7 and the fluorescence (ex. 605 nm, em. 675 nm) of the standard was compared to Cy5-LYZ in the same buffer. The fluorescent measurement evaluation exhibit that every fourth lysozyme was modified with a Cy5-dye.
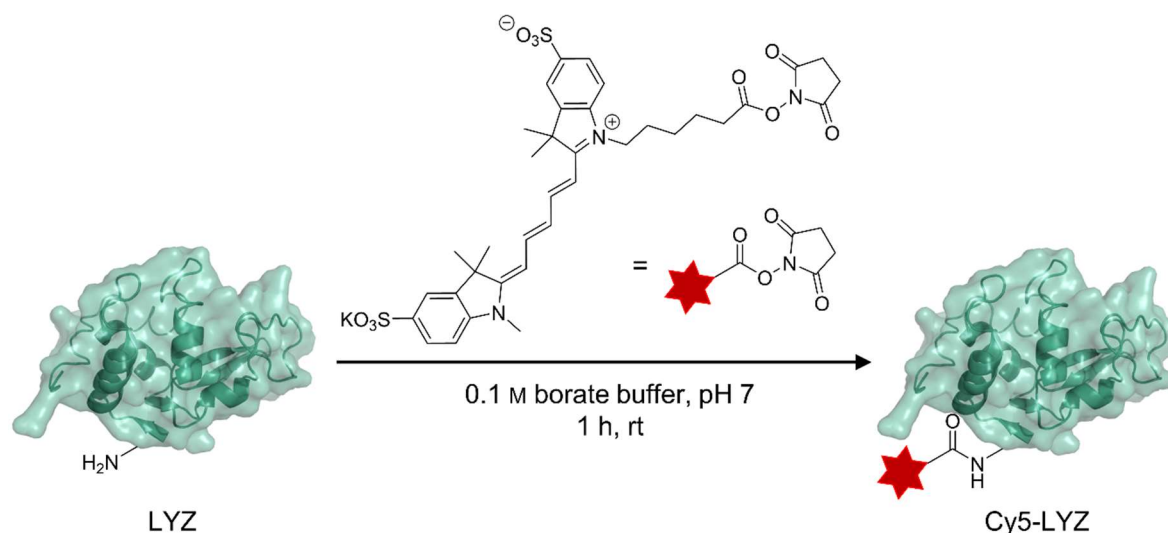
Figure 33: Labeling of LYZ with the fluorescent dye sulfo-cyanine 5 NHS ester. Primary amine on the LYZ surface reacts with the active ester of the dye, resulting in Cy5-LYZ.

Cy5-LYZ was used for encapsulation in LYZ_{mPEG}-nanoparticles (LYZ_{mPEG}-NP(Cy5-LYZ)), to ensure differentiation of the particle material LYZ_{mPEG} and encapsulated lysozyme. On the one hand, the distinction is suitable in order to find a purification method to remove not encapsulated Cy5-LYZ from LYZ_{mPEG} particle material and on the other hand, the subsequent determination of the encapsulated Cy5-LYZ amount is possible.

Nanoparticle Purification

In the first study of loaded LYZ_{mPEG}-nanoparticles, the gentamicin sulfate excess was removed by dialysis. However, this purification method is not purposeful. Considering the hydrophilicity of the gentamicin sulfate and there is no stimuli-responsiveness in the particle system, a payload release by diffusion in the exterior aqueous surrounding is suspected. As a result, during dialysis as purification method, drug release occurs simultaneously. Consequently, a purification method was searched, which provides a fast separation of the loaded particle system and free drug. Earlier studies had shown that the purification of LYZ_{mPEG}-nanoparticles by centrifugal devices is not a suitable method, because the centrifugation results in particle degradation due to harsh conditions.[129a] Based on these results LYZ_{mPEG}-nanoparticle purification by SEC was tested. Sephadex® G-100, a cross-linked dextran material, was selected as column content, in

consideration of good protein separation.[172] The separation behavior in the Sephadex®-G-100 column of LYZmPEG-NP(Cy5-LYZ), LYZmPEG-NP and Cy5-LYZ was compared. Samples were applied on the column and fractions were collected in a clear 96 well plate. An absorbance measurement of the samples in the well plate followed. Through the absorbance of aromatic amino acids of proteins, the separation behavior of empty nanoparticles, only consisting of LYZmPEG, was measured at 280 nm. And for analysis of free and encapsulated Cy5-LYZ, the absorbance was measured at 650 nm, caused by the excitation wavelength of the fluorescent dye. The result of this separation analysis by SEC is summarized in Figure 34.
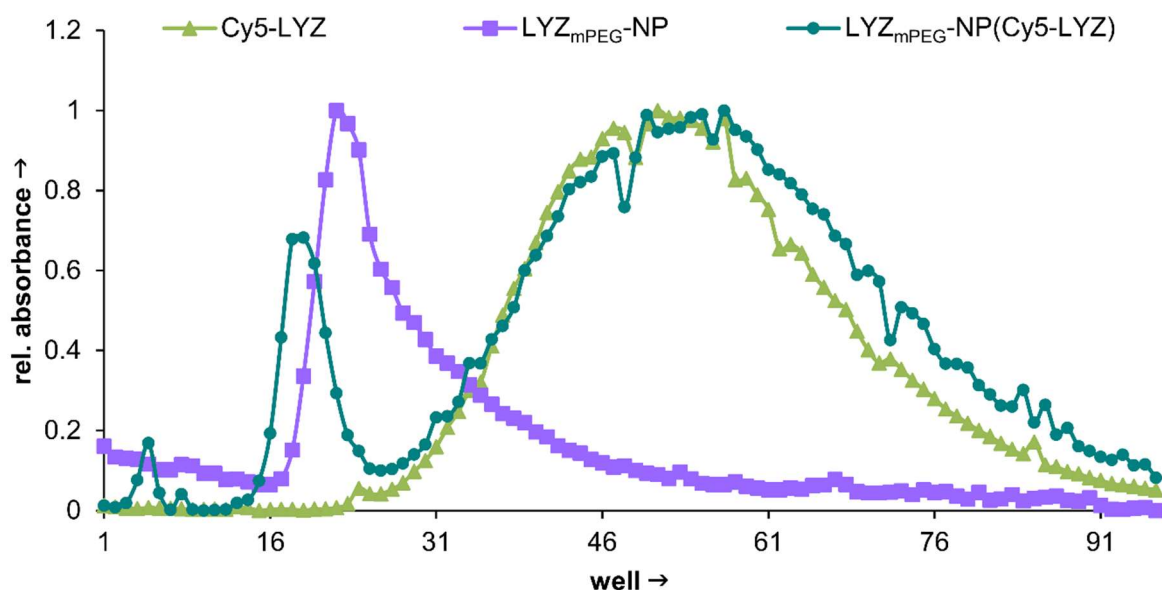
Figure 34: Separation behavior of Cy5-LYZ (bright green triangles), empty LYZmPEG-nanoparticles (purple squares) and Cy5-LYZ-loaded LYZmPEG-nanoparticles (dark green dots) by Sephadex® G-100. 147 μL fractions were collected in a clear 96 well plate. The absorbance of Cy5-LYZ and LYZmPEG-NP(Cy5_LYZ) was measured at 650 nm and of LYZmPEG-NP at 280 nm. Adapted from Steiert et al.[153], Copyright (2018) WILEY-VCH Verlag GmbH & Co. KGaA.

After separation of LYZmPEG-NP(Cy5-LYZ) by Sephadex® G-100, two peaks at 650 nm were identified. The first peak (fraction 16–24) coincides with the empty LYZmPEG-NP peak at 280 nm, indicating that this is the encapsulated Cy5-LYZ. The second peak (fraction 30–91) elutes like free Cy5-LYZ, which suggests that the separation of encapsulated and free Cy5-LYZ was successful. Fraction 16–24, containing LYZmPEG-NP(Cy5-LYZ), were collected to make sure, that the separation of free Cy5-LYZ is secured.

The purification by SEC results in a dilution of the nanoparticle system. Beyond that, it leads also to a nanoparticle loss due to not collecting the whole peak belonging to empty LYZmPEG-nanoparticles. This would have resulted in collecting free Cy5-LYZ. To ensure a complete nanoparticle purification, a nanoparticle loss was rather accepted. For determination of LYZmPEG-particle material concentration after purification, the

absorbance of purified empty LYZ$_{mPEG}$-NP was measured at 280 nm and compared to a standard curve of unpurified empty LYZ$_{mPEG}$-NP with a known concentration. The measurement results in a 180 μg mL^{-1} (7.86 μM) LYZ$_{mPEG}$ particle material concentration. The absorbance measurement of LYZ$_{mPEG}$-NP(Cy5-LYZ) would not have been effective, because the encapsulated Cy5-LYZ also absorbs at 280 nm, which would have resulted in a too high calculated nanoparticle concentration. Considering the same particle preparation and purification method, the equal particle material concentration of LYZ$_{mPEG}$-NP(Cy5-LYZ) is expected.

After nanoparticle purification, the Cy5-LYZ content in loaded LYZ$_{mPEG}$-nanoparticles was determined by fluorescent measurement (ex. 605 nm, em. 675 nm) resulting in an encapsulated Cy5-LYZ amount of 9.04 μg mL^{-1} (0.60 μM). Compared to the determined particle material concentration, it results in a loading ratio of 0.08 mol Cy5-LYZ per 1 mol LYZ$_{mPEG}$ (corresponding to an EE of 2.4% and an LC of 4.78wt%, calculated with eq. 1 and eq. 2). The low encapsulation efficiency can be explained by a very high loading feed of Cy5-LYZ during particle preparation. However, in this work, the improvement of the encapsulation efficiency was not pursued, due to the not encapsulated excess did not bother, as it could be easily removed using SEC. The determined loading capacity corresponds to the literature. For example, in PLGA microparticles, the protein bovine serum albumin (BSA) was successfully encapsulated with a loading capacity of 4.8%.[173] In an additional example of poly(lactic acid) (PLA) nanoparticles, a loading capacity of human serum albumin (HSA) of 2.3% was reached.[174] Both examples of polymer particles were prepared by the double emulsion technique.

Nanoparticle Analysis

After particle preparation and purification, the analysis of the empty and LYZ loaded LYZ$_{mPEG}$-nanoparticles follows. For size determination nanoparticle tracking analysis (NTA) was used. Normally, the most frequently used method for the size determination of nanoparticles is dynamic light scattering (DLS). In DLS, particles are scattering incident light depending on their size. The intensity of the scattered light is measured by the DLS and subsequently, the software calculates the particle size with the Stokes-Einstein equation. Advantages of DLS are the easy handling and the measurement is not time-consuming. Nevertheless, a drawback of this analytical method is that polydisperse samples end in unreliable results. In this regard, NTA measurements provide better results and additionally a better resolution compared to those of DLS.[175] Particles with a size between 30 nm and 1 μm can be analyzed by NTA. In this analytical method, particle size distribution is determined by a combination of light scattering and visualization with a charge-coupled device (CCD) camera. The camera is recording movements of the particles

due to Brownian molecular motion, which depends on the particle size. Subsequently, with a software the motions can be evaluated with the Stokes-Einstein equation, resulting in the hydrodynamic radius of the particles.[176] For nanoparticle analysis by NTA, the samples were diluted in a particle material concentration of 26 μg mL^{-1} and analyzed in three individual measurements with 30 seconds duration. Both, NTA measurements of empty (Figure 35a) and Cy5-LYZ loaded LYZ$_{mPEG}$-nanoparticles (Figure 35b) show a size distribution of around 200 nm, indicating that the encapsulation of native lysozyme results not in an increasing particle size.
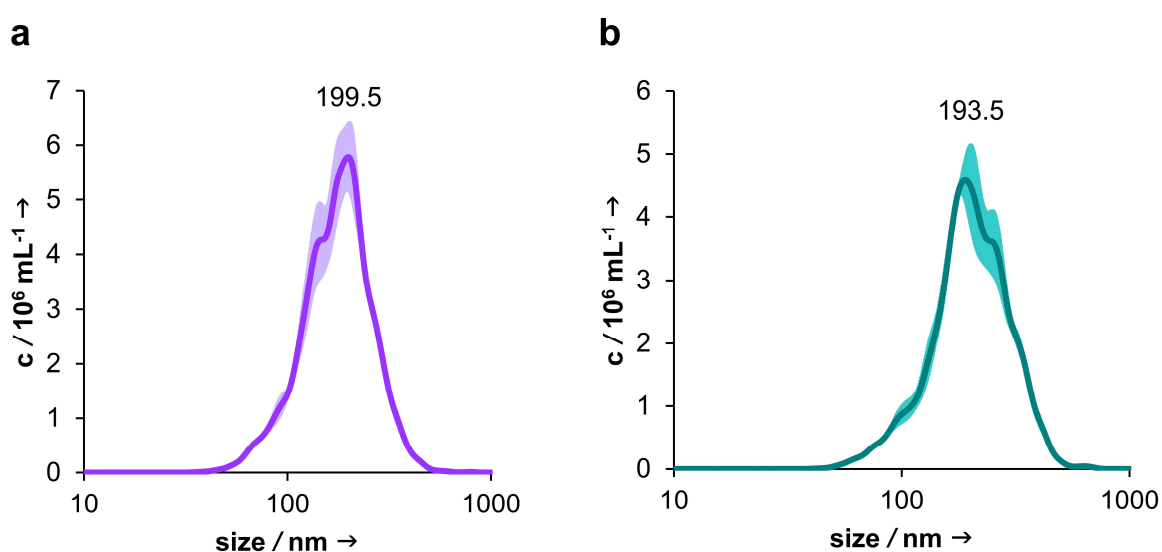
Figure 35: The size distribution of (a) empty and (b) Cy5-LYZ loaded LYZ$_{mPEG}$-nanoparticles determined by NTA measurements. Reproduced from Steiert *et al.*[153], Copyright (2018) WILEY-VCH Verlag GmbH & Co. KGaA.

A widespread method for visualization of nanoparticles is transmission electron microscopy (TEM). In this procedure, 5 μL of the samples (LYZ$_{mPEG}$-NP and LYZ$_{mPEG}$-NP(Cy5-LYZ)) were applied on a carbon-coated mesh copper grid and dried by removing the solvent with a filter paper at one side of the grid. In the microscope, electron beams interact with the sample, which leads to electron transmission by the atomic nuclei in the sample. This results in the contrast in a TEM-image, which is enlarged by several lenses, depicted on a screen and detected by a CCD camera.[177] The TEM image of empty (Figure 36a) and Cy5-LYZ loaded nanoparticles (Figure 36b) show a size around 200 nm, matching with the size obtained by NTA measurements. Furthermore, both larger TEM image sections show over the entire picture a narrow size distribution, indicating that the prepared particles are relatively monodisperse. A closer look at individual particles indicates density differences within the particles. Since proteins are denser materials compared to the attached PEG chains, the darker appearing areas inside the particles represent proteins. Nevertheless, the prepared nanoparticles are normally in solution and drying them on the grid can result in a size change. For this reason, the combination of

several analytical methods is advantageous, so the results of NTA measurements should gain more attention for size determination and TEM for the visualization of the shape.
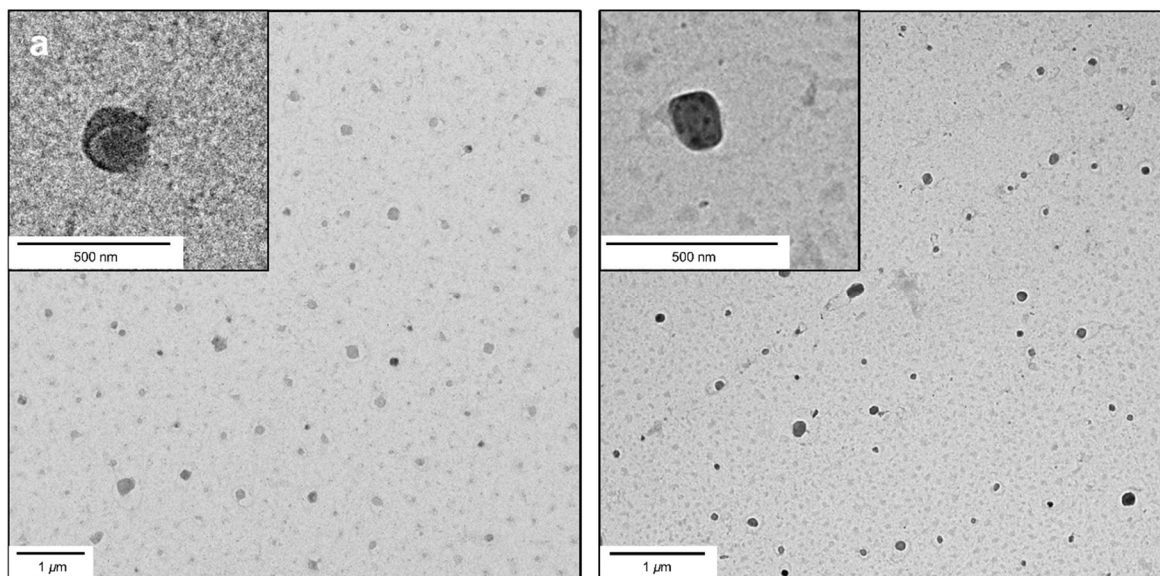
Figure 36: Visualization of (a) empty and (b) Cy5-LYZ loaded LYZ$_{mPEG}$-nanoparticles by TEM.

To analyze the charge of the prepared and purified nanoparticles, ζ-potential measurements were performed. The obtained value describes a potential difference between the particle surface and the surrounding solution. This method is used for the analysis of nanoparticle stability. The higher the obtained values, the more stable are the nanoparticle suspensions, due to the repulsion of similarly charged particles.[178] After purification empty LYZ$_{mPEG}$-nanoparticles show a ζ-potential of −10 mV (Table 5). In comparison, the Cy5-LYZ loaded particles show a value of −6.58 mV. Through the encapsulation of the positively charged lysozyme, it results in an increase of the net-charge. Both ζ-potential values indicate a reasonably well particle stability since LYZ-based nanoparticles with a similar value of −13 mV were stable over a time of minimum two months.[126b]

Table 5: Results of ζ-potential measurements of purified empty and Cy5-LYZ loaded LYZ$_{mPEG}$-nanoparticles. Adapted from Steiert *et al.*[153], Copyright (2018) WILEY-VCH Verlag GmbH & Co. KGaA.

sample	ζ-potential (mV)
LYZ$_{mPEG}$-NP	−10.00
LYZ$_{mPEG}$-NP(Cy5-LYZ)	−6.58

Cell-Viability Test using Human Cells

The prepared nanoparticle system should be biocompatible to human cells, which was examined using a cell viability test. For this investigation, the most common method is the MTT assay. In this approach, samples that should be analyzed, are incubated with human cells and after a sufficient incubation time, the yellow, water-soluble dye 3-(4,5-dimethyl-2-thiazolyl)-2,5-diphenyl-2H-tetrazolium bromide (MTT) is added. Through the positive charge of MTT, the dye can be taken up by the cells. By an active metabolism of cells, the MTT is reduced with NADH to the water-insoluble, purple formazan. After dissolving the formazan in DMSO, the amount of this dye can be calculated by measuring the absorbance at 570 nm. Considering that formazan could only be formed by an active metabolism, the absorbance directly correlates with the cell viability.[179]

For cell viability determination the human cervical cancer cells of Henrietta Lacks (HeLa cells) were used and incubated for 48 hours with purified empty and LYZ loaded LYZ$_{mPEG}$-nanoparticles, as well as the same concentration of free LYZ. In this assay, the fluorescent Cy5-LYZ could not be used due to absorbance of Cy5 at the same wavelength as formazan. For this reason, unmodified LYZ was encapsulated in the nanoparticle system and also for free LYZ analysis, the non-fluorescent labeled protein was used. All three samples in a concentration ranging between 0.14–4.37 μM particle material and an LYZ concentration from 0.01 to 0.31 μM show no toxicity (Figure 37). This result validates the biocompatibility of the particles, thus suitable as drug delivery material.
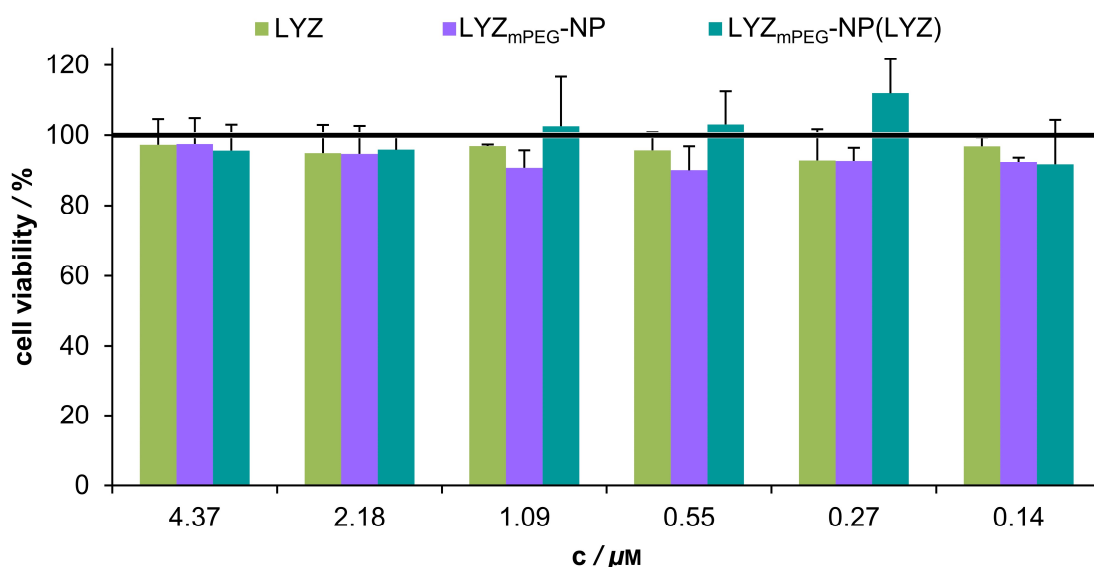
Figure 37: Results of the MTT assay for determination of the biocompatibility of empty and LYZ-loaded LYZ$_{mPEG}$-nanoparticles and an equivalent amount of free LYZ using HeLa cells. The concentration in the figure refers to the amount of LYZ$_{mPEG}$ particle material. Free LYZ was analyzed in concentrations ranging between 0.01–0.31 μM, to match the encapsulated amount in LYZ-loaded nanoparticles. Adapted from Steiert et al.[153], Copyright (2018) WILEY-VCH Verlag GmbH & Co. KGaA.

This result highlights the advantage of the developed LYZ$_{mPEG}$-nanoparticle system compared to the previously mentioned silica nanoparticles for LYZ delivery in section 1.3. Though these particles exhibit a good antibacterial activity[151], silica particles reveal toxicity against human cells[180].

Payload Release and Nanoparticle Stability

For a better understanding of the lysozyme release out of the LYZ$_{mPEG}$-nanoparticle, a dialysis experiment was carried out. After purification of the freshly prepared empty and Cy5-LYZ loaded nanoparticles, free Cy5-LYZ was diluted to the same concentration as the encapsulated Cy5-LYZ amount. The samples were placed in dialysis membranes (MWCO 20 kDa) and dialyzed against PBS (pH 7.4). Compounds with a smaller molecular weight as 20 kDa, like free or released Cy5-LYZ or LYZ$_{mPEG}$, would be washed out of the dialysis membrane. The particle stability and the release of Cy5-LYZ out of the particle compared to free Cy5-LYZ were analyzed over a period of 24 hours. Therefore, the samples were removed out of the dialysis membrane and evaluated by NTA and fluorescence measurements over time. The results of this experiment are summarized in Figure 38.

Free Cy5-LYZ is unobstructed in solution, and therefore it was removed very fast out of the dialysis membrane, as a result, more than 50% of the enzyme has already diffused out of the dialysis membrane after two hours (Figure 38a (light green line)). In contrast, the encapsulated Cy5-LYZ needs around 14 hours for the removal of more than 50% (Figure 38a (dark green line)). Thus, a delayed payload release out of the nanoparticle is observed. Empty nanoparticles were analyzed as a control. Fluorescence measurements show no change due to none payload (Figure 38a (purple line)). During the dialysis experiment, empty and Cy5-LYZ loaded particles were stable, which was analyzed by comparison of particle size and concentration in NTA measurement over time (Figure 38b (LYZ$_{mPEG}$-NP) and Figure 38c (LYZ$_{mPEG}$-NP(Cy5-LYZ)). Only marginal variations are noticeable, which are explainable by measurement inaccuracies. The NTA curves suggest, that the Cy5-LYZ removal by dialysis is not related to nanoparticle instability. It rather indicates that it happens by passive diffusion, which results in delayed payload release. Hydrophilic payloads have the tendency to diffuse to the outer hydrophilic environment. Consequently, no trigger for particle degradation or payload release is necessary. If a trigger would exist, it would only result in a faster payload release.

In comparison, the already mentioned PLGA microspheres with encapsulated BSA prepared by double emulsion revealed a similar release profile, since after one day around 60% of BSA was released. Nevertheless, in this publication, it was also shown that with increased usage of PVA concentrations for emulsion stabilization, the BSA release was slower. It is the result of decreased pore sizes within the particle. Thus, doubling the PVA

concentration has halved the release rate.[173] This confirms the assumption that the prepared LYZ$_{mPEG}$-nanoparticles are relatively wide-meshed due to the similar release profile of PLGA particles, only stabilized with a low extent of PVA.
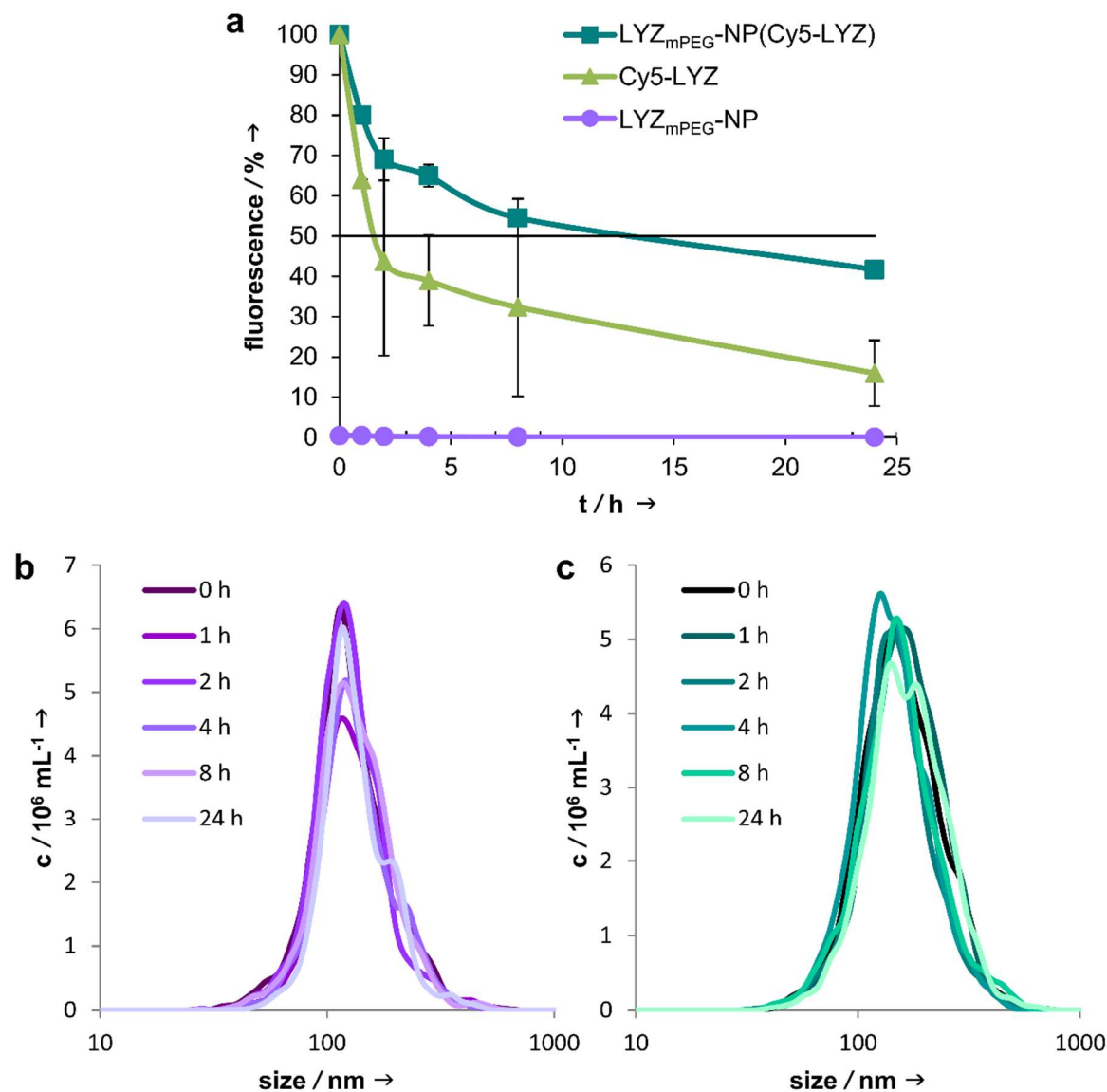
Figure 38: a) Comparison of fluorescence change of empty (purple), Cy5-LYZ loaded LYZ$_{mPEG}$-nanoparticles (dark green) and free Cy5-LYZ (bright green), during dialysis (MWCO 20 kDa) against PBS (pH 7.4) over a period of 24 hours. It demonstrates the delayed Cy5-LYZ release out of the nanoparticles. b) NTA measurements over time of empty LYZ$_{mPEG}$-nanoparticles and c) of Cy5-LYZ loaded LYZ$_{mPEG}$-nanoparticles during dialysis. In both NTA graphs no significant change of the particle size and concentration is observable, indicating that the Cy5-LYZ release happens by passive diffusion and not by particle degradation.

In addition, the advantage of LYZ$_{mPEG}$-NP(LYZ) could be highlighted compared to the previously described VLPs for LYZ encapsulation, which lacks in an LYZ release (see section 1.3).[149]

In summary, this chapter describes the successful LYZ$_{mPEG}$-nanoparticle preparation and encapsulation of native LYZ. The prepared particles show no toxicity and LYZ$_{mPEG}$-NP(LYZ) display a sustained LYZ release by passive diffusion.

3.1.3 SCREENING OF ANTIBACTERIAL ACTIVITY

After LYZ$_{mPEG}$-NP(LYZ) particle preparation, the following chapter will deal with the antibacterial activity of this particle system.

MIC Determination

For the antibacterial activity analysis of the lysozyme-loaded nanoparticles, in a first experiment, the minimal inhibitory concentration (MIC) should be determined. As described in the section of the gentamicin sulfate loaded particles, it defines the lowest concentration of antibacterial substances which results in no visible growth of bacteria. This experiment should get an impression in which concentration range the particles show antibacterial activity. A gram-positive bacteria strain was used for the antibacterial experiments, due to better accessibility of the peptidoglycan layer. Consequently, lysozyme shows a better activity against these bacteria compared to gram-negative ones. For this reason, the gram-positive bacteria strain *Micrococcus Luteus* (*M. Luteus*) was used for the investigations. It exists in dust and on human skin, as part of the natural bacterial flora.[181] In exceptional circumstances of immunosuppressed patients, this bacteria strain can cause endocarditis.[182] After preparation and purification of empty and Cy5-LYZ loaded LYZ$_{mPEG}$-nanoparticles, a loading concentration of 9.00 μg mL^{-1} Cy5-LYZ and a LYZ$_{mPEG}$ material concentration of 180 μg mL^{-1} was determined. For the investigation of more concentration values, the nanoparticles and the equivalent amount of Cy5-LYZ were diluted in PBS (pH 7.4). Subsequently, the samples were mixed with the bacteria strain *M. Luteus* and incubated at 37 °C overnight. The result of this antibacterial experiment is summarized in Table 6.

Free Cy5-LYZ and LYZ$_{mPEG}$-NP(Cy5-LYZ) show a MIC concentration of 0.56 μg mL^{-1}. Concentrations below result in turbidity due to bacteria growth. The same MIC values of free and encapsulated Cy5-LYZ indicate, that the particle preparation and encapsulation don't lead to an LYZ activity change. Incubation of the bacteria with empty nanoparticles show no bacteria growth inhibition. Consequently, a combinational effect of encapsulated Cy5-LYZ and LYZ$_{mPEG}$ particle material is not expected. As mentioned before during the encapsulation of gentamicin sulfate (section 3.1.2), the lysozyme PEGylation results in the shielding of the proteins' active site. Thus, the catalytic center is not easily accessible for big substrates, like bacteria. Concerning this, Wright *et al.* recently reported that already

the attachment of only two 2 kDa PEG chains on the lysozyme surface leads to a 50% decreased activity against *M. Luteus*.[183] Since LYZ$_{mPEG}$ bears twice as many PEG chains, it fits to our results in no antibacterial activity of empty LYZ$_{mPEG}$-nanoparticles.

Table 6: MIC determination of free Cy5-LYZ, purified Cy5-LYZ-loaded and empty nanoparticles against *M. Luteus* after 16 hours. The concentration in the table refers to the free and the encapsulated Cy5-LYZ concentration. (+) no visible bacteria growth is observable; (-) turbidity caused by bacteria growth.*the concentration of LYZ$_{mPEG}$-NP refers to the particle material LYZ$_{mPEG}$ and ranges from 2.81–90 μg mL^{-1}. It matches the amount of particle material of LYZ$_{mPEG}$-NP(Cy5-LYZ). Adapted from Steiert *et al.*[153], Copyright (2018) WILEY-VCH Verlag GmbH & Co. KGaA.

sample	concentration of encapsulated Cy5-LYZ [μg mL^{-1}]					
	4.50	2.25	1.12	0.56	0.28	0.14
Cy5-LYZ	+	+	+	+	-	-
LYZ$_{mPEG}$-NP(Cy5-LYZ)	+	+	+	+	-	-
LYZ$_{mPEG}$-NP*	-	-	-	-	-	-

In addition, it has to be considered, that the nanoparticle purification leads to a decreased LYZ$_{mPEG}$ particle material concentration. In view of that, a previous experiment has shown, that the incubation of *M. Luteus* with empty LYZ$_{mPEG}$-NP in a concentration of 234 μg mL^{-1} results in a bacteria growth inhibition (data not shown). However, in this test, only the particle dilution during purification was heeded, and not the additional particle loss. So, this experiment was performed with too high particle material concentrations. Nevertheless, this result proves a slightly antibacterial activity of the particle material, but not enough for a combined effect with encapsulated lysozyme after purification by SEC.

Time Kill Assay

In order to analyze the antibacterial activity of the lysozyme loaded nanoparticles more in detail, an advanced observation of the bacteria growth during incubation with the nanoparticles was carried out. Therefore, in a time kill assay, the change in turbidity due to bacteria growth was measured over time. For determination of the turbidity, also called optical density (OD), the absorbance at 600 nm was measured. Otherwise, the experimental setup was the same as at the MIC determination. Purified empty and Cy5-LYZ loaded LYZ$_{mPEG}$-nanoparticles, as well as the same amount of free Cy5-LYZ, were diluted to obtain a range of different concentrations. Subsequently, after mixing the samples with *M. Luteus*, the optical density was measured over a period of one day (Figure 39).
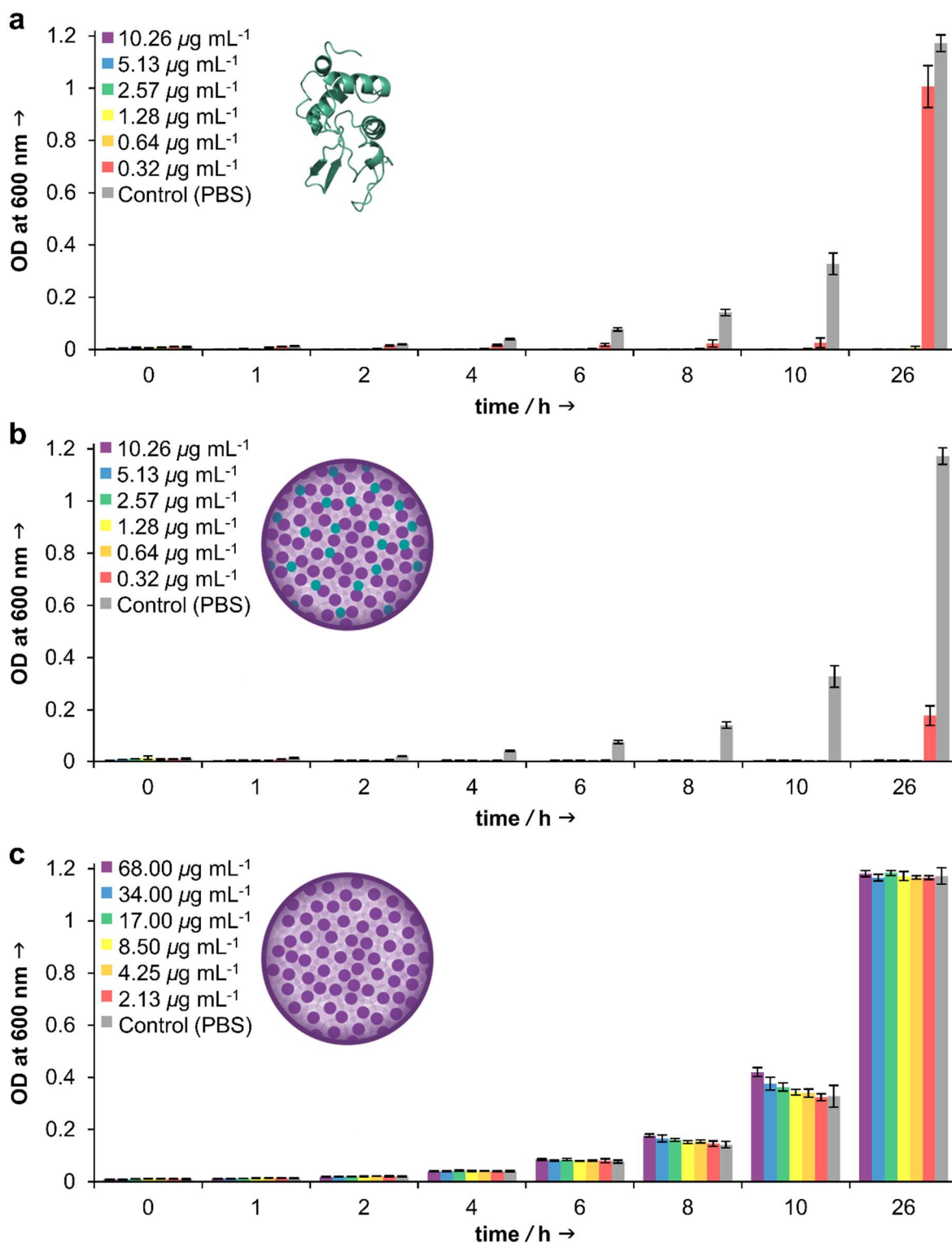
Figure 39: Optical density observation of *M. Luteus* over time, while incubated with free Cy5-LYZ (a), encapsulated Cy5-LYZ in LYZ$_{mPEG}$-NP (b) or empty LYZ$_{mPEG}$-NP (c). The concentrations in a) and b) refer to Cy5-LYZ, ranging from 0.32–10.26 μg mL^{-1}. In c) the concentration refers to the LYZ$_{mPEG}$ particle material, ranging between 2.13–68.00 μg mL^{-1} to correspond the amount of particle material of LYZ$_{mPEG}$-NP(Cy5-LYZ). Adapted from Steiert *et al.*[153], Copyright (2018) WILEY-VCH Verlag GmbH & Co. KGaA.

Free or encapsulated Cy5-LYZ concentrations greater or equal than 0.64 μg mL^{-1} incubated with *M. Luteus*, result in no bacteria growth over time (Figure 39a,b). Only at a lysozyme concentration of 0.32 μg mL^{-1} bacteria growth is observable, which is especially clearly visible after the incubation overnight. Encapsulated Cy5-LYZ seems to have a marginal greater antibacterial activity compared to free Cy5-LYZ, due to lower turbidity after 26 hours at a Cy5-LYZ concentration of 0.32 μg mL^{-1} (comparison of the red bars in Figure 39a,b). Again, empty nanoparticles show no antibacterial activity. Every analyzed concentration of LYZ$_{mPEG}$-NP results in the same optical density as the control, which is a mixture of bacteria and PBS (pH 7.4) (Figure 39c). Considering this outcome compared to the higher antibacterial activity of encapsulated Cy5-LYZ, this is not a result of a combined antibacterial effect of the particle material and the encapsulated enzyme. Rather, it is explainable by a sustained release, resulting in a prolonged impact on the peptidoglycan layer of *M. Luteus*. Furthermore, since the peptidoglycan layer is also a substrate of the LYZ$_{mPEG}$ particle material, it can lead to particle-bacteria interactions, but which is not enough for bacteria degradation. The following payload release in close bacteria proximity can also explain the slightly better inhibition of bacterial growth. In this context it also has to be considered that due to the negative ζ-potential, the nanoparticle probably does not favor interacting with the likewise negative charged bacteria cell wall. Particle proximity can only be explained by a substrate affinity.

Fluorescence Microscopy

For further investigations, Cy5-LYZ loaded LYZ$_{mPEG}$-nanoparticles were mixed with *M. Luteus* and analyzed by fluorescent microscopy (Figure 40).
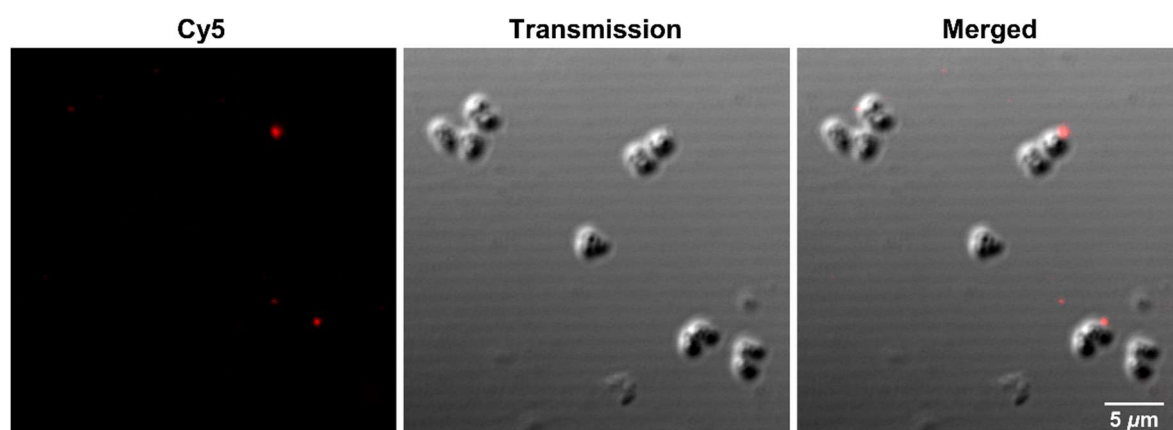
Figure 40: Fluorescence microscopy of *M. Luteus* mixed with Cy5-LYZ loaded LYZ$_{mPEG}$-nanoparticles. In the Cy5 channel (left picture), are individual signals of Cy5-LYZ detectable. The transmission picture displays the bacteria *M. Luteus* and the merged picture summarizes both channels. Considering the proximity of the Cy5 signal and the bacteria, presumably, it indicates the interaction of Cy5-LYZ with the peptidoglycan layer of *M. Luteus*. Reproduced from Steiert *et al.*[153], Copyright (2018) WILEY-VCH Verlag GmbH & Co. KGaA.

Figure 40 shows in the Cy5-channel scattered Cy5 signals. Probably demonstrating encapsulated Cy5-LYZ in LYZ$_{mPEG}$ particles or released individual Cy5-LYZ molecules. In the transmission channel, individual bacteria are recognizable. The merged picture of both channels demonstrates the proximity of the Cy5-signal and the outer part of the bacteria, presumably the bacteria cell wall. On the one hand, it could display the proximity of Cy5-LYZ loaded LYZ$_{mPEG}$ but more likely it indicates the interaction of released Cy5-LYZ with the bacteria cell wall, which will result in bacteria death. For clarification of this subject, in future, a more detailed analysis by fluorescence microscopy would be interesting for example by using a fluorescent-labeled particle material.

In summary, in the first project of this work, nanoparticles were successfully prepared by a double emulsion method after the PEGylation of LYZ. With this technique, it was possible to encapsulate hydrophilic payloads. Indeed, only the entrapment of the large antibacterial enzyme LYZ was fruitful, small antibiotics probably diffuse too fast out of the particle system. It was shown that the encapsulated LYZ was released by passive diffusion. Unfortunately, a combined effect of the particle material LYZ$_{mPEG}$ and the encapsulated native LYZ was not observed. However, the enclosed payload shows the same antibacterial activity as free LYZ, which proves that the encapsulation leads not to an impairment of the enzymatic activity during nanoparticle preparation. As a result, this protein-based nanoparticle system exhibit the potential to be commonly used for the delivery of various large hydrophilic drugs.

3.2 ACID-RESPONSIVE PROTEIN-BASED NANOPARTICLES

In the treatment of diseases, a stimuli-responsiveness of nanoparticles as a drug delivery system exhibits advantageous properties. These nanoparticles can disassemble after being exposed to a specific stimulus, which ensures a more controlled cargo release like described in section 1.1.4. For example, acid-sensitivity is a suitable tool for a triggered degradation in nanomedicine, considering that these particles have the ability to degrade in tumor tissues or during cellular uptake due to the acidic environment.[79] Until now, the drawback of the protein-based nanoparticle system developed in our group is the absence of such a triggered degradability of the nanoparticles. Concerning this, the protein modification with an acid degradable PEG will be outlined in this chapter. Additionally, as a result of the solubility switch of the protein-polymer conjugate, the nanoparticle preparation by the mild emulsion-based method will be discussed. The examination of nanoparticle degradability in slightly acid pH values will follow, which will be additionally analyzed by a triggered payload release.

The majority of the data in this section was published in Polymer Chemistry, Royal Society of Chemistry (Steiert *et al.*[184]), and is discussed in this work more in detail.

3.2.1 CYTOCHROME *c* SURFACE MODIFICATION AND ANALYSIS

First, the acid-labile PEG synthesis will be described. Subsequently, this polymer will be used for protein modification and the associated analysis will be discussed.

Synthesis of the acid-labile mP(EG-*co-iso*EPB)-NHS

The synthesis and the related analysis of the acid degradable PEG were performed in the group of ███ by ███████████████. Normally, PEG shows no acid degradability. This property was achieved by introducing vinyl ether moieties into the polymer backbone. Hawker *et al.* first described this kind of acid degradable PEG.[33a] The ████ group developed a new synthetic route to gain a lower dispersity of the polymer[33b] and to insert an end group which is necessary for protein modification. The detailed process of the polymer synthesis is summarized in Figure 41. As previously described in section 1.1.1, the polymer was synthesized by an anionic ring opening copolymerization (AROP) of ethylene oxide (EO) and 3,4-epoxy-1-butene (EPB), resulting in mP(EG-*co*-EPB). The obtained allyl residues were isomerized with a Wilkinson's catalysts $Rh^ICl(PPh_3)_3$ which results in pH-sensitive vinyl ether moieties (mP(EG-*co-iso*EPB)). Within the polymer name, *iso*EPB describes the pH-responsive vinyl ether cleavage sites.
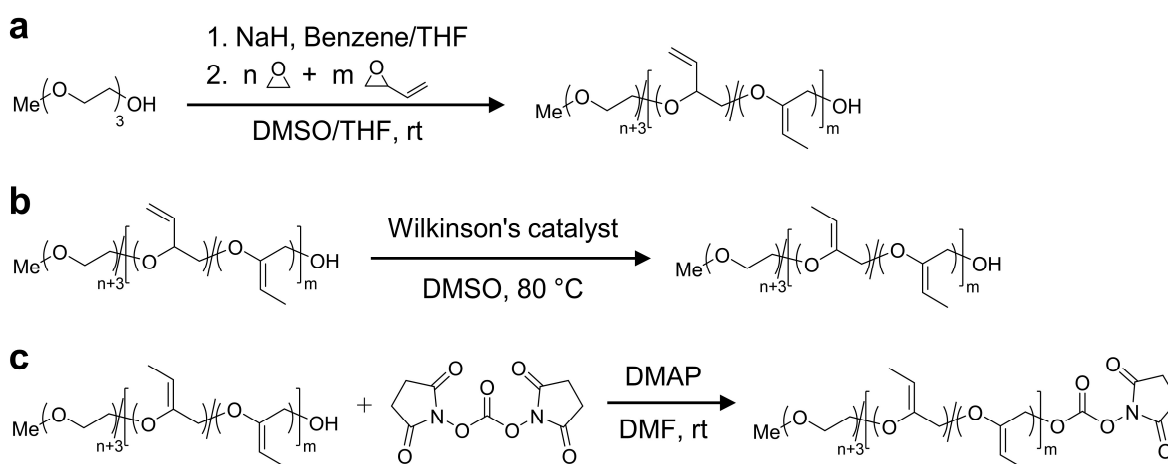
Figure 41: Synthesis route of mP(EG-*co-iso*EPB)-NHS; a) AROP of EO and EPB resulting mP(EG-*co*-EPB); b) Isomerization with a Wilkinson's catalysts to obtain mP(EG-*co-iso*EPB); c) Functionalization to an activated carbonate ester (mP(EG-*co-iso*EPB)-NHS) using NHS-DSC. The polymer synthesis was performed in the ███ group by ████████. Adapted from Steiert *et al.*[184], by permission of The Royal Society of Chemistry.

However, the end group functionalization comprised a difficulty. As described in section 3.1.1 lysine is the most addressed amino acid for protein modification. Favorite functionalization groups for lysine modification are for example activated carboxylic acids, like NHS or TFP-activated ester. For the installation of both functional groups, the polymer needs carboxylic acid end groups. However, due to the acidity of this group, proton donation is possible, resulting in vinyl ether degradation in the polymer backbone. For this reason, the polymer was synthesized with a hydroxyl-end-group in consideration of the lower acidity.[185] Subsequently, the polymer hydroxyl group was activated with *N,N'*-disuccinimidyl carbonate (NHS-DSC), which is also a frequently used method for PEG activation.[186] NHS-DSC consists of a carbonyl group with two NHS esters. The carbonyl group is highly reactive towards nucleophiles like the hydroxyl-end group of the polymer. As a reaction product, an activated succinimidyl carbonate ester (mP(EG-*co-iso*EPB)-NHS) is obtained.

After successful polymer synthesis, the detailed cleavage mechanism of mP(EG-*co-iso*EPB)-NHS in acidic conditions will be outlined. For easier description, only the acid-labile group, the vinyl ether moiety, is considered and not the whole polymer (Figure 42). First, a proton is transferred from a hydronium ion to the vinyl ether. The resulting cation intermediate directly reacts with a water molecule. The formed hemiketal decomposes quickly by building an alcohol and a ketone.[187]
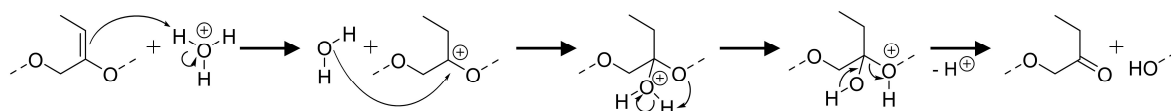
Figure 42: Cleavage mechanism of vinyl ether moieties. For easier description, only the decisive vinyl ether cleavage site is presented. First, the vinyl ether is protonated by a hydronium ion. The cationic intermediate subsequently reacts with water, which results in a hemiketal. A quick disintegration ends in an alcohol and a ketone.

The synthesis of two batches mP(EG-*co-iso*EPB)-NHS resulted in different molecular weights, NHS functionalization degrees and content of cleavage sites which is summarized in Table 7. The batch mP(EG-*co-iso*EPB)-NHS **1** was obtained with a molecular weight M_n of 4750 g mol^{-1}, a functionalization degree of 43% and an *iso*EPB content of 3 mol%. In contrast, the batch **2** shows a lower molecular weight M_n of 3320 g mol^{-1} and a lower functionalization degree of 37% but with 4 mol% more cleavage sites. The significantly lower number of cleavage sites of polymer **1** is due to the fact that the isomerization was not completely expired. For this reason, this polymer batch should only be considered as a model substance, for first conjugation and nanoparticle tests to get a general overview. However, the isomerization was improved in the synthesis of the second polymer batch. As a result, polymer **2** was used for investigations in depth.

Table 7: Comparison of molecular weight M_n, NHS functionalization degree and content of cleavage sites of two synthesized batches of mP(EG-*co-iso*EPB)-NHS. The synthesis was carried out in the ▆▆ group by ▆▆▆▆▆▆.

sample	M_n / g mol^{-1}	functionalization / %	*iso*EPB / mol%
mP(EG-*co-iso*EPB)-NHS **1**	4750	43	3
mP(EG-*co-iso*EPB)-NHS **2**	3320	37	7

For acidic degradation analysis of the polymer, **2** was dissolved in DCM, acidified with methanolic HCl (10%) and incubated overnight at room temperature. Subsequently, gel permeation chromatography (GPC) analysis was performed, which is a frequently used type of SEC for polymer analysis, separating polymers based upon their molecular weight.[188] It results in a molecular weight M_n shift from 3320 to 720 g mol^{-1}, indicating that polymer fragments with an average molar mass around 720 g mol^{-1} are formed during the degradation process (Figure 43). Furthermore, the molecular weight distribution increased from $Đ$=1.04 to $Đ$=1.53, pointing out that the produced cleavage product shows a polydispersity. Hence, looking precisely at the hydrolyzed polymer curve, polymer fragments between 200–3000 g mol^{-1} are obtained. Nevertheless, cleavage products larger than 600 Da are desirable due to kidney toxicity of PEG fragments between 200–600 Da.

Even though only very high PEG concentrations lead to it.[30] In order to avoid too small PEG fragments, the number of cleavage sites should not be increased.
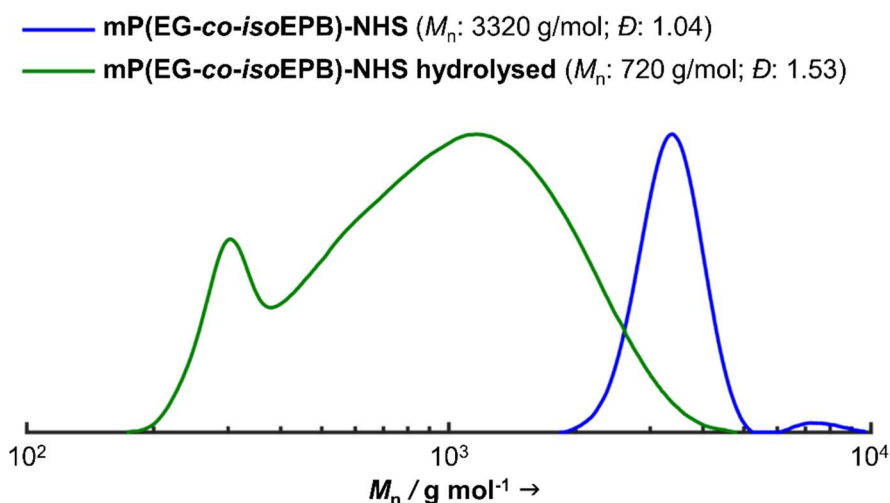
Figure 43: GPC analysis of mP(EG-*co-iso*EPB)-NHS **2** and after polymer **2** hydrolysis in acidic conditions. Polymer **2** has a molecular weight M_n of 3320 g mol^{-1} and narrow size distribution ($Đ$=1.04). Acidic cleavage results in a molecular weight M_n of 720 g mol^{-1} and an increased molecular weight distribution ($Đ$=1.53). Adapted from Steiert *et al.*[184], by permission of The Royal Society of Chemistry.

After the synthesis of the acid-sensitive polymer mP(EG-*co-iso*EPB)-NHS by ▮▮▮▮▮ ▮▮▮▮, this polymer was used for protein modification, which will be discussed in the following section.

Cytochrome *c* Modification with mP(EG-*co-iso*EPB)-NHS

In this project cytochrome *c* (Cyt), obtained from horse heart was used as a model protein. With a molecular weight of 12.4 kDa, this enzyme exhibit 19 lysine, which opens up many attachment points for polymers, comparatively to the small enzyme size. As already described in section 1.2.4 and 1.3, this enzyme has versatile roles in eukaryotes, like in the intrinsic apoptotic pathway.[135] As a result of this enzyme function, Cyt represents an interesting material in cancer therapy.

Cyt was modified with the acid degradable PEG to obtain a solubility switch (described in section 3.1.1, page 38). The enzyme PEGylation was carried out in an aqueous solution. Furthermore, basic pH conditions are required for deprotonating the ε-amines of lysine. As a result, the nucleophilic amines can attack the activated carbonate ester of the polymer. Succinimidyl carbonate linkages are highly reactive towards nucleophilic groups. Nevertheless, a disadvantage of this activated polymer is the hydrolysis of the functional group, resulting in NHS and CO_2 release. With increasing alkaline conditions, this process is accelerated.[154-155] Finding a compromise for these two decisive factors of amine

deprotonating and NHS hydrolysis, a pH value of 8.5 was chosen for enzyme modification. Figure 44 schematically demonstrates the Cyt modification with mP(EG-*co-iso*EPB)-NHS. All reactions for Cyt modification, which will be described below, were incubated overnight at 4 °C. During reaction time, a stable carbamate linkage between the enzyme and polymer was created. The reaction mixture was purified by SEC and additionally concentrated using centrifugal filters (MWCO 10 kDa). After freeze-drying, the modified enzyme (Cyt$_{degPEG}$) was obtained as a red solid.

In the first investigations, Cyt was modified with different excesses of mP(EG-*co-iso*EPB)-NHS **1**, to get an impression of the resulting acid-labile material. Subsequently, the outcomes were transferred to the enzyme modification with the second polymer batch. First, the Cyt PEGylation was tested with a 10-, 15- and 25-fold excess of mP(EG-*co-iso*EPB)-NHS **1** referring to the protein. The excess specification relates to the 43% functionalized polymer. As a result, this corresponds to a 4.3-, 6.45- and 10.72-fold excess, if only activated molecules are considered. Following, the excess will refer to the actually used eq, regardless of how much polymer has only been functionalized.
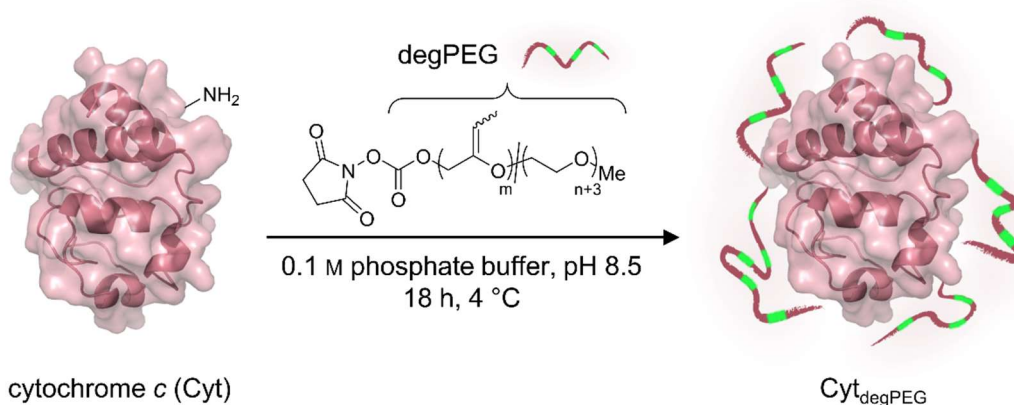
Figure 44: Surface PEGylation of cytochrome *c* (Cyt) with mP(EG-*co-iso*EPB)-NHS, resulting in schematically illustrated Cyt$_{degPEG}$. The curly bond of the polymer simplifies the two isomerization forms. The PEGylation takes place in aqueous conditions with a slightly basic pH value (pH 8.5). Adapted from Steiert *et al.*[184], by permission of The Royal Society of Chemistry.

Analysis of PEGylated Cytochrome *c*

The modified enzymes were analyzed by SDS-PAGE. Cyt$_{degPEG}$, modified with a 10-fold polymer **1** excess shows a broad band in the gel, beginning at the molecular weight of native Cyt of 12 kDa up to 170 kDa (Figure 45, lane 2). The smearing of protein-PEG conjugates in SDS-PAGEs is a typical behavior, which is described in the literature. Presumably, it is caused by interactions between SDS and polymer.[189] As a result, no exact size specification of the PEGylated enzyme is possible using this analytical method. However, considering that the broad band begins at the molecular weight of the native

Cyt, the SDS-PAGE indicates that the conversion to Cyt_{degPEG} was incompletely. Nevertheless, the PEGylation is sufficient in order to result in solubility in DCM and therefore this enzyme-polymer conjugate is applicable for nanoparticle preparation. The modification of Cyt with a 25-fold excess of polymer **1** resulted in a band between 40–170 kDa (Figure 45, lane 3). This corresponds to the expectation due to the higher polymer excess. At least 6 mP(EG-*co-iso*EPB)-NHS **1** chains (M_n=4750 g mol^{-1}) were successfully attached, considering the molecular weight increase from 12.4 kDa to at least 40 kDa. Using a lower mP(EG-*co-iso*EPB)-NHS **1** excess of 15, the band has shifted to a molecular weight from 24 kDa up to 170 kDa and no traces of native enzyme were observed (Figure 45, lane 4). This results in a supposition that at least two polymer **1** chains were successfully attached to the enzyme (11.6 kDa molecular weight increase). Also, these two Cyt_{degPEG} conjugates were soluble in DCM.
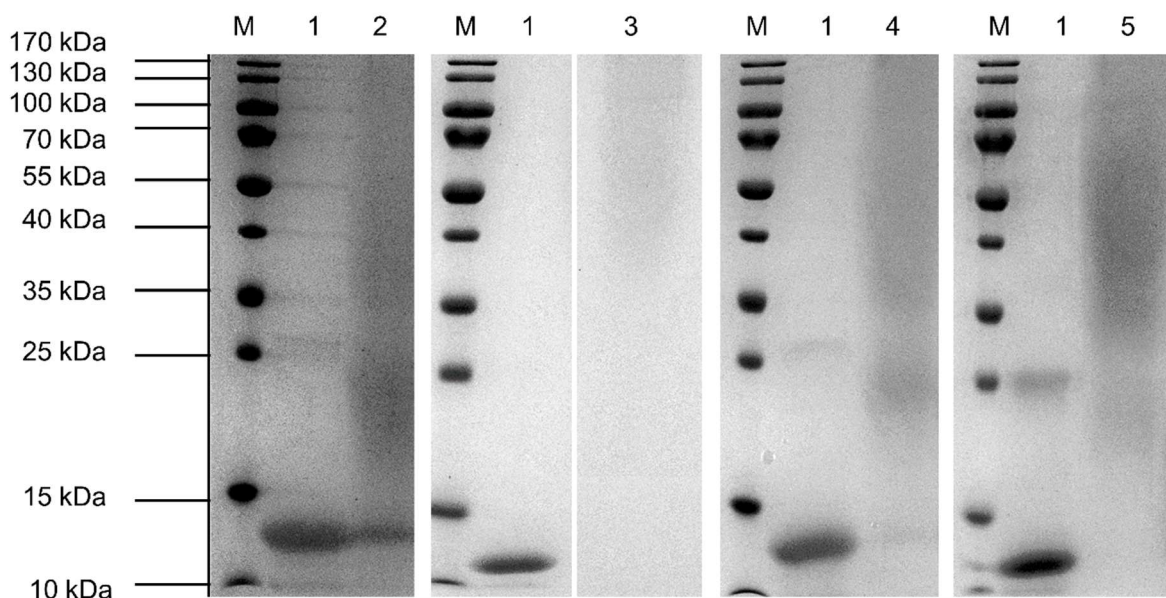
Figure 45: SDS-PAGE (15%) analysis after Cyt modification compared to native Cyt (lane 1). As protein marker (M) prestained protein ladder (10–170 kDa) was used. 120 μg of the Cyt_{degPEG} conjugates and 15 μg of the native enzyme were analyzed (first 90 V, 60 min; then 200 V, 60 min). Summary of SDS-PAGEs of Cyt-polymer conjugates after modification with a 10- (lane 2), 25- (lane 3) and 15-fold excess (lane 4) of mP(EG-*co-iso*EPB)-NHS **1**. Lane 5 shows the Cyt-polymer conjugate after enzyme modification using 17 eq of mP(EG-*co-iso*EPB)-NHS **2**. The SDS-PAGE shows the increase in molecular weight due to enzyme PEGylation. Only lane 2 shows traces of native enzyme, indicating that this conversion to Cyt_{degPEG} was incomplete.

The goal was, to find a low polymer concentration, which results in complete Cyt_{degPEG} conversion, while the product is soluble in DCM. All samples were soluble in DCM, but the Cyt modification with the 15-fold polymer excess showed the desired result. For this reason, this polymer concentration was used for further studies with mP(EG-*co-iso*EPB)-NHS **2**. Considering the lower functionalization of the second polymer batch, a slightly higher excess was applied. As a result, 17 eq of mP(EG-*co-iso*EPB)-NHS **2**

per enzyme were used for Cyt modification. The SDS-PAGE of this conjugate shows a broad band between 23–170 kDa (Figure 45, lane 5), indicating that at least three polymer chains (M_n=3320 g mol^{-1}) were successfully attached. The molecular weight is slightly lower compared to the conjugate modified with the polymer **1** excess of 15, even though one more polymer chain has been attached. This is attributed to the different molecular weights.

In the following section further analysis of the size, secondary structure and enzymatic activity of Cyt$_{degPEG}$ will be discussed. However, only the enzyme modification with the 17 eq of mP(EG-*co-iso*EPB)-NHS **2** will be considered. This enzyme-polymer conjugate shows the most promising results, which will be clarified later in section 3.2.2.

MALDI-ToF measurements revealed a molecular weight of 23.4 kDa (Figure 46), which matches the lowest area of the band in the SDS-PAGE of this enzyme-polymer conjugate. The increase of the molecular weight of 11 kDa corresponding to three attached polymer chains. This analytical method shows no traces of native enzyme too, indicating that the conversion to Cyt$_{degPEG}$ was complete.
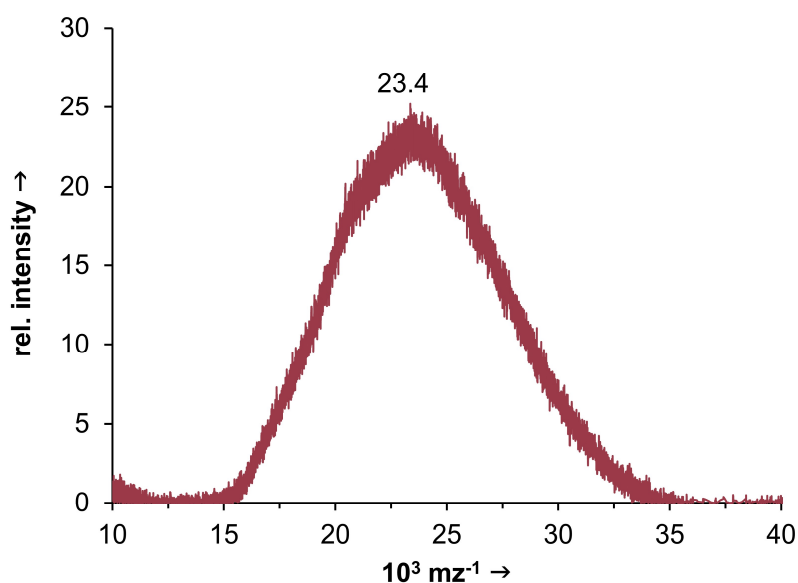
Figure 46: MALDI-ToF of Cyt$_{degPEG}$, synthesized with a 17-fold excess of mP(EG-*co-iso*EPB)-NHS **2**. Adapted from Steiert *et al.*[184], by permission of The Royal Society of Chemistry.

The investigation of the preserved secondary structure during PEGylation was analyzed by CD-spectroscopy. The spectrum of Cyt$_{degPEG}$ compared to the native enzyme show only minor changes (Figure 47). In a detailed investigation of the secondary structure elements by DichroWeb, the number of α-helices and β-sheets has only decreased around 1% each (Table 8). Around that percentage, the disordered structures have increased and in comparison, the number of turns shows almost no change. Nevertheless, the changes in secondary structure elements are so small, that they are negligible.
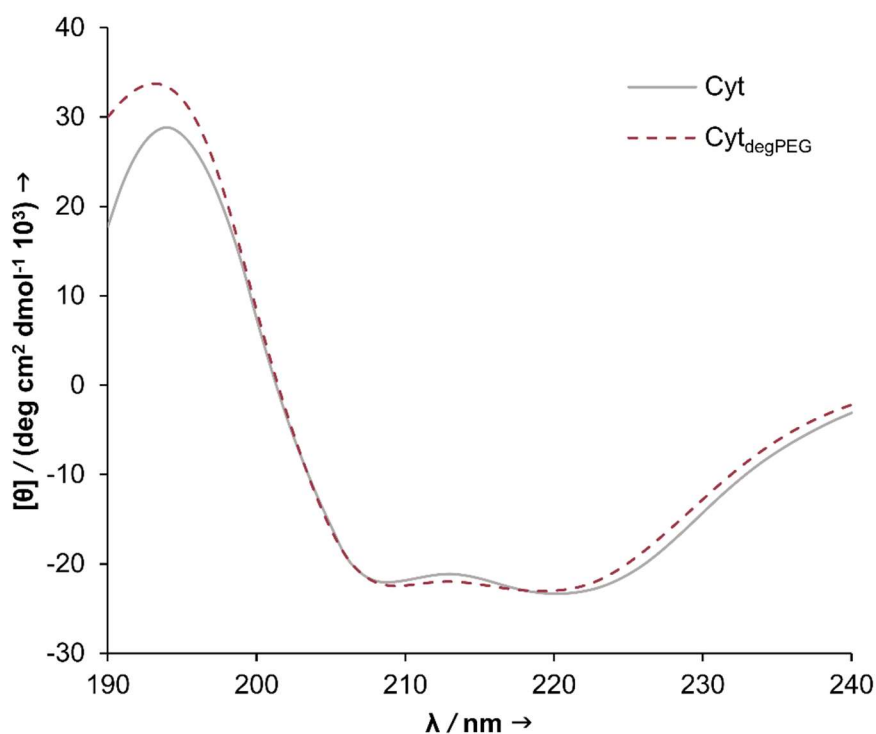
Figure 47: Circular dichroism spectra of native Cyt and modified Cyt with a 17-fold excess of mP(EG-*co*-*iso*EPB)-NHS **2** resulting in Cyt$_{degPEG}$. A comparison of both spectra results in only slight differences. A detailed comparison of secondary structure elements are summarized in Table 8. Adapted from Steiert *et al.*[184], by permission of The Royal Society of Chemistry.

Table 8: Detailed comparison of secondary structure elements of native Cyt and Cyt$_{degPEG}$ (in %) calculated by DichroWeb using CONTIN. Adapted from Steiert *et al.*[184], by permission of The Royal Society of Chemistry.

	Cyt	Cyt$_{degPEG}$
α-helices	64.4	63.1
β-sheet	3.9	2.5
turns	14.1	14.7
disordered	17.7	19.8

In addition to the described enzymatic functions in eukaryotes, Cyt has a natural peroxidase activity [134, 138], which was described in depth in section 1.2.4. For this reason, Cyt has the ability for the oxidation of various substrates in presence of H_2O_2.[136] For peroxidase activity investigation, 2-2'-azino-bis(3-ethylbenzthiazoline-6-sulfonic acid) (ABTS) is frequently used as artificial substrate. In this assay ABTS reacts with H_2O_2, catalyzed by peroxidases, resulting in a stable green radical cation (ABTS$^{\bullet+}$) which absorbs at 405 nm.[190] The detailed reaction mechanism is described in literature.[138]

For analysis, if the Cyt modification results in an alteration of the peroxidase activity, the described ABTS assay was used. Therefore, native Cyt and Cyt$_{degPEG}$ were incubated with

ABTS and H_2O_2. The formation of ABTS$^{\bullet+}$ was analyzed by measuring the absorbance at 405 nm over a period of three minutes. Slope comparison of the absorbance of the native enzyme and the PEGylated Cyt revealed a peroxidase activity of 93 ± 4% after enzyme modification (Figure 48). At this point, it must be emphasized, that in this reaction only small molecules are involved. For this reason, it is presumed that PEGylation leads not in the hindrance of substrate diffusion to the active site. Nevertheless, it can be concluded, that the modification of Cyt using 17 eq of mP(EG-*co*-*iso*EPB)-NHS **2** results in a negligible reduction of the initial peroxidase activity.
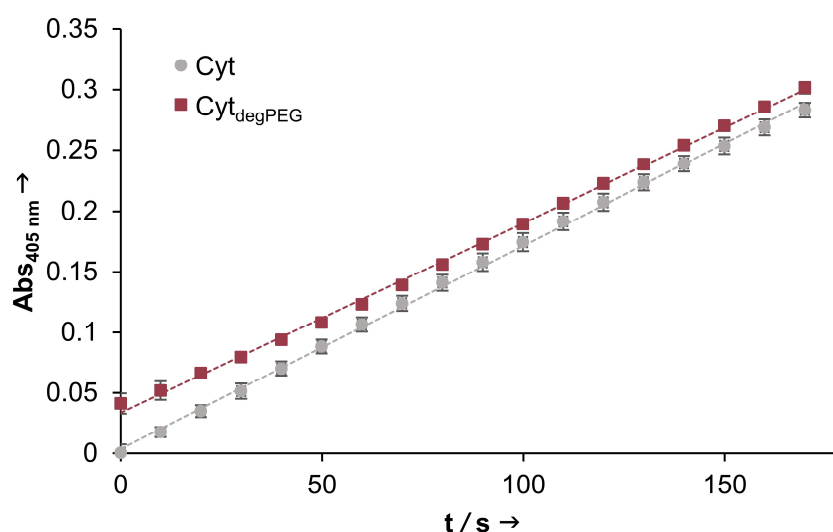
Figure 48: Result of the ABTS assay, comparing the enzymatic activity of native Cyt (grey slope) and Cyt$_{degPEG}$ (red slope) over a period of three minutes. In consideration of the peroxidase activity, the enzymes have the ability to react with ABTS in the presence of H_2O_2. It results in the ABTS$^{\bullet+}$ formation, which absorbs at 405 nm.

In summary, Cyt was successfully modified with the acid-sensitive PEG derivate mP(EG-*co*-*iso*EPB)-NHS, which results in almost no change in the secondary structure and in the enzymatic activity.

Protein-Polymer Degradation Study by SDS-PAGE and SEC

Following the Cyt modification using mP(EG-*co*-*iso*EPB)-NHS **2**, it was analyzed if the polymer is still degradable after enzyme attachment. Slightly acidic conditions should lead to vinyl ether cleavage in the polymer backbone. Considering that the cleavage sites are not directly at the functionalization group of the polymer, decomposition results in Cyt with small degradation fragments on the enzyme surface. For this reason, a completely unmodified Cyt cannot be regained. Figure 49 schematically demonstrates the Cyt$_{degPEG}$ cleavage in acidic conditions.
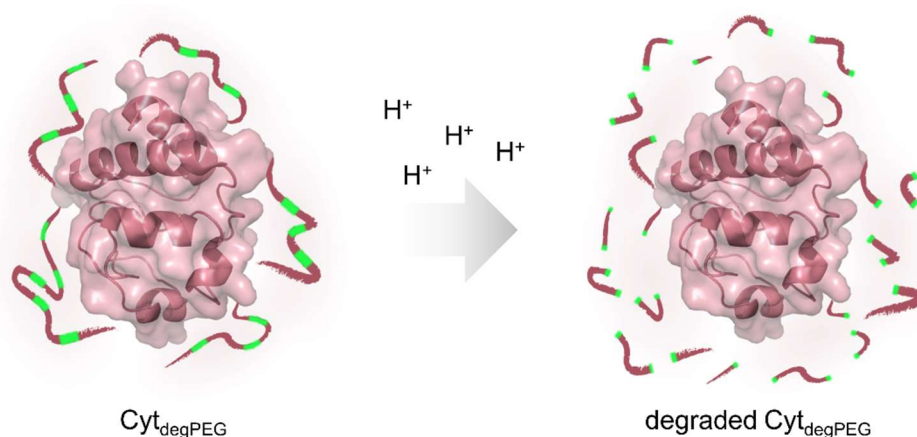
Figure 49: Schematical representation of polymer degradation of Cyt$_{degPEG}$ induced by protons. Acidic environment results in vinyl ether cleavage in the polymer backbone of the enzyme-polymer conjugate. Reproduced from Steiert *et al.*[184], by permission of The Royal Society of Chemistry.

For degradation analysis, the Cyt$_{degPEG}$ conjugate, which bears the polymer **2** chains, was incubated for one day at 37 °C in different acidic buffers and subsequently evaluated by SDS-PAGE (Figure 50).
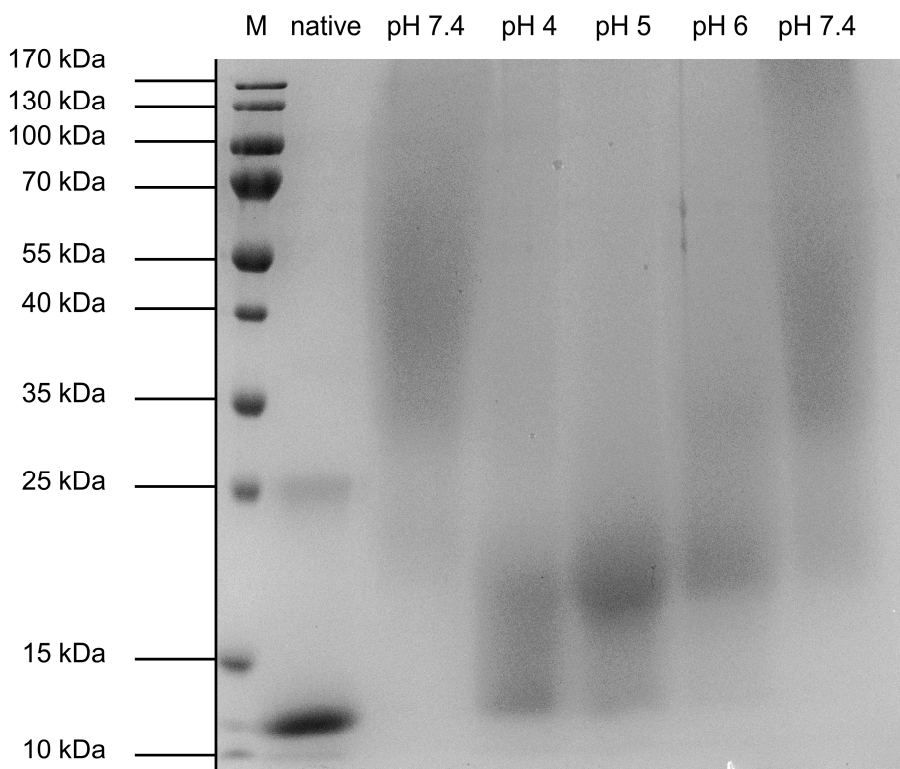
Figure 50: SDS-PAGE (15%) analysis of Cyt$_{degPEG}$ degradation. Cyt$_{degPEG}$ was incubated at 37 °C for 24 hours in different acidic and neutral buffers (pH 4, pH 5, pH 6 and pH 7.4). Subsequently, the samples were analyzed by SDS-PAGE and compared to freshly dissolved native Cyt and Cyt$_{degPEG}$ in *dd*-H$_2$O (left pH 7.4 lane). Reproduced from Steiert *et al.*[184], by permission of The Royal Society of Chemistry.

These samples were compared to native Cyt and Cyt$_{degPEG}$ (left pH 7.4 lane), which were freshly dissolved in water. Incubation in a buffer with pH 4 results in a downshifted band in the SDS-PAGE, nearly to the molecular weight of native Cyt. For this reason, this pH value seems to lead to complete polymer degradation. Nevertheless, the band is slightly smearing, which is presumably due to the polymer fragments on the enzyme surface. The incubation in a pH 5 buffer still leads to a good polymer cleavage on the enzyme surface, but not as completely as at pH 4. Furthermore, only slightly acid pH values like pH 6 are already resulting in polymer degradation (downshifted band compared to pH 7.4). Incubation of Cyt$_{degPEG}$ in physiological neutral conditions shows no change in molecular weight (left and right pH 7.4 lane). In summary, already mildly acidic conditions, as they exist in endo-lysosomal compartments, lead to a good vinyl ether degradation on the enzyme surface, while being stable in neutral surroundings.

For further examination of Cyt$_{degPEG}$ degradation, size exclusion chromatography (SEC) was used, in which bigger samples elutes faster than smaller ones. In this experiment, Cyt$_{degPEG}$ was incubated for 24 hours at the same pH values which were used for degradation analysis with SDS-PAGE (pH 7.4, pH 6, pH 5 and pH 4). After incubation time, the changed elution behavior of the samples was compared to native Cyt and freshly dissolved Cyt$_{degPEG}$ by SEC (Figure 51).
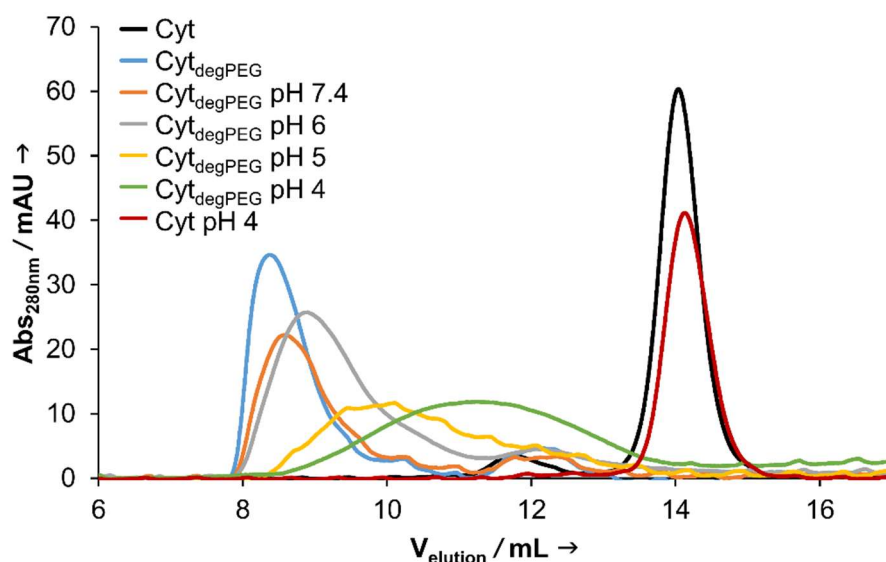
Figure 51: SEC analysis of freshly dissolved Cyt (black curve) and Cyt$_{degPEG}$ (blue curve) compared to Cyt$_{degPEG}$ incubated at various pH values at 37 °C for 24 hours (pH 7.4, orange; pH 6, grey; pH 5, yellow and pH 4, green). Native Cyt incubated at pH 4 behaves like freshly dissolved Cyt (red compared to back curve). Adapted from Steiert et al.[184], by permission of The Royal Society of Chemistry.

Since the native protein is smaller compared to Cyt$_{degPEG}$, it eluates last (Figure 51; black curve, 14 mL). Cyt$_{degPEG}$, which was incubated at pH 7.4 behaves similar to the Cyt-polymer conjugate which was dissolved freshly in dd-H$_2$O. It has the highest molecular

weight and elutes first (Figure 51; blue and orange curve, around 8.2–8.3 mL). Consequently, it can be summarized that Cyt_{degPEG} is stable at a pH of 7.4. Increasing the acidity results in expanded polymer cleavage, smaller sample sizes and longer elution times (Figure 51; grey, yellow and green curve). These results confirm with the Cyt_{degPEG} degradation analysis by SDS-PAGE. Additionally, the SEC curves show that the native enzyme is not fully regained after incubation in acidic conditions. The pH 4 Cyt_{degPEG} sample shows the biggest shift in elution behavior, nevertheless, a clear difference to native Cyt is recognizable. Again, this confirms, that polymer degradation fragments remain on the enzyme surface. Furthermore, it was analyzed by SEC that native Cyt, incubated at pH 4 for 24 hours elutes like freshly dissolved Cyt. It concludes, that changed elution behaviors are actually due to polymer degradation and not the consequence of enzyme denaturation.

In comparison, the previously described example of a protein-polymer conjugate developed by Yurkovetskiy *et al.* (see section 1.1.5), which bears several acid-sensitive acetal moieties in the polymer backbone need much more time for polymer cleavage. Thus, after 12 days only 50% of the acetal groups were degraded at pH 5.5[77], which emphasizes the better acid-sensitivity of this developed Cyt_{degPEG} conjugate.

In summary, the mP(EG-*co-iso*EPB) polymer in the Cyt_{degPEG} conjugate is degradable after protein attachment and thus, Cyt with small polymer fragment can be received. Following, the particle preparation based on Cyt_{degPEG} will be discussed.

3.2.2 CYT$_{DEGPEG}$ NANOPARTICLE PREPARATION AND DEGRADATION ANALYSIS

In this chapter, the preparation of nanoparticles based on Cyt_{degPEG} and the encapsulation of model compounds will be examined. The investigation of particle degradation in acidic conditions as well as the acid triggered release of the model compound will follow.

Cyt$_{degPEG}$ Nanoparticle Preparation

Based on the gained DCM solubility of the Cyt_{degPEG} conjugate, nanoparticles were prepared using a mild emulsion-based method (Figure 52). The goal after Cyt_{degPEG} nanoparticle (Cyt_{degPEG}-NP) formation is stability in physiological neutral conditions while degrading in an acidic environment. However, first prepared nanoparticle batches revealed that the desired particle properties depend on their composition. Based on obtained particle behavior, changes were made in the particle preparation. For this reason, nanoparticles with various differences were prepared, which were compared with each other.

Nevertheless, here, only the general differences in nanoparticle preparation will be mentioned superficially, while the subsequent chapter will discuss is more in-depth.

In this part of the thesis, the double emulsion method, as well as the single emulsion technique, were used for nanoparticle preparation. Both methods were previously described in section 1.2.2 and 3.1.2.
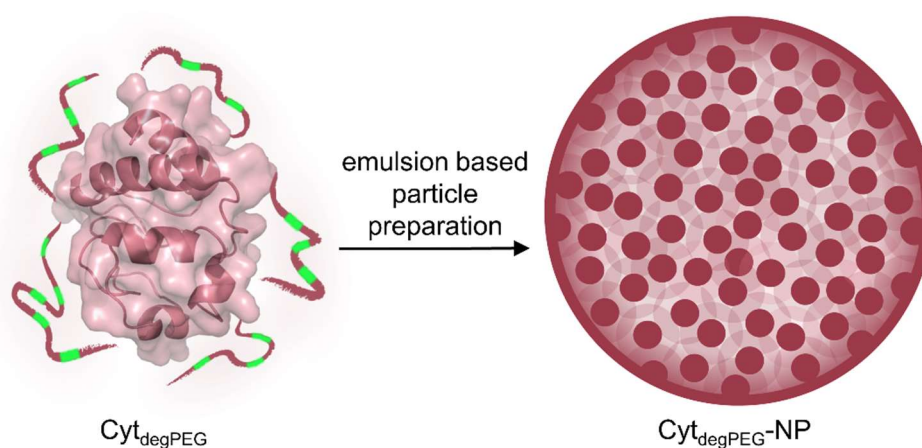
Figure 52: Schematic representation of Cyt$_{degPEG}$-nanoparticle preparation. Preparation techniques were either the double or the single emulsion method. Adapted from Steiert *et al.*[184], by permission of The Royal Society of Chemistry.

Since in this work the single emulsion method was not used yet, the detailed procedure is depicted in Figure 53. For encapsulation of a hydrophobic compound, it is dissolved in DCM together with Cyt$_{degPEG}$. For better comparison, both preparation methods were carried out with the same DCM (0.4 mL) and aqueous phase volume (2 mL).
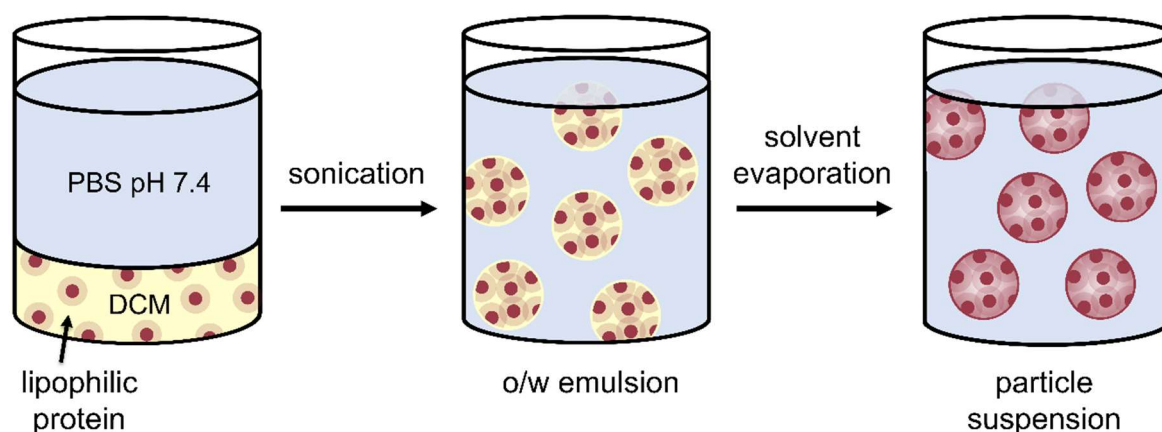
Figure 53: For the preparation of nanoparticles using the single emulsion method, Cyt$_{degPEG}$ as lipophilic conjugate is dissolved in DCM and covered with PBS pH 7.4. Sonication forms an oil-in-water (o/w) emulsion and volatile DCM removal results in the Cyt$_{degPEG}$-nanoparticle suspension.

Variations were not only made in the particle preparation technique, but also all described Cyt$_{degPEG}$ conjugates, modified with polymer **1** and **2** (see section 3.2.1), were used for

particle formation. And beyond, various amounts of Cyt_{degPEG} were applied to prepare nanoparticles.

The differences in particle preparation are summarized in Table 9. Firstly, it compiles, which polymer batch and excess was used for the enzyme modification and which technique was applied to prepare particles, the double or the single emulsion method. In addition, the table summarizes the amount of the Cyt_{degPEG} conjugate, which was used during particle preparation and if a payload was encapsulated. However, the exact particle compositions will be discussed in the following chapter, together with their influences of the particle stability and degradability. In this case, the nanoparticle size analysis will not yet be considered. Only after finding the optimal particle composition, it will be discussed in-depth.

Table 9: Summary of Cyt_{degPEG}-NP preparation. The polymer excess describes the polymer equivalents per mole protein during enzyme PEGylation. DE is the abbriviatioon of double emulsion and SE for the single emulsion particle preparation technique. The right column specify the Cyt_{degEPG} quantity used for the particle preparation.

polymer batch	polymer excess	particle preparation method	Cyt_{degPEG} / mg	payload
1	10	DE	2.5	-
1	15	DE	2.5	-
1	25	DE	2.5	-
1	15	DE	5	-
1	15	DE	1.75	-
1	15	DE	1.4	-
1	15	SE	1.75	-
1	15	SE	1.4	-
1	15	DE	1.75	+
1	15	SE	1.4	+
2	17	DE	1.6	+
2	17	DE	2.75	+
2	17	DE	3.0	+

Analysis of Nanoparticle Stability and Degradability and Payload Encapsulation

After formation of Cyt_{degPEG}-nanoparticles, the stability at physiological neutral conditions and the ability of degradation in acidic surroundings are expected. Decreased pH values lead to vinyl ether cleavage in the polymer backbone, resulting in Cyt bearing only small

polymer fragments on the surface. Considering that, the enzyme should regain its natural hydrophilicity. Within the particle this would result in losing unspecific, hydrophobic interactions, which lead to particle disassembly (Figure 54).

In the previous section, differences in the particle preparation where described, due to first tests revealed that the desired particle properties depend on their composition. For this reason, in this chapter, the differences of the prepared nanoparticles and their impact on stability and degradability in acidic conditions will be discussed. The obtained particle properties were crucial for the consequent changes, which were made in the following particle preparations. Accordingly, the alterations in particle composition will be gradually discussed in this chapter.
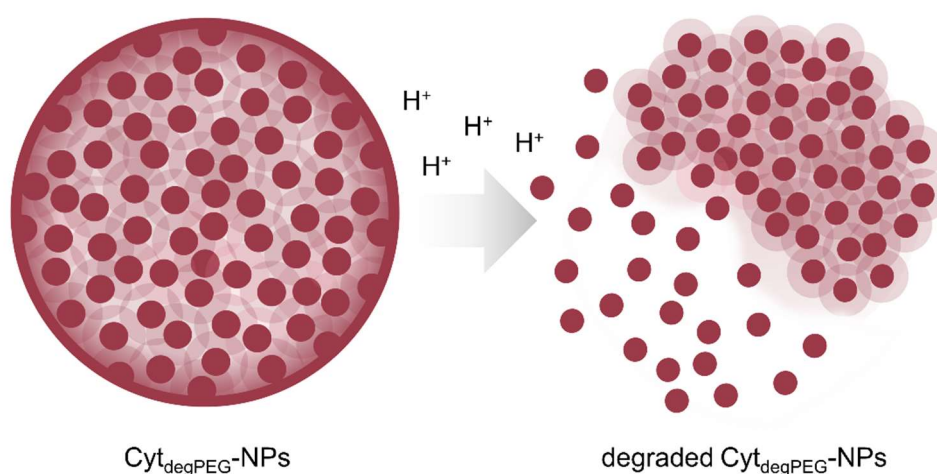
Figure 54: Schematic representation of Cyt_{degPEG}-nanoparticle disassembly in acidic conditions. Reproduced from Steiert *et al.*[184], by permission of The Royal Society of Chemistry.

For the stability and degradability investigations, freshly prepared nanoparticles were incubated in different pH values (pH 4, pH 5 and pH 7.4) at 37 °C over a period of 48 hours. The particles were analyzed by NTA measurements, in which the nanoparticle disassembly should lead to reduced particle number. The results of the examinations are summarized in Table 10 and detailed NTA curves of the degradation studies are in the appendix (section 6.4.2).

Table 10: Summary of Cyt_{degPEG}-NP degradation analysis. The polymer excess describes the polymer equivalents per mole protein during enzyme PEGylation. DE is the abbreviation of double emulsion and SE for the single emulsion particle preparation technique. (+) displays that something confirms and (-) that it does not confirm. (±) in the degradability column represents the particles degradation, but which is too slow.

polymer batch	polymer excess	particle preparation method	Cyt_{degPEG} / mg	payload	stability	degradability
1	10	DE	2.5	-	+	±
1	15	DE	2.5	-	+	±
1	25	DE	2.5	-	-	+
1	15	DE	5	-	+	-
1	15	DE	1.75	-	+	+
1	15	DE	1.4	-	-	+
1	15	SE	1.75	-	+	±
1	15	SE	1.4	-	+	+
1	15	DE	1.75	+	+	-
1	15	SE	1.4	+	+	-
2	17	DE	1.6	+	-	+
2	17	DE	2.75	+	+	+
2	17	DE	3.0	+	+	-

Influence of Cyt_{degPEG} Type: To start off the investigations, the nanoparticles were solely prepared by the double emulsion technique. In addition, in the first examination, the same amount of the Cyt_{degPEG} conjugates (2.5 mg) were used. Differences of the conjugates existed in the variation of the acid degradable polymer **1** excess (10-, 15- and 25-fold) during enzyme modification. These variations result in different nanoparticle stability and degradability behavior. Nanoparticles, based on Cyt_{degPEG}, which was modified with a 10-fold polymer **1** excess, lead to too stable nanoparticles. On the one hand, the particles show a constant particle number at pH 7.4 over two days, but on the other hand, they degrade too slowly in an acidic environment, due to nanoparticle concentration does not change after one day incubation time in decreased pH values. Only after two days, a clear particle number reduction could be noted. The particles consisting of the enzyme-polymer conjugate, modified with 15-equivalents of polymer **1**, show a similar effect. Indeed, the particles degrade faster, but still too slow. In contrast, particles built up of the modified enzyme with a 25-fold excess of **1**, decompose very good in acidic conditions but the particles were not stable at pH 7.4. The first degradation results of the Cyt_{degPEG}-nanoparticles reveal, that the degradability of the particle not only depends on the acid-

sensitive polymer but also on the overall particle composition. As a reminder, the three applied Cyt$_{degPEG}$ batches for particle preparation showed different molecular weights depending on the used excess of the polymer (section 3.2.1, Figure 45). In fact, in these nanoparticle stability experiments, more attached acid degradable polymer on the enzyme surface, result in lower stability of the prepared nanoparticles in physiological neutral and acidic conditions. Maybe it could be caused by reduced unspecific interactions between individual Cyt$_{degPEG}$ molecules within a particle, due to a higher proportion of the polymer. Since the particles composed of Cyt$_{degPEG}$, modified with 15 eq of the polymer **1**, revealed the best results in the first investigations, subsequent examinations were only carried out with this conjugate.

Influence of Cyt$_{degPEG}$ Amount: After the first findings of the nanoparticle system, next, the particle behavior consisting of different Cyt$_{degPEG}$ amounts were compared. Nanoparticles were prepared using 5 mg, 1.75 mg and 1.4 mg Cyt$_{degPEG}$ material, modified with 15 eq of the polymer **1**. On the one hand, 5 mg was chosen for the preparation to find out how the particles behave, when a very large amount of particle material is used. However, since in the first results already 2.5 mg of this conjugate revealed too stable particles, it was assumed that a smaller amount of material for particle preparation leads to the desirable properties. For this reason, 1.75 mg and 1.4 mg were further picked as particle material amounts. The particles consisting of 5 mg enzyme-polymer material were too stable, resulting in no particle degradation in acidic conditions. In contrast, particles, which were built up of 1.4 mg Cyt$_{degPEG}$, degrade at pH 4 and pH 5, but also at pH 7.4 over a period of two days. Only the Cyt$_{degPEG}$-nanoparticles, which were prepared with 1.75 mg show the desired results. These nanoparticles reveal a constant particle number at pH 7.4 and a rapid degradation behavior at pH 4 and pH 5 during an incubation time of 48 hours. The particle number decreases faster at pH 4 compared to pH 5, which was expected due to higher acidity. These results substantiate the hypothesis that the particle degradation behavior correlates with the particle composition. More particle material leads to more unspecific interactions. Following that, acidic cleavage of the polymer backbone cannot result in particle disassembly. Nevertheless, unspecific interactions between individual Cyt$_{degPEG}$ molecules are needed, since particles prepared with too less material are not stable in neutral conditions. In order to find the most favorable unspecific interactions, the optimal compositions of the particles have to be discovered. As described, for double emulsion the optimal particle composition was identified with 1.75 mg Cyt$_{degPEG}$, modified with 15 eq of the polymer **1**.

Single Emulsion Preparation: In further studies, the nanoparticle behavior of particles prepared by single emulsion was analyzed. To start off these investigations, the same Cyt$_{degPEG}$ material, modified with a 15-fold polymer **1** excess and the same amount, used for the optimal double emulsion particles (1.75 mg) was applied for the single emulsion

technique. The resulting particles were too stable, which didn't degrade in an acidic environment. The difference of both nanoparticle preparation methods is, that during the double emulsion method, there is an inner water core. Presumably, the water droplets reduce the hydrophobic interactions of individual Cyt_{degPEG} molecules during particle formation. Considering, that this reducing effect does not exist in the single emulsion method, the particle formation with this method results in more unspecific interactions of individual enzyme-polymer conjugates. 1.4 mg Cyt_{degPEG} was determined to be the optimal amount for nanoparticle preparation method by single emulsion. Over a period of two days, the prepared particles were stable at pH 7.4, but show a fast decreased particle number at pH 4 and a little bit slower degradation behavior at pH 5.

Influence of Payload: After the detection of the optimal particle compositions in the double and single emulsion, model compounds should be encapsulated into these particles to analyze an acid triggered payload release. As hydrophobic payload, Curcumin (CUR) was used for encapsulation by the single emulsion method (Cyt_{degPEG}-NP(CUR)). This yellow, natural compound is extracted out of the turmeric plant and it is considered as a potential anticancer drug.[191] Oregon-green™488-dextran (OGD, 10 kDa) was chosen as a hydrophilic payload for encapsulation by the double emulsion technique (Cyt_{degPEG}-NP(OGD)). As already investigated previously in this work, only large hydrophilic compounds remain in the particles (section 3.1.2). Small payloads fast diffuse out in the exterior water phase due to their hydrophilicity. For this reason, a large model compound was selected, which is already fluorescent-labeled for easier analysis. After CUR or OGD encapsulation, the nanoparticles were purified by dialysis to remove the not encapsulated drugs. However, both kinds of particles didn't degrade in acidic conditions, presumably due to further unspecific interactions by the payload. For this reason, if a payload should be encapsulated in the Cyt_{degPEG}-particles, in the following the optimal particle composition has to be investigated together with the encapsulated payload. Only considering the particle material without the payload is not sufficient. Additionally, only the encapsulation of the hydrophilic compounds was further examined. Taking into account that drug encapsulation has an influence on the particle stability, the assumption was that particles could rather disassemble if a payload has an additional intrinsic motivation to diffuse in the exterior aqueous phase. For first investigations, non-fluorescent labeled dextran (10 kDa) was encapsulated (Cyt_{degPEG}-NP(DEX)), since it is cheaper, but behave like OGD.

However, since the polymer **1** batch was depleted after these findings, further nanoparticles had to be prepared using Cyt_{degPEG} modified with a 17-fold excess of polymer **2**. Compared to the last examined Cyt_{degPEG} material, instead of two polymer chains, three were attached to the enzyme surface and additionally, more vinyl ether moieties are within the polymer backbone.

In comparison to preceding examinations, a lower Cyt_{degPEG} amount of 1.6 mg was used for particle preparation, since in previous approaches the particles with encapsulated OGD were too stable. Even though DEX was encapsulated, these particles were not stable enough. Concerning the changed amount of polymer chains and cleavage sites, it confirms the first nanoparticle degradation results, that also the Cyt_{degPEG} material composition has an effect on nanoparticle stability. Cyt_{degPEG}-NP(DEX) preparation using 2.75 mg of this Cyt_{degPEG} material revealed the desired degradation behavior. The nanoparticles were stable in physiological neutral conditions and degrade fast at pH 4. At pH 5 the particles also disassemble, but only after 24 hours (Figure 55). Already using 0.25 mg more Cyt_{degPEG} material, the resulting particles were too stable.
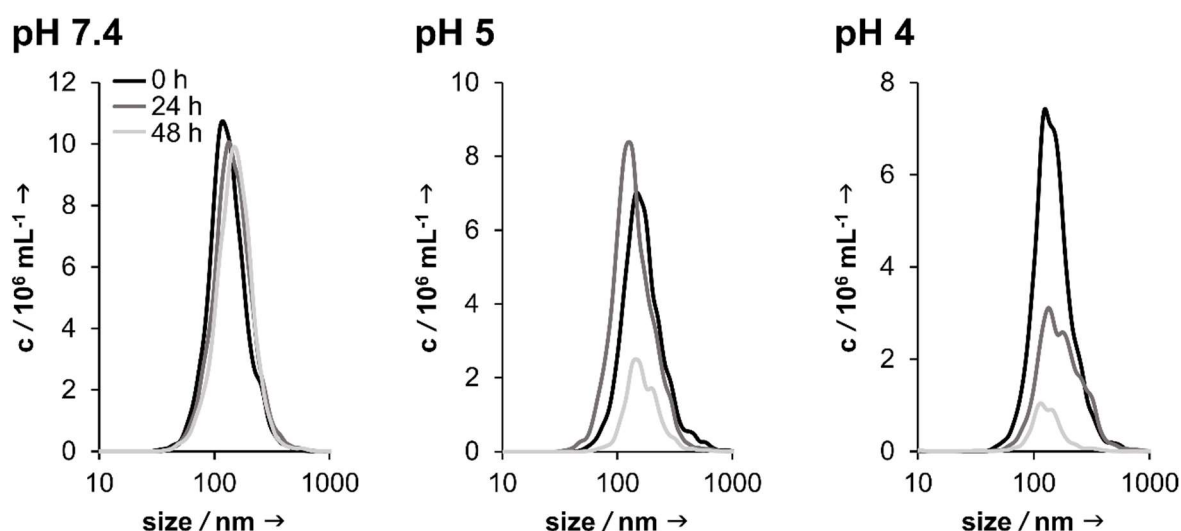
Figure 55: NTA measurements for Cyt_{degPEG}-NP(DEX) degradation analysis in acidic conditions. Nanoparticles consisting of Cyt_{degPEG}, which was modified with 17 eq of polymer **2**. 2.75 mg of this enzyme-polymer conjugate was used for the particle preparation by the double emulsion technique. Nanoparticles were mixed with different buffers (pH 7.4, pH 5 and pH 4) and incubated at 37 °C for 48 hours. For analysis, NTA measurements were performed over time (black: 0 h, grey: 24 h; light grey: 48 h).

The advantage of the developed Cyt_{degPEG}-nanoparticles becoming obvious when comparing to the already mentioned particles of self-assembled BSA-DMDOMA conjugates (see section 1.2.3). These particles bear acid-sensitive dioxolane moieties in the polymer backbone, which require extreme acid pH values for particle degradation (pH 1).[130] In contrast, the Cyt_{degPEG}-nanoparticles need a much milder acidic environment for particle disassembly, occurring for example in the endo-lysosomal pathway. Although, it required efforts to prepare Cyt_{degPEG}-particles with these desirable properties, however, an optimal particle composition using the double emulsion technique could be found. 2.75 mg Cyt_{degPEG}, modified with 17 eq of **2,** was applied for the particle preparation using a double emulsion technique for the encapsulation of DEX. For this reason, the following

sections, which will outline the detailed particle analysis and payload release, will only deal with this optimal particle batch.

Analysis of Nanoparticle Size, Morphology and Toxicity

The morphology, size and charge of this optimal composition of Cyt_{degPEG}-NP(DEX) (2.75 mg Cyt_{degPEG}, modified with 17 eq of **2**) prepared by double emulsion, was analyzed by NTA, TEM and ζ-potential measurements. Cyt_{degPEG}-NP(DEX) show an average size of 141 nm, measured by NTA (Figure 56). In comparison, the other prepared nanoparticle compositions discussed in the previous section revealed mode sizes between 110–180 nm (Table 19 in appendix). Nevertheless, no trend in Cyt_{degPEG} material amount, preparation method, payload encapsulation and particle size were recognizable. Size differences can be explained by variations during particle preparation.
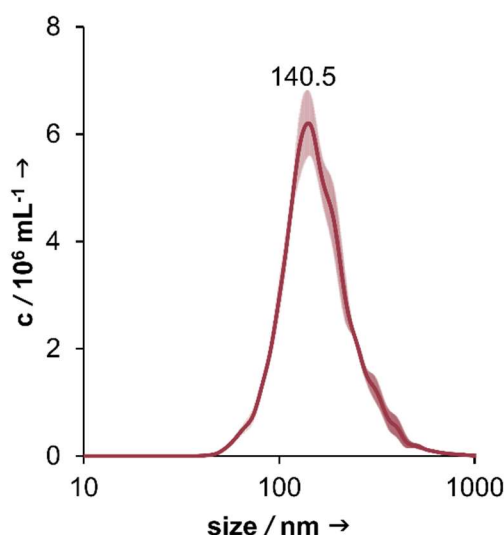
Figure 56: Size distribution of Cyt_{degPEG}-NP(DEX) determined by NTA measurement. Adapted from Steiert *et al.*[184], by permission of The Royal Society of Chemistry.

Morphology analysis of Cyt_{degPEG}-NP(DEX) by TEM confirms the size obtained by NTA. The overview image shows a narrow size distribution of different Cyt_{degPEG}-particles on the grid (Figure 57a). In contrast, Figure 57b reveals a detailed particle structure image. Small black dots inside the particle are probably individual enzymes, which are surrounded by less dense polymer chains. Furthermore, the demarcation of the particle seems diffuse, due to polymer chains, directed to the outside.
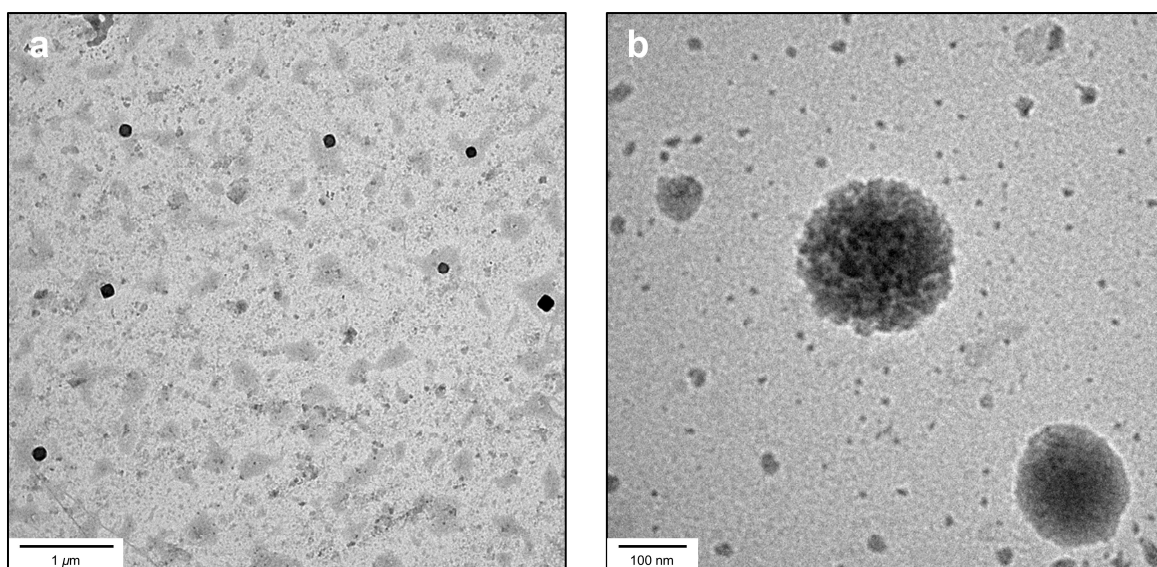
Figure 57: TEM images of Cyt_{degPEG}-NP(DEX) for size distribution (a) and morphology analysis (b). In parts adapted from Steiert *et al.*[184], by permission of The Royal Society of Chemistry.

The ζ-potential measurements revealed a value of −2 mV, which is a nearly neutral charge of Cyt_{degPEG}-NP(DEX) (Table 11). Consequently, that would mean, that the particles are not stable. Nevertheless, in the stability analysis, the nanoparticles didn't reveal a particle disassembly within two days. Furthermore, it was previously described in the literature that PEGylation can lead to a shielding effect of charge, resulting in nearly neutral particles.[192] Since the TEM image shows less dense material at the outer edge of the particle, this may indicate that PEG is directed to the outside of the particle, which could result in the described shielding effect. Additionally, during particle compositions discussion, it was shown that the unspecific interactions within the particles result in nanoparticle stability. For this reason, stable particles are expected, despite nearly neutral particle charge. Nevertheless, in the future, a detailed study of a long-term stability of the nanoparticles would be of interest.

Table 11: Result of ζ-potential measurement of dextran loaded Cyt_{degPEG}-nanoparticles. Adapted from Steiert *et al.*[184], by permission of The Royal Society of Chemistry.

sample	ζ-potential (mV)
Cyt_{degPEG}-NP(DEX)	−1.98 ± 0. 21

For the investigation of the cell viability of the Cyt_{degPEG}-NP(DEX) system, an MTT assay with HeLa cells was performed (Figure 58). After 48 hours native Cyt and Cyt_{degPEG} cause no toxicity up to concentrations of 23.50 μM. In literature it is described, that native Cyt cannot pass cytoplasm membranes.[193] As a result of the membrane impermeability, Cyt cannot induce apoptosis in the cell cytoplasm. Considering that Cyt_{degPEG}-material shows

as well no toxicity, presumably, the modified Cyt is also membrane impermeable. In contrast, Cyt$_{degPEG}$-NP(DEX) shows toxic effects in all analyzed concentrations. In the highest Cyt$_{degPEG}$-NP(DEX) concentration the cell viability is reduced by 31%. Presumably, nanoparticles are taken up in cells by endocytosis.[60] Within this pathway, the particles would degrade due to acidity in endosome vesicles.[194] Release in the cytosol would result in free Cyt bearing only small polymer fragments on the surface. This modified enzyme could induce apoptosis by binding APAF1.[135] Since this is a hypothesis for induced nanoparticle toxicity, this issue has to be analyzed in future investigations more in detail. Nevertheless, as a drug delivery system in cancer therapy additional nanoparticle toxicity in cancer cells would be favorable.

In comparison, in our group an MTT test of nanoparticles consisting of non-stimuli-responsive Cyt-PEG conjugates, reveal a cell viability of 90% at particle concentrations of 17.30 μM.[127] Here, the Cyt-PEG conjugate remains intact intracellularly since in the conjugate is no stimuli-responsiveness. As a result, the interaction of Cyt-PEG and APAF1 is sterically hindered, causing decreased apoptosis. In consideration of the above-mentioned hypothesis, this comparison pointing out that using the acid-sensitive Cyt$_{degPEG}$-nanoparticles, an almost unmodified Cyt is recovered intracellularly, increasing the induction of apoptosis.
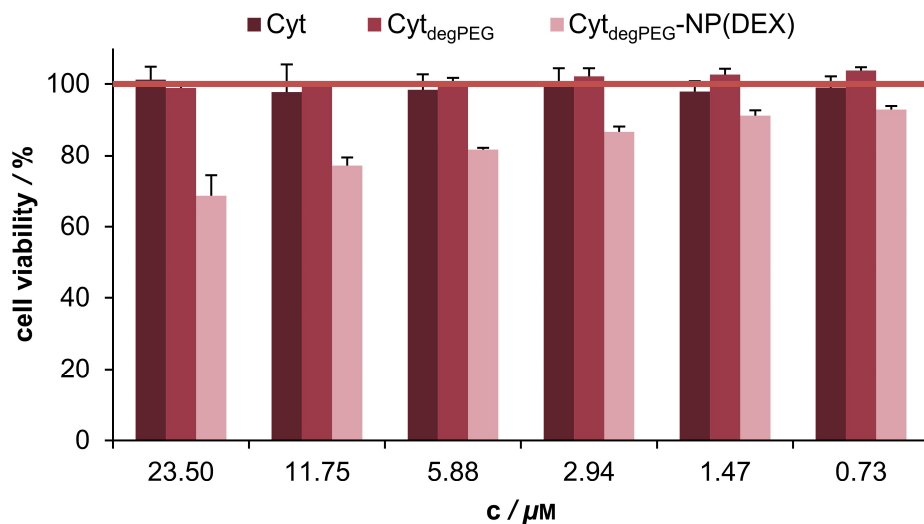
Figure 58: MTT assay results of native Cyt, Cyt$_{degPEG}$ and Cyt$_{degPEG}$-NP(DEX) incubated with HeLa-cells for 48 hours. The concentration refers to the Cyt material. Adapted from Steiert *et al.*[184], by permission of The Royal Society of Chemistry.

After detailed nanoparticle analysis, the following section will discuss the acid triggered payload release due to nanoparticle disassembly.

Payload Release from Nanoparticles

The following section will only consider the optimal particle composition. As mentioned before, 2.75 mg Cyt_{degPEG}, modified with 17 eq of **2,** was used for the particle preparation by double emulsion while encapsulation DEX. However, for investigations of acid triggered payload release, the fluorescent DEX variant (OGD) was encapsulated in Cyt_{degPEG}-nanoparticles.

For the removal of not encapsulated OGD, dialysis was performed for 4 hours against H_2O. To ensure that most free OGD with a molecular weight of 10 kDa will be removed during dialysis, an MWCO of 100 kDa was used. After nanoparticle purification, the encapsulated OGD amount was determined by fluorescent measurement (ex. 490 nm, em. 527 nm) and comparison of an OGD-standard. It results in an OGD concentration of 2.41 μM, which corresponds to an encapsulation efficiency of 50% compared to the initially used OGD feed (calculated by eq. 1). In comparison to the used particle material concentration of 58.76 μM (2.75 mg in 2 mL), it leads to 0.04 mol OGD per 1 mol Cyt_{degPEG}. Since the Cyt_{degPEG}-NP(DEX) exhibits a total weight of 2.80 mg, a loading content of 1.72 wt% OGD is obtained (calculated by eq. 2). This loading content is a little bit lower compared to LYZ_{mPEG}-NP(Cy5-LYZ) of the first project (4.78 wt%). The lower loading content is due to a lower initial OGD feed. However, this results in a higher encapsulation efficiency of 50% compared to 2.4% of the first project in this work.

For OGD release investigation out of the Cyt_{degPEG}-NP(OGD) system triggered in acidic conditions, a dialysis experiment was carried out. After nanoparticle purification by dialysis for 4 hours against H_2O the OGD loaded particles were mixed 1:1 either with pH 7.4, pH 5 or pH 4 buffer. Subsequently, the nanoparticles mixtures were placed in dialysis membranes (MWCO 140 kDa). Particles were dialyzed against the corresponding buffer mix, in order to maintain the pH value inside of the dialysis membrane. This issue is important in this experiment due to OGD fluorescent intensity depends on the pH value.[195] For the same reason, the nanoparticles were mixed with corresponding buffers before they were placed in the dialysis membrane. The dialysis experiment was carried out at 37 °C to mimic natural body temperature. Free compounds smaller than 140 kDa, like OGD or Cyt_{degPEG}, would be washed out of the dialysis membrane. The particle stability or rather particle degradation and payload release were investigated over a period of 48 hours. The particle suspensions were removed out of the dialysis membrane, particle stability was analyzed by NTA and the OGD payload release by fluorescent measurements (ex. 490 nm, em. 527 nm). The results of this experiment are summarized in Figure 59.

a

b
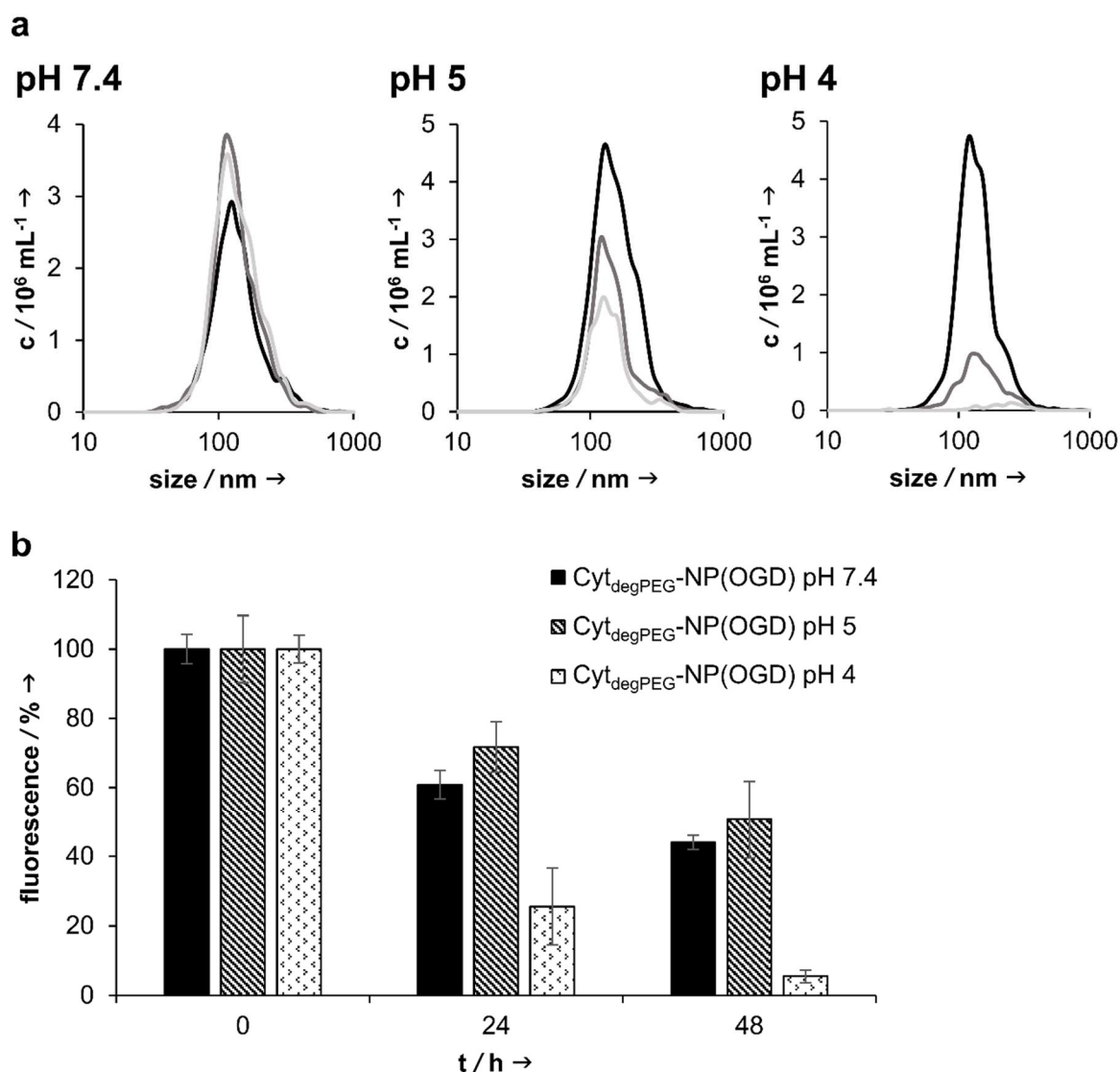
Figure 59: a) NTA measurements Cyt$_{degPEG}$-NP(OGD) during dialysis against pH 7.4, pH 5, pH 4 at 37 °C over 48 hours (black: 0 h, grey: 24 h; light grey: 48 h); b) Investigation of payload release by measuring changes of fluorescence during dialysis against pH 7.4, pH 5, pH 4 at 37 °C over 48 hours. Black bars show fluorescent changes of Cyt$_{degPEG}$-NP(OGD) dialyzed against pH 7.4, striped bars against pH 5 and angular patterned bars against pH 4. The fluorescent decrease indicates a payload release out of the particles. Adapted from Steiert *et al.*[184], by permission of The Royal Society of Chemistry.

As analyzed during particle compositions the Cyt$_{degPEG}$-NPs(OGD) were stable at physiological neutral conditions, the particle concentration does not change significantly over a period of 48 hours. In comparison at pH 5, a small particle concentration decrease was observed after 24 hours and after 48 hours the concentration was almost halved. At pH 4 a distinct particle degradation is observable. In Figure 59b, the same OGD release of around 55% at pH 7.4 and pH 5 was observed. As described previously in this work, the hydrophilic payload can release the particle by passive diffusion. Though, a pH value of 5 results in a reduced particle number but it seems to be not enough for an increased payload

release. Nevertheless, a good payload release was examined at pH 4. Already after 24 hours, 75% of the OGD is released successfully and after 48 hours nearly all OGD was removed. This result proves the acid triggered OGD release by Cyt$_{degPEG}$-nanoparticle degradation.

In summary, in this chapter, an acid-sensitive nanoparticle system was successfully developed. The particles are based on Cyt modified with a PEG, which contains acid-sensitive vinyl ether moieties. Nanoparticles were prepared using a mild double emulsion method and as hydrophilic model compounds, DEX respectively OGD, were successfully encapsulated. Additionally, an acid triggered payload release could be shown at a pH value of 4.

3.3 REDUCTIVE-RESPONSIVE PROTEIN-BASED NANOPARTICLES

Another common trigger for nanoparticle disassembly is redox-responsiveness. The most common reductive cleavable moiety is gained through disulfide bonds. However, many proteins lack in thiols. For this reason, an attachment of an artificial thiol group would be necessary. An interesting method to avoid pre-enzyme thiolation is the use of a so-called disulfide-self-immolative linker. It is an appealing method for the incorporation of disulfide linkages in thiol-free materials.[81]

In the third project of this work an enzyme modification with PEG, bearing a disulfide-self-immolative linker will be presented. The nanoparticle preparation by a mild emulsion method will be discussed, which is based on the solubility switch of the protein-polymer conjugate. Following, the nanoparticle degradability in reductive conditions will be investigated, which should lead to native enzyme recovery. In the following sections, the results of this third project are presented and discussed in detail.

3.3.1 CYTOCHROME *C* SURFACE MODIFICATION AND ANALYSIS

At the beginning of this chapter, the synthesis of the linker molecule for PEG in order to obtain the self-immolative ability will be described. The discussion of protein modification using this polymer will follow. Supplementary, to highlight the advantage of this linker, the protein will be modified using PEG without the self-immolative ability. Furthermore, at the end of this section, the analysis of the protein-polymer conjugate will be discussed.

Polymer Linker Synthesis and Activation

The synthesis of this disulfide-self-immolative-mPEG (DS-SIL-mPEG) was performed in the group of ███ ███████ by ███████████████. However, partly the second and third synthesis steps were carried out in addition by myself. The synthesis route is summarized in Figure 60. First, 2-mercaptoethan-1-ol was activated with 2,2'-dipyridyl disulfide. Subsequently, a thiol-exchange reaction between 2-(pyridin-2-yldisulfaneyl) ethan-1-ol and poly(ethylene glycol) methyl ether thiol (mPEG-SH) resulted in mPEG-(disulfaneyl)ethan-1-ol. Since the hydroxyl-group is not reactive enough for enzyme modification, it was electrophilic activated using 4-nitrophenyl chloroformate under an argon atmosphere at room temperature. The last reaction step yield in 84% of mPEG-DS-SIL nitro phenyl carbonate (carbonate-DS-SIL-mPEG). However, only 25% of the polymer was functionalized, which was calculated by ^{1}H-NMR integration (Figure 98). The reaction conditions may not have been completely inert, which could result in 4-nitrophenyl chloroformate hydrolysis. In

addition, this hydrolysis occurs increasingly at higher temperatures. Consequently, the reaction at a decreased temperature could improve the functionalization degree.[196] Since the non-functionalized polymer has no effect on the further reaction, no effort has been made to improve the functionalization. Nevertheless, in the future, this would be of interest, in order to use less material in the following application.

a

b

c
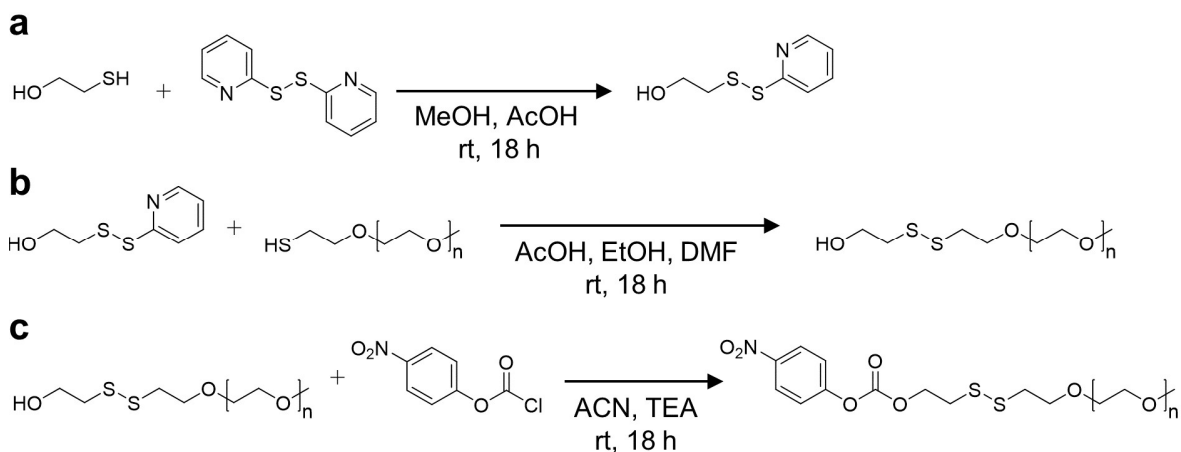
Figure 60: Synthesis route of carbonate-DS-SIL-mPEG. a) Activation of 2-mercaptoethan-1-ol using 2,2'-dipyridyl disulfide (53% yield); b) Subsequently, reaction with mPEG-SH follows (80% yield); c) Electrophilic activation of the resulting mPEG-(disulfaneyl)ethan-1-ol was carried out using 4-nitrophenyl chloroformate (84% yield, 25% functionalized). The synthesis was performed in the ▮▮▮ group by ▮▮▮▮▮ and in parts by myself.

For highlighting the benefits of the self-immolative ability of carbonate-DS-SIL-mPEG, additionally, a reductive-labile enzyme-PEG conjugate was prepared, without this special property. Therefore, mPEG-SH was activated with 2,2'-dipyridyl disulfide (Figure 61), which can be used for enzyme-SH modification. First, to ensure that the polymer is not present as a disulfide, mPEG-SH was reduced using two equivalents tris(2-carboxyethyl)phosphin (TCEP). Since TCEP reduces selective disulfide bonds and is unreactive toward many other functional groups, it is often used as a reducing agent in biochemistry.[197] Furthermore, TCEP has the advantage over the reducing agent dithiothreitol (DTT), that it is more stable in aqueous solution and it reduces disulfide linkages irreversibly.[198] Subsequently, after an overnight reaction, 21 eq of 2,2'-dipyridyl disulfide was added and incubated overnight. On the one hand, this high excess was used considering that the reducing agent is still in the reaction solution and on the other hand to prevent homocoupling of mPEG-SH. The mixture was purified by SEC and after freeze-drying, the activated polymer (mPEG-S-S-Py) was obtained as a white solid in a yield of 67%. However, despite the lower yield compared to carbonate-DS-SIL-mPEG, the functionalization degree of mPEG-S-S-Py was 89%, which was calculated by ^{1}H-NMR integration (Figure 99). After activation, the pyridine disulfide group of mPEG-S-S-Py has the ability to react with thiol-containing molecules by forming a new disulfide linkage.
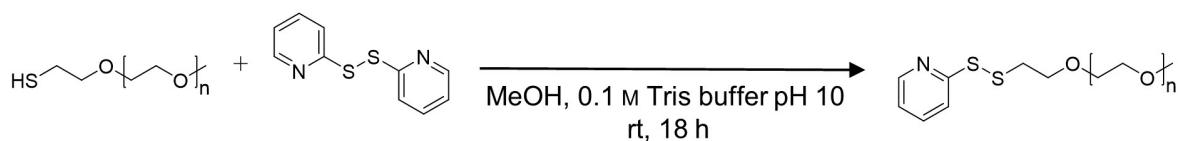
Figure 61: Thiol activation of mPEG-SH using 2,2'-dipyridyl disulfide, which results in mPEG-S-S-Py (67% yield, 89% functionalized).

During linker synthesis and mPEG activation, both used mPEG-SH chains have a molecular weight of 2 kDa. After presenting the PEG linker synthesis and activation, the following section will focus on the protein PEGylation.

Cytochrome *c* PEGylation

Like in the second project of this work, Cyt was also used as a model enzyme for the reductive-labile PEGylation. The Cyt PEGylation using the carbonate-DS-SIL-mPEG takes place in aqueous solution with a slightly alkaline buffer (pH 8). Like described in the other two projects in this work, in basic conditions, amines of the lysine are deprotonated, resulting in the ability to nucleophilic attack the polymer. The carbonate ester of the polymer has the disadvantage of hydrolysis instability, which is expended in increasing basic buffers.[154-155] For this reason, a pH value of 8 was chosen as a compromise. Cyt was modified with a 30-fold excess of carbonate-DS-SIL-mPEG per enzyme, incubated for 48 hours at room temperature (Figure 62). The excess specification relates to the 25% functionalized polymer. As a result, this corresponds to a 7.5-fold excess, if only activated molecules are considered.
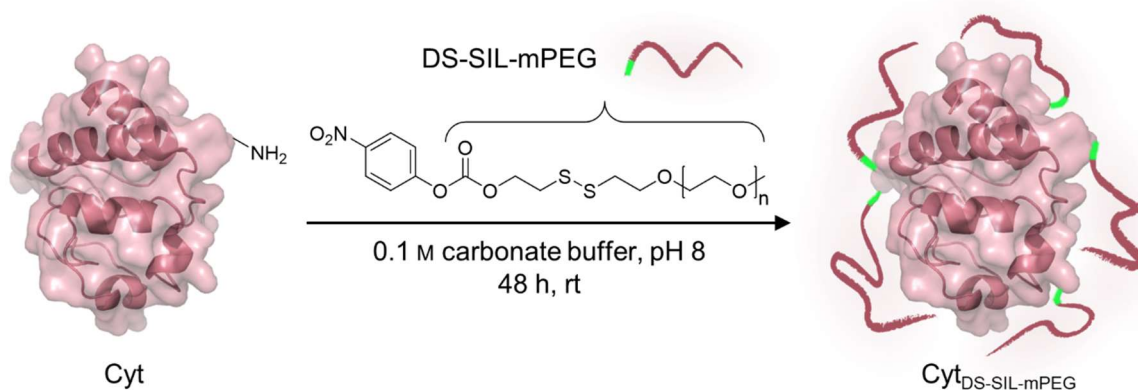
Figure 62: Surface PEGylation of Cyt using carbonate-DS-SIL-mPEG, which results in the schematical illustrated Cyt$_{DS-SIL-mPEG}$. The reaction takes place in aqueous solution at a slightly basic pH value (pH 8).

The conjugation reaction results in a carbamate linkage between Cyt and the polymer. The mixture containing the enzyme-polymer conjugate was purified by centrifugal filters (MWCO 10 kDa) and after freeze-drying $Cyt_{DS-SIL-mPEG}$ was obtained as red solid.

As mentioned before, enzyme PEGylation was also performed with mPEG-S-S-Py, which is highly reactive towards free thiol groups. Considering, Cyt has no free thiol, artificial SH-groups are introduced on the enzyme surface. Therefore, a suitable linker molecule is N-succinimidyl-S-acetylthiopropionate (SATP). Cyt amines react with the electrophilic NHS ester of the SATP linker, resulting in an acetyl protected sulfhydryl group on the enzyme surface (Figure 63). For Cyt modification, 19 eq of SATP per enzyme was used. SATP was dissolved in DMSO and combined with Cyt in aqueous solution. After an incubation time of 1 hour, the mixture was purified by centrifugal filters (MWCO 10 kDa). After freeze-drying Cyt_{SATP} was obtained as red solid. The acetylation of the sulfhydryl group protects the thiol group for oxidation to undesired disulfides,[199] consequently long-time storage of Cyt_{SATP} is possible.
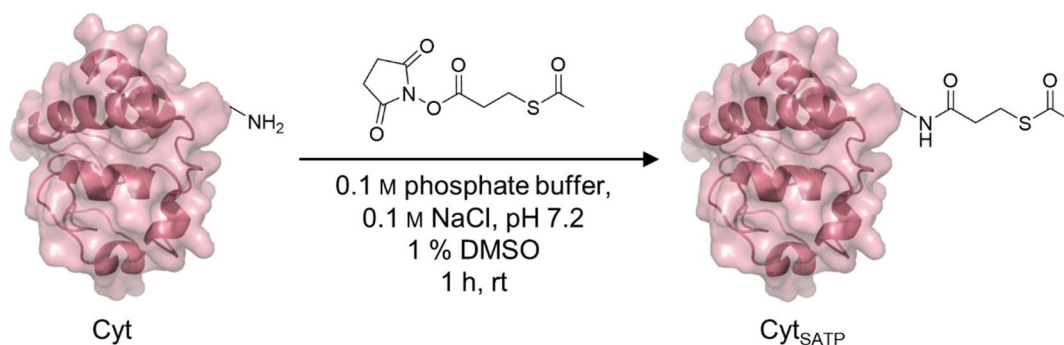
Figure 63: Introducing of protected thiol-groups on Cyt using SATP.

The Cyt modification with SATP results in a decreased number of primary amines. For this reason, the SATP modification degree can be indirectly determined by a comparison of the amine number of native Cyt and Cyt_{SATP}. An advantage over a direct thiol quantification method is that this assay can be carried out without deprotecting the sulfhydryl groups of SATP. A TNBS assay was used for primary amine quantification. During this assay, amines react with 2,4,6-trinitrobenzene sulfonic acid (TNBS) resulting in a highly orange-colored product whose absorbance can be determined at 335 nm.[200] This assay revealed around three primary amines in Cyt_{SATP}. Consequently, 16 SATP molecules were successfully attached, due to the original 19 amines of the native enzyme.

For subsequent PEGylation of Cyt_{SATP} the acetyl protecting group has to be removed, resulting in Cyt_{SH} with free thiols (Figure 64a). Accordingly, Cyt_{SATP} was incubated with a deacetylation solution containing an excess of the reducing agent hydroxylamine. After two hours of incubation time, the mixture was purified by centrifugal filters (MWCO 10 kDa) for hydroxylamine removal. The resulting enzyme with free thiol groups

was immediately used for PEGylation. Therefore, Cyt_{SH} was mixed with mPEG-S-S-Py in an aqueous buffer (pH 7.4) containing EDTA. In a thiol-disulfide exchange reaction, the thiol of the enzyme reacts with the pyridyl-disulfide activated polymer. It yields in $Cyt_{S-S-mPEG}$ as asymmetric disulfide product (Figure 64b) after the elimination of the inert 2-pyridinethione leaving group.[201] Unwanted Cyt_{SH} oxidation to homo-dimerization products is weakened by EDTA in the reaction solution,[202] which ensures that only the desired enzyme-polymer conjugate is obtained. For Cyt_{SH} PEGylation 10 eq of mPEG-S-S-Py per enzyme were used. Since only 89% of the polymer was functionalized, the specification corresponds to an 8.9-fold excess, if only activated molecules are considered. After overnight reaction at room temperature, the enzyme-polymer conjugate was purified by centrifugal filters (MWCO 10 kDa) and lyophilization results in $Cyt_{S-S-mPEG}$ as red solid.
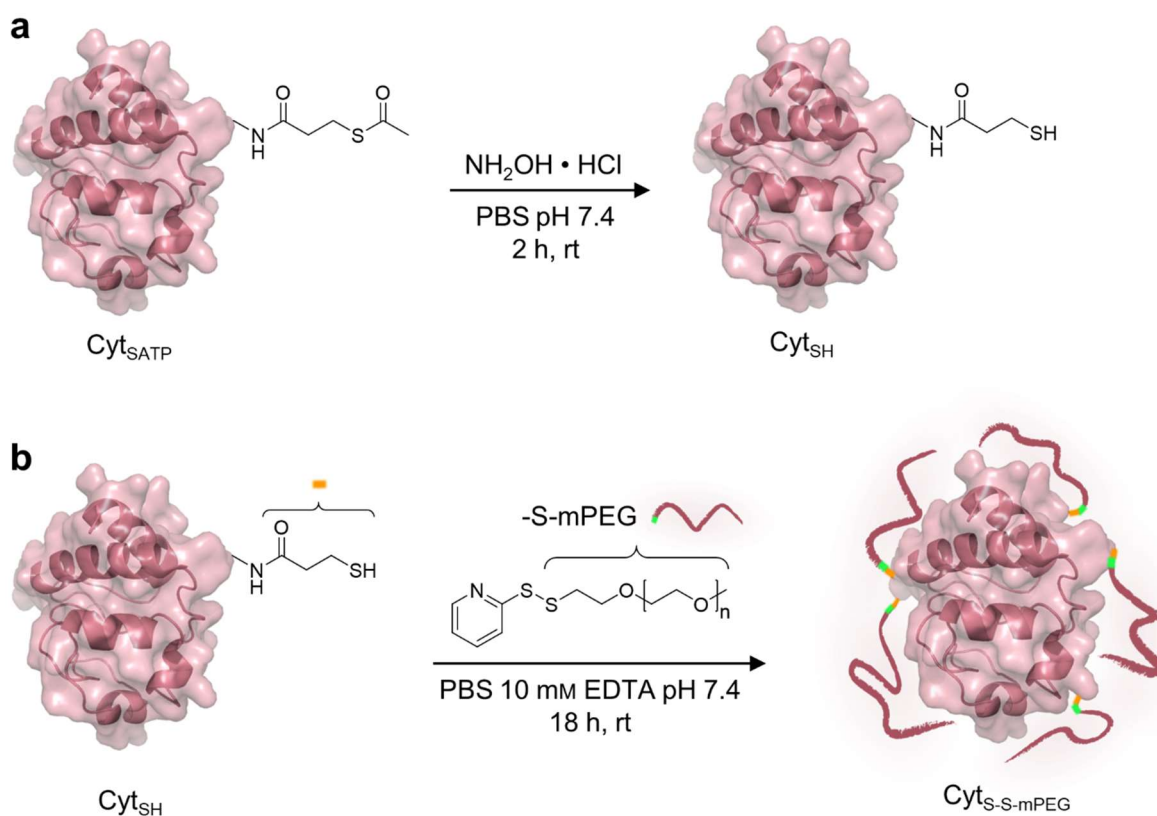
Figure 64: Synthetic route of Cyt_{SATP} PEGylation using mPEG-S-S-Py. a) First, SATP on the enzyme surface was deprotected with hydroxylamine. b) Immediately, the free thiol group was PEGylated with mPEG-S-S-Py in a thiol-disulfid exchange reaction, resulting in $Cyt_{S-S-mPEG}$.

After describing both enzyme PEGylation methods, a detailed analysis of the enzyme-polymer conjugate follows. The aim of attention is on the preparation of nanoparticles consisting of the enzyme-polymer conjugate with the self-immolative ability. As a result, the following chapter focuses only on the analysis of $Cyt_{DS-SIL-mPEG}$.

Analysis of PEGylated Cytochrome *c*

The SDS-PAGE was performed with a loading buffer, which contains no β-mercaptoethanol (section 5.3.4), in order not to reduce the disulfide bond of the enzyme-polymer conjugate. The resulting SDS-PAGE of Cyt$_{DS\text{-}SIL\text{-}mPEG}$ show small traces of native Cyt and a broad smear from 17–100 kDa (Figure 65). Considering the molecular weight of native Cyt of 12.4 kDa, it indicates that at least two polymer chains were successfully attached on the enzyme surface of Cyt$_{DS\text{-}SIL\text{-}mPEG}$.
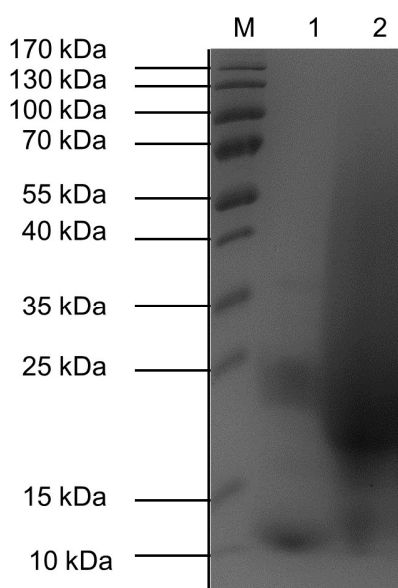
Figure 65: SDS-PAGE (15%) analysis of Cyt$_{DS\text{-}SIL\text{-}mPEG}$ (lane 2) compared to native Cyt (lane 1). As protein marker (M) prestained protein ladder (10–170 kDa) was used. 120 μg of the Cyt$_{DS\text{-}SIL\text{-}mPEG}$ conjugate and 15 μg of the native enzyme were analyzed (first 90 V, 60 min; then 200 V, 60 min). The SDS-PAGE shows an increased molecular weight of Cyt$_{DS\text{-}SIL\text{-}mPEG}$ due to enzyme PEGylation. Only minor traces of native enzyme are observable, indicating that this conversion to Cyt$_{DS\text{-}SIL\text{-}mPEG}$ occurred not fully completely.

MALDI-ToF measurement show a similar result, but several maxima were detected (Figure 66). Beginning at 14.5 kDa up to 27.1 kDa local maxima are observable in 2.1 kDa steps, displaying the exact number of attached polymer chains. Since the attached polymer has a molecular weight of 2.1 kDa, due to additional 0.1 kDa of the linker molecule, it concludes that 1 up to 7 polymers were attached to Cyt. The global maximum is detected at 22.9 kDa, indicating that most enzymes bear 5 DS-SIL-mPEG chains. Furthermore, also small traces of native Cyt are recognizable in the MALDI-ToF spectrum. Nevertheless, Cyt$_{DS\text{-}SIL\text{-}mPEG}$ is fully soluble in DCM and therefore suitable for nanoparticle preparation.
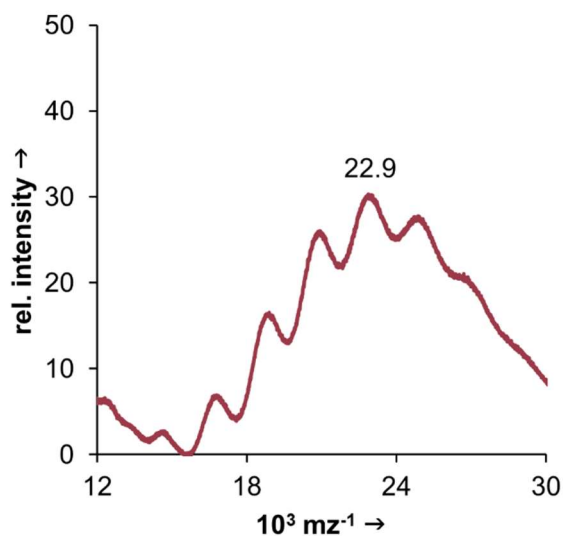
Figure 66: MALDI-ToF of Cyt$_{DS\text{-}SIL\text{-}mPEG}$ with several local maxima, which confirm the increase in molecular weight. Also, minor traces of native Cyt are detectable in the MALDI-ToF.

For analysis of structural integrity after enzyme PEGylation, CD spectroscopy was performed. The CD spectrum of Cyt$_{DS\text{-}SIL\text{-}mPEG}$ in Figure 67 shows only minimal changes in the secondary structure.
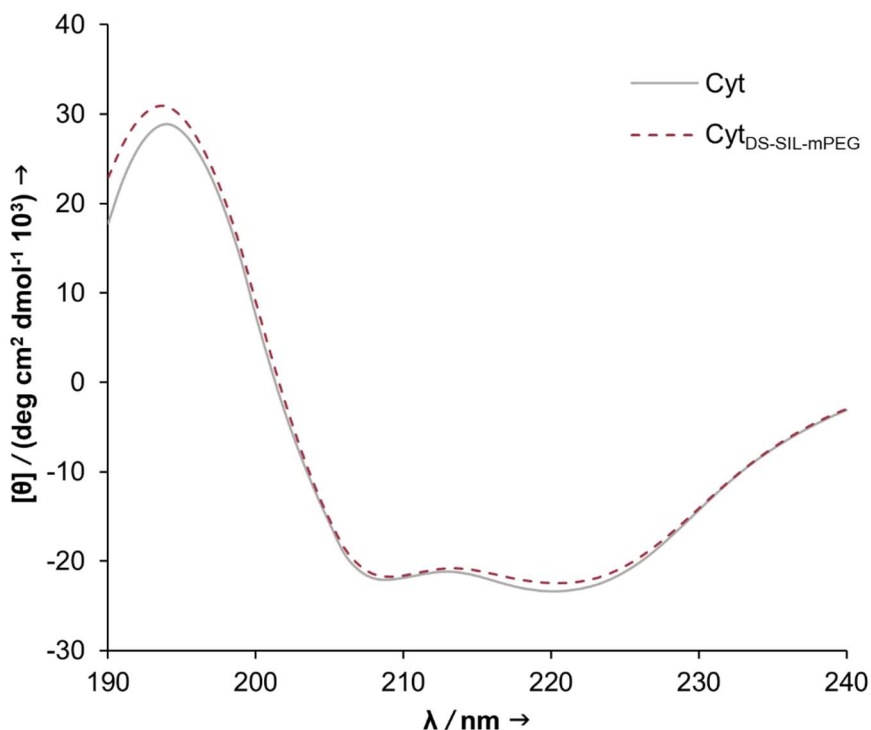
Figure 67: Circular dichroism spectra of native Cyt (grey) and Cyt$_{DS\text{-}SIL\text{-}mPEG}$ (dotted, red). Comparison of both CD spectra shows only minor differences, suggesting that Cyt PEGylation with carbonate-DS-SIL-mPEG results in nearly no impairment of the secondary structure. Detailed analysis of secondary structure elements is summarized in Table 12.

During a detailed comparison of secondary structure elements, it is observable that all three, α-helices, β-sheets and turns, decrease around 3-4% (Table 12). As a result, the disordered structures increased around the sum of the other structural changes of 11%. Nevertheless, it is only a marginal change in secondary structure and for this reason, considered as negligible.

Table 12: Detailed calculated secondary structure elements of native Cyt and Cyt$_{DS-SIL-mPEG}$ (in %) by DichroWeb using CONTIN.

	Cyt	Cyt$_{DS-SIL-mPEG}$
α-helices	64.4	61.0
β-sheet	3.9	0.4
turns	14.1	10.3
disordered	17.7	28.4

For the investigation, if the PEGylation of Cyt using carbonate-DS-SIL-mPEG results in an enzymatic activity change, an ABTS assay was carried out, which is described in detail in section 3.2.1. Native Cyt and Cyt$_{DS-SIL-mPEG}$ were incubated with ABTS and H_2O_2. The ABTS$^{\bullet+}$ formation was analyzed over a period of three minutes by measuring the absorbance at 405 nm (Figure 68). The PEGylated Cyt reveals an enzymatic activity of $101.1 \pm 2.4\%$ calculated by comparison of ABTS cation radical formation slopes. Consequently, the ABTS assay proves no impairment of the enzymatic activity of Cyt$_{DS-SIL-mPEG}$ compared to native Cyt.
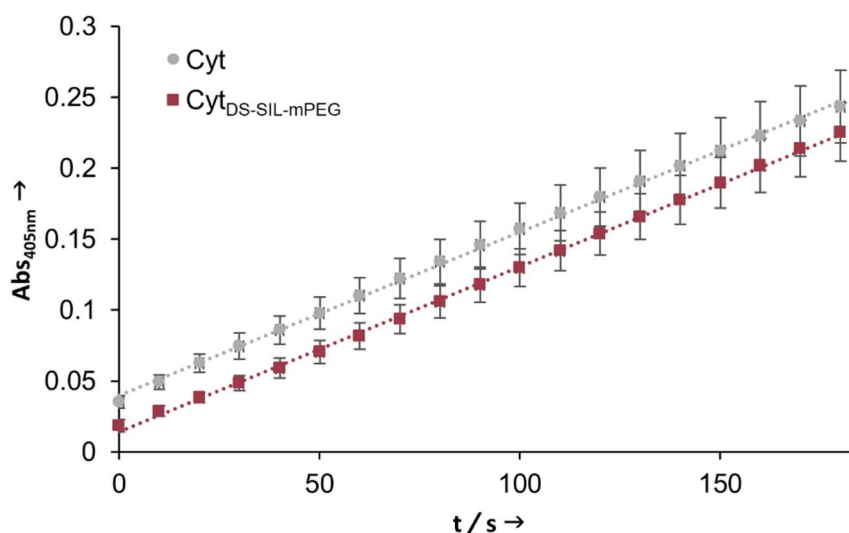
Figure 68: Result of the ABTS assay, comparing the enzymatic activity of native Cyt (grey slope) and Cyt$_{DS-SIL-mPEG}$ (red slope) over a period of three minutes. In consideration of the peroxidase activity, the enzymes have the ability to react with ABTS in presence of H_2O_2 by formation of ABTS$^{\bullet+}$, which absorbs at 405 nm.

In summary, Cyt$_{DS\text{-}SIL\text{-}mPEG}$ analysis has proven the successful enzyme PEGylation, due to molecular weight increase. Furthermore, it was shown, that the enzyme modification results in preserved secondary structure and enzymatic activity.

Protein-Polymer Degradation Study by SDS-PAGE

After the PEGylation of Cyt using carbonate-DS-SIL-mPEG, the self-immolative ability of the attached PEG chains was analyzed in reductive conditions and compared to Cyt$_{S\text{-}S\text{-}mPEG}$. Here, reductive conditions lead to disulfide cleavage, resulting in thiol-mPEG and Cyt$_{SH}$, which still bears the deprotected SATP linker group (Figure 69a). In this case, the native enzyme will not be recovered. The reduction of the disulfide-bond of Cyt$_{DS\text{-}SIL\text{-}mPEG}$ leads also to a free thiol-group, but in contrast, this group initiates a further reaction. The thiol reacts with the carbamate linker group, resulting in the five-membered cyclic side product 1,3-oxathiolan-2-one and thiol-mPEG (Figure 69b). In this cleavage mechanism, the native Cyt is recovered.
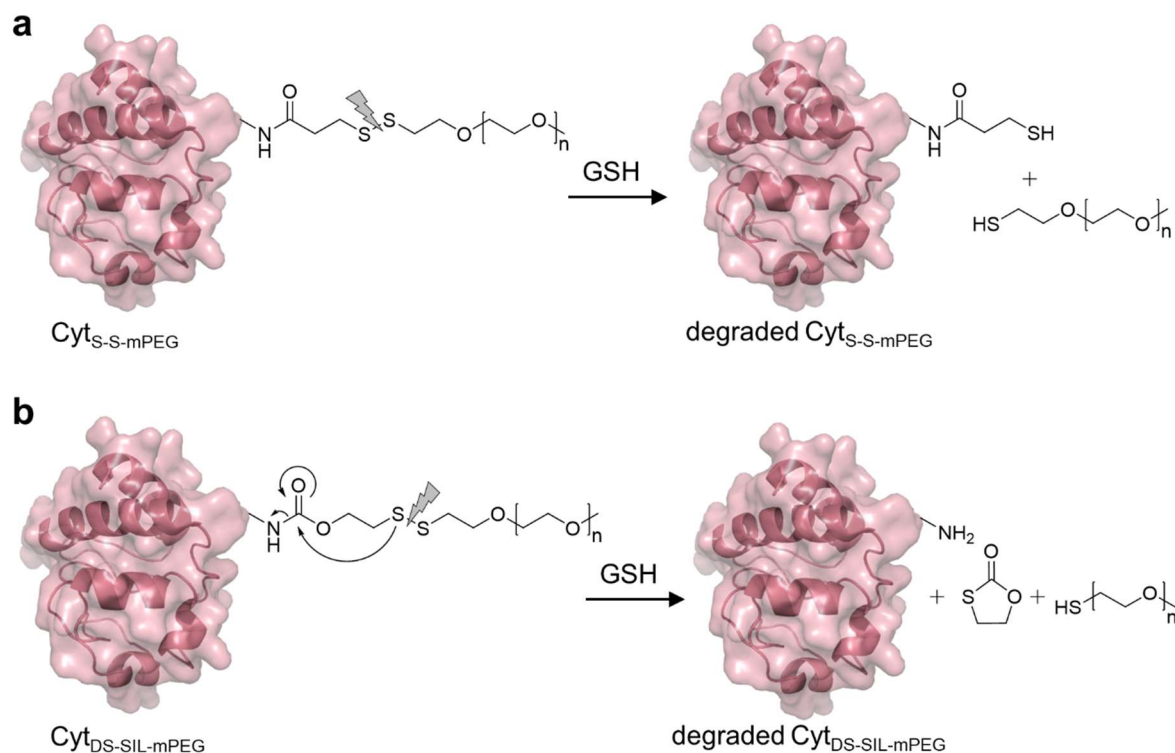
Figure 69: Schematic representation of reductive cleavage of Cyt$_{S\text{-}S\text{-}mPEG}$ (a) and Cyt$_{DS\text{-}SIL\text{-}mPEG}$ (b) using GSH. Reduction results in Cyt$_{S\text{-}S\text{-}mPEG}$ still bearing the deprotected SATP linker. In contrast, native Cyt is obtained during Cyt$_{DS\text{-}SIL\text{-}mPEG}$ reduction due to the self-immolative linker between Cyt and thiol-mPEG.

As already mentioned in section 1.1.4, inside of cells, the tripeptide glutathione (GSH) has the ability to reduce the disulfide bond. The extracellular GSH concentration is only in the submicromolar range and in contrast inside of cells it is present in high concentration up

to 10 mM.[66] For reductive degradation comparison, $Cyt_{S-S-mPEG}$ and $Cyt_{DS-SIL-mPEG}$ were incubated for one day at 37 °C in an aqueous 10 mM GSH solution. This GSH concentration was chosen to mimic intracellular reductive conditions. In addition, both enzyme-polymer conjugates were incubated in PBS pH 7.4 buffer as control. All samples were analyzed using a non-reducing SDS-PAGE and compared to freshly dissolved enzyme-polymer conjugates in dd-H$_2$O (Figure 70).
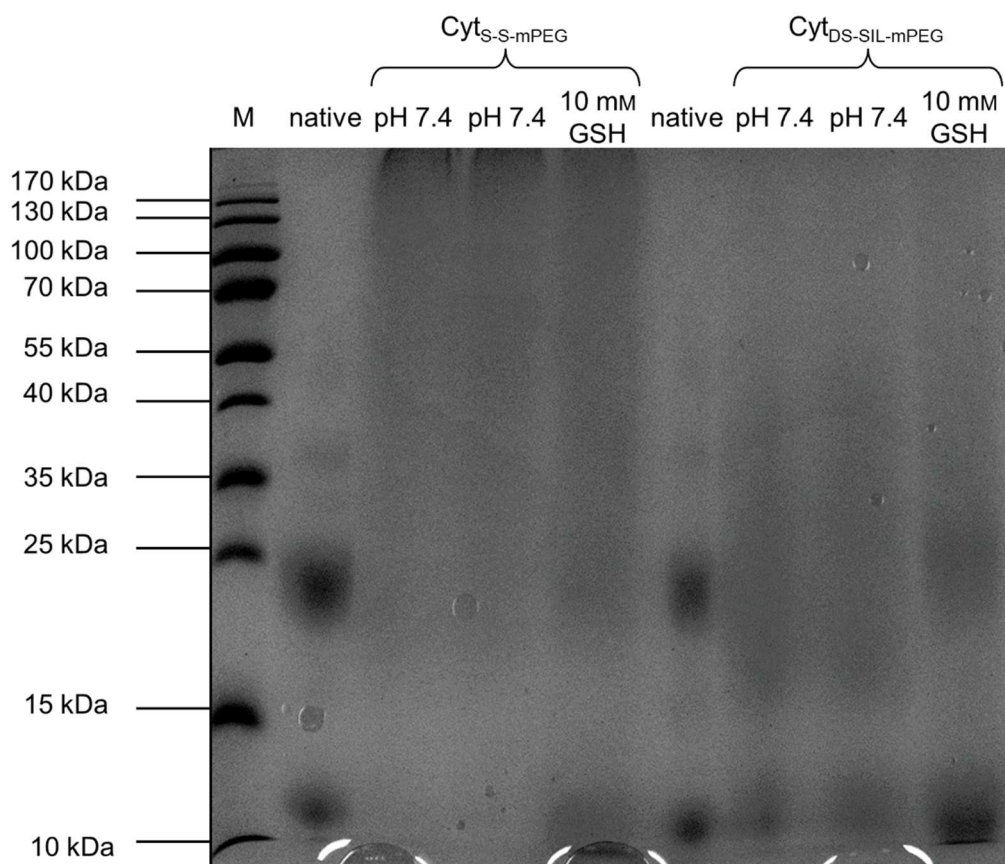
Figure 70: SDS-PAGE (15%) analysis of $Cyt_{S-S-mPEG}$ and $Cyt_{DS-SIL-mPEG}$ degradation. The enzyme-polymer conjugates were incubated for 24 hours at 37 °C in PBS pH 7.4 as control ($Cyt_{S-S-mPEG}$ right pH 7.4, $Cyt_{DS-SIL-mPEG}$ right pH 7.4) or in a 10 mM GSH containing aqueous buffer ($Cyt_{S-S-mPEG}$ 10 mM GSH, $Cyt_{DS-SIL-mPEG}$ 10 mM GSH). Subsequently, the samples were analyzed by a non-reductive SDS-PAGE and compared to freshly dissolved enzyme-polymer conjugates ($Cyt_{S-S-mPEG}$ left pH 7.4, $Cyt_{DS-SIL-mPEG}$ left pH 7.4) and native Cyt in dd-H$_2$O.

Freshly dissolved $Cyt_{S-S-mPEG}$ ($Cyt_{S-S-mPEG}$ left pH 7.4 lane) shows a broad smear from around 20 kDa up to 170 kDa. The control sample, incubated in PBS pH 7.4 reveals no change in the molecular weight ($Cyt_{S-S-mPEG}$ right pH 7.4 lane), indicating the stability of this enzyme-polymer conjugate in non-reductive conditions. $Cyt_{S-S-mPEG}$ treated with 10 mM GSH ($Cyt_{S-S-mPEG}$ 10 mM GSH lane) show in the SDS-PAGE a minor band at the molecular weight of native Cyt (Figure 70, native). However, the broad smear is still strongly visible. It can be concluded that the disulfide bond of $Cyt_{S-S-mPEG}$ was moderately cleaved, but only a small part. In contrast, $Cyt_{DS-SIL-mPEG}$ incubated in reductive conditions

shows an intense band at a molecular weight of native Cyt and of the Cyt dimer (Cyt$_{DS\text{-}SIL\text{-}mPEG}$ 10 mM GSH lane). Though there is also a broad smear visible, but only lightly, indicating that most of Cyt$_{DS\text{-}SIL\text{-}mPEG}$ were reductive cleaved. The control sample (Cyt$_{DS\text{-}SIL\text{-}mPEG}$ right pH 7.4 lane), incubated in PBS pH 7.4, show again no change in molecular weight compared to the freshly dissolved sample (Cyt$_{DS\text{-}SIL\text{-}mPEG}$ left pH 7.4 lane). It proves the stability of Cyt$_{DS\text{-}SIL\text{-}mPEG}$ in non-reductive conditions. Comparison of Cyt$_{S\text{-}S\text{-}mPEG}$ and Cyt$_{DS\text{-}SIL\text{-}mPEG}$ summarize that reductive cleavage of the self-immolative linker works much better. It could be explained by a rapid and efficient self-catalyzed cleavage of the self-immolative linker in reductive conditions. For this reason, Cyt$_{S\text{-}S\text{-}mPEG}$ is no longer considered in the further work.

The reductive cleavage of Cyt$_{DS\text{-}SIL\text{-}mPEG}$ was further detailed analyzed by MALDI-ToF. Therefore, the enzyme-polymer conjugate was incubated for 24 hours at 37 °C in an aqueous 10 mM GSH solution. For comparison, Cyt$_{DS\text{-}SIL\text{-}mPEG}$ was dissolved in PBS pH 7.4 and treated equally. After one day incubation time, MALDI-ToF measurements were performed and compared to freshly dissolved Cyt$_{DS\text{-}SIL\text{-}mPEG}$ in *dd*-H$_2$O (Figure 71).
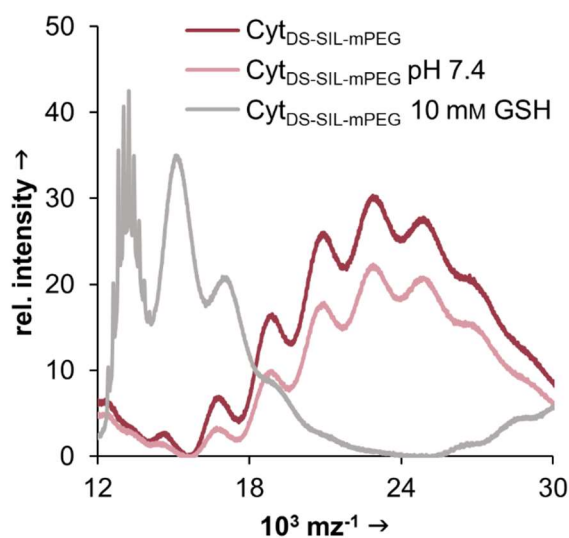
Figure 71: MALDI-ToF analysis of Cyt$_{DS\text{-}SIL\text{-}mPEG}$ degradation. Therefore, Cyt$_{DS\text{-}SIL\text{-}mPEG}$ was incubated for 24 hours at 37 °C in PBS pH 7.4 (light red curve) or in a 10 mM GSH containing aqueous buffer (grey curve). Subsequently, MALDI-ToF measurements were performed and compared to freshly dissolved Cyt$_{DS\text{-}SIL\text{-}mPEG}$ in *dd*-H$_2$O (dark red curve).

The freshly dissolved and the incubated sample in PBS pH 7.4 shows no change in the MALDI-ToF spectra (Figure 71, dark red and light red curve). The reduced sample with GSH displays a decreased molecular weight (Figure 71, grey curve). Locale maxima are shown between 12.4 kDa and 14.0 kDa in 0.2 kDa steps and at 15.1 kDa and 17.2 kDa. The smallest molecular weight corresponds to the native Cyt. The maxima between 12.6 and 14.0 kDa seem to correlate to Cyt bearing still between 2 and 16 linker molecules with a molecular weight of around 0.1 kDa. In literature, it is described that the cyclization-

elimination is slower compared to other self-immolative depolymerization mechanisms.[203] For this reason, probably longer incubation times are necessary for complete linker removal. In Figure 71, peaks of the grey curve at a higher molecular weight of 15.1 and 17.2 kDa display Cyt with one or two DS-SIL-mPEG chains and additional six linker molecules. Consequently, on the one hand within the 24 hours incubation time nearly all PEG chains were successfully reductive cleaved off, but not all self-immolative linker molecules degraded. Nevertheless, the degradation of Cyt$_{DS-SIL-mPEG}$ seems to work well in reductive conditions.

In summary of this section, Cyt$_{DS-SIL-mPEG}$ shows a better reductive cleavage compared to Cyt$_{S-S-mPEG}$ in the SDS-PAGE. Additionally, degradation analysis using MALDI-ToF measurements confirm the reductive decomposition of Cyt$_{DS-SIL-mPEG}$. Unfortunately, after 24 hours not only native Cyt is obtained, but also Cyt bearing still linker molecules and PEG chains. For this reason, in the future, longer incubation times would be of interest to ensure complete linker degradation. The following section will demonstrate the particle preparation based on Cyt$_{DS-SIL-mPEG}$.

3.3.2 NANOPARTICLE PREPARATION AND PARTICLE ANALYSIS

This chapter discusses the nanoparticle preparation based on Cyt$_{DS-SIL-mPEG}$ material and the succeeding particle analysis.

Nanoparticle Preparation by Single Emulsion

Since Cyt$_{DS-SIL-mPEG}$ is soluble in DCM, nanoparticles with the single emulsion method can be prepared, resulting in a Cyt$_{DS-SIL-mPEG}$-NP suspension. Here, 1.75 mg Cyt$_{DS-SIL-mPEG}$ was used for the particle preparation, which will be discussed in section 3.3.3 more in detail.

Determination of the Nanoparticle Size by NTA Measurement

Cyt$_{DS-SIL-mPEG}$-nanoparticles were analyzed in their size, morphology and charge by NTA, TEM and ζ-potential measurements. Using NTA, Cyt$_{DS-SIL-mPEG}$-NP shows an average size of around 130 nm (Figure 72). This size is comparable to Cyt$_{degPEG}$-nanoparticles in section 3.2.2. Presumably, this indicates that in general particles based on Cyt-PEG conjugates and prepared by the emulsion technique results in sizes around 130 nm.
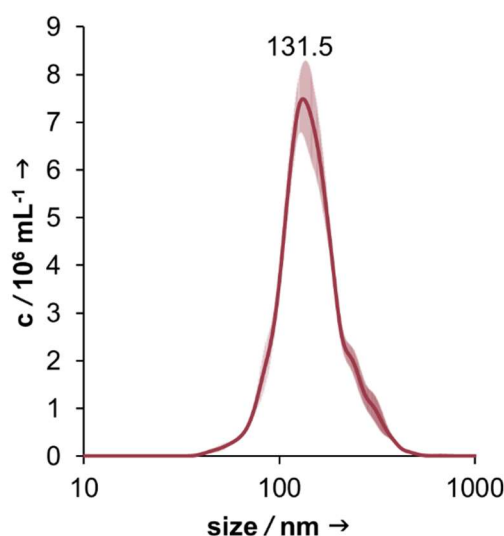
Figure 72: Size determination of Cyt$_{DS\text{-}SIL\text{-}mPEG}$-NP by NTA-measurement.

The size of Cyt$_{DS\text{-}SIL\text{-}mPEG}$-NP determined by NTA approves with the TEM images (Figure 73a). Furthermore, this image illustrates an overall uniform size distribution. Supplementary, the detailed view of Figure 73b summarizes nanoparticles with sizes between 50 and 200 nm.
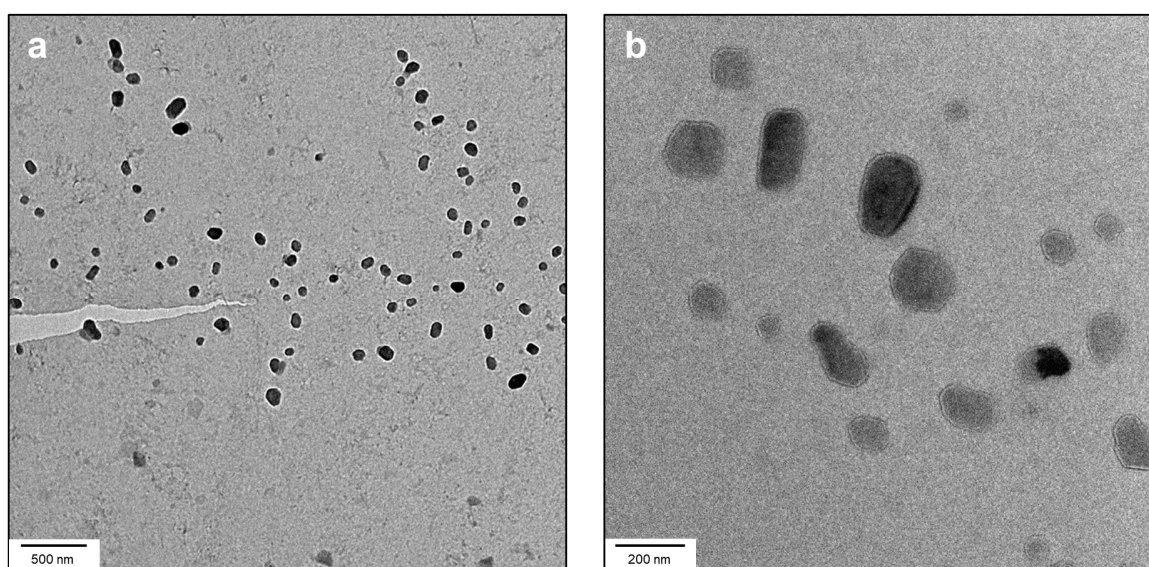
Figure 73: TEM images of Cyt$_{DS\text{-}SIL\text{-}mPEG}$-NP for size distribution analysis; a) shows an overall image and b) a zoomed-in area.

The ζ-potential measurement of Cyt$_{DS\text{-}SIL\text{-}mPEG}$-NP results in a value of around −2.1 mV (Table 13), which is comparable to the ζ-potential of Cyt$_{degPEG}$-NPs. Also here, the ζ-potential of the nanoparticle suspension is very low, which normally points out an instability. Nevertheless, as described previously PEG-chains can result in charge shielding. For this reason, the low value does not necessarily reveal that the particles are

unstable. However, in the future, a long-time stability investigation of Cyt$_{DS-SIL-mPEG}$-NPs would be of interest.

Table 13: Results of ζ-potential measurement of Cyt$_{DS-SIL-mPEG}$-nanoparticles.

sample	ζ-potential (mV)
Cyt$_{DS-SIL-mPEG}$-NP	-2.08 ± 0.27

Determination of the Cell Viability of HeLa Cells by MTT Assay

For the investigation of the cell viability of the reductive-labile Cyt$_{DS-SIL-mPEG}$ system, an MTT assay was performed (Figure 74). Therefore, native Cyt, Cyt$_{DS-SIL-mPEG}$ and Cyt$_{DS-SIL-mPEG}$-NPs in the same concentrations (0.51–16.37 μM) were incubated with HeLa cells for 48 hours.
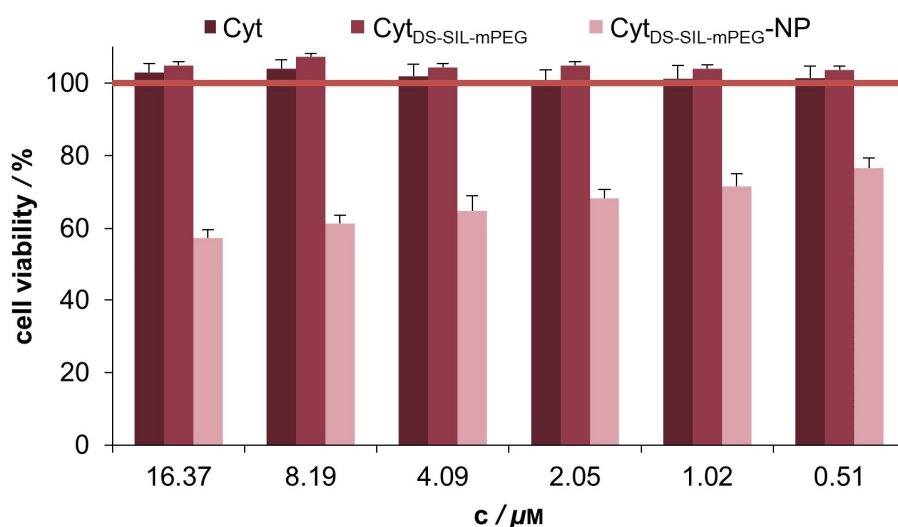
Figure 74: MTT assay results of native Cyt, Cyt$_{DS-SIL-mPEG}$ and Cyt$_{DS-SIL-mPEG}$-NPs incubated with HeLa cells for 48 hours. The given concentrations refer to the Cyt material.

Also, this result coincides with the MTT assay of the Cyt$_{degPEG}$-system. Native Cyt and Cyt$_{DS-SIL-mPEG}$ cannot pass the cell membrane, resulting in no toxicity in these human cells. In contrast, Cyt$_{DS-SIL-mPEG}$-NPs show a toxic effect in all analyzed concentration. At the highest concentration of 16.37 μM the cell viability is reduced by 43%. Nanoparticles are taken up by the HeLa cells, presumably by endocytosis. After the release of the particles in the cytosol, the high GSH concentration leads to Cyt$_{DS-SIL-mPEG}$ reduction. Consequently, native Cyt is obtained in the cytosol, resulting in the initiation of the apoptosis pathway. Comparison of Cyt$_{DS-SIL-mPEG}$-NPs with Cyt$_{degPEG}$-NPs, reveal higher toxicity of the reductive-labile particles. Already 2.05 μM Cyt$_{DS-SIL-mPEG}$-NPs induce the same toxicity of 31% reduced cell viability as 23.50 μM Cyt$_{degPEG}$-NPs. Presumably, the reason for that is the

reduction of $Cyt_{DS-SIL-mPEG}$ to native Cyt. The regained Cyt has the unrestricted ability to bind the apoptosome, which results in apoptosis. In contrast, acidic degradation of Cyt_{degPEG} in cells leads to Cyt which still bears polymer fragments on the enzyme surface. Probably, this modified enzyme has not the same binding ability to the apoptosome due to steric hindrance. This would explain the higher cytotoxicity of $Cyt_{DS-SIL-mPEG}$-NPs, which highlights the advantage of using a self-immolative linker during enzyme PEGylation.

3.3.3 NANOPARTICLE DEGRADATION ANALYSIS

After proving the lability of the $Cyt_{DS-SIL-mPEG}$ material under reductive conditions, and the ability for nanoparticle preparation, the degradation of the particles under reductive conditions was investigated. In order to compare different compositions, nanoparticles were freshly prepared with either 1.4 mg or 1.75 mg of $Cyt_{DS-SIL-mPEG}$ using the single emulsion technique. For degradation, the nanoparticles were 1:1 mixed with an aqueous 20 mM GSH solution, resulting in a final 10 mM GSH concentration. Again, this GSH concentration was used to correspond to the intracellular one. As control $Cyt_{DS-SIL-mPEG}$-NPs were diluted in the same manner using PBS pH 7.4. The mixtures were incubated at 37 °C and the change in nanoparticle concentration was observed using NTA measurements. The results are summarized in Figure 75.

The nanoparticles, consisting of 1.4 mg of the enzyme-polymer conjugate and incubated in PBS pH 7.4 show a halved particle concentration after one day (Figure 75a). During the following two days, the particles further halved, but afterward, the particle numbers have stabilized. The degradation of this particle batch in GSH solution takes place very fast, so after three days of incubation time, there are almost no particles observable. The particles consisting of 1.75 mg $Cyt_{DS-SIL-mPEG}$ material incubated in PBS pH 7.4, show a similar effect (Figure 75b). However, the number of particles only decreased around one third. Overall, after one day the particle number then changes barely noticeably. For this reason, this particle batch seems to be more stable. In contrast, the degradation in GSH takes longer. Only after nine days, nearly no particles were observable, compared to three days for the 1.4 mg particle batch.

It has to be noted, that the biggest change of particle concentration of both controls is within the first day. Presumably, the sample dilution results in particle instability. Nevertheless, this effect was weaker when using more $Cyt_{DS-SIL-mPEG}$ material. This result demonstrates a trend: the more $Cyt_{DS-SIL-mPEG}$ material is used, the more stable are the prepared nanoparticles in PBS pH 7.4, but it also results then in a slower degradation in GSH solution. Unlike the acid-labile NPs, in this case, an optimal particle composition does not exist, a compromise has to be found. In comparison to the acid-labile Cyt_{degPEG}-NPs,

this nanoparticle system is not fully stable and it is more difficult to degrade. Presumably, it is explainable due to $Cyt_{DS-SIL-mPEG}$ has only one cleavage site between the enzyme and the polymer. It could be supposed, that after cleavage of $Cyt_{DS-SIL-mPEG}$ within the particle, the unspecific interactions between individual enzyme-polymer conjugates are still too strong, and one cleavage site is not sufficient to disturb these interactions.
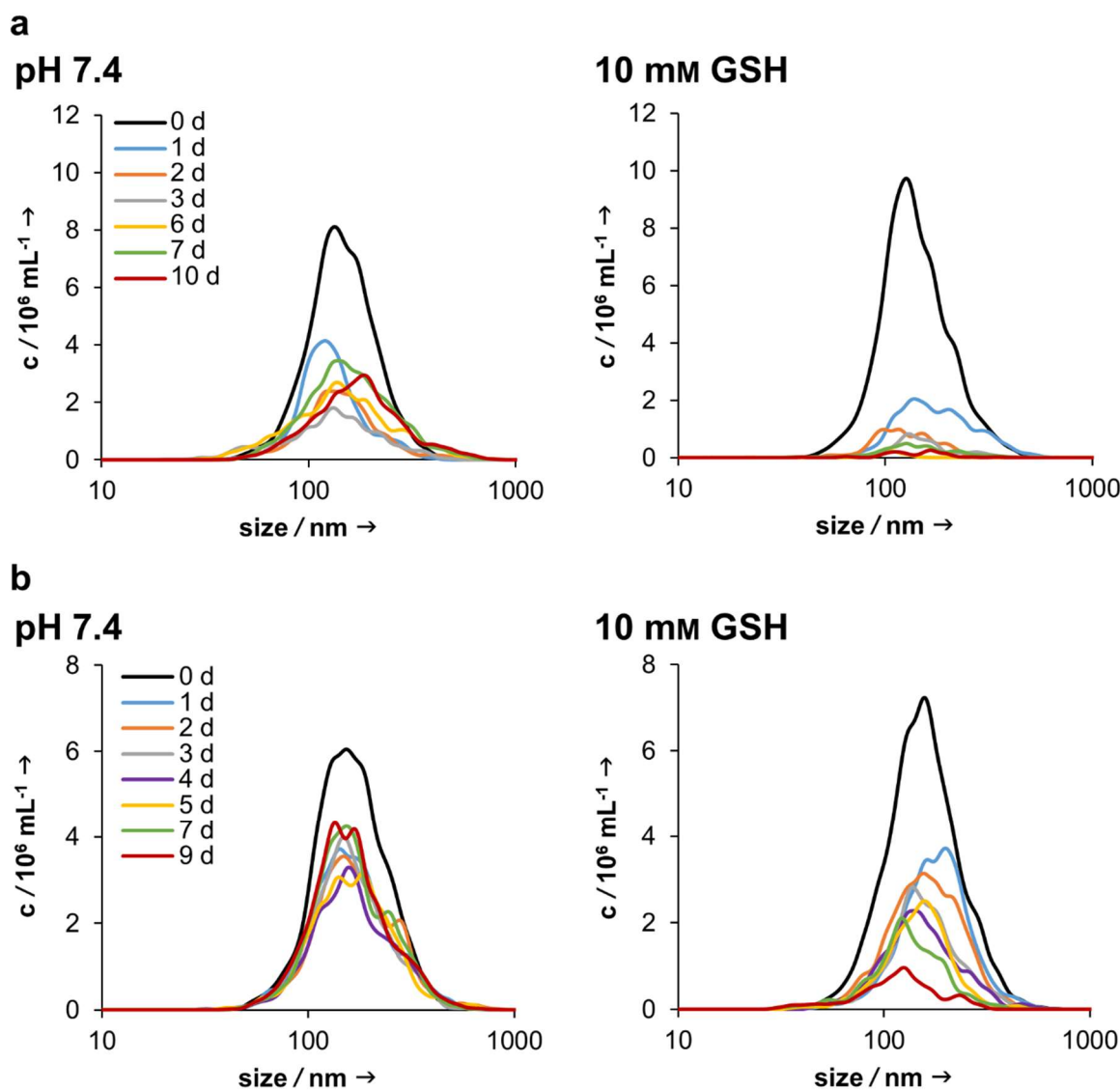
Figure 75: NTA measurements for $Cyt_{DS-SIL-mPEG}$-NP degradation analysis in reductive conditions. Nanoparticles were either prepared with 1.4 mg (a) or 1.75 mg (b) $Cyt_{DS-SIL-mPEG}$ by single emulsion. Nanoparticles were 1:1 mixed with different buffers (pH 7.4, 20 mM GSH) and incubated at 37 °C. For analysis, NTA measurements were performed over time.

In this case, a compromise that includes sufficient stability and a slow degradation was found in the particle consisting of 1.75 mg $Cyt_{DS-SIL-mPEG}$ conjugate. For this reason, only this particle composition was used for further in-depth investigations on particle stability and degradability. It was investigated if degradation of control particles relates to a $Cyt_{DS-SIL-mPEG}$ instability in PBS pH 7.4 and on the other hand if the slow reductive particle

degradation correlates to a slow Cyt$_{DS-SIL-mPEG}$ conjugate cleavage. Therefore, Cyt$_{DS-SIL-mPEG}$-particles were again mixed with PBS pH 7.4 as control and 20 mM GSH solution for reductive degradation. The particles were incubated at 37 °C and after 48 hours, the samples were analyzed by SDS-PAGE (Figure 76) and MALDI-ToF (Figure 77) and compared to untreated Cyt$_{DS-SIL-mPEG}$-NPs.
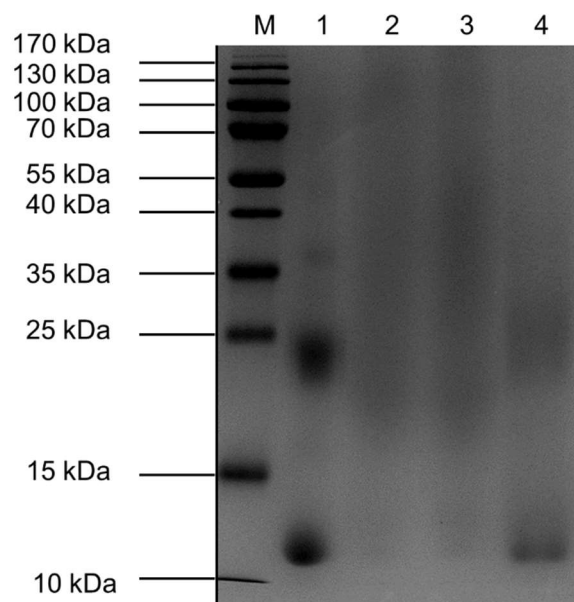
Figure 76: SDS-PAGE (15%) analysis of Cyt$_{DS-SIL-mPEG}$-NP degradation, prepared by single emulsion using 1.75 mg of the enzyme-polymer conjugate. The nanoparticles were mixed and incubated for 48 hours at 37 °C in PBS pH 7.4 as control (lane 3) or in a 20 mM GSH containing aqueous buffer (lane 4). Subsequently, the samples were analyzed by a non-reductive SDS-PAGE and compared to untreated particles (lane 2) and native Cyt (lane 1) in *dd*-H$_2$O.

Both methods lead to similar results compared to that of Cyt$_{DS-SIL-mPEG}$ material degradation analysis (section 3.3.1). Since the Cyt$_{DS-SIL-mPEG}$-NPs show the same sizes in the SDS-PAGE und in MALDI-ToF compared to Cyt$_{DS-SIL-mPEG}$, this indicates, that the particles disassembly throughout both analytical methods. Otherwise, higher molecular weights of the particles compared to the Cyt$_{DS-SIL-mPEG}$ material would have been detected. Nevertheless, these investigations allow a conclusion concerning the particle material behavior. The particles incubated in PBS pH 7.4 show in the SDS-PAGE and in the MALDI-ToF no native Cyt (Figure 76 lane 3, Figure 77 light red curve). Furthermore, no change between the control particles, which were incubated in PBS pH 7.4, and untreated particles (Figure 76 lane 2, Figure 77 dark red curve) are observable. Considering that control particles and untreated nanoparticles show no differences in both analytical methods, it can be concluded, that the decrease of the particle concentration in PBS pH 7.4 does not relate to Cyt$_{DS-SIL-mPEG}$ cleavage. In contrast, particles incubated in GSH show almost only native Cyt (Figure 76 lane 4, Figure 77 grey curve). Nevertheless, after GSH treatment, in the SDS-PAGE a small smear is still observable. Presumably, this is caused by one non-

cleaved PEG chain, which could be detected in the MALDI-ToF. However, in summary, this result exhibits a nearly complete reductive cleavage of $Cyt_{DS-SIL-mPEG}$, even if after two days only half of the particles are degraded. These results could confirm the above-mentioned hypothesis that after successful linker cleavage in reductive conditions, the unspecific interactions within the particle are still predominantly available. Thus, particle disassembly occurs only slowly.
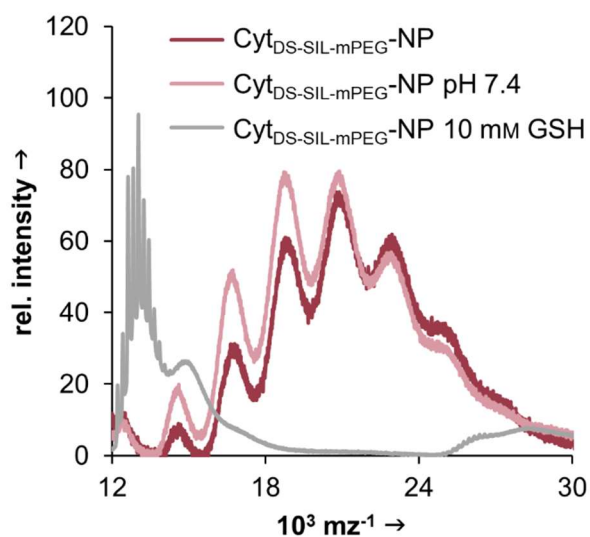
Figure 77: MALDI-ToF analysis of $Cyt_{DS-SIL-mPEG}$-NP degradation. Therefore, $Cyt_{DS-SIL-mPEG}$-NPs were 1:1 mixed and incubated for 48 hours at 37 °C in PBS pH 7.4 (light red curve) or in a 20 mM GSH containing aqueous buffer (grey curve). Subsequently, MALDI-ToF measurements were performed and compared to untreated $Cyt_{DS-SIL-mPEG}$-NPs (dark red curve).

For morphology analysis of the incubated $Cyt_{DS-SIL-mPEG}$-NPs, TEM images were recorded. Therefore, the mixed particles (PBS pH 7.4 or 20 mM GSH solution) were incubated at 37 °C for 9 days, concerning that the particles need that time to disassemble almost completely in reductive conditions (see Figure 75). The resulting TEM images are summarized in Figure 78. Control $Cyt_{DS-SIL-mPEG}$-NPs in PBS pH 7.4 show particles in the known size distribution (Figure 78a). In comparison, the TEM image of reductive degraded particles shows almost exclusively small black dots and no particular systems (Figure 78b). Native Cyt has a diameter of around 3 nm,[204] which is supposedly represented in the image. The black dots are also observable in the control image, but probably it is $Cyt_{DS-SIL-mPEG}$ due to non-reductive conditions. Much more important is to emphasize, that particles are observable in the control and there are none in the reduced batch.
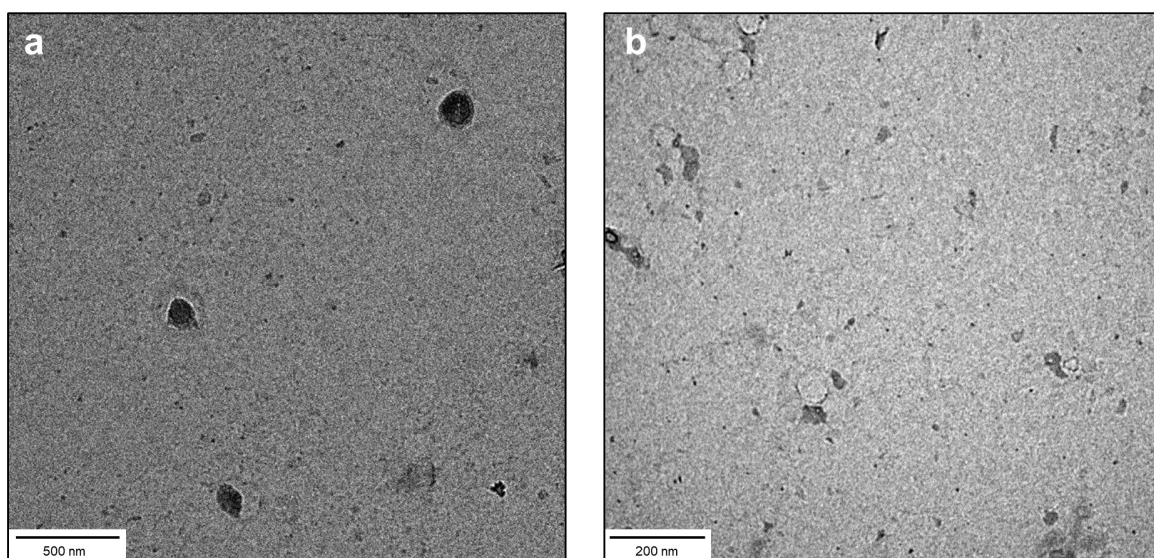
Figure 78: TEM analysis of Cyt$_{DS-SIL-mPEG}$-NP degradation. Therefore, Cyt$_{DS-SIL-mPEG}$-NPs were 1:1 mixed and incubated for 9 days at 37 °C in PBS pH 7.4 (a) or in a 20 mM GSH containing aqueous buffer (b). Subsequently, samples were applied on a grid and analyzed by TEM.

For comparison of the developed Cyt$_{DS-SIL-mPEG}$-nanoparticles with a literature described example, a nanogel, which was already described in section 1.1.5, will be considered since it is similarly composed like Cyt$_{DS-SIL-mPEG}$. In this example, a polymer bearing the same self-immolative linker as Cyt$_{DS-SIL-mPEG}$, but in the polymer side chain, and it was conjugated to lipase, inducing a nanogel formation. In reductive conditions, the lipase recovery was proven in SDS-PAGE analysis.[85] However also a smear to greater molecular weights was observable, indicating that the enzyme recovery was also not completely. However, a 0.6 M DTT solution was used for this investigation, which does not represent intracellular conditions. Accordingly, these results highlight the advantage of the developed Cyt$_{DS-SIL-mPEG}$-nanoparticles, which could already decompose in mild physiological conditions.

In summary, in the third project of this thesis, the preparation of a reductive-labile protein-based nanoparticle system was developed. Cyt was PEGylated using a polymer with a self-immolative ability. Subsequently, particles were prepared using the single emulsion method. Incubation of the particles in reductive conditions shows a slow particle degradation and it nearly results in regaining the native enzyme.

4 CONCLUSION AND OUTLOOK

In summary, the main goal of this thesis was the development of dynamic protein-based nanoparticle systems. On the one hand, the encapsulation of hydrophilic payloads using the double emulsion method was further evolved and in addition different stimuli-responsive groups were introduced in this type of nanocarrier.

Lysozyme Nanoparticles for the Delivery of Hydrophilic Antibacterial Payloads

In the first project of this thesis, the double emulsion technique was successfully transferred to PEGylated LYZ as a nanoparticle backbone. At first, LYZ was modified using TFP-activated mPEG, resulting in high surface PEGylation while negligible affecting the secondary structure of the enzyme and likewise the activity was only reduced about 19%. However, the enzymatic activity was tested using an artificial substrate, which is distinct smaller compared to the bacterial cell wall, the natural substrate. The polymer attachment on the enzyme surface changed the solubility behavior in organic solvents, which enables the emulsion-based nanoparticle preparation resulting in around 200 nm sized particles. The encapsulation of the small antibiotic gentamicin sulfate achieved not the desired results, presumably due to the small size this drug diffused out of the particle system too fast. For this reason, a larger hydrophilic antibacterial payload was enclosed in this nanocarrier. Referring to the natural antibiotic properties, native LYZ was chosen as biotherapeutic, whose encapsulation was successful. The slow sustained release of this enzyme was observed while the nanoparticles were stable, accordingly the biotherapeutic released by passive diffusion. The encapsulation of the native LYZ does not affect the enzymatic activity, which was proven against the gram-positive bacteria strain *M. Luteus* (Figure 79). Nevertheless, a combined effect of the encapsulated native LYZ and the particle material could not be observed, presumably, the high surface PEGylation leads to a too distinctive shielding of the active site of LYZ$_{mPEG}$. Finally, this particle system with the encapsulated biotherapeutic was tested to be non-toxic to human cells. Thus, it ensures that these nanoparticles could be applied as drug delivery systems.
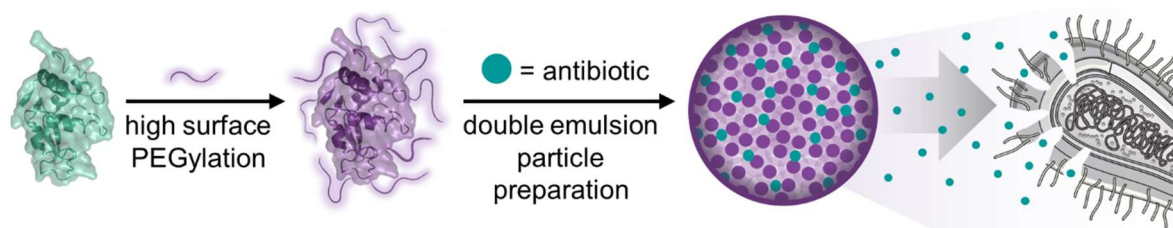
Figure 79: Encapsulation of native LYZ as a natural antibiotic in LYZ$_{mPEG}$-nanoparticles using a double emulsion technique. Native LYZ release results in bacteria death.

In the future, the development of a positively charged particle material would be of interest. The new received positive nanoparticles could interact with the negatively charged bacterial cell wall of both, gram-positive and –negative ones. If an antibiotic would be encapsulated in this particle material, it would result in a more site-specific drug release. For example, in addition to the PEG attachment, spermine molecules could be introduced on the enzyme surface to gain a positive charge. However, it also would be possible to directly attach target structures to the particle surface. Since bacteria secrete different toxins but also enzymes like lipase, antibodies or enzyme substrates could be attached to the particle surface for active targeting. For example, polycaprolacton (PCL) represents a lipase substrate, which could be attached to the particle surface material. In addition, bacterial colonies lead locally in a pH value reduction. As a result, an acid stimuli-responsiveness in the nanoparticle backbone would be of interest. This would allow a site-specific drug release at bacterial infections, respectively nearly native LYZ recovery from the particle material, which could be used as biotherapeutic.
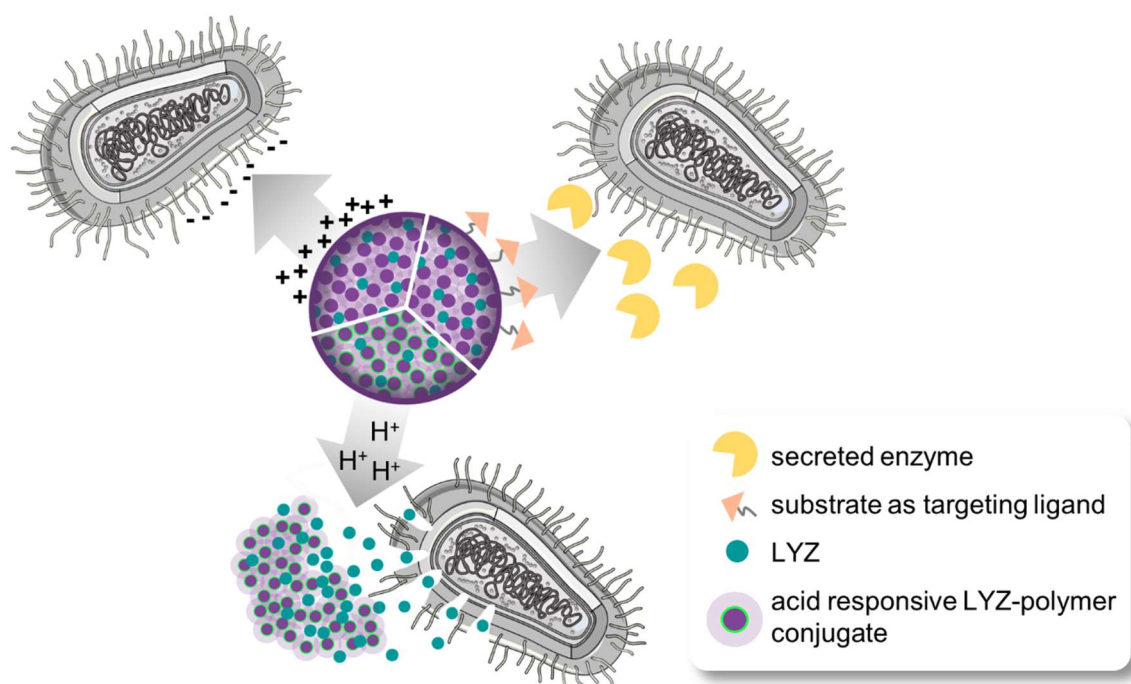
Figure 80: Future perspective concerning protein-based nanoparticle systems for the treatment of bacterial infections.

Acid-Responsive Protein-based Nanoparticles

For the improvement of the protein-based nanoparticle system, the idea was to introduce a stimuli-responsiveness in the nanoparticle backbone. For this reason, in the second part of this thesis, an acid degradable particle variant was developed (Figure 81a). The degradability was obtained by a cleavable PEG with vinyl ether moieties distributed in the polyether backbone. Herein, Cyt was used as a model enzyme. The high surface

modification of this enzyme using the degradable PEG, only slightly affected the enzymatic structure and activity. The acid lability of the polymer backbone was revealed even after the attachment on the enzyme surface. Already a mildly acidic environment of pH 6 was sufficient for polymer degradation while being stable at physiological neutral conditions. In addition to the gained stimuli-responsiveness, the polymer attachment to Cyt led to a solubility of this conjugate in DCM, which allows the preparation of protein-nanoparticles by the emulsion-based technique with sizes around 140 nm. The resulting particles revealed complexity in being stable at physiological neutral conditions while degrading at acidic pH values due to polymer backbone cleavage. It emerged that the nanocarrier composition had a strong influence on particle stability or rather a degradability. For example, the composition of the enzyme-polymer conjugate, like the number of attached polymer chains and cleavage sites affects the particle stability and degradability. However, also the amount of enzyme-polymer conjugates used during particle preparation and the encapsulation of model compounds in the nanoparticle system caused a changed behavior of the particles. Nevertheless, optimal particle compositions could be evaluated. Oregon-green dextran was successfully encapsulated into the particle system as a model compound and a stimuli-responsive release was observed at a pH value of 4. An MTT assay revealed a toxicity of these nanoparticles against human cells due to the natural apoptotic activity of Cyt, which is an interesting aspect considering these stimuli-responsive nanoparticles as an anticancer drug delivery system.

Taking into account that the two stimuli-responsive protein-based nanoparticles in this thesis can be compared with each other, the outlook of these two topics will be discussed together after the next paragraph at the end of this chapter.

Reductive-Responsive Protein-based Nanoparticles

In the third project of this thesis, a traceless Cyt polymer modification was successfully evaluated, which was redox-responsive due to using a disulfide self-immolative PEG (Figure 81b). The enzyme PEGylation leads to almost no structural alterations in the enzyme and its activity was not affected. Reductive conditions, as it occurs intracellularly, lead to the disulfide cleavage, inducing a cyclization reaction, which results in unmodified, native Cyt. However, within one day incubation time in a redox-active environment, most Cyt molecules still bear small linker groups, indicating that the reaction time was not sufficient enough to trigger the complete self-immolative reaction. Nevertheless, Cyt could be nearly regained after incubation in cellular reductive conditions. The enzyme-polymer conjugate was soluble in DCM and therefore suitable for the preparation of protein-based nanoparticles by the emulsion-based technique, where particles with around 130 nm were obtained. Unfortunately, the optimal particle composition could not be found, unlike the

acid-labile particles in the second project of this thesis. Probably, the reason is that only one cleavage site is available between the enzyme and polymer, resulting in a minor detraction of the unspecific interactions in the nanoparticle system during cleavage. Nevertheless, a comprise was reached by reasonably good stability in non-reductive conditions, while the particles slowly degrade over 9 days in attendance of physiological redox-active agents. Additional particle analysis confirmed the particle stability as well as the degradability by regaining the almost unmodified, native Cyt due to the disulfide self-immolative linker cleavage. In a cell viability analysis, these nanoparticles exhibited higher toxicity compared to the acid-sensitive Cyt particles. The reason for that is the recovery of the nearly unmodified Cyt through the intracellular reductive conditions, resulting in a more unhindered apoptosome interaction, which leads to an increasingly induced cell death.
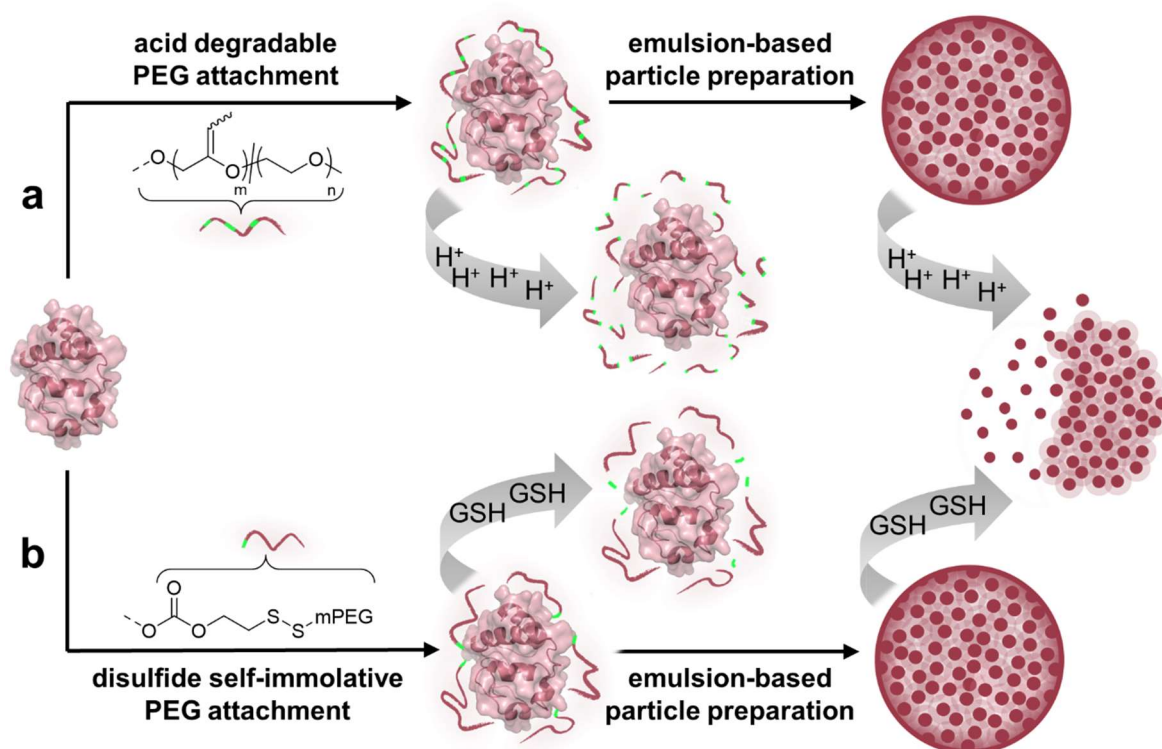
Figure 81: Acid- (a) and redox-responsive (b) nanoparticles based on PEGylated Cyt. Both particle types were prepared by using the emulsions technique and each had the ability to degrade after exposure with certain stimuli.

Outlook for both stimuli-responsive protein-based nanoparticle systems

The stimuli-responsive protein-based nanoparticles developed in this thesis can pursue the same or similar goals. First, changes in the number and sites of cleavage moieties will be considered and subsequently, further particle analysis and applications will take into account.

In the future, referring to the acid-sensitive nanoparticles, the attachment of a vinyl ether linker between Cyt and PEG should be compared to the analyzed cleavable polymer backbone with several vinyl ether moieties. In this regard, possible changes in particle stability and degradability should be investigated, when the same responsive group appears only once as a linker. In addition, the results could be compared to the protein nanoparticles bearing the disulfide self-immolative linker, if these particles also degrade slower. Conversely, in addition to the disulfide self-immolative linker of the developed redox-responsive protein nanoparticles, several disulfide linkages can be introduced in the PEG backbone. Thereupon, it can be investigated whether the particles disassemble better in reductive conditions due to whole polymer backbone cleavage while maintaining the recovery of the native enzyme.

Additionally, in the future, the closer investigation of the structure and composition of both stimuli-responsive protein-based nanoparticles would be an interesting approach. For example, using scanning electron microscopy (SEM), a combination of chemical and optical characterization could be provided. Furthermore, differential centrifugal sedimentation (DCS) can be used amongst other things for the particle density investigation. The different particle compositions barely varied in size but the densities may be different, which can be compared using DCS. Thus, the relationships between particle stability and degradability could be examined more in detail.

In addition, the detailed *in vitro* cellular uptake of the nanoparticles, as well as the intracellular particle disassembly and enzyme recovery would be interesting aspects that could be explored in the future using, for example, confocal microscopy.
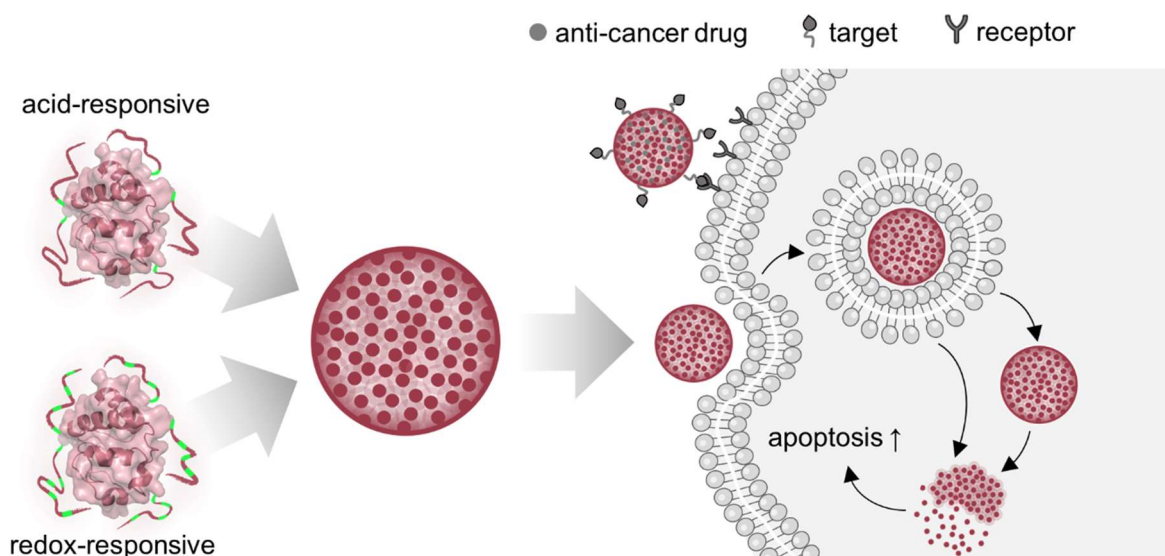
Figure 82: Future perspective of the stimuli-responsive protein-based nanoparticle system.

Furthermore, concerning the natural apoptotic property of the regained Cyt out of the particle backbone, the further prosecution of these particles would be an interesting approach in cancer treatment. Thus, these nanoparticle systems could be used for the delivery of anticancer drugs, like doxorubicin, which potentially increases the intracellular toxic effect through the particle material itself.

All in all, two different stimuli-responsive protein-based nanoparticle systems were successfully developed. These nanocarriers have the potential to be used as drug delivery systems, allowing a fast drug release in the presence of intrinsic stimuli, like the acidic environment in the endo-lysosomal pathway after cellular uptake or the increased intracellular reductive conditions. And especially concerning the self-immolative ability of the Cyt particles, nearly native enzyme could be regained. This opens up the possibility that the particle material itself could be used as a natural drug.

5 EXPERIMENTAL SECTION

5.1 MATERIALS

5.1.1 REAGENTS AND SOLVENTS

Chemical	Supplier	CAS
2,2'-azinobis-(3-ethylbenzthiazoline-6-sulfonate) (ABTS	Alfa Aesar	30931-67-0
Acetic acid	Sigma-Aldrich	64-19-7
Acetone	Sigma-Aldrich	67-64-1
Acetonitrile	TCI, Belgium	75-05-8
Ammonium persulfate (APS)	Carl Roth	7727-54-0
Boric acid	Sigma-Aldrich	10043-35-3
Bromphenol blue	Sigma-Aldrich	115-39-9
Chloroform-*d*	Deutero	865-49-6
Coomassie Brilliant Blue G	Sigma-Aldrich	6104-58-1
Curcumin	TCI	458-37-7
Cytochrome *c* from horse heart	Serva Electrophoresis	9007-43-6
Dichloromethane anhydrous, ≥99.8%, contains 40–150 ppm amylene as stabilizer	Sigma-Aldrich	75-09-2
N,N'-Dicyclohexylcarbodiimide	TCI	538-75-0
Diethyl ether	Carl Roth	69-29-7
Dimethyl sulfoxide anhydrous, ≥99.9%	Sigma-Aldrich	67-68-5
Dextran; M_W 10 000	Pharmacosmos	9004-54-0
Dextran, Oregon Green® 488; M_W 10 000	Life Technologies	
DMEM GlutaMAX™ (Dulbecco's Modified Eagle's Medium high glucose)	Sigma-Aldrich, USA	
Ethanol	Fisher Scientific, USA	64-17-5
Ethylenediaminetetraacetic acid (EDTA)	Sigma-Aldrich	60-00-4
Ethylenediaminetetraacetic acid disodium salt dihydrate	Sigma-Aldrich	6381-92-6
Fetal Calf Serum (FCS)	Life Technologies	
Gentamicin sulfate	Sigma-Aldrich	1405-41-0
L-Glutathione reduced	Sigma-Aldrich	70-18-8

Chemical	Supplier	CAS
Glycerol	Sigma-Aldrich	56-81-5
Glycine	Sigma-Aldrich	56-40-6
Hydrochloric acid 37%	Carl Roth	7647-01-0
Hydrochloric acid 1 M	Carl Roth	7647-01-0
Hydrogen peroxide solution 30%	Sigma-Aldrich	7722-84-1
Hydroxylamine hydrochloride	Sigma-Aldrich	5470-11-1
Lysozyme from chicken egg white	Sigma-Aldrich	12650-88-3
Methanol	Sigma-Aldrich	67-56-1
4-Methylumbelliferyl β-D-N,N',N''-triacetylchitotriosid	Sigma-Aldrich	53643-13-3
PageRuler Prestained Protein Ladder (SM0671)	Thermo Scientific	
Phosphate buffered saline (10x concentrate, BioPerformance Certified)	Sigma-Aldrich	
Penicillin-streptomycin (5000 U/mL) Gibco™	Thermo Scientific	
Polyethylene glycol (2000) α-methoxy-ω-carboxy	Rapp Polymere	
Polyethylene glycol methyl ether thiol (2000)	Sigma-Aldrich	
Potassium phosphate	Sigma-Aldrich	7778-53-2
Roti®-Load 1	Carl Roth	
Rotiphorese® Gel 30	Carl Roth	
Sephadex® G-75 Medium	Sigma-Aldrich	37224-29-6
Sephadex® G-100 Medium	Sigma-Aldrich	9050-94-6
Sodium acetate	Sigma-Aldrich	127-09-3
Sodium carbonate	Carl Roth	497-19-8
Sodium chloride	Carl Roth	7647-14-5
Sodium dihydrogen phosphate	Amresco, USA	7558-80-7
Sodium dodecyl sulfate	Carl Roth	151-21-3
Sodium hydroxide	Carl Roth	1310-73-2
Sodium hydroxide solution 1 M	Carl Roth	
Sodium pyruvate (100 mM) Gibco™	Thermo Scientific	
Sodium sulfate	Carl Roth	7757-82-6
N-succinimidyl-S-acetylthiopropionate (SATP)	Thermo Scientific	
Sulfo-Cyanine 5 NHS-Ester (Cy5-NHS)	Lumiprobe	
Sulfuric acid	Sigma-Aldrich	7664-93-9
2,3,5,6-Tetrafluorophenol	Alfa Aesar	769-39-1

Chemical	Supplier	CAS
N,N,N',N'-Tetramethylethylenediamine (TEMED)	VWR	110-18-9
3-(4,5-dimethyl-2-thiazolyl)-2,5-diphenyl-2H-tetrazolium bromide (MTT)	Sigma-Aldrich	298-93-1
2,4,6-Trinitrobenzene sulfonic acid (TNBS)	Alfa Aesar	2508-19-2
Tris(2-carboxyethyl)phosphine hydrochloride (TCEP)	Carl Roth	51805-45-9
Trizma® base	Sigma-Aldrich	77-86-1
Trypsin from bovine pancreas	Sigma-Aldrich	9002-07-7

5.1.2 BUFFERS AND MEDIA

Purified water (Direct-Q®) was used for the preparation of all buffers and media. Adjustment of the pH values was performed with NaOH or HCl if not otherwise stated. Before usage all buffers were filtered through a sterile syringe filter with a pore size of 0.22 μm (CME membrane, Rotilabo®).

Acetate Buffer (0.1 M, pH 4)
1.24 g sodium acetate (Sigma-Aldrich, M_W 82.03 g mol^{-1}) and 5.10 g acetic acid (Sigma-Aldrich, M_W 60.05 g mol^{-1}) were dissolved in *dd*-H2O (1 L) and the pH was adjusted to pH 4.

Acetate Buffer (0.1 M, pH 5)
5.25 g sodium acetate (Sigma-Aldrich, M_W 82.03 g mol^{-1}) and 2.16 g acetic acid (Sigma-Aldrich, M_W 60.05 g mol^{-1}) were dissolved in *dd*-H2O (1 L) and the pH was adjusted to pH 5.

APS 10% in water
100 mg APS (Carl Roth, M_W 228.20 g mol^{-1}) was dissolved in *dd*-H$_2$O (1 mL).

Borate Buffer (0.1 M, pH 7)
6.2 g boric acid (Sigma-Aldrich, M_W 61.83 g mol^{-1}) were dissolved in *dd*-H2O (1 L) and adjusted to pH 7.

Borate Buffer (0.1 M, pH 9)
6.2 g boric acid (Sigma-Aldrich, M_W 61.83 g mol^{-1}) were dissolved in *dd*-H2O (1 L) and adjusted to pH 9.

Carbonate Buffer (0.1 M, pH 8)

10.60 g sodium carbonate (Carl Roth, M_W 105.99 g mol^{-1}) were dissolved in *dd*-H2O (1 L) and adjusted to pH 8.

CD Buffer (10 mM K$_3$PO$_4$, 50 mM Na$_2$SO$_4$, pH 7)

2.12 g potassium phosphate (Sigma-Aldrich, M_W 212.27 g mol^{-1}) and 7.10 g sodium sulfate (Carl Roth, M_W 142.04 g mol^{-1}) were dissolved in *dd*-H2O (1 L) and adjusted to pH 7 with NaOH and H$_2$SO$_4$.

Coomassie Staining Solution

250 mg Coomassie Brilliant Blue G (Sigma-Aldrich, M_W 854.02 g mol^{-1}) were dissolved in a mixture of water (45 mL), ethanol (45 mL) and acetic acid (10 mL).

Deacetylation Solution

7 mg hydroxylamine hydrochloride (Sigma-Aldrich, M_W 69.49 g mol^{-1}) and 1.5 mg ethylenediamine-tetraacetic acid disodium salt dihydrate (Sigma-Aldrich, M_W 372.24 g mol^{-1}) and were dissolved in 180 μL PBS buffer (pH 7.4). This buffer was freshly prepared before each usage.

Destaining Solution for Coomassie Stained Gels

A mixture of ethanol (450 mL), water (450 mL) and acetic acid (100 mL) was used.

DMEM for HeLa Cells

DMEM GlutaMAX™ (high glucose) with phenol red was mixed with 10% FCS, 1% pyruvate and 1% penicillin-streptomycin.

Glycine Buffer (0.1 M, pH 10)

7.5 g glycine (Sigma-Aldrich, M_W 75.07 g mol^{-1}) and 5.8 g sodium chloride (Carl Roth, M_W 58.44 g mol^{-1}) were dissolved in *dd*-H$_2$O (1 L) and adjusted to pH 10.

Glycine Buffer (0.5 M, pH 12)

37.5 g glycine (Sigma-Aldrich, M_W 75.07 g mol^{-1}) and 5.8 g sodium chloride (Carl Roth, M_W 58.44 g mol^{-1}) were dissolved in *dd*-H$_2$O (1 L) and adjusted to pH 12.

Loading Buffer for Non-Reductive SDS-PAGES

8 mg bromophenol blue (Sigma-Aldrich, M_W 669.96 g mol^{-1}), 2.3 g Tris (Sigma-Aldrich, M_W 121.14 g mol^{-1}) and 30 mL glycerol (Sigma-Aldrich, M_W 92.09 g mol^{-1}) were dissolved in dd-H_2O to a final volume of 100 mL.

PBS Buffer (pH 7.4)

PBS 10x concentrate (Sigma-Aldrich, 100 mL) was diluted with dd-H_2O (900 mL); containing 154 mM NaCl, 8 mM Na_2HPO_4 and 2 mM KH_2PO_4 with a final pH of 7.4.

PBS Buffer (10 mM EDTA, pH 7.4)

2.9 g ethylenediaminetetraacetic acid (Sigma-Aldrich, M_W 292.24 g mol^{-1}) were dissolved in 1 L PBS buffer (pH 7.4).

Phosphate Buffer (0.1 M, pH 5.2)

12 g sodium dihydrogen phosphate (Amresco, M_W 119.98 g mol^{-1}) were dissolved in dd-H_2O (1 L) and adjusted to pH 5.2.

Phosphate Buffer (0.1 M, pH 6.0)

12 g sodium dihydrogen phosphate (Amresco, M_W 119.98 g mol^{-1}) were dissolved in dd-H_2O (1 L) and adjusted to pH 6.0.

Phosphate Buffer (0.1 M, 0.15 M NaCl, pH 7.2)

12 g sodium dihydrogen phosphate (Amresco, M_W 119.98 g mol^{-1}) and 8.8 g sodium chloride (Carl Roth, M_W 58.44 g mol^{-1}) were dissolved in dd-H_2O (1 L) and adjusted to pH 7.2.

Phosphate Buffer (0.1 M, pH 7.4)

12 g sodium dihydrogen phosphate (Amresco, M_W 119.98 g mol^{-1}) were dissolved in dd-H_2O (1 L) and adjusted to pH 7.4.

Phosphate Buffer (0.1 M, 10 mM GSH, pH 7.4)

6.1 mg L-glutathione reduced (Sigma-Aldrich, M_W 307.32 g mol^{-1}) were dissolved in 2 mL phosphate buffer (0.1 M, pH 7.4). This buffer was freshly prepared before each usage.

Phosphate Buffer (0.1 M, 20 mM GSH, pH 7.4)

12.3 mg L-glutathione reduced (Sigma-Aldrich, M_W 307.32 g mol^{-1}) were dissolved in 2 mL phosphate buffer (0.1 M, pH 7.4). This buffer was freshly prepared before each usage.

Phosphate Buffer (10 mM, pH 7.4)

1.2 g sodium dihydrogen phosphate (Amresco, M_W 119.98 g mol^{-1}) were dissolved in *dd*-H$_2$O (1 L) and adjusted to pH 7.4.

Phosphate Buffer (0.1 M, pH 8.5)

12 g sodium dihydrogen phosphate (Amresco, M_W 119.98 g mol^{-1}) were dissolved in *dd*-H$_2$O (1 L) and adjusted to pH 8.5.

Running Buffer for Gel Electrophoresis (5x concentrated)

15.1 g Tris (Sigma-Aldrich, M_W 121.14 g mol^{-1}) and 94 g glycine (Sigma-Aldrich, M_W 75.07 g mol^{-1}) and a solution of SDS in *dd*-H$_2$O (20%, 25 mL) were dissolved in *dd*-H$_2$O to a final volume of 1 L.

SDS 20% in Water

20 g sodium dodecyl sulfate (Carl Roth, M_W 288.38 g mol^{-1}) were dissolved in *dd*-H$_2$O to a final volume of 100 mL.

Tris Buffer (0.1 M, 0.1 M NaCl, pH 10)

12.1 g Tris (Sigma-Aldrich, M_W 121.14 g mol^{-1}) and 5.8 g sodium chloride (Carl Roth, M_W 58.44 g mol^{-1}) were dissolved in *dd*-H$_2$O (1 L) and adjusted to pH 10.

Tris Buffer (1 M, pH 6.8)

121.1 g Tris (Sigma-Aldrich, M_W 121.14 g mol^{-1}) were dissolved in *dd*-H$_2$O (1 L) and adjusted to pH 6.8.

Tris Buffer (1.5 M, pH 8.8)

181.7 g Tris (Sigma-Aldrich, M_W 121.14 g mol^{-1}) were dissolved in *dd*-H$_2$O (1 L) and adjusted to pH 8.8.

5.1.3 DISPOSABLES

Consumables	Manufacturer
Amicon® Ultra 15 mL, MWCO 10 kDa	Merck Millipore
CELLSTAR® cell culture flasks 25 cm^2, 75 cm^2, 175 cm^2	Greiner Bio-One
Coverslips, precision (thickness: 0.17 ± 0.005 mm, borosilicate glass)	Carl Roth GmbH
96-deep-well-plate	Serva Electrophoresis
Disposable cuvettes, polystyrene	Carl Roth GmbH
Disposable hypodermic needles (size: 21 G)	B. Braun
Disposable pipettes 2 mL, 5 mL, 10 mL, 20 mL	Sarstedt
Disposable syringes 1 mL, 2 mL, 5 mL, 10 mL, 20 mL	B. Braun
Eppendorf Tubes 1.5 mL, 2 mL, 5 mL	Eppendorf
Eppendorf Tubes 1.5 mL, black	Eppendorf
Filtropur S 0.2 (sterile, non-pyrogenic)	Sarstedt
Float-A-Lyzer®G2 Dialysis Device (MWCO 100 kDa)	Spectrum Labs
Folded Capillary Zeta Cell	Malvern
Glass pipettes	Carl Roth GmbH
Locking clips for dialysis	Carl Roth GmbH
Microplate 12-well, flat bottom, clear, sterile	Greiner Bio-One
Microplate 96-well, flat bottom, clear	Sarstedt
Microplate 96-well, flat bottom, clear, sterile	Greiner Bio-One
Microplate 96-well, flat bottom, clear, UV-Star®	Greiner Bio-One
Microplate 96-well, flat bottom, black	Greiner Bio-One
Microscope slides (soda-lime glass, 76 x 26 mm, 1 mm thick)	Carl Roth GmbH
NAP™-25 Columns Sephadex™ G-25 DNA Grade	GE Healthcare
NMR tubes	Sigma-Aldrich
Parafilm	VWR
Pipette tips 2 μL, 250 μL, 1000 μL	Sarstedt
Slide-A-Lyzer™ Dialysis Cassettes (MWCO 10 kDa)	Thermo Scientific
Tubes 13 mL, 100x16 mm, polypropylene	Sarstedt
Tubes 15 mL, 120x17 mm, polypropylene	Sarstedt
Tubes 50 mL, 114x28 mm, polypropylene	Sarstedt
Xpress Micro-Dialyzer MD100 (MWCO 140 kDa)	Serva Electrophoresis
Xpress Micro-Dialyzer MD300 (MWCO 20 kDa)	Serva Electrophoresis

5.1.4 CELL LINES AND BACTERIA STRAINS

HeLa Cells

An epithelioid cervix carcinoma cell line, established from a cervical cancer tissue sample of Henrietta Lacks in 1951. Cells were a kind gift from the group of ███████████ ██

MC4100 Bacteria

The gram-negative *E. coli* strain MC4100 was used from the group of ████████ ██ ██████.

***M. Luteus* Bacteria**

The gram-positive bacteria strain *M. Luteus* was used from the group of ████████ ██ ██████

5.2 EQUIPMENT

Absorbance and Fluorescence Measurements

Equipment: Infinite® Pro M200 Plate Reader, Tecan Group Ltd., Switzerland. Analysis was carried out using i-control 1.7 software and Microsoft Excel.

Absorbance measurements were performed with clear 96-well microplates (flat bottom). Absorbance measurements to determine protein concentration (λ=280 nm) were performed with 96-well UV-Star plates. Fluorescence measurements were performed with black 96-well microplates (flat bottom). The excitation and emission wavelengths of the used fluorophores are summarized in Table 14.

Table 14: Excitation and emission maxima of the used fluorescent samples.

Fluorescent dye	$\lambda_{em.}$ / nm	$\lambda_{ex.}$ / nm
4-Methylumbelliferone	380	460
Cy5	605	675
OGD	490	527

Bath-Sonicator

Equipment: Sonorex Super RK 102 H, Bandelin electronic GmbH & Co. KG, Berlin, Germany.

Samples were sonicated until complete dissolving could be observed.

Biological Safety Cabinet

Equipment: Herasafe™, Kendro Laboratory Products, Langenselbold, Germany.

All cell culture experiments were performed in a sterile environment using a biological safety cabinet.

Centrifuges

Equipment: Heraeus™ Multifuge™ X3R, Thermo Scientific, Waltham, Massachusetts, USA.

Heraeus™ Megafuge™ 8 R, Thermo Scientific, Waltham, Massachusetts, USA.

Centrifugation was performed at the indicated times in each experiment.

Centrifugal Filter Units

Equipment: Amicon Ultra-4, regenerated cellulose, MWCO 10 kDa, Merck Millipore Ireland.

The separation of low molecular and biopolymers was carried out using centrifugal filter units with 4 mL loading capacity. They were centrifuged at 7500 g for 10 min unless otherwise stated.

Circular Dichroism (CD) Spectroscopy

Equipment: J-815 Circular Dichroism Spectrometer, JASCO International co., LTD., Hachioji, Tokyo, Japan.

Analysis was carried out using the software Spectra Manager 2.12 00.

Measurements were performed at 20 °C in 1 mm path length quartz cuvettes (Hellma Analytics).

Dialysis

Equipment: Xpress Micro-Dialyzer MD300, MWCO 20 kDa, Serva Electrophoresis GmbH, Heidelberg, Germany.

Xpress Micro-Dialyzer MD100, MWCO 140 kDa, Serva Electrophoresis GmbH, Heidelberg, Germany.

Float-A-Lyzer®G2 Dialysis Device, MWCO 100 kDa, Spectrum Labs, Rancho Dominguez, California, USA.

Slide-A-Lyzer™ Dialysis Cassette, MWCO 10 kDa, Thermo Scientific, Waltham, Massachusetts, USA.

Dialysis with Micro-Dialyzer MD300 (MWCO 6–8 kDa) was performed against PBS (pH 7.4) in a 96-deep-well-plate under constant shaking. The buffer was changed 5-times in 24 hours.

Dialysis with Micro-Dialyzer MD100 (MWCO 140 kDa) was performed against PBS (pH 7.4), 1:1 mixture of PBS (pH 7.4) and 0.1 M acetate buffer pH 5 or 1:1 mixture of PBS (pH 7.4) and 0.1 M acetate buffer pH 4 in 2 mL Eppendorf Tubes under constant shaking at 37 °C. The buffer was changed 6-times in every 24 hours.

Dialysis with Float-A-Lyzer®G2 (MWCO 100 kDa) was performed against H_2O. The water was changed every hour.

Dialysis with Slide-A-Lyzer™ (MWCO 10 kDa) was performed against H_2O. The water was changed 5-times in 24 hours.

Incubator

Equipment: Heraeus® BB15 FUNCTION Line, Thermo Scientific, Waltham, Massachusetts, USA.

Cell incubations were performed in a humidified incubator at 37 °C with 5% CO_2 atmosphere.

Inert Gas

Equipment: Argon gas bomb in 99.998% purity N46, Air Liquide Deutschland GmbH, Düsseldorf, Germany.

Argon was used as inert gas to flood flasks and reaction containers. Balloons were attached to the reaction flasks to prevent the contact of reagents with air.

Lyophilizer

Equipment: ALPHA 1-4 LSC, Martin Christ Gefriertrocknungsanlagen GmbH, Osterode am Harz, Germany.

Samples were dissolved or suspended in water, frozen in liquid nitrogen and then stored in the lyophilizer for freeze-drying for at least one day.

Mass Spectrometry (MALDI-ToF MS)

Equipment: Axima CFR MALDI-ToF mass spectrometer, Shimadzu, Columbia, Maryland, USA.

rapifleX MALDI-ToF/ToF mass spectrometer, Bruker, Billerica, Massachusetts, USA.

Analysis was performed in positive ion and linear mode of the spectrometer. Sinapic acid was used as matrix and CH_3CN/H_2O 1/1 as solvent.

Microscopy

Equipment: Leica TCS SP5 Microscope, Leica Microsysteme Vertrieb GmbH Mikroskopie und Histologie, Wetzlar, Germany.

Images were taken using the software LAS AF Lite and further processed with Fiji software.

TCS SP5 is a microscope provided by the Microscopy Core Facility, IMB, Mainz, Germany. With 4 PMTs, 4 laser lines (405 / 458, 476, 488, 496, 514 / 561 / 633 nm lines), 6 objectives (10x/0.3 dry; 20x/0.7 dry; 20x/0.7 imm; 40x/1.3 oil; 63x/1.4 oil; 63x/1.2 water) and a fast resonance scanner. Here the oil objective lens HC PL APO CS2 63.0x/1.40 OIL UV was used.

Nanoparticle Tracking Analysis (NTA)

Equipment: NanoSight LM 10, NanoSight Ltd., Amesbury, Wiltshire, United Kingdom.

Analysis was carried out using Nanosight NTA 3.4 software.

Nanoparticle Tracking Analysis (NTA) was performed with a NanoSight LM 10 microscope (Malvern Instruments) equipped with a green laser (532 nm) and a sCMOS camera. All samples were prepared in aqueous buffer with dilutions stated in every experiment. Movements of the particles were recorded as videos for 30 seconds at 25 °C in three individual measurements. The size calculation was performed with NTA software version 3.4.

Nuclear Magnetic Resonance (NMR)

Equipment: Bruker Topspin Fourier 300 MHz.

For standard analytical purpose, ^{1}H-NMR spectra were recorded at 300 MHz. The experiments were performed at room temperature (rt) using the indicated solvents. The chemical shifts were reported in ppm against the solvent signal of TMS. For the description of the signals the following abbreviations were used: s = singlet, d = doublet, t = triplet, q = quartet, m = multiplet, br = broad signal. Integrals were calculated by using MestReNova Software. Assignments were carried out according to literature. Peaks resulting from solvent residues were determined by literature.[205]

Particle Sonicator

Equipment: Bandelin Ultrasonic Homogenisator Sonoplus UW 70 (v220-240w), microtip
              MS 73 SH70G Stufenhorn 20 kHz, BANDELIN electronic GmbH & CO. KG,
              Berlin, Germany.

Sonication of all nanoparticle samples was carried out while cooling the samples on an ice bath (Settings: power 75%, cycle 70% MS 72/D).

pH Measurement

Equipment: SevenCompact™ pH/Ion S220 with a InLab® Micro special electrode,
              Mettler Toledo, Mettler-Toledo Ltd., Beaumont Leys, Leicester, United
              Kingdom.

The pH-meter was calibrated with commercial available buffer standards (pH 4.00, pH 7.00, and pH 11.00).

Rotary Evaporation

Equipment: RV06-ML Janke-Kunkel rotary evaporator; HB4 basic water bath, IKA-
              Werke GmbH & Co. KG, Staufen im Breisgau, Germany.

              CVC24 vacuum controller; 1715550193 membrane pump, Vacuubrand,
              Wertheim, Germany.

Sample concentration under reduced pressure was performed by rotary evaporation in a water bath at rt or 45 °C and the adjusted pressure for the used solvent.

Sample Incubation

Equipment: Thermomixer pro, CellMedia, Elsteraue, Germany.

Samples were incubated either at 4 °C or 37 °C and shaken with 1000 rpm.

Scales

Equipment: Mettler Toledo Excellence Plus.

Sartorius™ M-Prove™ Scales AY303, Sartorius, Göttingen, Germany.

Samples below 500 mg were weighed on the fine balance from Mettler. For samples above 500 mg, the standard laboratory balance from Sartorius was used.

Solvents

All solvents were either bought dry or dried before use.

SDS Gel Electrophoresis

Equipment: Mini Vertical Electrophoresis Unit Hoefer SE260, Hoefer Inc., Holliston, Massachusetts, USA.

GelDoc XR+ with Image Lab™ Software, Bio-Rad Laboratories Inc., Hercules, California, USA.

FUSION PULSE TS with Image Master assistant™ Software, Vilber Lourmat Deutschland GmbH, Eberhardzell, Germany.

The exact procedure is described in section 5.3.4.

Transmission Electron Microscopy (TEM)

Equipment: Tecnai T12 (FEI, acceleration voltage: 120keV, electron source: LaB6 BIO-TWIN cathode, TVIPS-F416 Camera), Hillsboro, Oregon, USA.

300-mesh copper carbon grids from Plano GmbH were used for sample preparation.

Water

Equipment: Direct-Q® 5 UV Remote Water Purification System, Merck Millipore, Germany.

Water (*dd*-H2O) for buffers and particle washing steps was purified by a Direct-Q® 5 UV Remote Water Purification System.

Zeta potential

Equipment: Malvern Zetasizer Nano ZS, Malvern Instruments GmbH, Herrenberg, Germany.

ζ-potential measurements were performed with a Zetasizer Nano ZS instrument (Malvern). Three measurements with automatic measurement duration (between 10 and 100 runs)

were performed. The refractive index (RI) of the dispersant (preset: water) was set to 1.330 and the viscosity to 0.8872 cP. The RI of the particles was set to 1.45 with a dielectric constant of 78.5. Samples were analyzed in a clear disposable folded capillary cell at 25 °C.

5.3 PROTEIN PEGYLATION

5.3.1 POLYMER FUNCTIONALIZATION

Functionalization of Methoxypolyethylene Glycol with Tetrafluorophenol (TFP-mPEG)

The activation of mPEG with 2,3,5,6-tetrafluorophenol (TFP) was performed as described previously.[126b] α-methoxy-ω-carboxy PEG 2000 (Rapp Polymer, Germany) (400 mg, 0.20 mmol) and 2,3,5,6-tetrafluorophenol (36 mg, 0.21 mmol) were dissolved under argon atmosphere in 30 mL dried dichloromethane (DCM). *N,N'*-dicyclohexylcarbodiimide (DCC) (50 mg, 0.24 mmol) was added and stirred at rt for 24 h. The mixture was diluted with 50 mL acetone, filtered and the solvent was removed under pressure. After repetition of the last step, 313 mg TFP-mPEG (0.14 mmol, 70% yield) was obtained as a slightly yellow solid.

^{1}H NMR (300 MHz, CDCl$_3$, Me$_4$Si) δ(ppm) = 7.05-6.93 (m, 1H, aromatic), 6.50 (s, br, 1H, amine), 3.64 (s, 165H, PEG), 3.37 (s, 3H, -CH$_3$), 3.04 (t, 2H, -CH$_2$-), 2.63 (t, 2H, -CH$_2$-)

Synthesis of mPEG-(disulfaneyl)ethan-1-ol

The carbonate-DS-SIL-mPEG synthesis required a three-step procedure. The first step, the synthesis of 2-(pyridine-2-yldisulfanyl)ethan-1-ol, was solely carried out in the group of ▇▇▇▇▇▇▇▇▇▇▇▇▇▇▇▇▇▇▇▇▇▇▇▇, by ▇▇▇▇▇▇▇▇▇. Following reactions for the mPEG-(disulfaneyl)ethan-1-ol and mPEG-DS-SIL nitrophenyl carbonate synthesis was firstly performed by ▇▇▇▇▇▇▇▇, subsequently, it was carried out by myself.

mPEG-SH (50 mg, 0.025 mmol) was dissolved in a mixture of 0.2 mL AcOH, 2.0 mL EtOH and 2.0 mL DMF under argon atmosphere. To this, a solution of 2-(pyridin-2-yldisulfaneyl) ethan-1-ol (18.7 mg, 0.1 mmol), which was synthesized in the group of ▇▇▇▇▇▇▇ ▇▇▇▇▇▇▇▇▇▇▇▇▇▇▇▇▇▇, by ▇▇▇▇▇▇▇▇▇ in a mixture of 0.05 mL AcOH, 0.5 mL EtOH and 0.5 mL DMF was added dropwise. The reaction was stirred overnight at rt, following by most solvent removal under vacuum. The residue was precipitated in cold Et$_2$O. After centrifugation (12 000 g, 15 min) the supernatant was removed and this

washing procedure with Et$_2$O was repeated two times. The precipitate was dissolved in *dd*-H$_2$O and lyophilization results in mPEG-(disulfaneyl)ethan-1-ol (41.49 mg, 0.020 mmol, 80% yield).

^{1}H NMR (300 MHz, CDCl$_3$, Me$_4$Si) δ(ppm) = 3.87 (t, 2H, OH-CH$_2$-), 3.64 (s, 184H, PEG), 3.55 (m, 2H, -CH$_2$-O-), 3.39 (t, 2H, -CH$_2$-S-), 3.37 (s, 3H, -CH$_3$), 2.88 (t, 2H, -S-CH$_2$-)

Synthesis of disulfide-self-immolative (DS-SIL) nitrophenol carbonate mPEG (carbonate-DS-SIL-mPEG)

mPEG-(disulfaneyl) ethan-1-ol (41.49 mg, 0.020 mmol) was dissolved in 3 mL anhydrous acetonitrile under argon atmosphere. The solution was cooled to 0 °C. After the addition of trimethylamine (3.82 μL, 0.02 mmol), subsequently a solution of 4-nitrophenyl chloroformate (20 mg, 0.1 mmol) in 1 mL anhydrous acetonitrile was added. The reaction was allowed to slowly warm up to rt. After 5 hours, additional 4-nitrophenyl chloroformate (20 mg, 0.1 mmol) in 1 mL anhydrous acetonitrile was added. The reaction was stirred overnight at rt, following by removal of the solvent. The residue was dissolved in DMF and precipitated in cold Et$_2$O. After centrifugation (12 000 g, 15 min) the supernatant was removed and the washing step with Et$_2$O was repeated two times. The precipitate was dissolved in *dd*-H$_2$O and lyophilization results in mPEG-DS-SIL nitrophenyl carbonate (37.87 mg, 0.017 mmol, 84% yield, 25% functionalized).

^{1}H NMR (300 MHz, CDCl$_3$, Me$_4$Si) δ(ppm) = 8.28 (d, 0.5H, aromatic), 7.40 (d, 0.5H, aromatic), 3.64 (s, 157H, PEG), 3.38 (s, 3H, -CH$_3$), 3.11 (s, br, 4H, -CH$_2$-S-S-CH$_2$-)

Protection of the thiol group of mPEG-SH with 2,2'-dipyridyldisulfide (mPEG-S-S-Py)

First, due to possible oxidation of the free thiol-group, polyethylene glycol methyl ether thiol (mPEG-SH) (212.42 mg, 0.1 mmol) was reduced with TCEP (60.89 mg, 0.2 mmol). Therefore, mPEG-SH (212.42 mg, 0.1 mmol) and TCEP (60.89 mg, 0.2 mmol) were combined in 2 mL *dd*-H$_2$O and stirred overnight at rt. After the reaction time, 2,2'-dipyridyldisulfide (467.06 mg, 2.1 mmol) in 1.75 mL methanol was mixed with the reduced mPEG-SH. Then, 2.5 mL 0.1 M Tris buffer (0.1 M NaCl, pH 10) was added and the reaction mixture was allowed to stir overnight at rt. The product was purified by size exclusion chromatography (NAP™-25 Columns Sephadex™ G-25 DNA Grade, GE Healthcare, UK, buffer: *dd*-H$_2$O). Freeze-drying results in mPEG-S-S-Py (141.44 mg, 0.067 mmol, 67%, 89% functionalized) as a white powder.

¹H NMR (300 MHz, CDCl₃, Me₄Si) δ(ppm) = 8.59 (s, br, 1H, aromatic), 8.27 (s, br, 2H, aromatic), 7.51 (s, br, 1H, aromatic), 3.64 (s, 167H, PEG), 3.37 (s, 3H, -CH₃), 3.20 (s, br, 2H, -S-CH₂-)

5.3.2 PROTEIN FUNCTIONALIZATION

SATP Modification of Cytochrome *c* (Cyt$_{SATP}$)

20 mg horse heart cytochrome *c* [EC 232-700-9] (1.6 μmol) were dissolved in 4 mL 0.1 M phosphate buffer (0.15 M sodium chloride, pH 7.2) and combined with 7.52 mg *N*-succinimidyl-*S*-acetylthiopropionate (SATP) (30.6 μmol) in DMSO (40 μL). The mixture was stirred for 1 h at rt. The modified protein was purified by centrifugal filters (Amicon® Ultra 4 centrifugal filter membranes, regenerated cellulose, MWCO 10 kDa, 7500 *g*, 10 min, 4 °C, Merck Millipore) for four times with *dd*-H₂O. The product was lyophilized (ALPHA 1-2 LD plus) subsequently.

TNBS Assay for Amine Quantification of Native Cyt and Cyt$_{SATP}$

The number of primary amino groups of Cyt$_{SATP}$ was determined by a TNBS assay. Cyt$_{SATP}$ was dissolved in 0.1 M borate buffer pH 9 in a concentration of 23 μM. Native Cyt was used as an external standard in a concentration range of 2.5–20 μM in 0.1 M borate buffer pH 9. 500 μL of Cyt$_{SATP}$ and the Cyt standard were mixed with 3 μL 2.5% TNBS solution in black Eppendorf tubes. The mixtures were incubated at 37 °C for 2 h. Subsequently, 100 μL of each solution were pipetted in a clear 96-well plate and the absorbance was measured in triplets at 335 nm (Infinite® 200 PRO (Tecan) plate reader). For all samples, blank measurements without TNBS were carried out at 335 nm and subtracted as background from each measurement.
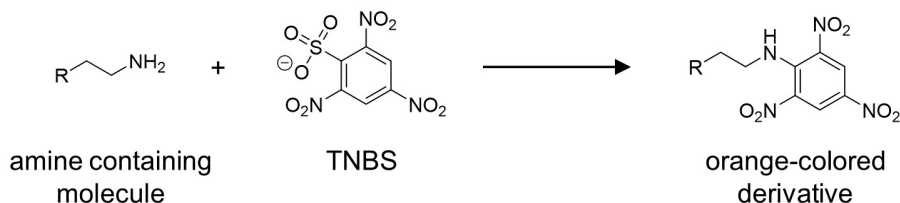
Figure 83: Primary amine reacts with 2,4,6-trinitrobenzene sulfonic acid (TNBS), resulting in an orange product whose absorbance can be detected at 335 nm.

Fluorescence Labeling of LYZ (Cy5-LYZ)

Lysozyme (30.65 mg, 2.10 μmol) was dissolved in 3 mL of 0.1 M borate buffer (pH 7) and combined with sulfo-cyanin 5 NHS-ester (Cy5, 1.00 mg, 1.31 μmol). The mixture was stirred for 1 h at rt and shielded from light. The modified protein was purified by size exclusion chromatography (NAP™-25 Columns Sephadex™ G-25 DNA Grade, GE Healthcare, UK, buffer: *dd*-H$_2$O). After lyophilisation, a fluffy blue product was obtained.

The fluorescent labeling was quantified by measuring the fluorescence (ex. 605 nm; em. 675 nm) of the modified protein in comparison to free Cy5 in triplets of 100 μL, using an Infinite® 200 PRO (Tecan) plate reader. The Cy5 standard was prepared in 0.1 M borate buffer (pH 7.0). Cy5-LYZ was dissolved in the same buffer and diluted to a final concentration of 20.07 μM, according to an M$_W$ of 14.95 kDa (LYZ modified with one Cy5 molecule). The Cy5 content of the protein solution was 5.22 μM, leading to a Cy5 per protein ratio of 0.26:1. This means approx. every 4th protein was modified with a fluorophore.

5.3.3 PROTEIN PEGYLATION

Lysozyme PEGylation with TFP-mPEG (LYT$_{mPEG}$)

15 mg lysozyme from chicken egg white [EC 3.2.1.17] (1.0 μmol) and 50 mg TFP-mPEG (0.023 mmol) were dissolved in 3 mL 0.1 M carbonate buffer pH 8 and stirred for 48 h at rt. The mixture was purified by size exclusion chromatography (NAP^{TM}-25 Columns Sephadex^{TM} G-25 DNA Grade, GE Healthcare, UK, buffer: *dd*-H$_2$O). The product was collected and lyophilized (ALPHA 1-2 LD plus).

Cytochrome *c* PEGylation with mP(EG-*co*-*iso*EPB)-NHS (Cyt$_{degPEG}$)

Horse heart cytochrome *c* [EC 232-700-9] (0.4 μmol) and mP(EG-*co*-*iso*EPB)-NHS were dissolved in 0.1 M phosphate buffer pH 8.5 and stirred overnight at 4 °C (specific compositions are summarized in Table 15). The mixture was purified by column chromatography (Sephadex® G-75 medium, Sigma-Aldrich, buffer: *dd*-H$_2$O). After collecting the first fraction yielding the product, the modified protein was concentrated with Amicon® Ultra 4 centrifugal filter membranes (regenerated cellulose, MWCO 10 kDa, 7500 *g*, 10 min, 4 °C, Merck Millipore). The product was lyophilized (ALPHA 1-2 LD plus).

Table 15: Reaction compositions of Cyt$_{degPEG}$ synthesis.

Cyt / mg	Cyt / µmol	polymer batch	polymer eq	polymer / mg	V (buffer) / mL
5	0.4	**1**	10	16.1	1
5	0.4	**1**	15	24.2	1
2.5	0.2	**1**	25	20.2	0.5
5	0.4	**2**	17	27.4	1

Cytochrome *c* PEGylation with carbonate-DS-SIL-mPEG (Cyt$_{DS\text{-}SIL\text{-}mPEG}$)

3 mg Cytochrome *c* [EC 232-700-9] (0.24 µmol) and 14.52 mg carbonate-DS-SIL-mPEG (7.26 µmol, 25% functionalized) were dissolved in 600 µL 0.1 M carbonate buffer pH 8 and stirred for 48 h at rt. The mixture was purified by centrifugal filters (Amicon® Ultra 4 centrifugal filter membranes, regenerated cellulose, MWCO 10 kDa, 7500 *g*, 10 min, 4 °C, Merck Millipore) for four times with *dd*-H$_2$O. The product was lyophilized (ALPHA 1-2 LD plus) subsequently.

Cyt$_{SATP}$ PEGylation with mPEG-S-S-Py (Cyt$_{S\text{-}S\text{-}mPEG}$)

To deprotect the thiol groups of the SATP-linker, 5 mg Cyt-SATP (0.4 µmol) were dissolved in 1 mL PBS (pH 7.4) and mixed with 100 µL deacetylation solution (see section 5.1.2). The mixture was stirred for 2 h at rt and purified by centrifugal filters (Amicon® Ultra 4 centrifugal filter membranes, regenerated cellulose, MWCO 10 kDa, 7500 *g*, 10 min, 4 °C, Merck Millipore) for three times with PBS containing 10 mM EDTA. The protein was subsequently used for PEGylation. 8.06 mg mPEG-S-S-Py (4.0 µmol) were dissolved in PBS containing 10 mM EDTA and combined with the deprotected Cyt$_{SATP}$ resulting in a total volume of 1 mL. The mixture was stirred overnight at rt. The reaction mixture was purified by centrifugal filters (Amicon® Ultra 4 centrifugal filter membranes, regenerated cellulose, MWCO 10 kDa, 7500 *g*, 10 min, 4 °C, Merck Millipore) for four times with *dd*-H$_2$O. The product was lyophilized (ALPHA 1-2 LD plus) subsequently.

5.3.4 Analysis of PEGylated Proteins

SDS Gel Electrophoresis

SDS-PAGE for protein analysis was carried out like described elsewhere.[159] For all SDS-PAGES a 15% polyacrylamide separation gel (Table 16) with a thickness of 0.75 mm

(T Spacer, Hoefer, USA) was prepared. The stacking gel was prepared according to Table 16 and added on the top of the separation gel.

The native enzymes (1 mg mL^{-1}) and PEGylated enzymes (2–8 mg mL^{-1}) were dissolved in the denoted concentration in water. 15 μL of the protein-solutions were denaturized by adding 5 μL of Roti®-Load 1 and heated in a boiling water bath for 15 min. In the case of retaining disulfide bonds, 5 μL of the non-reducing loading buffer (Table 17) were combined with 15 μL of the protein-solutions and the mixtures were not incubated in a boiling water bath. 20 μL of each mixture was completely pipetted into one pocket of the gel. Empty pockets were loaded with loading buffer. As marker 5 μL of prestained protein ladder (10–170 kDa) was used. A voltage of 90 mV was applied for 60 min, following by a voltage of 200 mV for further 60 min. The gel was stained using a coomassie staining solution. Images of SDS-PAGE gels were taken with GelDoc™ XR+ (Bio-Rad Laboratories Inc.) and processed with the Image Lab™ Software (camera filter 1) or with FUSION PULSE TS (Vilber Lourmat Deutschland GmbH) and processed with the 'Image Master' assistant™ Software (camera filter 2).

Table 16: Composition of the 15% separation with a total volume of 5 mL and the stacking gel with a total volume of 2 mL for SDS-PAGE analysis.

components	separation gel	stacking gel
H_2O in mL	1.125	1.37
Rotiphorese® 30 in mL	2.5	0.34
1.5 M Tris (pH 8.8) in mL	1.3	-
1 M Tris (pH 6.8) in mL	-	0.26
20% SDS in mL	0.025	0.01
10% APS in mL	0.05	0.02
TEMED in mL	0.002	0.002

Table 17: Composition of the non-reductive loading buffer for SDS-PAGE analysis.

components	quantity
bromphenole blue	8 mg
Tris	2.27 g
glycerin	30 mL
dd-H_2O	to 100 mL

MALDI-ToF MS Measurement

The MALDI-ToF measurements were obtained with a Shimadzu Axima CFR MALDI-ToF mass spectrometer. This mass spectrometer is equipped with a nitrogen laser, which pulsed the samples every 3 ns at 337 nm. Furthermore, rapifleX MALDI-ToF/ToF mass spectrometer was used, equipped with a 10 kHz scanning Smartbeam 3D Laser (Nd:YAG at 355 nm) and 10 bit 5 GHZ Digitizer. Samples were dissolved in CH_3CN/TFA 0.1% or CH_3CN/H_2O 1/1 with concentrations of around 1 mg mL^{-1}. Sinapic acid was used as matrix and applied on a multistage target before 1 μL of the sample was also applied and dried by evaporation. The sample was measured in positive ion and linear mode of the spectrometer.

Circular Dichroism (CD)

The CD measurements were recorded with a Jasco J-815 Circular Dichroism spectrometer at 20 °C using the Spectra Manager 2.08.04 software. Native enzymes were analyzed with a concentration of 0.1 mg mL^{-1} in 10 mM K_3PO_4/50 mM Na_2SO_4 buffer (pH 7). PEGylated enzymes were dissolved in the same buffer and their concentration was adjusted to the same value as native enzyme by absorbance at 280 nm (for PEGylated LYZ) or 409 nm (for PEGylated Cyt). Measurements were made in quartz cells with a path length of 1 mm. The resolution during the collection of all data points was 0.1 nm. The measurements were performed in triplets and the spectrum of the buffer was subtracted as background. Secondary structure was determined with DichroWeb using the analysis program CONTIN (reference set 7).[206]

Enzymatic Activity of PEGylated Lysozyme

LYZ$_{mPEG}$ and native LYZ were dissolved in 0.1 M phosphate buffer (pH 5.2) in a concentration of 2 μM. 4-Methylumbelliferyl-β-D-*N,N',N''*-triacetylchitotriosid ((GlcNAc)$_3$MeU) was dissolved in 0.1 M phosphate buffer (pH 5.2) in a concentration of 20 μM and incubated at 42 °C for 5 min. 200 μL of LYZ$_{mPEG}$ or native LYZ was mixed with 200 μL of the (GlcNAc)3MeU-solution and incubated at 42 °C. After 0 min, 10 min, 30 min and every next half hour (until 2.5 h were over) the catalytic activity of 50 μL of the incubated solution was stopped with 300 μL 0.5 M glycine buffer (pH 12) and stored in the fridge. In the end, the fluorescence of 100 μL of all samples was measured in triplets in a 96 well plate (Infinite® 200 PRO (Tecan) plate reader, ex. 380 nm; em. 460 nm).
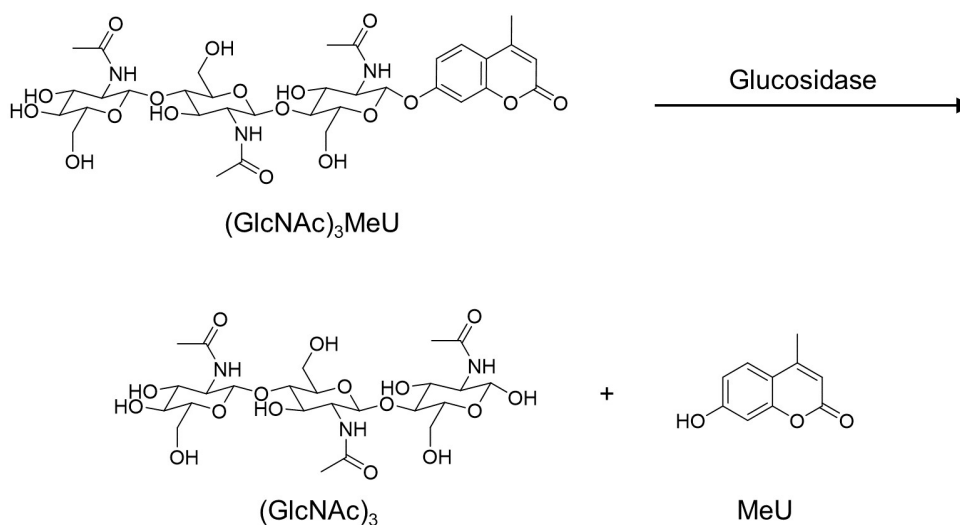
Figure 84: Cleavage of the 4-Methylumbelliferyl-β-D-*N,N',N''*-triacetylchitotriosid substrate ((GlcNAc)₃MeU) by the glycosidase activity of LYZ. The cleaved 4-methylumbelliferone (MeU) results in a fluorescent signal, which can be detected (ex. 380 nm; em. 460 nm).

Enzymatic Activity of PEGylated Cytochrome *c*

The enzymatic activity of native Cyt, Cyt$_{degPEG}$ and Cyt$_{DS-SIL-mPEG}$ were analyzed using an 2,2'-azinobis-(3-ethylbenzthiazoline-6-sulfonate) (ABTS) assay. 10 mM phosphate buffer pH 7.4 was used as working buffer. 100 μL of ABTS solution (2 mM) was mixed with 50 μL of samples (native Cyt or Cyt$_{degPEG}$, 22.6 μM) in a 96-well-microplate (flat bottom). The reaction was initiated by adding 50 μL of an H$_2$O$_2$ solution (2 mM in *dd*-H$_2$O). Subsequently, the change in absorbance at 405 nm was measured for 3 minutes (Infinite® 200 PRO (Tecan) plate reader). The absorbance of the background (100 μL ABTS with 50 μL sample, but instead of H$_2$O$_2$ solution only 50 μL *dd*-H$_2$O) was subtracted from each measurement.
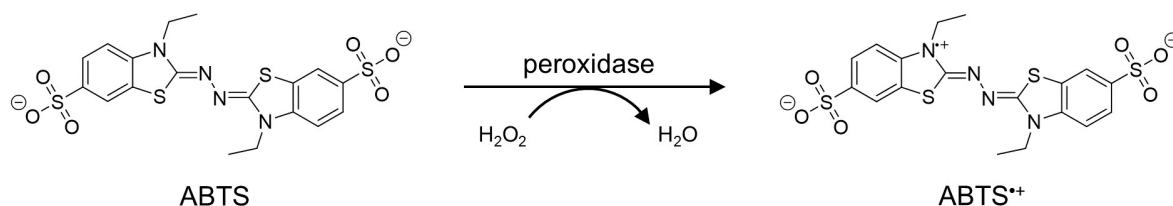
Figure 85: Peroxidase catalyzed reaction of ABTS and H$_2$O$_2$, resulting in the green ABTS radical cation (ABTS•⁺), whose absorbance can be detected at 405 nm.

5.3.5 DEGRADATION ANALYSIS OF PEGYLATED PROTEINS

Analysis of Cyt$_{degPEG}$ Degradation by SDS-PAGE

Cyt$_{degPEG}$ was dissolved in 0.1 M sodium acetate buffer pH 4 or pH 5 or 0.1 M phosphate buffer pH 6 or pH 7.4 in concentrations of 8 mg mL^{-1}. These samples were incubated for

24 h at 37 °C and shaken with 1000 rpm. Native Cyt (1 mg mL^{-1}) and Cyt$_{degPEG}$ (8 mg mL^{-1}) was freshly dissolved in *dd*-H$_2$O. 15 μL of the protein-solutions were denaturized by adding 5 μL of Roti®-Load 1 and heated in a boiling water bath for 15 min. The different samples were analyzed with a 15% polyacrylamide gel.

Analysis of Cyt$_{degPEG}$ Degradation by SEC

Cyt$_{degPEG}$ was dissolved in a concentration of 150 μM in 0.1 M sodium acetate buffer (pH 4, pH 5) or in 0.1 M phosphate buffer (pH 6, pH 7.4). Similarly, native Cyt (150 μM) was dissolved in 0.1 M sodium acetate buffer pH 4 as control. These samples were incubated for 24 h at 37 °C and shaken at 1000 rpm. For comparison, native Cyt (150 μM) and Cyt$_{degPEG}$ (150 μM) were freshly dissolved in *dd*-H$_2$O and measured directly. 150 μL of the protein-solutions were analyzed with size exclusion chromatography. The SEC runs were performed on a 24 mL high-resolution size exclusion column (Superdex™ 75 10/300 GE Healthcare Bio-Sciences AB) at 4 °C with a flow rate of 0.8 mL in PBS pH 7.4.

Degradation Analysis of Redox-Sensitive PEGylated Enzymes by SDS-PAGE

Cyt$_{DS-SIL-mPEG}$ and Cyt$_{S-S-mPEG}$ were dissolved in concentrations of 8 mg mL^{-1} in 0.1 M phosphate buffer pH 7.4 or 0.1 M phosphate buffer pH 7.4 with 10 mM GSH. These samples were incubated for 24 h at 37 °C and shaken with 1000 rpm. Native Cyt (1 mg mL^{-1}) and the PEGylated enzymes (8 mg mL^{-1}) were freshly dissolved in *dd*-H$_2$O. 5 μL of the non-reductive loading buffer was combined with 15 μL of each protein-solutions. The different samples were analyzed with a 15% polyacrylamide gel.

5.4 NANOPARTICLE PREPARATION

5.4.1 DOUBLE EMULSION-BASED NANOPARTICLE PREPARATION

Preparation of LYZ$_{mPEG}$-based Nanoparticles by Double Emulsion Technique

LYZ$_{mPEG}$ (5 mg) was dissolved in 0.8 mL DCM. After adding 100 μL *dd*-H$_2$O, the solution was sonicated on ice for 15 s. To the resulting emulsion, 4 mL of ice-cold PBS buffer (pH 7.4) was added and treated again with ultrasonic pulses for 30 s. The majority of DCM in the w/o/w emulsion was removed under reduced pressure (15 min, 700 mbar, rt, 280 rpm). Remaining traces of DCM were evaporated by stirring at rt for 45 min, resulting in an opaque nanoparticle suspension.

For the encapsulation of GS, 100 μL of GS-solution in dd-H$_2$O (2 mg mL^{-1}) was added to the DCM solution before carrying out the first sonication step (instead of 100 μL dd-H$_2$O).

For the encapsulation of LYZ or Cy5-LYZ, 100 μL of enzyme-solution in dd-H$_2$O (40 mg mL^{-1}) was added to the DCM solution at the first sonication step (instead of 100 μL dd-H$_2$O). These nanoparticles were purified by SEC (see section 5.4.3).

Preparation of Nanoparticles Consisting of Cyt$_{degPEG}$ by Double Emulsion Technique

Cyt$_{degPEG}$ (1.4 mg, 1.6 mg 1.75 mg, 2.5 mg, 2.75 mg, 3.0 mg or 5 mg) was dissolved in 0.4 mL DCM. After adding 50 μL of dd-H$_2$O the two phases were sonicated on ice for 15 s. To the resulting emulsion, 2 mL of ice-cold PBS buffer (pH 7.4) was added and treated again with ultrasonic pulses for 30 s. The DCM of the w/o/w emulsion was evaporated by stirring at rt overnight, resulting in an opaque nanoparticle suspension.

For the encapsulation of Oregon-Green™488-dextran (OGD) or dextran (DEX) in Cyt$_{degPEG}$-NPs, 50 μL of an OGD/DEX solution (10 kDa dextran, 2 mg mL^{-1} in PBS pH 7.4) was added to the DCM solution at the first sonication step (instead of 50 μL dd-H$_2$O).

5.4.2 SINGLE EMULSION-BASED NANOPARTICLE PREPARATION

For the preparation of protein-based nanoparticles by single emulsion the PEGylated enzymes Cyt$_{degPEG}$ or Cyt$_{DS-SIL-mPEG}$ (1.4 mg or 1.75 mg) were dissolved in ice-cold dichloromethane (DCM, 0.4 mL) and covered by 2 mL ice-cold PBS buffer (pH 7.4). The mixture was sonicated for 45 s on ice, using an ultrasonicator (Bandelin Ultrasonic Homogenisator Sonoplus UW 70 (v220-240w), microtip MS 73 SH70G Stufenhorn 20 kHz). The emulsion was stirred in a well-ventilated hood overnight for evaporation of DCM.

For the encapsulation of curcumin (CUR) in Cyt$_{degPEG}$-NPs, 40 μg CUR and 1.4 mg Cyt$_{degPEG}$ were combined in 0.4 mL DCM, covered with 2 mL ice-cold PBS buffer (pH 7.4) and further treated like described before.

5.4.3 NANOPARTICLE PURIFICATION AFTER ENCAPSULATION OF FLUORESCENT COMPOUNDS

Purification of loaded LYZ$_{mPEG}$-Nanoparticles

GS-loaded LYZ$_{mPEG}$-nanoparticle were freshly prepared and purified by dialysis (Float-A-Lyzer®G2 Dialysis Device, MWCO 100 kDa, Spectrum Labs) against H$_2$O for 8 h.

The LYZ$_{mPEG}$-nanoparticle with encapsulated Cy5-LYZ suspensions were purified by size exclusion chromatography (Sephadex® G-100, medium, Sigma-Aldrich, Germany, buffer: PBS, pH 7.4). 0.5 mL of the nanoparticle suspension was applied onto the column. 147 μL was collected per fraction in a clear 96 well plate. The absorbance of the Cy5-labeled protein was analyzed at 650 nm and the unlabeled ones at 280 nm. Fractions 16–24 (V=1.32 mL) were selected for the collection of purified Cy5-LYZ loaded LYZ$_{mPEG}$-NP in order to separate from free Cy5-LYZ. The purification was repeated to a total of four times (V$_{total}$=5.3 mL).

Purification of Cyt$_{degPEG}$-based Nanoparticles

CUR-loaded Cyt$_{degPEG}$-NP were freshly prepared and purified by dialysis (Slide-A-Lyzer™ Dialysis Cassette, MWCO 10 kDa, Thermo Scientific) against H$_2$O for 1 d to remove not encapsulated CUR.

OGD-loaded Cyt$_{degPEG}$-NP were freshly prepared and purified by dialysis (Float-A-Lyzer®G2 Dialysis Device, MWCO 100 kDa, Spectrum Labs) against H$_2$O for 4 h to remove not encapsulated OGD.

5.4.4 DETERMINATION OF LYZ$_{mPEG}$-NANOPARTICLE CONCENTRATION AFTER PURIFICATION

To calculate the concentration of the LYZ$_{mPEG}$-nanoparticle suspension after purification, the absorbance at 280 nm of a linear dilution of unpurified empty nanoparticles with known concentrations was used as standard. The standard and the purified NP were measured in triplets of 100 μL using an Infinite® 200 PRO (Tecan) plate reader. The absorbance of the background (PBS pH 7.4) was subtracted from each measurement. The direct measurement of LYZ-loaded particles is not possible, due to the additional absorbance of encapsulated lysozyme. However, since the particle preparation and purification are identical, the same particle concentration is expected.

5.4.5 DETERMINATION OF CY5-LYZ CONCENTRATION

After purification of the LYZ$_{mPEG}$-nanoparticle suspension, the Cy5-LYZ content of the particles was determined by measuring the fluorescence (ex. 605 nm, em. 675 nm) of the particle suspension in comparison to a Cy5-LYZ standard in triplets of 100 μL using an Infinite® 200 PRO (Tecan) plate reader. The fluorescence of the background (PBS pH 7.4) was subtracted from each measurement. The Cy5-LYZ loading can vary and has to be determined for each new particle batch.

5.4.6 DETERMINATION OF OGD CONCENTRATION

After purification of the Cyt$_{degPEG}$-nanoparticles, the OGD content of the particles was determined by measuring the fluorescence (ex. 490 nm, em. 527 nm) of the particle suspension in comparison to an OGD standard in triplets of 100 μL using an Infinite® 200 PRO (Tecan) plate reader. The fluorescence of the background (PBS pH 7.4) was subtracted from each measurement.

5.4.7 ENCAPSULATION EFFICIENCY AND LOADING CAPACITY

The amount of the loaded fluorescent drug into the protein-based nanoparticles was determined by the following eq. 1 and eq. 2. The amount in mol of the encapsulated drug was calculated by multiplication of the determined encapsulated concentration with the total volume of the purified particles (V(LYZ$_{mPEG}$-nanoparticles)=5.3 mL, V=(Cyt$_{degPEG}$-nanoparticles)=2 mL). The mass in g was calculated by multiplication of the mol with the molecular weight (M$_W$(Cy5-LYZ)=14946.76 g mol^{-1}; M$_W$(OGD)=10000 g mol^{-1}). The mass of LYZ$_{mPEG}$ was determined with the calculated LYZ$_{mPEG}$-nanoparticle concentration multiplied with the total volume of the purified particle (5.3 mL). The mass of Cyt$_{degPEG}$ was calculated with the initial concentration which was used for the particle preparation (1.375 mg mL^{-1}) multiplied with the total volume of the purified particle (2 mL).

$$\text{EE (mol\%)} = \frac{n_{drug,encapsulated}}{n_{drug,feed}} \cdot 100\% \qquad \text{eq. 1}$$

$$\text{LC (wt\%)} = \frac{m_{drug,encapsulated}}{m_{drug,encapsulated} + m_{PEGylated\ protein}} \cdot 100\% \qquad \text{eq. 2}$$

5.4.8 CHARACTERIZATION OF PARTICLE SIZE, CHARGE AND SHAPE

Determination of Particle Size by Nanoparticle Tracking Analysis

Particle size and particle degradation were determined by Nanoparticle Tracking Analysis (NTA). NTA was performed on a NanoSight LM 14 equipped with a green laser (532 nm) and a marlin charged coupled device (CCD) camera. PEGylated Cyt-based particles were diluted in a ratio of 1:50, 1:25, or 1:12.5. LYZ_{mPEG}-based nanoparticles which were purified by size exclusion chromatography (180 μg mL^{-1} in PBS pH 7.4) were diluted in a ratio of 1:7 in PBS (pH 7.4). The samples were loaded into the measurement cell. Movements of particles in the samples were recorded as videos for 30 seconds at 25 °C. The videos were analyzed with the NanoSight NTA 3.1 software showing the mean values of three individual measurements.

Table 18: Software settings for NTA measurements of nanoparticles.

Capture:	Screen Gain 1.0
	Camera level 11
Process:	Screen Gain 1.0
	Detection Threshold 5

Determination of Particle Surface Charge by Measuring Zeta Potential

ζ-potential measurements were performed with a Zetasizer Nano ZS instrument (Malvern). Three measurements with automatic measurement duration (between 10 and 100 runs) were performed. The refractive index (RI) of the dispersant (preset: water) was set to 1.330 and the viscosity to 0.8872 cP. The RI of the particles was set to 1.45 with a dielectric constant of 78.5. All nanoparticles were analyzed without dilution. Samples were analyzed in a clear disposable folded capillary cell at 25 °C.

Determination of Particle Shape by Transmission Electron Microscopy (TEM)

Nanoparticle suspensions were drop-casted on a 300-mesh copper carbon grid from Plano GmbH for TEM measurements (5 μL). The image acquisition was done with a transmission electron microscope Tecnai T12 (FEI, acceleration voltage: 120 kV, electron source: LaB6 BIO-TWIN cathode) equipped with a 4K CCD camera (Tietz).

5.4.9 NANOPARTICLE STABILITY ANALYSIS AND PAYLOAD RELEASE

Nanoparticle Degradation Analysis of Cyt$_{degPEG}$-NPs

The stability of Cyt$_{degPEG}$-NPs were analyzed by NTA measurements over time at different pH values. 500 μL NP suspension was mixed with either 500 μL 0.1 M sodium acetate buffer pH 4, 500 μL 0.1 M sodium acetate buffer pH 5 or 500 μL PBS pH 7.4 as control. The mixtures were incubated at 37 °C and shaken at 1000 rpm. After 0 h, 24 h and 48 h NTA measurements were performed with the same dilutions. The dilutions were carried out in the corresponding buffers (0.1 M sodium acetate buffer pH 4 or pH 5 or PBS pH 7.4).

Nanoparticle Degradation Analysis of Cyt$_{DS\text{-}SIL\text{-}mPEG}$-NPs

The stability of Cyt$_{DS\text{-}SIL\text{-}mPEG}$-NPs were analyzed by NTA measurements over time at different pH values. 900 μL NP suspension was mixed with either 900 μL 0.1 M phosphate buffer pH 7.4 containing 20 mM GSH or 500 μL PBS pH 7.4 as control. The mixtures were incubated at 37 °C and shaken at 1000 rpm. NTA measurements were performed over time with the same dilutions. The dilutions were carried out in the corresponding buffers (0.1 M phosphate buffer pH 7.4 containing 10 mM GSH or PBS pH 7.4).

Determination of Cy5-LYZ Release and LYZ$_{mPEG}$-Nanoparticle Stability

Cy5-LYZ loaded LYZ$_{mPEG}$-nanoparticles and empty nanoparticles were freshly prepared and purified. Subsequently, the encapsulated amount of Cy5-LYZ was determined (7.29 μg mL^{-1}, method in section 5.4.5) and the same amount of free Cy5-LYZ was dissolved in PBS (pH 7.4). The samples (300 μL) were dialyzed (Xpress Micro-Dialyzer MD300, MWCO 20 kDa, Serva) against PBS pH 7.4 at rt and analyzed by fluorescence measurement (Infinite® 200 PRO (Tecan) plate reader, ex. 605 nm, em. 675 nm) and NTA size measurements over a period of 24 h.

Determination of OGD Release and Cyt$_{degPEG}$-Nanoparticle Degradation

The degradation of Cyt$_{degPEG}$-NP and the release of OGD under acidic conditions was analyzed using a dialysis experiment. After nanoparticle purification to remove not encapsulated OGD, the particles were then mixed in a 1:1 ratio with either 0.1 M sodium acetate buffer pH 4, 0.1 M sodium acetate buffer pH 5 or PBS pH 7.4 as control. 100 μL of these mixtures were dialyzed (Xpress Micro-Dialyzer MD100, MWCO 140 kDa, Serva) against the corresponding buffer mix (1:1 mix of 0.1 M sodium acetate buffer pH 4 and PBS

pH 7.4, 0.1 M sodium acetate buffer pH 5 and PBS pH 7.4 or PBS pH 7.4 alone) at 37 °C. The particle degradation and OGD release were analyzed by NTA size measurements and a fluorescence readout (ex. 490 nm, em. 527 nm; Infinite® 200 PRO (Tecan) plate reader) over a period of 48 h. The data for the 0-hour value was measured directly after mixing of the nanoparticle suspension with the appropriate buffer.

5.4.10 TOXICITY OF PEGYLATED PROTEINS AND NPs

Cell Viability by MTT Assay

HeLa cell lines were grown in Dulbecco's Modified Eagle Medium (DMEM) supplemented with 10% (v/v) fetal calf serum (FCS), 1% pyruvate and 1% penicillin-streptomycin. Cell incubations were performed in a humidified incubator at 37 °C with 5% CO_2 atmosphere. All used buffers were either autoclaved, sterile filtered or already sterile when supplied and were preheated to 37 °C. Cells were grown in 75 cm^2 or 25 cm^2 standard cell culture flasks.

The cell viability of human HeLa cells in presence of native enzymes, PEGylated enzymes and nanoparticles was determined using the MTT method. Cells were seeded in 96 well plates with a density of $1.5 \cdot 10^4$ cells per well and allowed to attach overnight. After removal of the cell culture media, 100 μL of different dilutions of the samples were added as triplets to the well plate. After an incubation time of 48 h (37 °C, 5% CO_2) a solution of 3-(4,5-dimethyl-2-thiazolyl)-2,5-diphenyl-2H-tetrazolium bromide (MTT) in medium (40 μL, 3.0 mg mL^{-1}) was added directly to each well and the plate was incubated for additional 20 min. The medium was then replaced and a mixture of DMSO (200 μL per well) and 0.1 M glycine buffer (25 μL per well, pH 10) was added. After a shaking time of 15 min, 50 μL per well of this purple DMSO solution was added to another clear-bottom 96-well assay plate (Greiner Bio-One) containing a mixture of 0.1 M glycine buffer (17 μL per well, pH 10) and DMSO (133 μL per well). The absorbance at 570 nm was measured using an Infinite® 200 PRO (Tecan) plate reader. The absorbance at 690 nm was subtracted as background. Cell viability was normalized to the absorbance measured from untreated cells.

For analysis of the cell viability of materials of the LYZ$_{mPEG}$ project, Cy5-LYZ loaded LYZ$_{mPEG}$-nanoparticles were prepared freshly and purified by size exclusion chromatography (Sephadex® G-100). Empty and loaded LYZ$_{mPEG}$-nanoparticles were diluted with culture media to particle concentrations of 0.14–4.37 μM. The concentrations of free LYZ were 0.01–0.31 μM in order to match the amount in the corresponding LYZ-loaded NPs.

For analysis of the cell viability of materials of the Cyt_{degPEG} project native Cyt, Cyt_{degPEG} and freshly prepared Cyt_{degPEG}-nanoparticles were diluted with culture media to concentrations of 0.73–23.50 μM.

For analysis of the cell viability of materials of the $Cyt_{DS-SIL-mPEG}$ project native Cyt, $Cyt_{DS-SIL-mPEG}$ and freshly prepared $Cyt_{DS-SIL-mPEG}$-nanoparticles were diluted with culture media to concentrations of 0.51–16.37 μM.
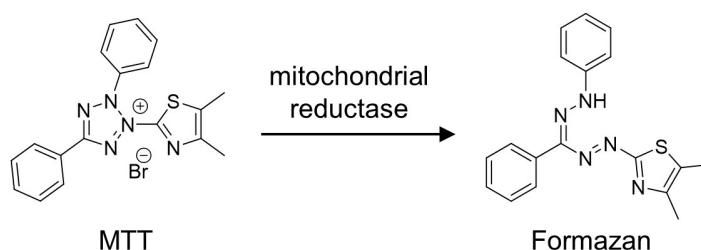
Figure 86: Reduction of the water-soluble 3-(4,5-dimethyl-2-thiazolyl)-2,5-diphenyl-2H-tetrazolium bromide (MTT) to the water-insoluble formazan by the mitochondrial reductase in cells.

Determination of Antimicrobial Activity by MIC

Micrococcus Luteus (*M. Luteus*) was cultivated overnight in LB medium. The next day the overnight culture of the bacteria was diluted in 25 mL LB media (1:100) and allowed to grow to log phase. Empty nanoparticles and Cy5-LYZ-loaded nanoparticles were freshly prepared and purified with Sephadex® G-100. The concentration of encapsulated Cy5-LYZ (8.99 μg mL^{-1}) was determined with a Cy5-LYZ standard (method in section 5.4.5). For the MIC determination, the amount of free and encapsulated Cy5-LYZ was adjusted to match. Similarly, the concentrations of empty particles were matched with the Cy5-LYZ-loaded particles. All particles and free Cy5-LYZ were diluted with PBS (pH 7.4) and mixed (1 mL each) with 1 mL of *M. Luteus* (OD = 0.075). The final concentrations of encapsulated and free Cy5-LYZ were 4.50–0.14 μg mL^{-1}, empty nanoparticles were analyzed in a concentration range between 90–2.81 μg mL^{-1} of particle material. All initial mixtures of the samples and the bacteria were clear. After an incubation time of 16 hours at 37 °C and 210 rpm, the turbidity was observed visually and by measuring the optical density (OD) at 600 nm using a PowerWave™ XS microplate spectrophotometer (BioTek).

Determination of Antimicrobial Activity by Time Kill Assay

M. Luteus from a freezer stock (1 mL) were thawed in 25 mL LB medium. 25 μL were then directly further diluted with 25 mL LB medium (1:1000), to prevent that the bacteria will enter the stationary phase during overnight growing. The next day the bacteria were diluted to an optical density of 0.1. Empty nanoparticles and nanoparticles with

encapsulated Cy5-LYZ were freshly prepared and purified with Sephadex® G-100. The concentration of encapsulated Cy5-LYZ (20.52 μg mL^{-1}) was determined with a Cy5-LYZ standard (method in section 5.4.5). The amount of free and encapsulated Cy5-LYZ was adjusted to match. Similarly, the concentrations of empty particles were matched with the Cy5-LYZ-loaded particles. Empty and LYZ-loaded nanoparticles, as well as free Cy5-LYZ, were diluted with PBS (pH 7.4). 100 μL of the samples and 100 μL of *M. Luteus* (OD = 0.1) were mixed in a sterile 96 well plate and analyzed in triplets. The final concentrations of free and encapsulated Cy5-LYZ were 10.26–0.32 μg mL^{-1}, empty nanoparticles were analyzed in a concentration range between 68.00–2.13 μg mL^{-1} of particle material. The 96 well plate was incubated on an orbital shaker (700 rpm) at 37 °C. As positive control, PBS (pH 7.4) was mixed with the bacteria. Each sample (PBS, Cy5-LYZ, Cy5-LYZ loaded LYZ$_{mPEG}$-NP, empty LYZ$_{mPEG}$-NP) was mixed with LB medium and subtracted from the measurements as background. The OD at 600 nm was measured over time with an Infinite® 200 PRO (Tecan) plate reader.

5.4.11 *M. LUTEUS* FLUORESCENCE MICROSCOPY

10 μL of *M. Luteus* (OD = 1.1) in LB-medium were mixed with 10 μL of purified Cy5-LYZ loaded nanoparticles with a concentration of 9.56 μg mL^{-1} Cy5-LYZ. 5 μL of this mixture was analyzed between an untreated coverslip (borosilicate, 0.17 mm, Carl Roth, Germany) and a microscope slide (Carl Roth, Germany) by fluorescence microscopy.

Imaging of *M. Luteus* mixed with LYZ$_{mPEG}$-NP(Cy5-LYZ) was performed with a Leica TCS SP5 Microscope, equipped with an oil objective lens HC PL APO CS2 63.0x/1.40 OIL UV. The Cy5 was excited with a 633 nm HeNe laser, while the emission was collected between 696 and 737 nm using a PMT detector. Image analysis was performed with Fiji software.

6 APPENDIX

6.1 LIST OF ABBREVIATIONS

Abbreviation	Meaning
Abs	absorbance
AcOH	acetic acid
ABTS	2,2'-azinobis-(3-ethylbenzthiazoline-6-sulfonate)
APAF1	apoptotic protease-activating factor-1
approx.	approximately
APS	ammonium persulfate
AROP	anionic ring opening copolymerization
ATP	adenosine triphosphate
BSA	bovine serum albumin
c	concentration
c	centi-
carbonate-DS-SIL-mPEG	4-nitrophenyl carbonate activated DS-SIL-mPEG
CCD	marlin charged coupled device
CD	circular dichroism
CDCl$_3$	deuterated chloroform
CUR	curcumin
Cy5	sulfo-cyanine 5 NHS ester
Cy5-LYZ	Cy5-labeled lysozyme
Cyt	cytochrome c
Cyt$_{degPEG}$	Cyt modified with mP(EG-co-isoEPB)-NHS
Cyt$_{degPEG}$-NP	nanoparticles based on Cyt$_{degPEG}$
Cyt$_{degPEG}$-NP(CUR)	CUR loaded Cyt$_{degPEG}$-NPs
Cyt$_{degPEG}$-NP(DEX)	DEX loaded Cyt$_{degPEG}$-NPs
Cyt$_{degPEG}$-NP(OGD)	OGD loaded Cyt$_{degPEG}$-NPs
Cyt$_{DS-SIL-mPEG}$	Cyt modified with carbonate-DS-SIL-mPEG
Cyt$_{DS-SIL-mPEG}$-NP	nanoparticles based on Cyt$_{DS-SIL-mPEG}$
Cyt$_{SH}$	deprotected thiol of Cyt$_{SATP}$

Abbreviation	Meaning
Cyt_{SATP}	Cyt modified with SATP
$Cyt_{S-S-mPEG}$	Cyt_{SH} modified with mPEG-S-S-Py
δ	Chemical shift (ppm) downfield from TMS
d	day
d	deci-
dd-	double distilled
d_6	deuterated (6-times)
Da	Dalton
DAPI	4',6-diamidino-2-phenylindole
DCC	*N,N'*-dicyclohexylcarbodiimide
DCM	dichloromethane
DE	double emulsion
deg	degree
DEX	dextran
DLS	dynamic light scattering
DMEM	Dulbecco's modified Eagle's medium
DMF	dimethylformamide
DMSO	dimethyl sulfoxide
DS-SIL	disulfide-self-immolative
DS-SIL-mPEG	mPEG containing a DS-SIL-linker
DTT	dithiothreitol
Đ	polydispersity index
E. coli	*Escherichia coli*
EDTA	ethylenediaminetetraacetic acid
EE	encapsulation efficiency
e.g.	exempli gratia (for example)
em.	emission
EO	ethylene oxide
EPB	3,4-epoxy-1-butene
EPR	enhanced permeability and retention
eq.	equation
eq	equivalent
et al.	*et alii* (and others)

Abbreviation	Meaning
Et$_2$O	diethylether
EtOAc	ethyl acetate
EtOH	ethanol
ex.	excitation
FCS	fetal calf serum
FDA	Food and Drug Administration
g	gram
g	gravity of earth
GlcNAc	*N*-acetylglucosamine
GPC	gel permeation chromatography
GS	gentamicin sulfate
GSH	L-glutathione reduced
h	hour(s)
H$_2$O	water
HeLa	tumor cells from the patient Henrietta Lacks
^{1}H-NMR	proton NMR
HSA	human serum albumin
i.a.	inter alia (among other things)
k	kilo-
λ	wavelength
L	liter
LC	loading capacity
LYZ	lysozyme
LYZ$_{mPEG}$	LYZ modified with TFP-mPEG
LYZ$_{mPEG}$-NP	nanoparticles based on LYZ$_{mPEG}$
LYZ$_{mPEG}$-NP(Cy5-LYZ)	Cy5-LYZ loaded LYZ$_{mPEG}$-NPs
LYZ$_{mPEG}$-NP(GS)	GS loaded LYZ$_{mPEG}$-NPs
LYZ$_{mPEG}$-NP(LYZ)	LYZ loaded LYZ$_{mPEG}$-NPs
μ	micro-
m	mass
m	meter
m	milli-
M	molar

Abbreviation	Meaning
MALDI-ToF MS	matrix-assisted laser desorption / ionization time of flight
MC4100	*E. coli* strain
MeOH	methanol
MIC	minimum inhibitory concentration
min	minute
M. Luteus	*Micrococcus Luteus*
M_n	number average molecular weight
mPEG	methoxypoly(ethylene glycol)
mP(EG-*co*-EPB)	allyl ether moieties containing mPEG
mP(EG-*co*-*iso*EPB)	vinyl ether moieties containing mPEG
mP(EG-*co*-*iso*EPB)-NHS	succinimidyl carbonate activated mP(EG-*co*-*iso*EPB)
mPEG-SH	mPEG ether thiol
mPEG-S-S-Py	pyridyl disulfide activated mPEG
MS	mass spectroscopy
MTT	3,(4,5-dimethyl-2-thiazolyl)-2,5-diphenyl-2H-tetrazolium bromide
M_W	molecular weight
MWCO	molecular weight cut-off
n	nano-
NADH	nicotinamide adenine dinucleotide
NHS	*N*-hydroxysuccinimide
NHS-DSC	*N,N'*-disuccinimidyl carbonate
NMR	nuclear magnetic resonance
NP	nanoparticle
NTA	nanoparticle tracking analysis
OD	optical density
OGD	oregon-green™488-dextran
(o/w)	oil-in-water
PBS	phosphate buffered saline
PDB	protein data bank
PEG	poly(ethylene glycol)
PLA	poly(lactic acid)
PLGA	poly(lactic *co*-glycolic acid)

Abbreviation	Meaning
PVA	polyvinyl alcohol
rel.	relative
RI	refractive index
ROS	reactive oxygen species
rt	room temperature
SATP	*N*-succinimidyl-*S*-acetylthiopropionate
SD	standard deviation
SDS	sodium dodecyl sulfate
SDS-PAGE	sodium dodecyl sulfate polyacrylamide gel electrophoresis
SE	single emulsion
SEC	size exclusion chromatography
[θ]	molar ellipticity
t	time
TCEP	tris(2-carboxyethyl)phosphin
TEM	trasmission electron microscopy
TEMED	tetramethylethylenediamine
TFP	2,3,5,6-tetrafluorophenol
TFP-mPEG	TFP activated mPEG
TMS	tetramethylsilane
TNBS	2,4,6-trinitrobenzene sulfonic acid
U	units
USA	United States of America
UV	ultraviolet
V	volume
(w/o)	water-in-oil
(w/o/w)	water-in-oil-in-water
wt%	percentage by mass

6.2 COLLABORATION PARTNER

███████

██

████████████████

███████████████████████████████

██████████

███

██████████████████████████████

6.3 BIBLIOGRAPHY

[1]   M. C. Roco, *J. Nanopart. Res.* **2011**, *13*, 427-445.
[2]   Z. Abdin, M. A. Alim, R. Saidur, M. R. Islam, W. Rashmi, S. Mekhilef, A. Wadi, *Renewable Sustainable Energy Rev.* **2013**, *26*, 837-852.
[3]   L. M. Katz, K. Dewan, R. L. Bronaugh, *Food Chem. Toxicol.* **2015**, *85*, 127-137.
[4]   S. S. Mukhopadhyay, *Nanotechnol., Sci. Appl.* **2014**, *7*, 63-71.
[5]   V. D. Krishna, K. Wu, D. Su, M. C. J. Cheeran, J.-P. Wang, A. Perez, *Food Microbiol.* **2018**, *75*, 47-54.
[6]   S. Soares, J. Sousa, A. Pais, C. Vitorino, *Front. Chem.* **2018**, *6*, 360-360.
[7]   R. Singh, J. W. Lillard, *Exp. Mol. Pathol.* **2009**, *86*, 215-223.
[8]   A. MaHam, Z. Tang, H. Wu, J. Wang, Y. Lin, *Small* **2009**, *5*, 1706-1721.
[9]   F. Salahpour Anarjan, *Nano-Struct. Nano-Objects* **2019**, *19*, 100370.
[10]   Y. H. Choi, H.-K. Han, *J. Pharm. Invest.* **2018**, *48*, 43-60.
[11]   C. L. Ventola, *Pharmacy and Therapeutics* **2017**, *42*, 742-755.
[12]   J. Shi, P. W. Kantoff, R. Wooster, O. C. Farokhzad, *Nat. Rev. Cancer* **2017**, *17*, 20-37.
[13]   J. Nicolas, S. Mura, D. Brambilla, N. Mackiewicz, P. Couvreur, *Chem. Soc. Rev.* **2013**, *42*, 1147-1235.
[14]   A. Z. Mirza, F. A. Siddiqui, *Int. Nano Lett.* **2014**, *4*, 94.
[15]   P. Ghosh, G. Han, M. De, C. K. Kim, V. M. Rotello, *Adv. Drug Delivery Rev.* **2008**, *60*, 1307-1315.
[16]   M. Vallet-Regí, M. Colilla, I. Izquierdo-Barba, M. Manzano, *Molecules* **2017**, *23*, 47.
[17]   S.-J. Choi, J. K. Lee, J. Jeong, J.-H. Choy, *Mol. Cell. Toxicol.* **2013**, *9*, 205-210.
[18]   T. Sun, Y. S. Zhang, B. Pang, D. C. Hyun, M. Yang, Y. Xia, *Angew. Chem., Int. Ed.* **2014**, *53*, 12320-12364.
[19]   I. Ekladious, Y. L. Colson, M. W. Grinstaff, *Nat. Rev. Drug Discovery* **2019**, *18*, 273-294.
[20]   A. Puri, K. Loomis, B. Smith, J.-H. Lee, A. Yavlovich, E. Heldman, R. Blumenthal, *Crit. Rev. Ther. Drug Carrier Syst.* **2009**, *26*, 523-580.
[21]   M. W. Kim, S.-H. Kwon, J. H. Choi, A. Lee, *Int. J. Mol. Sci.* **2018**, *19*, 3859.
[22]   Y. Barenholz, *J. Controlled Release* **2012**, *160*, 117-134.
[23]   D. Bobo, K. J. Robinson, J. Islam, K. J. Thurecht, S. R. Corrie, *Pharm. Res.* **2016**, *33*, 2373-2387.
[24]   U. Kedar, P. Phutane, S. Shidhaye, V. Kadam, *Nanomedicine* **2010**, *6*, 714-729.
[25]   J. S. Lee, J. Feijen, *J. Controlled Release* **2012**, *161*, 473-483.
[26]   P. Kesharwani, K. Jain, N. K. Jain, *Prog. Polym. Sci.* **2014**, *39*, 268-307.
[27]   a) S. Tran, P.-J. DeGiovanni, B. Piel, P. Rai, *Clin. Transl. Med.* **2017**, *6*, 44; b) F. Canal, J. Sanchis, M. J. Vicent, *Curr. Opin. Biotechnol.* **2011**, *22*, 894-900.
[28]   a) A. Abuchowski, J. R. McCoy, N. C. Palczuk, T. van Es, F. F. Davis, *J. Biol. Chem.* **1977**, *252*, 3582-3586; b) A. Abuchowski, T. Van Es, N. Palczuk, F. Davis, *J. Biol. Chem.* **1977**, *252*, 3578-3581.
[29]   V. Gupta, S. Bhavanasi, M. Quadir, K. Singh, G. Ghosh, K. Vasamreddy, A. Ghosh, T. J. Siahaan, S. Banerjee, S. K. Banerjee, *J. Cell Commun. Signal.* **2019**, *13*, 319-330.
[30]   K. Knop, R. Hoogenboom, D. Fischer, U. S. Schubert, *Angew. Chem., Int. Ed.* **2010**, *49*, 6288-6308.
[31]   a) P. Wilson, P. C. Ke, T. P. Davis, K. Kempe, *Eur. Polym. J.* **2017**, *88*, 486-515; b) M. Barz, R. Luxenhofer, R. Zentel, M. J. Vicent, *Polym. Chem.* **2011**, *2*, 1900-1918.
[32]   B. S. Tucker, B. S. Sumerlin, *Polym. Chem.* **2014**, *5*, 1566-1572.

[33]   a) P. Lundberg, B. F. Lee, S. A. van den Berg, E. D. Pressly, A. Lee, C. J. Hawker, N. A. Lynd, *ACS Macro Lett.* **2012**, *1*, 1240-1243; b) M. Worm, D. Leibig, C. Dingels, H. Frey, *ACS Macro Lett.* **2016**, *5*, 1357-1363.

[34]   J. Ewald, J. Blankenburg, M. Worm, L. Besch, R. E. Unger, W. Tremel, H. Frey, H. Pohlit, *Chem. - Eur. J.* **2019**, *Advance online publication.* https://doi.org/10.1002/chem.201905310

[35]   a) A. Jain, S. K. Singh, S. K. Arya, S. C. Kundu, S. Kapoor, *ACS Biomater. Sci. Eng.* **2018**, *4*, 3939-3961; b) Y. Zhang, T. Sun, C. Jiang, *Acta Pharm. Sin. B* **2018**, *8*, 34-50; c) T. Miao, J. Wang, Y. Zeng, G. Liu, X. Chen, *Adv. Sci. (Weinheim, Ger.)* **2018**, *5*, 1700513.

[36]   F. Foerster, D. Bamberger, J. Schupp, M. Weilbächer, L. Kaps, S. Strobl, L. Radi, M. Diken, D. Strand, A. Tuettenberg, P. R. Wich, D. Schuppan, *Nanomedicine (London, U. K.)* **2016**, *11*, 2663-2677.

[37]   D. Bamberger, D. Hobernik, M. Konhäuser, M. Bros, P. R. Wich, *Mol. Pharmaceutics* **2017**, *14*, 4403-4416.

[38]   a) B. B. Breitenbach, I. Schmid, P. R. Wich, *Biomacromolecules* **2017**, *18*, 2839-2848; b) B. B. Breitenbach, E. Steiert, M. Konhäuser, L.-M. Vogt, Y. Wang, S. H. Parekh, P. R. Wich, *Soft Matter* **2019**, *15*, 1423-1434.

[39]   a) P. Ma, R. J. Mumper, *J. Nanomed. Nanotechnol.* **2013**, *4*, 1000164; b) E. Miele, G. P. Spinelli, E. Miele, F. Tomao, S. Tomao, *Int. J. Nanomed.* **2009**, *4*, 99-105; c) M. R. Green, G. M. Manikhas, S. Orlov, B. Afanasyev, A. M. Makhson, P. Bhar, M. J. Hawkins, *Ann. Oncol.* **2006**, *17*, 1263-1268.

[40]   a) G. Manoukian, F. Hagemeister, *Expert Opin. Biol. Ther.* **2009**, *9,* 1445-1451; b) T. M. Kuzel, *Clin. Lymphoma* **2000**, *1*, S33-S36.

[41]   J. Reinholz, K. Landfester, V. Mailänder, *Drug Delivery* **2018**, *25*, 1694-1705.

[42]   S. Schöttler, K. Landfester, V. Mailänder, *Angew. Chem., Int. Ed.* **2016**, *55*, 8806-8815.

[43]   C. Corbo, R. Molinaro, A. Parodi, N. E. Toledano Furman, F. Salvatore, E. Tasciotti, *Nanomedicine (London, U. K.)* **2016**, *11*, 81-100.

[44]   E. Fröhlich, *Int. J. Nanomed.* **2012**, *7*, 5577-5591.

[45]   M. P. Xiong, Y. Bae, S. Fukushima, M. L. Forrest, N. Nishiyama, K. Kataoka, G. S. Kwon, *ChemMedChem* **2007**, *2*, 1321-1327.

[46]   S. Schöttler, G. Becker, S. Winzen, T. Steinbach, K. Mohr, K. Landfester, V. Mailänder, F. R. Wurm, *Nat. Nanotechnol.* **2016**, *11*, 372.

[47]   B. Du, M. Yu, J. Zheng, *Nat. Rev. Mater.* **2018**, 358-374.

[48]   F. Alexis, E. Pridgen, L. K. Molnar, O. C. Farokhzad, *Mol. Pharmaceutics* **2008**, *5*, 505-515.

[49]   E. Blanco, H. Shen, M. Ferrari, *Nat. Biotechnol.* **2015**, *33*, 941-951.

[50]   Y. Matsumura, H. Maeda, *Cancer Res.* **1986**, *46*, 6387-6392.

[51]   H. Hashizume, P. Baluk, S. Morikawa, J. W. McLean, G. Thurston, S. Roberge, R. K. Jain, D. M. McDonald, *Am. J. Pathol.* **2000**, *156*, 1363-1380.

[52]   G. Bergers, L. E. Benjamin, *Nat. Rev. Cancer* **2003**, *3*, 401-410.

[53]   D. F. Baban, L. W. Seymour, *Adv. Drug Delivery Rev.* **1998**, *34*, 109-119.

[54]   Y. Nakamura, A. Mochida, P. L. Choyke, H. Kobayashi, *Bioconjugate Chem.* **2016**, *27*, 2225-2238.

[55]   R. Toy, P. M. Peiris, K. B. Ghaghada, E. Karathanasis, *Nanomedicine (London, U. K.)* **2014**, *9*, 121-134.

[56]   M. Longmire, P. L. Choyke, H. Kobayashi, *Nanomedicine (London, U. K.)* **2008**, *3*, 703-717.

[57]   S. K. Golombek, J.-N. May, B. Theek, L. Appold, N. Drude, F. Kiessling, T. Lammers, *Adv. Drug Delivery Rev.* **2018**, *130*, 17-38.

[58] J. Zhao, M. H. Stenzel, *Polym. Chem.* **2018**, *9*, 259-272.

[59] S. Behzadi, V. Serpooshan, W. Tao, M. A. Hamaly, M. Y. Alkawareek, E. C. Dreaden, D. Brown, A. M. Alkilany, O. C. Farokhzad, M. Mahmoudi, *Chem. Soc. Rev.* **2017**, *46*, 4218-4244.

[60] P. Foroozandeh, A. A. Aziz, *Nanoscale Res. Lett.* **2018**, *13*, 339.

[61] N. D. Donahue, H. Acar, S. Wilhelm, *Adv. Drug Delivery Rev.* **2019**, *143*, 68-96.

[62] J. H. Lee, Y. Yeo, *Chem. Eng. Sci.* **2015**, *125*, 75-84.

[63] S. Mura, J. Nicolas, P. Couvreur, *Nat. Mater.* **2013**, *12*, 991-1003.

[64] S. Uthaman, K. M. Huh, I.-K. Park, *Biomater. Res.* **2018**, *22*, 22.

[65] C. Wang, T. Zhao, Y. Li, G. Huang, M. A. White, J. Gao, *Adv. Drug Delivery Rev.* **2017**, *113*, 87-96.

[66] H. J. Forman, H. Zhang, A. Rinna, *Mol. Aspects Med.* **2009**, *30*, 1-12.

[67] E. Fleige, M. A. Quadir, R. Haag, *Adv. Drug Delivery Rev.* **2012**, *64*, 866-884.

[68] S. Binauld, M. H. Stenzel, *ChemComm* **2013**, *49*, 2082-2102.

[69] S. J. Sonawane, R. S. Kalhapure, T. Govender, *Eur. J. Pharm. Sci.* **2017**, *99*, 45-65.

[70] a) H. Wei, R.-X. Zhuo, X.-Z. Zhang, *Prog. Polym. Sci.* **2013**, *38*, 503-535; b) N. Deirram, C. Zhang, S. S. Kermaniyan, A. P. R. Johnston, G. K. Such, *Macromol. Rapid Commun.* **2019**, *40*, 1800917.

[71] J. Li, X. Zhang, M. Zhao, L. Wu, K. Luo, Y. Pu, B. He, *Biomacromolecules* **2018**, *19*, 3140-3148.

[72] a) M. Huo, J. Yuan, L. Tao, Y. Wei, *Polym. Chem.* **2014**, *5*, 1519-1528; b) N. V. Rao, H. Ko, J. Lee, J. H. Park, *Front. Bioeng. Biotechnol.* **2018**, *6*, 110.

[73] H. Sun, B. Guo, R. Cheng, F. Meng, H. Liu, Z. Zhong, *Biomaterials* **2009**, *30*, 6358-6366.

[74] H. S. Han, T. Thambi, K. Y. Choi, S. Son, H. Ko, M. C. Lee, D.-G. Jo, Y. S. Chae, Y. M. Kang, J. Y. Lee, J. H. Park, *Biomacromolecules* **2015**, *16*, 447-456.

[75] a) Q. Feng, R. Tong, *Bioeng. Transl. Med.* **2016**, *1*, 277-296; b) J. D. Bargh, A. Isidro-Llobet, J. S. Parker, D. R. Spring, *Chem. Soc. Rev.* **2019**, *48*, 4361-4374; c) A. Grotzky, Y. Manaka, T. Kojima, P. Walde, *Biomacromolecules* **2011**, *12*, 134-144; d) K. Maier, E. Wagner, *J. Am. Chem. Soc.* **2012**, *134*, 10169-10173.

[76] C. Seidler, D. Y. W. Ng, Y. Wu, T. Weil, *Supramol. Chem.* **2016**, *28*, 742-746.

[77] A. Yurkovetskiy, S. Choi, A. Hiller, M. Yin, C. McCusker, S. Syed, A. J. Fischman, M. I. Papisov, *Biomacromolecules* **2005**, *6*, 2648-2658.

[78] T. Steinbach, G. Becker, A. Spiegel, T. Figueiredo, D. Russo, F. R. Wurm, *Macromol. Biosci.* **2017**, *17*, 1600377.

[79] W. Gao, J. M. Chan, O. C. Farokhzad, *Mol. Pharmaceutics* **2010**, *7*, 1913-1920.

[80] C. G. Decker, H. D. Maynard, *Eur. Polym. J.* **2015**, *65*, 305-312.

[81] C. F. Riber, A. A. A. Smith, A. N. Zelikin, *Adv. Healthcare Mater.* **2015**, *4*, 1887-1890.

[82] P. Ruiz-Sanchis, M. Wohl Benjamin, A. A. Smith Anton, K. Zuwala, J. Melchjorsen, M. Tolstrup, N. Zelikin Alexander, *Adv. Healthcare Mater.* **2014**, *4*, 65-68.

[83] a) G. Liu, X. Wang, J. Hu, G. Zhang, S. Liu, *J. Am. Chem. Soc.* **2014**, *136*, 7492-7497; b) A. Sagi, R. Weinstain, N. Karton, D. Shabat, *J. Am. Chem. Soc.* **2008**, *130*, 5434-5435; c) Y. Xie, T. Murray-Stewart, Y. Wang, F. Yu, J. Li, L. J. Marton, R. A. Casero, D. Oupický, *J. Controlled Release* **2017**, *246*, 110-119; d) C. A. Blencowe, A. T. Russell, F. Greco, W. Hayes, D. W. Thornthwaite, *Polym. Chem.* **2011**, *2*, 773-790.

[84] J. Chen, M. Zhao, F. Feng, A. Sizovs, J. Wang, *J. Am. Chem. Soc.* **2013**, *135*, 10938-10941.

[85] Y. Guo, Y. Zhang, Z. Niu, Y. Yang, *Colloids Surf., B* **2019**, *184*, 110526.

[86] G. Wang, H. Uludag, *Expert Opin. Drug Delivery* **2008**, *5*, 499-515.

[87] G. Jutz, P. van Rijn, B. Santos Miranda, A. Böker, *Chem. Rev.* **2015**, *115*, 1653-1701.

[88]   R. L. M. van Montfort, E. Basha, K. L. Friedrich, C. Slingsby, E. Vierling, *Nat. Struct. Biol.* **2001**, *8*, 1025-1030.

[89]   T. Douglas, M. Young, *Science* **2006**, *312*, 873-875.

[90]   a) L. Schoonen, J. C. M. van Hest, *Nanoscale* **2014**, *6*, 7124-7141; b) L. A. Lee, Z. Niu, Q. Wang, *Nano Res.* **2009**, *2*, 349-364.

[91]   M. Tarhini, H. Greige-Gerges, A. Elaissari, *Int. J. Pharm.* **2017**, *522*, 172-197.

[92]   U. Shimanovich, G. J. L. Bernardes, T. P. J. Knowles, A. Cavaco-Paulo, *Chem. Soc. Rev.* **2014**, *43*, 1361-1371.

[93]   N. T. Southall, K. A. Dill, A. D. J. Haymet, *J. Phys. Chem. B* **2002**, *106*, 521-533.

[94]   C. Weber, C. Coester, J. Kreuter, K. Langer, *Int. J. Pharm.* **2000**, *194*, 91-102.

[95]   H. B. Wijayanti, N. Bansal, H. C. Deeth, *Compr. Rev. Food Sci. Food Saf.* **2014**, *13*, 1235-1251.

[96]   M. Martins, A. Loureiro, N. G. Azoia, C. Silva, A. Cavaco-Paulo, *Trends Biotechnol.* **2016**, *34*, 496-505.

[97]   M. J. J., R. C. Oppenheim, P. Speiser, *Pharm. Acta Helv.* **1978**, *53*, 17-23.

[98]   a) K. Langer, S. Balthasar, V. Vogel, N. Dinauer, H. von Briesen, D. Schubert, *Int. J. Pharm.* **2003**, *257*, 169-180; b) B. von Storp, A. Engel, A. Boeker, M. Ploeger, K. Langer, *J. Microencapsulation* **2012**, *29*, 138-146.

[99]   a) L. P. Herrera Estrada, J. A. Champion, *Biomater. Sci.* **2015**, *3*, 787-799; b) S. Sundar, J. Kundu, S. C. Kundu, *Sci. Technol. Adv. Mater.* **2010**, *11*, 014104; c) W. Lohcharoenkal, L. Wang, Y. C. Chen, Y. Rojanasakul, *BioMed Res. Int.* **2014**, *2014*, 180549.

[100]   Q. Li, C. Liu, X. Zhao, Y. Zu, Y. Wang, B. Zhang, D. Zhao, Q. Zhao, L. Su, Y. Gao, B. Sun, *Int. J. Nanomed.* **2011**, *6*, 397-405.

[101]   L. H. Estrada, S. Chu, J. A. Champion, *J. Pharm. Sci.* **2014**, *103*, 1863-1871.

[102]   S. Yu, P. Yao, M. Jiang, G. Zhang, *Biopolymers* **2006**, *83*, 148-158.

[103]   C. Bengoechea, I. Peinado, D. J. McClements, *Food Hydrocolloids* **2011**, *25*, 1354-1360.

[104]   a) L. Yang, F. Cui, D. Cun, A. Tao, K. Shi, W. Lin, *Int. J. Pharm.* **2007**, *340*, 163-172; b) A. O. Elzoghby, W. M. Samy, N. A. Elgindy, *J. Controlled Release* **2012**, *157*, 168-182.

[105]   K. Piradashvili, M. Fichter, K. Mohr, S. Gehring, F. R. Wurm, K. Landfester, *Biomacromolecules* **2015**, *16*, 815-821.

[106]   O. G. Jones, D. J. McClements, *Compr. Rev. Food Sci. Food Saf.* **2010**, *9*, 374-397.

[107]   S. Bae, K. Ma, T. H. Kim, E. S. Lee, K. T. Oh, E.-S. Park, K. C. Lee, Y. S. Youn, *Biomaterials* **2012**, *33*, 1536-1546.

[108]   W. Wang, Y. Huang, S. Zhao, T. Shao, Y. Cheng, *ChemComm* **2013**, *49*, 2234-2236.

[109]   Y. Wu, D. Y. W. Ng, S. L. Kuan, T. Weil, *Biomater. Sci.* **2015**, *3*, 214-230.

[110]   R. Falatach, C. McGlone, M. S. Al-Abdul-Wahid, S. Averick, R. C. Page, J. A. Berberich, D. Konkolewicz, *ChemComm* **2015**, *51*, 5343-5346.

[111]   E. M. Pelegri-O'Day, E. W. Lin, H. D. Maynard, *J. Am. Chem. Soc.* **2014**, *136*, 14323-14332.

[112]   a) G. N. Grover, H. D. Maynard, *Curr. Opin. Chem. Biol.* **2010**, *14*, 818-827; b) L. A. Canalle, D. W. P. M. Löwik, J. C. M. van Hest, *Chem. Soc. Rev.* **2010**, *39*, 329-353.

[113]   C. Boyer, X. Huang, M. R. Whittaker, V. Bulmus, T. P. Davis, *Soft Matter* **2011**, *7*, 1599-1614.

[114]   a) Y. Wu, S. Ihme, M. Feuring-Buske, S. L. Kuan, K. Eisele, M. Lamla, Y. Wang, C. Buske, T. Weil, *Adv. Healthcare Mater.* **2013**, *2*, 884-894; b) L. Zhang, Z. Lu, X. Li, Y. Deng, F. Zhang, C. Ma, N. He, *Polym. Chem.* **2012**, *3*, 1958-1961; c) Y. Wu, E. K. Shih, A. Ramanathan, S. Vasudevan, T. Weil, *Biointerphases* **2012**, *7*, 1-10.

[115] H.-A. Klok, *Macromolecules* **2009**, *42*, 7990-8000.

[116] M. A. Gauthier, H.-A. Klok, *ChemComm* **2008**, *23*, 2591-2611.

[117] W. B. Liechty, D. R. Kryscio, B. V. Slaughter, N. A. Peppas, *Annu. Rev. Chem. Biomol. Eng.* **2010**, *1*, 149-173.

[118] Y. Xia, S. Tang, B. D. Olsen, *ChemComm* **2013**, *49*, 2566-2568.

[119] a) C. N. Lam, M. Kim, C. S. Thomas, D. Chang, G. E. Sanoja, C. U. Okwara, B. D. Olsen, *Biomacromolecules* **2014**, *15*, 1248-1258; b) A. Huang, J. M. Paloni, A. Wang, A. C. Obermeyer, H. V. Sureka, H. Yao, B. D. Olsen, *Biomacromolecules* **2019**, *20*, 3713-3723.

[120] a) Y. Jiang, H. Lu, A. Dag, G. Hart-Smith, M. H. Stenzel, *J. Mater. Chem. B* **2016**, *4*, 2017-2027; b) Y. Jiang, M. Stenzel, *Macromol. Biosci.* **2016**, *16*, 791-802.

[121] Y. Jiang, M. Liang, D. Svejkar, G. Hart-Smith, H. Lu, W. Scarano, M. H. Stenzel, *ChemComm* **2014**, *50*, 6394-6397.

[122] J. Zhang, Y. Lei, A. Dhaliwal, Q. K. T. Ng, J. Du, M. Yan, Y. Lu, T. Segura, *Biomacromolecules* **2011**, *12*, 1006-1014.

[123] a) N. C. Mougin, P. van Rijn, H. Park, A. H. E. Müller, A. Böker, *Adv. Funct. Mater.* **2011**, *21*, 2470-2476; b) P. van Rijn, H. Park, K. Özlem Nazli, N. C. Mougin, A. Böker, *Langmuir* **2013**, *29*, 276-284.

[124] X. Huang, M. Li, D. C. Green, D. S. Williams, A. J. Patil, S. Mann, *Nat. Commun.* **2013**, *4*, 2239.

[125] L.-H. Xue, C.-Y. Xie, S.-X. Meng, R.-X. Bai, X. Yang, Y. Wang, S. Wang, B. P. Binks, T. Guo, T. Meng, *ACS Macro Lett.* **2017**, *6*, 679-683.

[126] a) M. Fach, L. Radi, P. R. Wich, *J. Am. Chem. Soc.* **2016**, *138*, 14820-14823; b) L. Radi, M. Fach, M. Montigny, E. Berger-Nicoletti, W. Tremel, P. R. Wich, *MedChemComm* **2016**, *7*, 1738-1744.

[127] L. Radi, PhD thesis, Johannes Gutenberg-University Mainz **2018**.

[128] a) M. Iqbal, N. Zafar, H. Fessi, A. Elaissari, *Int. J. Pharm.* **2015**, *496*, 173-190; b) W. Wang, M.-J. Zhang, L.-Y. Chu, *Curr. Opin. Pharmacol.* **2014**, *18*, 35-41; c) J. P. Rao, K. E. Geckeler, *Prog. Polym. Sci.* **2011**, *36*, 887-913.

[129] a) E. Steiert, master thesis, Johannes Gutenberg-University Mainz **2016**; b) M. Fach, PhD thesis, Johannes Gutenberg-University Mainz **2016**.

[130] N. Vanparijs, R. De Coen, D. Laplace, B. Louage, S. Maji, L. Lybaert, R. Hoogenboom, B. G. De Geest, *ChemComm* **2015**, *51*, 13972-13975.

[131] L. Wang, L. Liu, B. Dong, H. Zhao, M. Zhang, W. Chen, Y. Hong, *Acta Biomater.* **2017**, *54*, 259-270.

[132] J. Xu, J. Wang, J. C. Luft, S. Tian, G. Owens, A. A. Pandya, P. Berglund, P. Pohlhaus, B. W. Maynor, J. Smith, B. Hubby, M. E. Napier, J. M. DeSimone, *J. Am. Chem. Soc.* **2012**, *134*, 8774-8777.

[133] W. Müller-Esterl, in *Biochemie*, 1. ed., Springer Spektrum, Heidelberg, Germany, **2004**, pp. 158-158.

[134] D. Alvarez-Paggi, L. Hannibal, M. A. Castro, S. Oviedo-Rouco, V. Demicheli, V. Tórtora, F. Tomasina, R. Radi, D. H. Murgida, *Chem. Rev.* **2017**, *117*, 13382-13460.

[135] Y.-L. P. Ow, D. R. Green, Z. Hao, T. W. Mak, *Nat. Rev. Mol. Cell Biol.* **2008**, *9*, 532-542.

[136] R. Radi, L. Thomson, H. Rubbo, E. Prodanov, *Arch. Biochem. Biophys.* **1991**, *288*, 112-117.

[137] C. Garrido, L. Galluzzi, M. Brunet, P. E. Puig, C. Didelot, G. Kroemer, *Cell Death Differ.* **2006**, *13*, 1423-1433.

[138] I. S. Isaac, J. H. Dawson, *Essays Biochem.* **1999**, *34*, 51-69.

[139] L. Callewaert, C. W. Michiels, *J. Biosci.* **2010**, *35*, 127-160.

[140] a) D. Moldenhauer, J. P. Fuenzalida Werner, C. A. Strassert, F. Gröhn, *Biomacromolecules* **2019**, *20*, 979-991; b) C. Cai, U. Bakowsky, E. Rytting, A. K. Schaper, T. Kissel, *Eur. J. Pharm. Biopharm.* **2008**, *69*, 31-42.

[141] V. A. Proctor, F. E. Cunningham, D. Y. C. Fung, *Crit. Rev. Food Sci. Nutr.* **1988**, *26*, 359-395.

[142] S. S. Usmani, G. Bedi, J. S. Samuel, S. Singh, S. Kalra, P. Kumar, A. A. Ahuja, M. Sharma, A. Gautam, G. P. S. Raghava, *PLoS One* **2017**, *12*, e0181748.

[143] A. Mullard, *Nat. Rev. Drug Discovery* **2019**, *18*, 85-89.

[144] H. A. D. Lagassé, A. Alexaki, V. L. Simhadri, N. H. Katagiri, W. Jankowski, Z. E. Sauna, C. Kimchi-Sarfaty, *F1000Research* **2017**, *6*, 113.

[145] G. M. Keating, *BioDrugs* **2013**, *27*, 413-418.

[146] B. J. Bruno, G. D. Miller, C. S. Lim, *Ther. Delivery* **2013**, *4*, 1443-1467.

[147] a) S. Santra, C. Kaittanis, J. M. Perez, *Mol. Pharmaceutics* **2010**, *7*, 1209-1222; b) A. Macone, S. Masciarelli, F. Palombarini, D. Quaglio, A. Boffi, M. C. Trabuco, P. Baiocco, F. Fazi, A. Bonamore, *Sci. Rep.* **2019**, *9*, 11749.

[148] W. Gao, S. Thamphiwatana, P. Angsantikul, L. Zhang, *Wiley Interdiscip. Rev.: Nanomed. Nanobiotechnol.* **2014**, *6*, 532-547.

[149] L. Schoonen, S. Maassen, R. J. M. Nolte, J. C. M. van Hest, *Biomacromolecules* **2017**, *18*, 3492-3497.

[150] A. Abouhmad, T. Dishisha, M. A. Amin, R. Hatti-Kaul, *Biomacromolecules* **2017**, *18*, 1600-1608.

[151] H. Song, Y. Ahmad Nor, M. Yu, Y. Yang, J. Zhang, H. Zhang, C. Xu, N. Mitter, C. Yu, *J. Am. Chem. Soc.* **2016**, *138*, 6455-6462.

[152] a) D. S. Pisal, M. P. Kosloski, S. V. Balu-Iyer, *J. Pharm. Sci.* **2010**, *99*, 2557-2575; b) S.-j. Cao, S. Xu, H.-m. Wang, Y. Ling, J. Dong, R.-d. Xia, X.-h. Sun, *AAPS PharmSciTech* **2019**, *20*, 190.

[153] E. Steiert, L. Radi, M. Fach, P. R. Wich, *Macromol. Rapid Commun.* **2018**, *39*, 1800186.

[154] M. J. Roberts, M. D. Bentley, J. M. Harris, *Adv. Drug Delivery Rev.* **2012**, *64*, 116-127.

[155] D. Pfister, M. Morbidelli, *J. Controlled Release* **2014**, *180*, 134-149.

[156] E. Steiert, intership protocol, Johannes Gutenberg-University Mainz, **2016**.

[157] M. R. Lockett, M. F. Phillips, J. L. Jarecki, D. Peelen, L. M. Smith, *Langmuir* **2008**, *24*, 69-75.

[158] Y. Wang, I. Teraoka, F. Y. Hansen, G. H. Peters, O. Hassager, *Macromolecules* **2010**, *43*, 1651-1659.

[159] U. K. Laemmli, *Nature* **1970**, *227*, 680-685.

[160] B. Domon, R. Aebersold, *Science* **2006**, *312*, 212-217.

[161] N. J. Greenfield, *Nat. Protoc.* **2006**, *1*, 2876-2890.

[162] M.-P. Mingeot-Leclercq, Y. Glupczynski, P. M. Tulkens, *Antimicrob. Agents Chemother.* **1999**, *43*, 727-737.

[163] J. E. Peters, T. E. Thate, N. L. Craig, *J. Bacteriol.* **2003**, *185*, 2017-2021.

[164] P. Wild, A. Gabrieli, E. M. Schraner, A. Pellegrini, U. Thomas, P. M. Frederik, M. C. A. Stuart, R. Von Fellenberg, *Microsc. Res. Tech.* **1997**, *39*, 297-304.

[165] T. J. Silhavy, D. Kahne, S. Walker, *Cold Spring Harbor Perspect. Biol.* **2010**, *2*, a000414.

[166] U. Posadowska, M. Brzychczy-Włoch, E. Pamula, *Acta Bioeng. Biomech.* **2015**, *17*, 41-48.

[167] a) J. Kim, J. W. Grate, P. Wang, *Chem. Eng. Sci.* **2006**, *61*, 1017-1026; b) S. N. Dean, K. B. Turner, I. L. Medintz, S. A. Walper, *Ther. Delivery* **2017**, *8*, 577-595; c) H.-C. Mahler, A. Allmendinger, in *Protein Therapeutics*, Wiley-VCH Verlag GmbH & Co.

KGaA, Weinheim, Germany, **2017**, pp. 469-491; d) M. Vellard, *Curr. Opin. Biotechnol.* **2003**, *14*, 444-450.

[168] A. J. Hale, C. A. Smith, L. C. Sutherland, V. E. A. Stoneman, V. L. Longthorne, A. C. Culhane, G. T. Williams, *Eur. J. Biochem.* **1996**, *236*, 1-26.

[169] Z. Gu, A. Biswas, M. Zhao, Y. Tang, *Chem. Soc. Rev.* **2011**, *40*, 3638-3655.

[170] G. Mattson, E. Conklin, S. Desai, G. Nielander, M. D. Savage, S. Morgensen, *Mol. Biol. Rep.* **1993**, *17*, 167-183.

[171] T. Arakawa, Y. Kita, S. N. Timasheff, *Biophys. Chem.* **2007**, *131*, 62-70.

[172] J. Porath, P. Flodin, *Chromatographia* **1987**, *23*, 365-369.

[173] Y.-Y. Yang, T.-S. Chung, N. Ping Ng, *Biomaterials* **2001**, *22*, 231-241.

[174] M. F. Zambaux, F. Bonneaux, R. Gref, P. Maincent, E. Dellacherie, M. J. Alonso, P. Labrude, C. Vigneron, *J. Controlled Release* **1998**, *50*, 31-40.

[175] S. Bhattacharjee, *J. Controlled Release* **2016**, *235*, 337-351.

[176] V. Filipe, A. Hawe, W. Jiskoot, *Pharm. Res.* **2010**, *27*, 796-810.

[177] Z. L. Wang, *J. Phys. Chem. B* **2000**, *104*, 1153-1175.

[178] S. Das, A. Chaudhury, *AAPS PharmSciTech* **2011**, *12*, 62-76.

[179] T. Mosmann, *J. Immunol. Methods* **1983**, *65*, 55-63.

[180] I.-Y. Kim, E. Joachim, H. Choi, K. Kim, *Nanomedicine: NBM* **2015**, *11*, 1407-1416.

[181] M. T. Madigan, T. D. Brock, in *Brock Mikrobiologie*, 13. ed., Pearson, München, Germany, **2013**, pp. 761-761.

[182] G. Miltiadous, M. Elisaf, *J. Med. Case Rep.* **2011**, *5*, 251.

[183] T. A. Wright, R. C. Page, D. Konkolewicz, *Polym. Chem.* **2019**, *10*, 434-454.

[184] E. Steiert, J. Ewald, A. Wagner, U. A. Hellmich, H. Frey, P. R. Wich, *Polym. Chem.* **2020**, *11*, 551-559.

[185] D. D. Perrin, B. Dempsey, E. P. Serjeant, in *pKa Prediction for Organic Acids and Bases*, Springer Netherlands, Dordrecht, **1981**, pp. 1-11.

[186] T. Miron, M. Wilchek, *Bioconjugate Chem.* **1993**, *4*, 568-569.

[187] A. J. Kresge, D. S. Sagatys, H. L. Chen, *J. Am. Chem. Soc.* **1977**, *99*, 7228-7233.

[188] Y. V. Kissin, *J. Polym. Sci., Part A: Polym. Chem.* **1995**, *33*, 227-237.

[189] C. Y. Zheng, G. Ma, Z. Su, *Electrophoresis* **2007**, *28*, 2801-2807.

[190] H. Cai, X. Liu, J. Zou, J. Xiao, B. Yuan, F. Li, Q. Cheng, *Chemosphere* **2018**, *193*, 833-839.

[191] R. K. Maheshwari, A. K. Singh, J. Gaddipati, R. C. Srimal, *Life Sci.* **2006**, *78*, 2081-2087.

[192] a) M. Tobío, R. Gref, A. Sánchez, R. Langer, M. J. Alonso, *Pharm. Res.* **1998**, *15*, 270-275; b) T. Niidome, M. Yamagata, Y. Okamoto, Y. Akiyama, H. Takahashi, T. Kawano, Y. Katayama, Y. Niidome, *J. Controlled Release* **2006**, *114*, 343-347.

[193] I. I. Slowing, B. G. Trewyn, V. S. Y. Lin, *J. Am. Chem. Soc.* **2007**, *129*, 8845-8849.

[194] Y.-B. Hu, E. B. Dammer, R.-J. Ren, G. Wang, *Transl. Neurodegener.* **2015**, *4*, 18.

[195] I. Vergne, P. Constant, G. Lanéelle, *Anal. Biochem.* **1998**, *255*, 127-132.

[196] O. A. El Seoud, F. Siviero, *J. Phys. Org. Chem.* **2006**, *19*, 793-802.

[197] J. A. Burns, J. C. Butler, J. Moran, G. M. Whitesides, *J. Org. Chem.* **1991**, *56*, 2648-2650.

[198] E. B. Getz, M. Xiao, T. Chakrabarty, R. Cooke, P. R. Selvin, *Anal. Biochem.* **1999**, *273*, 73-80.

[199] R. J. S. Duncan, P. D. Weston, R. Wrigglesworth, *Anal. Biochem.* **1983**, *132*, 68-73.

[200] a) A. F. S. A. Habeeb, *Anal. Biochem.* **1966**, *14*, 328-336; b) R. B. Sashidhar, A. K. Capoor, D. Ramana, *J. Immunol. Methods* **1994**, *167*, 121-127.

[201] B. Sui, C. Cheng, P. Xu, *Adv. Ther. (Weinheim, Ger.)* **2019**, *2*, 1900062.

[202]   a) R. Stevens, L. Stevens, N. C. Price, *Biochem. Educ.* **1983**, *11*, 70; b) J. R. Winther,
        C. Thorpe, *Biochim. Biophys. Acta* **2014**, *1840*, 838-846; c) S. Chandrasekhar, D. E.
        Epling, A. M. Sophocleous, E. M. Topp, *J. Pharm. Sci.* **2014**, *103*, 1032-1042.

[203]   G. I. Peterson, M. B. Larsen, A. J. Boydston, *Macromolecules* **2012**, *45*, 7317-7328.

[204]   L. M. Dejean, S. Martinez-Caballero, S. Manon, K. W. Kinnally, *Biochim. Biophys.*
        Acta, Mol. Basis Dis. **2006**, *1762*, 191-201.

[205]   H. E. Gottlieb, V. Kotlyar, A. Nudelman, *J. Org. Chem.* **1997**, *62*, 7512-7515.

[206]   S. M. Kelly, T. J. Jess, N. C. Price, *Biochim. Biophys. Acta, Proteins Proteomics* **2005**,
        1751, 119-139.

6.4 SUPPLEMENTAL DATA

6.4.1 ADDITIONAL DATA OF THE LYSOZYME NANOPARTICLES FOR DELIVERY OF HYDROPHILIC ANTIBACTERIAL PAYLOADS PROJECT
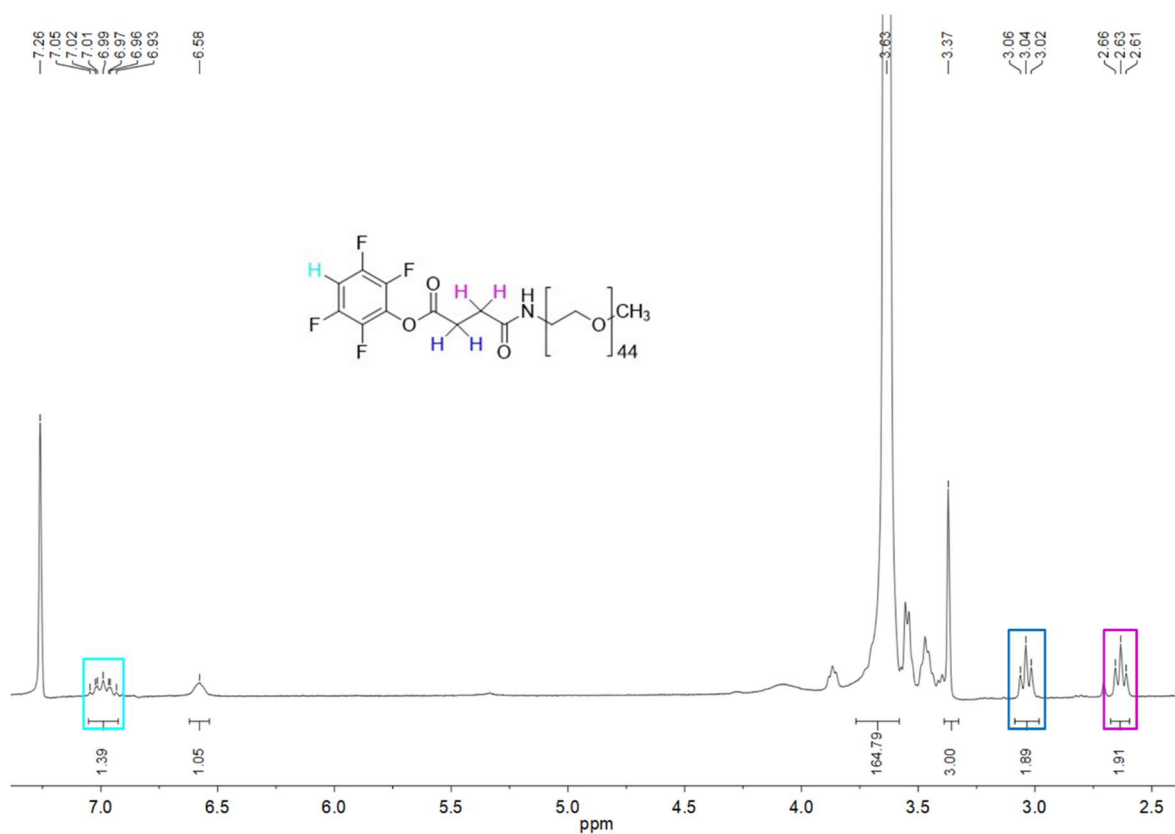
¹H-NMR

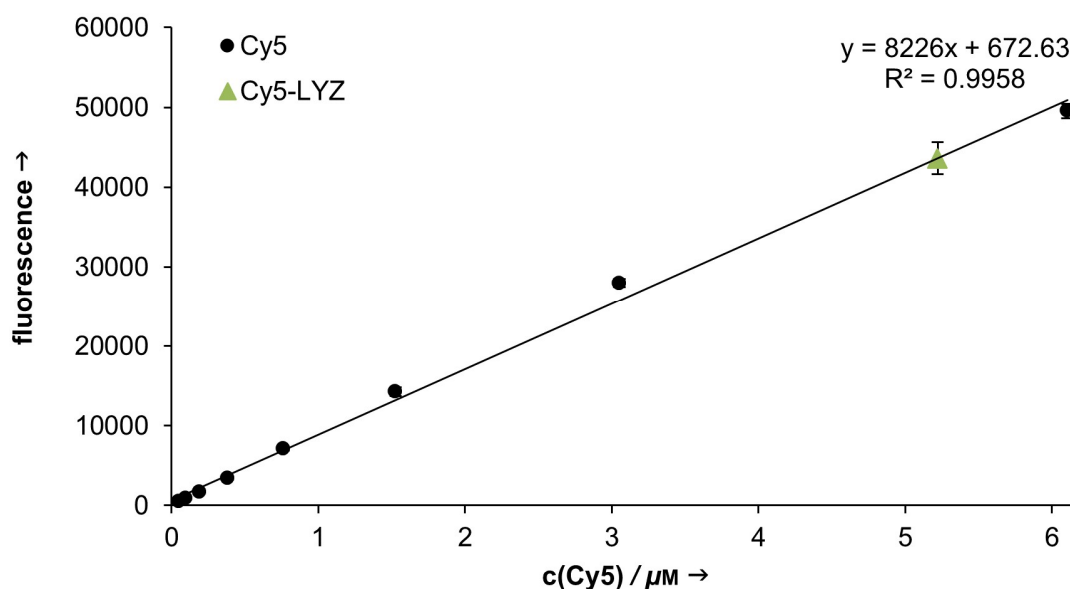Figure 87: ¹H-NMR of TFP-mPEG.

Graphs of Standard Curves

Figure 88: Determination of the Cy5 content of Cy5-LYZ (green triangle) by using a dilution of Cy5 (black dots). Adapted from Steiert *et al.*[153], Copyright (2018) WILEY-VCH Verlag GmbH & Co. KGaA.
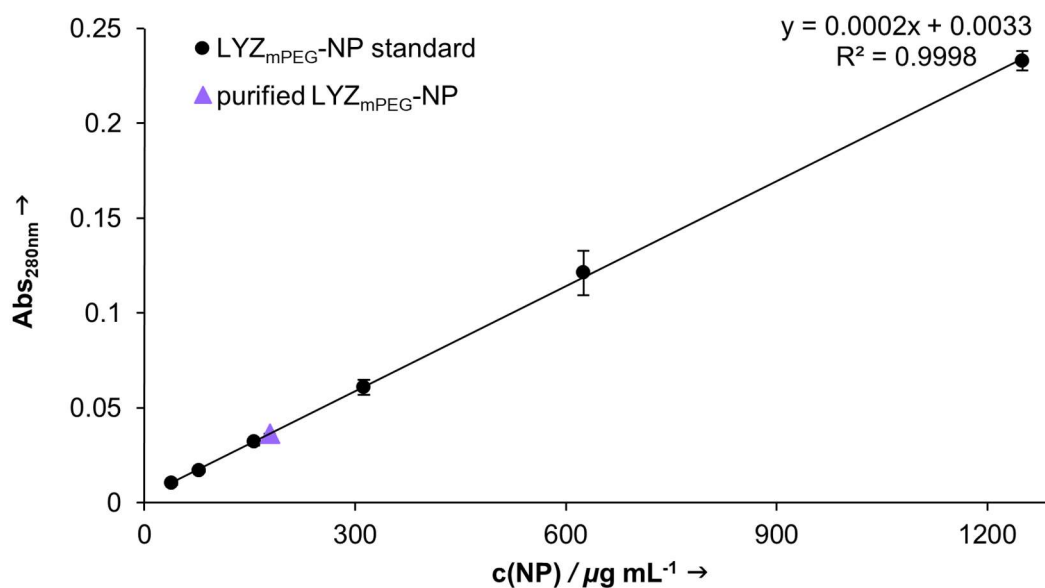
Figure 89: Determination of LYZ_{mPEG}-NP concentration (purple triangle) after purification by size exclusion chromatography by linear regression of unpurified LYZ_{mPEG}-NPs as standard (black dots). Adapted from Steiert *et al.*[153], Copyright (2018) WILEY-VCH Verlag GmbH & Co. KGaA.

Figure 90: Determination of encapsulated Cy5-LYZ in LYZ$_{mPEG}$-NP(Cy5-LYZ) (dark green square) using Cy5-LYZ as standard (light green triangles). Adapted from Steiert *et al.*[153], Copyright (2018) WILEY-VCH Verlag GmbH & Co. KGaA.

6.4.2 ADDITIONAL DATA OF THE ACID-RESPONSIVE PROTEIN-BASED NANOPARTICLES PROJECT
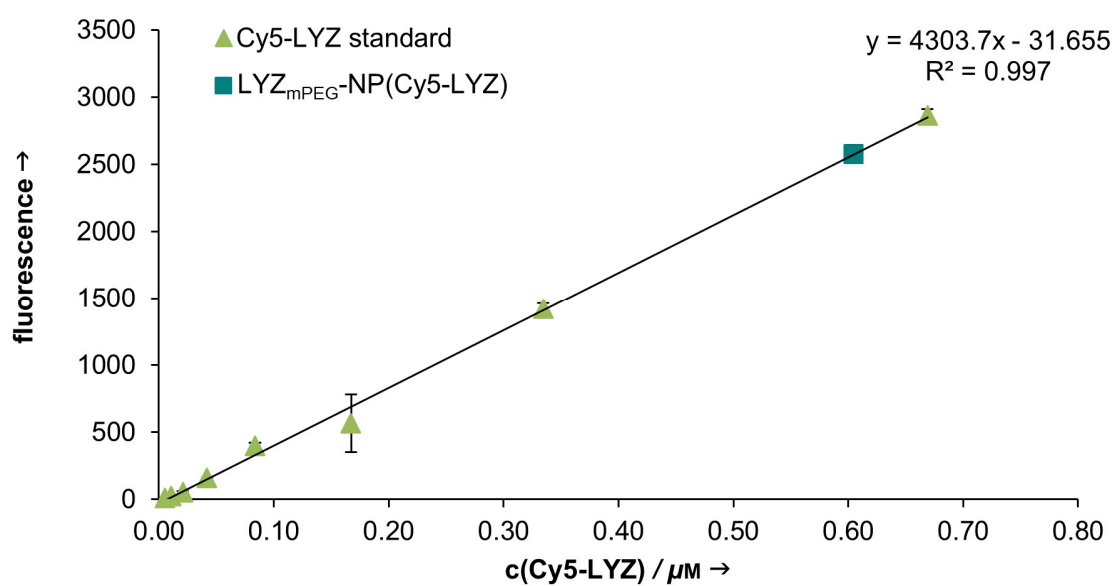
Particle Composition Analysis

Figure 91: NTA measurements for Cyt_{degPEG}-NP degradation analysis in acidic conditions. Nanoparticles consisting of Cyt_{degPEG}, which was modified with 10 eq (a), 15 eq (b) or 25 eq (c) of polymer **1**. 2.5 mg of these enzyme-polymer conjugates were used for the particle preparation by the double emulsion technique. Nanoparticles were mixed with different buffers (pH 7.4, pH 5 and pH 4) and incubated at 37 °C for 48 hours. For analysis, NTA measurements were performed over time (black: 0 h, grey: 24 h; light grey: 48 h).

Figure 92: NTA measurements for Cyt$_{degPEG}$-NP degradation analysis in acidic conditions. Nanoparticles consisting of Cyt$_{degPEG}$, which was modified with 15 eq of polymer **1**. 5 mg (a), 1.75 mg (b) or 1.4 mg (c) of this enzyme-polymer conjugate was used for the particle preparation by the double emulsion technique. Nanoparticles were mixed with different buffers (pH 7.4, pH 5 and pH 4) and incubated at 37 °C for 48 hours. For analysis, NTA measurements were performed over time (black: 0 h, grey: 24 h; light grey: 48 h).
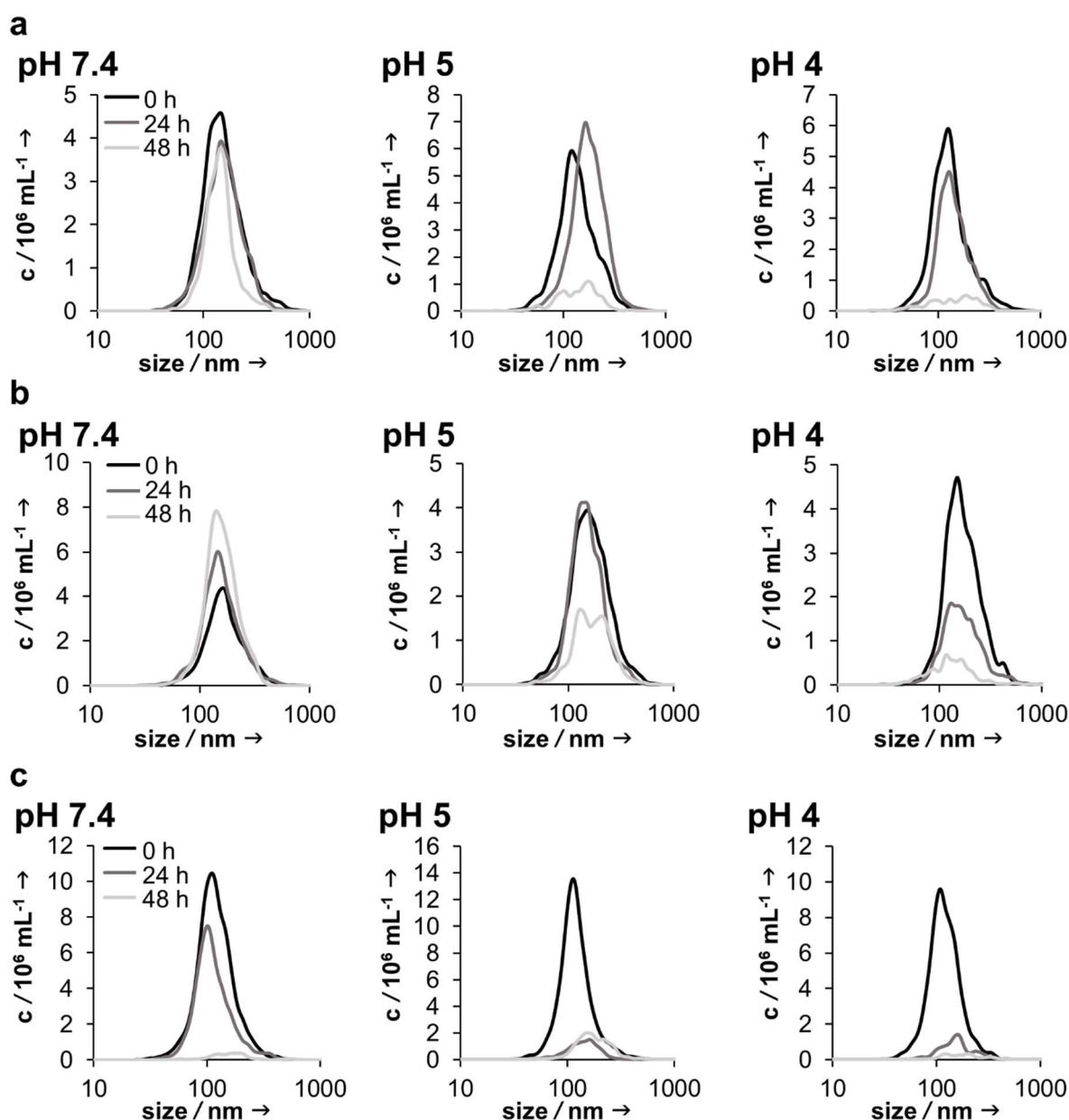
Figure 93: NTA measurements for Cyt$_{degPEG}$-NP degradation analysis in acidic conditions. Nanoparticles consisting of Cyt$_{degPEG}$, which was modified with 15 eq of polymer **1**. 1.75 mg (a) or 1.4 mg (b) of this enzyme-polymer conjugate was used for the particle preparation by the single emulsion technique. Nanoparticles were mixed with different buffers (pH 7.4, pH 5 and pH 4) and incubated at 37 °C for 48 hours. For analysis, NTA measurements were performed over time (black: 0 h, grey: 24 h; light grey: 48 h).
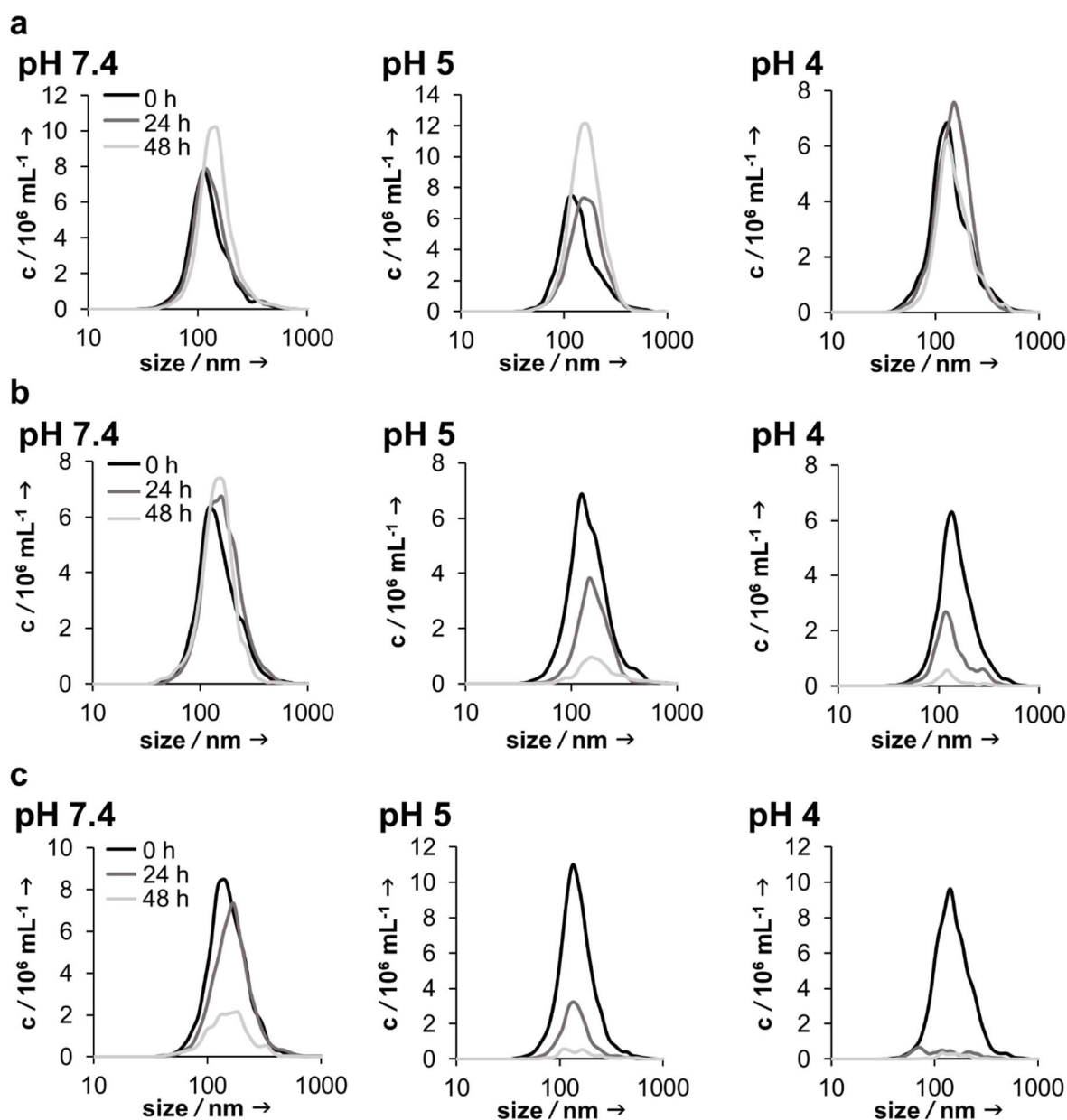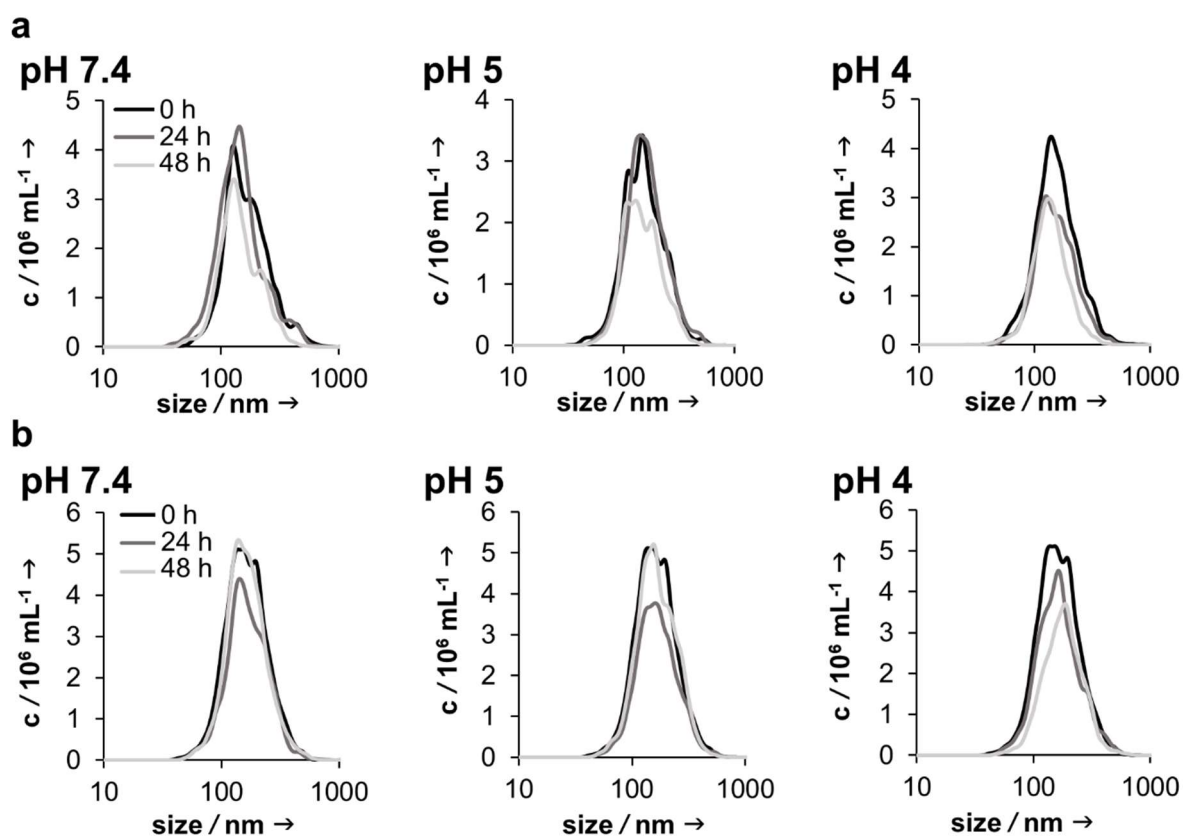
Figure 94: NTA measurements for Cyt$_{degPEG}$-NP degradation analysis in acidic conditions. Nanoparticles consisting of Cyt$_{degPEG}$, which was modified with 15 eq of polymer **1**. a) 1.75 mg of this enzyme-polymer conjugate was used for the particle preparation by the double emulsion technique during OGD encapsulation. b) 1.4 mg of this enzyme-polymer conjugate was used for the particle preparation by the single emulsion technique during CUR encapsulation. Both nanoparticle batches were mixed with different buffers (pH 7.4, pH 5 and pH 4) and incubated at 37 °C for 48 hours. For analysis, NTA measurements were performed over time (black: 0 h, grey: 24 h; light grey: 48 h).
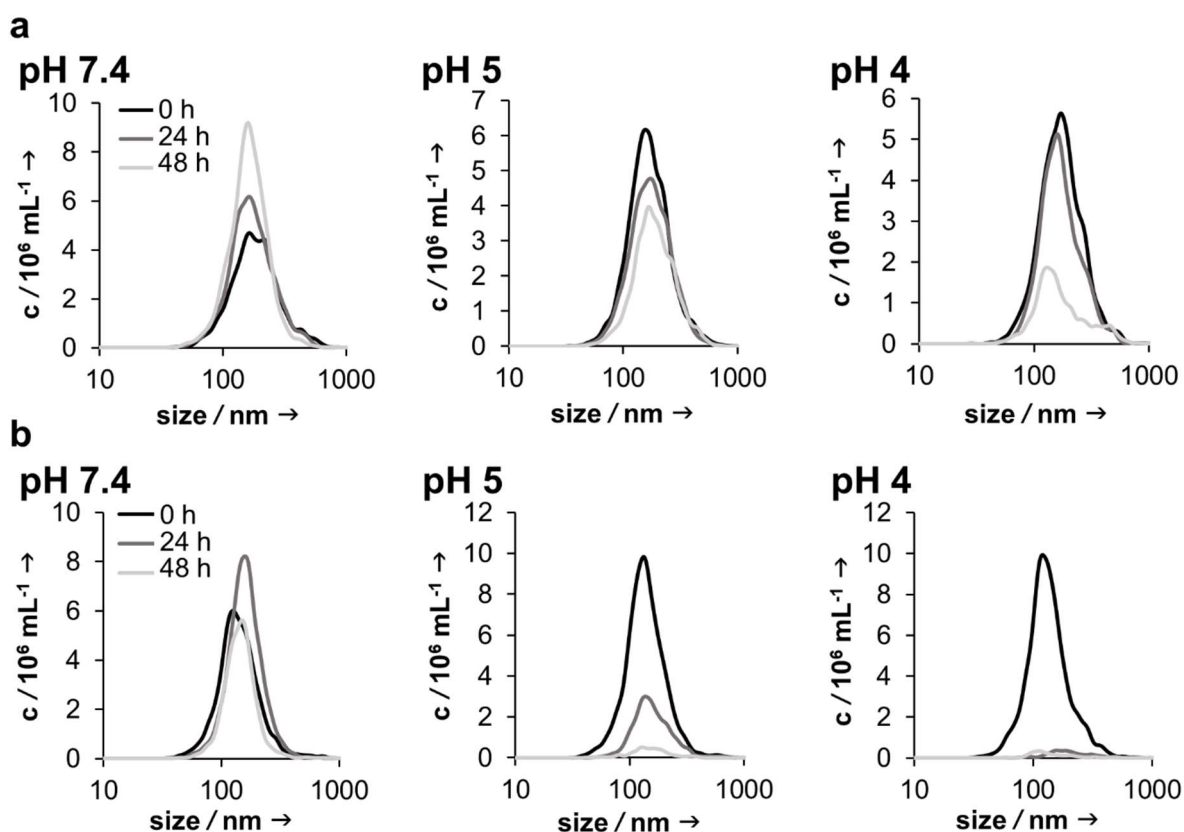
Figure 95: NTA measurements for Cyt$_{degPEG}$-NP(DEX) degradation analysis in acidic conditions. Nanoparticles consisting of Cyt$_{degPEG}$, which was modified with 17 eq of polymer **2**. 1.6 mg (a) or 3.0 mg (b) of this enzyme-polymer conjugate was used for the particle preparation by the double emulsion technique. Nanoparticles were mixed with different buffers (pH 7.4, pH 5 and pH 4) and incubated at 37 °C for 48 hours. For analysis, NTA measurements were performed over time (black: 0 h, grey: 24 h; light grey: 48 h).
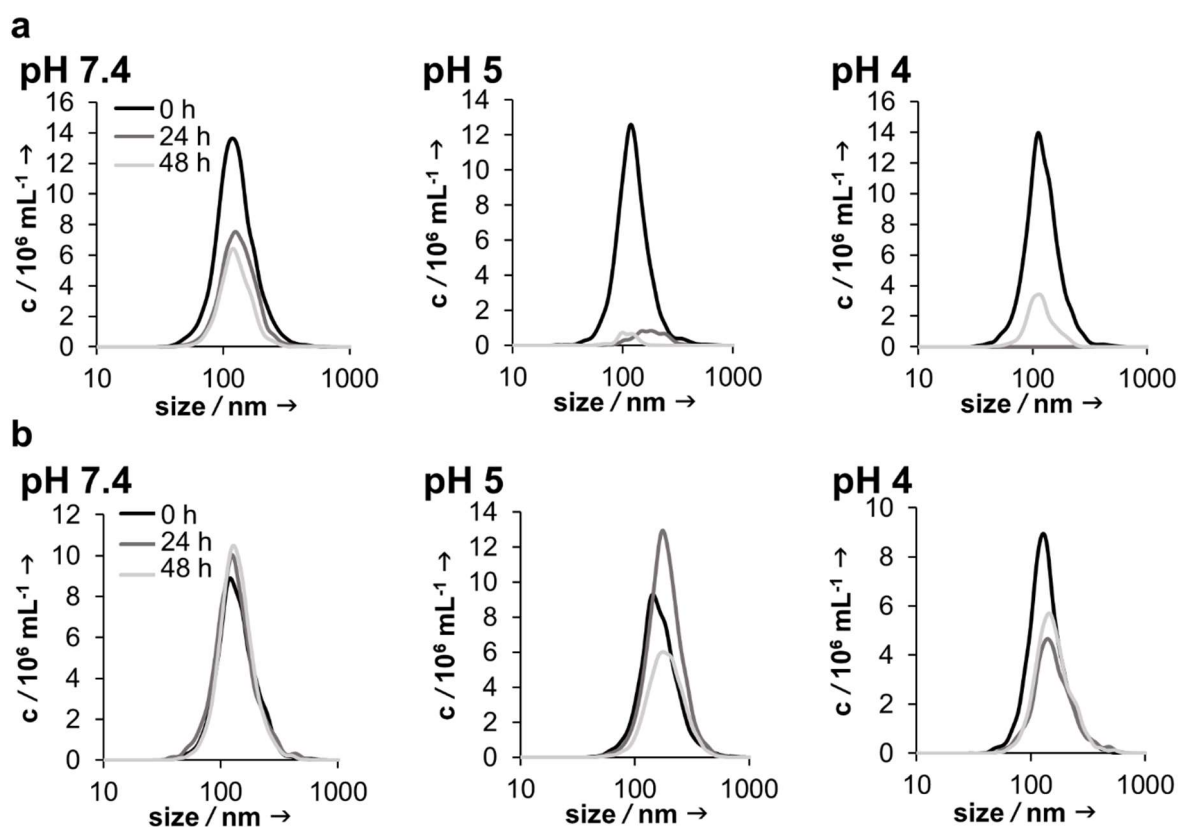
Table 19: Detailed size analysis of different Cyt_{degPEG}-nanoparticles compositions by NTA measurements. Three individual measurements were performed per sample.

polymer batch	polymer excess	particle preparation method	Cyt_{degPEG} /mg	mean / nm	mode / nm	SD / nm
1	10	DE	2.5	211.4 ± 12.3	135 ± 9.6	125.3 ± 18.8
1	15	DE	2.5	217.9 ± 7.5	158.2 ± 7.0	106.0 ± 5.7
1	25	DE	2.5	148.7 ± 1.6	110.3 ± 1.1	69.0 ± 2.8
1	15	DE	5	173.9 ± 5.2	112.5 ± 3.2	105.1 ± 3.7
1	15	DE	1.75	195.6 ± 8.9	126.8 ± 6.0	105.2 ± 10.3
1	15	DE	1.4	193.7 ± 4.4	137.1 ± 4.2	103.9 ± 9.5
1	15	SE	1.75	246.1 ± 6.5	180.6 ± 20.4	125.4 ± 2.9
1	15	SE	1.4	197.2 ± 9.8	134.4 ± 10.6	136.8 ± 12.9
1	15	DE	1.75	208.8 ± 4.3	161.9 ± 19.0	92.1 ± 7.4
1	15	SE	1.4	230.6 ± 19.5	142.3 ± 15.2	123.3 ± 16.9
2	17	DE	1.6	154.0 ± 2.3	121.3 ± 3.6	70.4 ± 4.6
2	17	DE	2.75	215.9 ± 7.0	141.2 ± 2.1	137.7 ± 5.9
2	17	DE	3.0	174.7 ± 5.6	131.2 ± 7.8	92.8 ± 10.3

Graph of Standard Curve
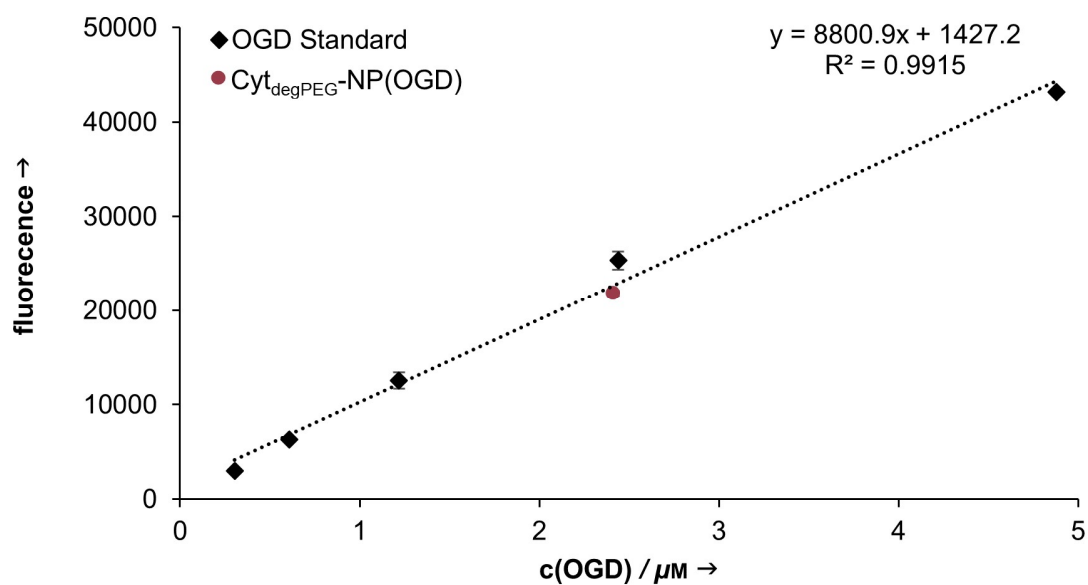
Figure 96: Determination of encapsulated OGD in Cyt_{degPEG}-NP(OGD (red dot) using OGD as standard (black squares). Adapted from Steiert *et al.*[184], by permission of The Royal Society of Chemistry.

6.4.3 ADDITIONAL DATA OF THE REDUCTIVE-RESPONSIVE PROTEIN-BASED NANOPARTICLES PROJECT

¹H-NMR
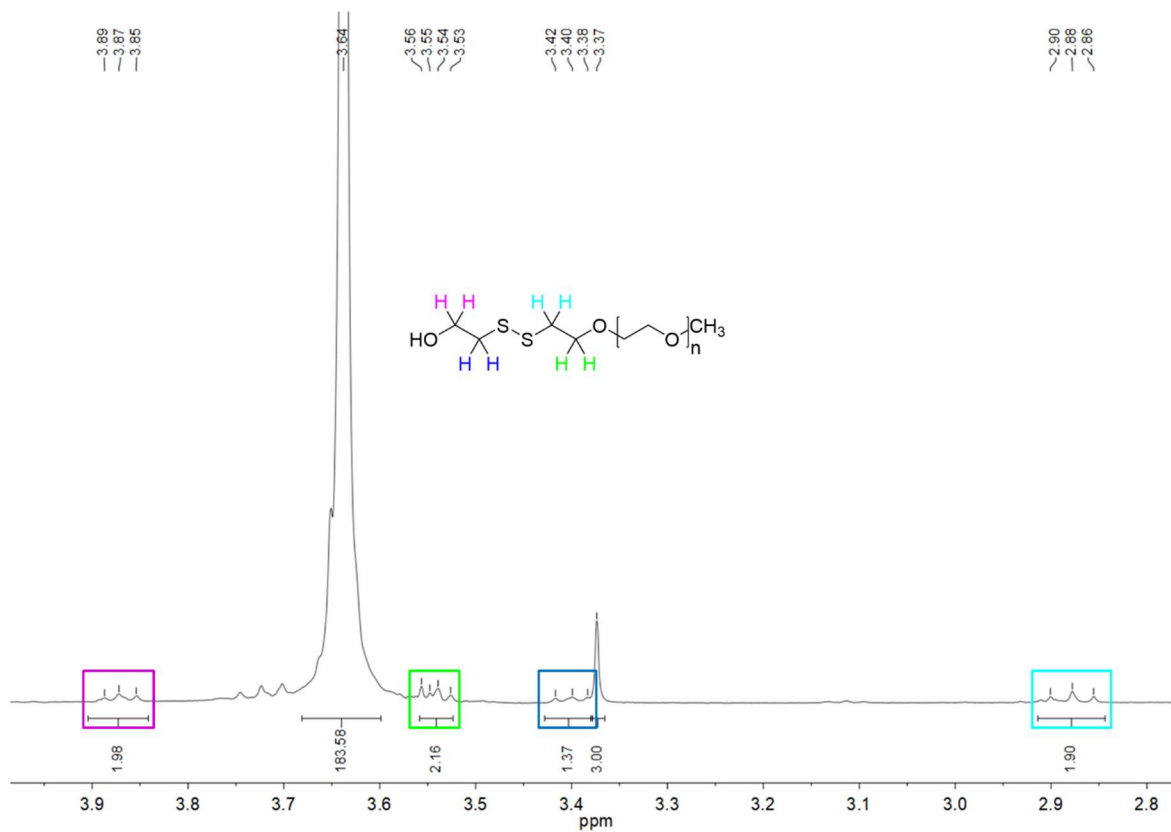
Figure 97: ¹H-NMR of mPEG-(disulfaneyl)ethan-1-ol.
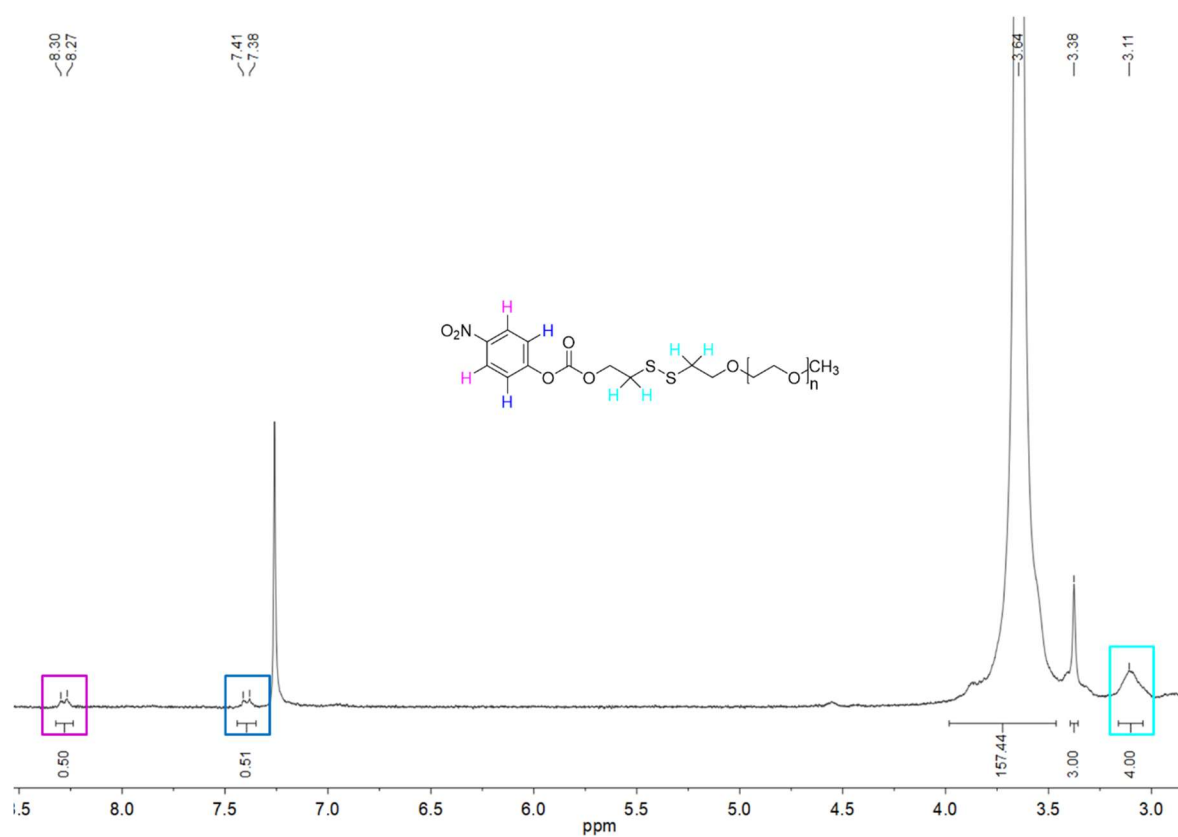
Figure 98: ^{1}H-NMR of disulfide-self-immolative nitrophenol carbonate mPEG.
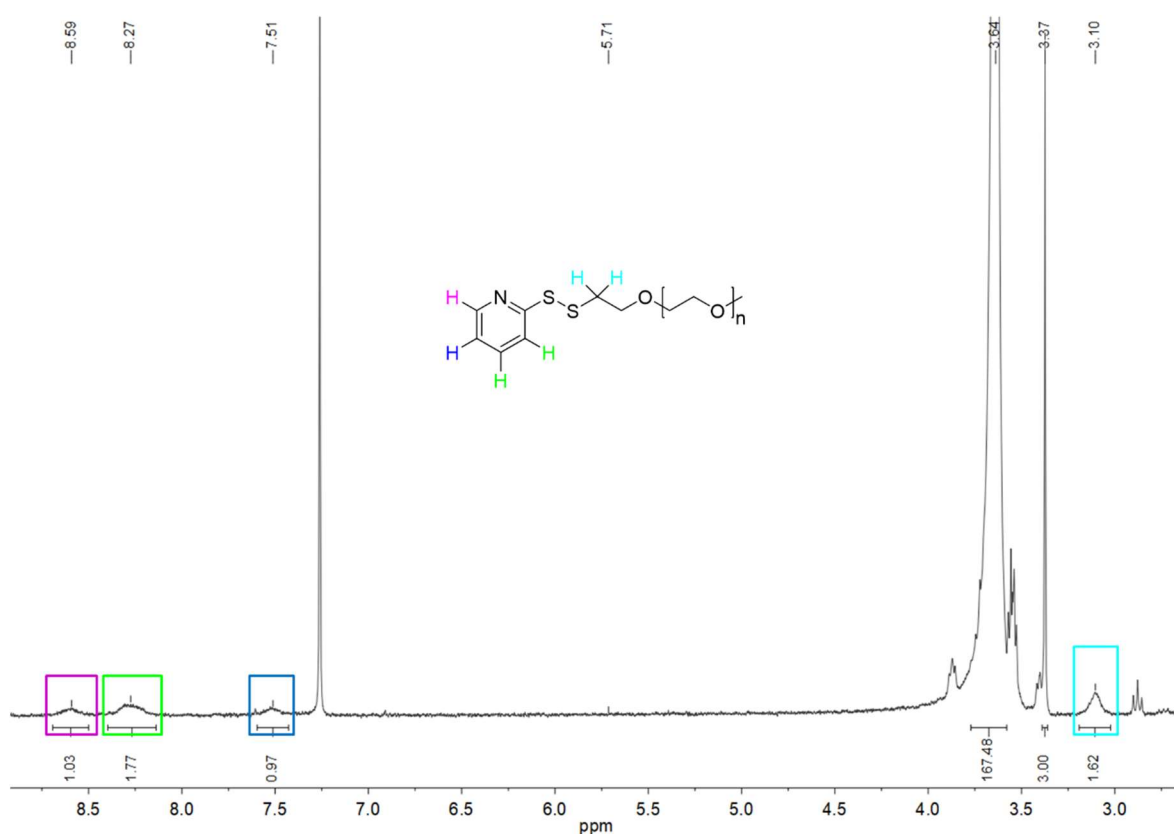
Figure 99: ^{1}H-NMR of mPEG-S-S-Py.

Graph of Standard Curve
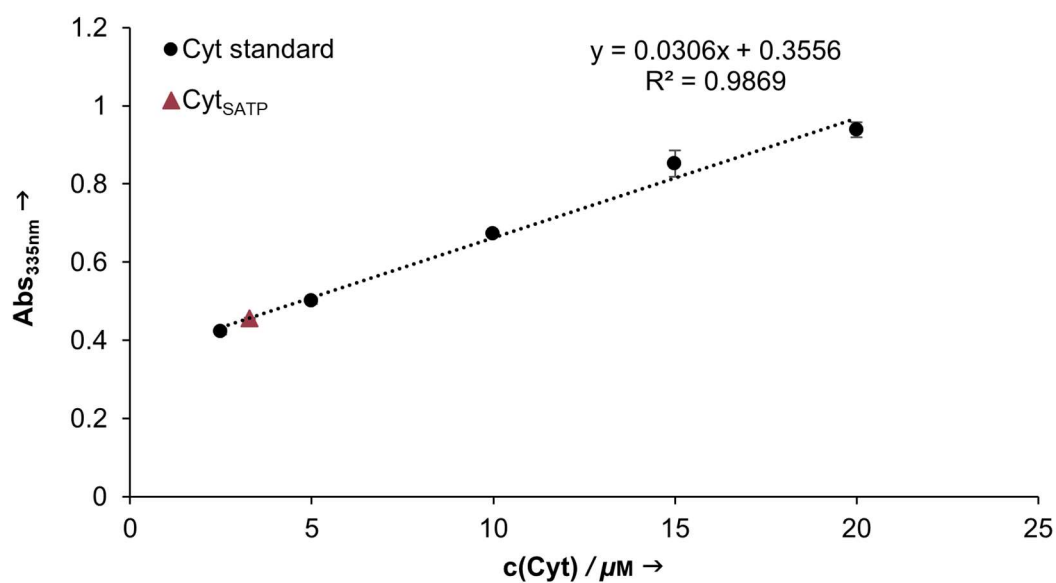
Figure 100: TNBS assay for primary amine quantification using a Cyt standard (black dots). Cyt$_{SATP}$ was analyzed with a concentration of 23 μM (red square). The assay detects 2.72 ± 0.04 primary amino groups in Cyt$_{SATP}$, in relation, native Cyt bears 19 amines. Consequently, 16 SATP molecules were introduced on the Cyt surface.

Curriculum Vitae

██████████

████████████████████████

██

██████████████████████████

██

██████████████████████████████████

█████████

████████████████████████████████
██
████████████████████████████████████

████████

██
████████████████
██
███
███████████████████████████████████
████████████
█████████████████████████████████████
████████████████████████████████████
███
███
████████████
██
████████████████████████████████

██████████████████
██
████████████████████████
████████████████████

██
███
████████████████████████████
████████████████████████████████

██
████████████████████████████

██
                        ██████████████
                        ███

██████████
██
                        ████████████████████████████████████

████████████████████████████

████████████
        ██
            ██
            ██████████
        ██
            ██
            ██
            ██████████
        ██
            ███
            ████████████████████████████████████
        ██
            ████████████████████████████
        ██
            ███████████████████████████████████████

████████████████████████████
        ██
            ██████████
        ██
            ███████
        ██
            ████████████████████
        ██
            ████████████████████
        ██
            ████████████████████████████